General Disclaimer

One or more of the Following Statements may affect this Document

- This document has been reproduced from the best copy furnished by the organizational source. It is being released in the interest of making available as much information as possible.

- This document may contain data, which exceeds the sheet parameters. It was furnished in this condition by the organizational source and is the best copy available.

- This document may contain tone-on-tone or color graphs, charts and/or pictures, which have been reproduced in black and white.

- This document is paginated as submitted by the original source.

- Portions of this document are not fully legible due to the historical nature of some of the material. However, it is the best reproduction available from the original submission.

Produced by the NASA Center for Aerospace Information (CASI)

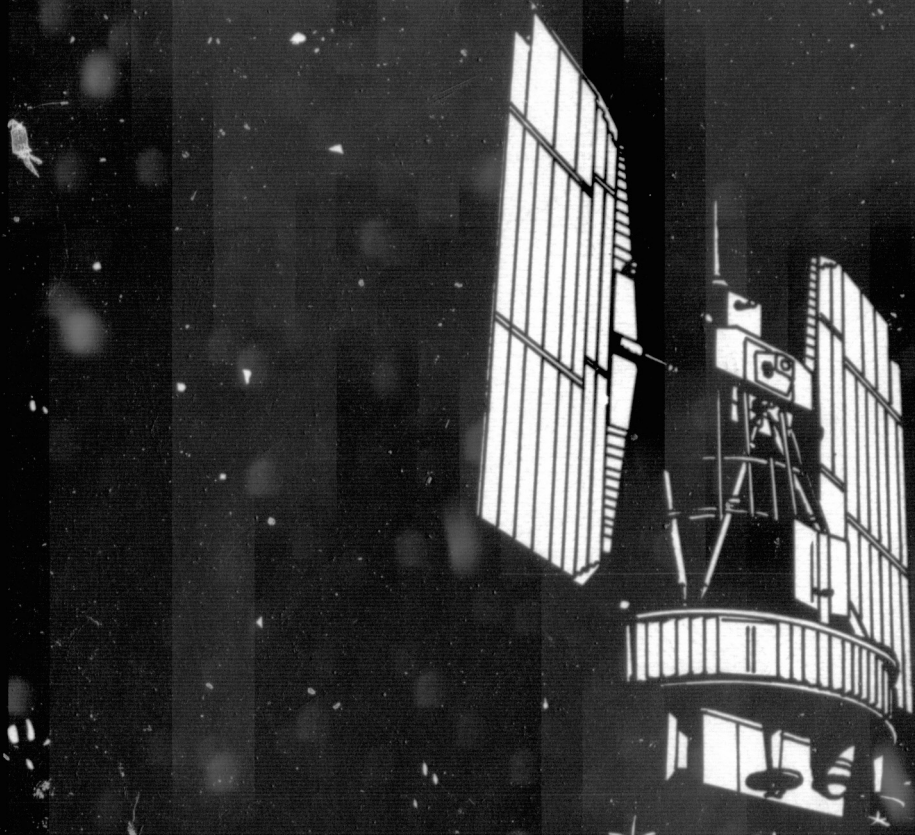
03

E7.5-10324
CR-148926

(E75-10324) ANALYSIS OF ERTS-1 IMAGERY OF WYOMING AND ITS APPLICATION TO EVALUATION OF WYOMING'S NATURAL RESOURCES Final Report, Jul. 1972 - Dec. 1974 (Wyoming Univ.) 303 p HC $9.25 CSCL 08F G3/43

N75-26468

Unclas 00324



FINAL REPORT: CONTRACT NAS 5-21799 1434A

January, 1975 R.S. HOUSTON, R.W. MARRS and L.E. BORGMAN

RECEIVED
JUN 18 1975
SIS/902.6

University of Wyoming Remote Sensing Laboratory

TYPE III FINAL REPORT

on

ANALYSIS OF ERTS-1 IMAGERY OF WYOMING AND ITS APPLICATION TO EVALUATION OF WYOMING'S NATURAL RESOURCES

"Made available under NASA sponsorship in the interest of early and wide dissemination of Earth Resources Survey Program information and without liability for any use made thereof."

By: Robert S. Houston, Ronald W. Marrs, and Leon E. Borgman

With Contributions From: S. S. Agard, R. Barton, D. L. Blackstone, R. M. Breckenridge, E. R. Decker, J. Earle, M. A. Evans, N. Froman, R. C. Gordon, K. E. Kolm, R. B. Parker, F. R. Redfern, D. Strickland, and B. J. Tomes

Color
Original photography may be purchased from:
EROS Data Center
10th and Dakota Avenue
Sioux Falls, SD 57198

Department of Geology
University of Wyoming
Laramie, Wyoming 82071

January, 1975

Prepared For:

NASA/GODDARD SPACE FLIGHT CENTER
GREENBELT, MARYLAND 20771

TECHNICAL REPORT STANDARD TITLE PAGE

1. Report No.	2. Government Accession No.	3. Recipient's Catalog No.

4. Title and Subtitle	5. Report Date
FINAL REPORT: ANALYSIS OF ERTS-1 IMAGERY OF WYOMING AND ITS APPLICATION TO EVALUATION OF WYOMING'S NATURAL RESOURCES	January, 1975
	6. Performing Organization Code
7. Author(s) R. S. Houston, R. W. Marrs, and L. E. Borgman	8. Performing Organization Report No. ERTS-WYO-FINAL
9. Performing Organization Name and Address Department of Geology University of Wyoming Laramie, Wyoming 82071	10. Work Unit No.
	11. Contract or Grant No. NAS 5-21799
	13. Type of Report and Period Covered July, 1972 - December, 1974
12. Sponsoring Agency Name and Address NASA/Goddard Space Flight Center Greenbelt, Maryland 20771 Tech. Monitor: Frederick Gordon, Jr.	14. Sponsoring Agency Code

15. Supplementary Notes

16. Abstract

The data provided by the Earth Resources Technology Satellite is unquestionably an important new tool for earth resource applications. Successful applications demonstrated by investigators include: 1) general geologic mapping, 2) structural and tectonic studies, 3) landforms and surface processes, 4) mineral exploration, 5) land-use inventories, 6) hydrologic studies, 7) investigations in agriculture and forestry, and 8) environmental quality and ecology. The chief advantages of the ERTS-1 data for geologic studies are the synoptic view, spectral information, and seasonal coverage. The spectral data and the repetitive aspect are even more important for land use and vegetation studies. The main limitations of the ERTS data are low resolution and lack of stereoscopic coverage. Computer techniques were not used successfully as a means of automated mapping or interpretation, but can provide a (very powerful) tool to assist the interpreter in some applications.

17. Key Words (Selected by Author(s))	18. Distribution Statement
Geology, Vegetation, Land-use, Computer Analysis	

19. Security Classif. (of this report)	20. Security Classif. (of this page)	21. No. of Pages	22. Price*
unclassified	unclassified		

*For sale by the Clearinghouse for Federal Scientific and Technical Information, Springfield, Virginia 22151.

Figure 2. Technical Report Standard Title Page

PREFACE

The chief objective of the University of Wyoming ERTS-1 investigation (contract NAS 5-21799) was to develop expertise in the application of ERTS data in resource studies and to evaluate the ERTS-1 data in these applications. The study began prior to the ERTS-1 launch in July of 1972 and will continue through October, 1975 under contract modification 7 (10 January, 1975). The original objectives were achieved by December, 1974 and results of those studies are summarized in this report. These studies emphasized geologic applications of the ERTS data but also included hydrologic, agricultural, land-use, and ecologic evaluations of the ERTS-1 data.

Results of these studies were mostly positive. The regional, repetitive coverage proved invaluable in several applications and the spectral information provided by the ERTS multispectral scanner allowed investigators to make many subtle distinctions regarding lithologic units, possible mineral deposits, soil moisture, and vegetation condition. Major limitations of the ERTS data are its lack of stereoscopic geometry and low resolution.

CONTENTS

	PAGE
INTRODUCTION	1
LABORATORY AND OPERATIONAL RESEARCH	1
DISSEMINATION OF DATA	5
Public	5
Scientific	6
OBJECTIVES	8
PERSONNEL	9
RESULTS OF THE INTERPRETATION OF ERTS IMAGERY	13
Geology	13
Geologic Mapping	13
Topical Mapping	15
Mineral Exploration	19
Structural Geology	22
Geothermal	27
Agriculture and Forestry	27
Hydrology	32
Environmental Quality	37
Ecology	41
Other Applications	49
USE OF AIRCRAFT IMAGERY	49
DEVELOPMENT OF COMPUTER PROCESSING TECHNIQUES	50
Minicomputer Output Possibilities	51
Sequential Q-mode Factor Pattern Recognition Techniques	53
Frequency Space Cluster Search	56
Multivariate Ratio Techniques	57
COST BENEFIT ESTIMATES	59
SUMMARY	61
APPENDICES	62
A. Summary of applications of ERTS-1 imagery to land-use studies in Wyoming	63
B. Application of remote-sensing data to geologic problems encountered by the Wyoming Geological Survey	79
C. Summary of a study of regional geomorphologic relationships in the Wyoming Basin province	81

PAGE

D. The use of satellite imagery and aerial photography for making lithologic distinctions 84

E. Geologic mapping from ERTS-1 imagery 101

F. Geologic applications of ERTS-1 in volcanic terrane 109

G. Geologic map of Carbon County, Wyoming interpreted from ERTS-1 imagery 123

H. Utility of high-altitude color photography for geologic mapping 136

I. Mapping of large glacial features using ERTS-1 imagery 138

J. Estimating available water contained in snow-pack 143

K. ERTS imagery applied to mapping of sand dunes 154

L. Tectonics and linear elements interpreted from ERTS 157

M. Structural geology of south-central Wyoming . . 158

N. Mapping of major fractures with ERTs imagery 164

O. Analysis of photo linear elements, Bighorn-Pryor Mountains, Montana and Wyoming 169

P. Analysis of photo linear elements, Laramie Mountains, Wyoming 174

Q. Geology of photo linear elements, Great Divide Basin, Wyoming 182

R. Tectonic analysis of southwestern Wyoming from ERTS-1 imagery 188

S. Comparison of ERTS imagery with S-190A, S-190B, and aerial photographs for lineation mapping 192

T. Vegetation analysis in the Laramie Basin, Wyoming from ERTS-1 imagery 198

U. Identification of irrigated crops 204

V. ERTS-1 imagery as a tool for mapping major vegetation zones in Wyoming 210

W. The use of ERTS data for range mapping and estimation of above-ground green biomass 228

X. Mapping of seleniferous soil units 240

Y. Programs employed in Q-mode factor analysis ERTS-1 multispectral data 242

REFERENCES 276

LIST OF FIGURES

		PAGE
Figure 1.	ERTS-1 false-color infrared mosaic of Wyoming	2
Figure 2.	Snow scene of the Laramie Range (ERTS-1 image 1514-17104-4), Changes in topographic expression of sedimentary units along the west flank of the Laramie Range correspond to facies changes . . .	18
Figure 3.	ERTS-1 mosaic of Sweetwater County, Wyoming compared to a structure contour map representing the top of the Cretaceous Dakota Formation	26
Figure 4.	Snow scene of Yellowstone National Park (portion of ERTS-1 image 1213-17415-7), Numbers indicate thermal areas detectable as zones of melted snow or ice	28
Figure 5.	Color-additive comparison of ERTS-1 imagery of the Laramie Basin obtained in autumn, 1972 (1047-17184-7) and summer 1973 (1353-17190-7), The striking contrast in surface water distribution is readily apparent in this duo-tone composite	34
Figure 6.	A red-band ERTS-1 image of the Laramie Basin (1353-17190-5) showing contrasts in basin lakes related to water depth and turbidity (compare with Fig. 7) . . .	35
Figure 7.	A duo-tone image composite of the Laramie Basin area (ERTS-1 image 1353-17190 bands 5 and 7), this composite shows surface waters in contrasting colors which can be interpreted in terms of the water depth and turbidity	36
Figure 8.	Rawlins area land use interpreted from ERTS-1 imagery	39
Figure 9.	Snow scene of the Casper area, central Wyoming (ERTS-1 image 1534-17211-7)	42
Figure 10.	Isodensity contour map of the Casper area	43
Figure 11a.	A portion of ERTS-1 image 1515-17160-4 showing a smoke plume from a fire at the American Quasar #1 Patterson well north of Douglas, Wyoming	44

LIST OF FIGURES (cont'd)

		PAGE
Figure 11b.	A ground-level view of the fire at the American Quasar #1 Patterson well . .	44
Figure 12.	Emmission plumes from trona mills and other industrial sites in southwestern Wyoming	45
Figure 13a.	Snow distribution and area of available winter range in the winter periods November, 1972 and January, 1973	47
Figure 13b.	Snow distribution and area of available winter range in the winter periods April, 1973 and February, 1974 . . .	48
Figure A-1.	Index map showing the location of the Powder River Basin test area	65
Figure A-2.	Land-use classification map for the Powder River Basin; Wyoming	66
Figure A-3.	Flood plains of major streams in the Powder River Basin as mapped from ERTS-1 imagery	68
Figure A-4.	Map of forest and range land in a portion of the Bighorn Mountains	69
Figure A-5.	Range map of part of the Powder River Basin test site	70
Figure A-6.	Soil map of the west-central portion of the Powder River Basin	72
Figure A-7.	Areas of equivalent slope estimated from drainage pattern and density	73
Figure A-8.	Coal reserves of the central Powder River Basin	74
Figure A-9.	Areas of potential mineral resource development along the west flank of the Bighorn Mountains	76
Figure A-10.	Land use maps of Casper, Wyoming	78
Figure B-1.	Geomorphic section of the Wyoming Basin	82
Figure D-1.	Map of Wyoming showing identification numbers of best ERTS-1 images	85
Figure D-2.	Index map showing Skylab S-190A coverage of Wyoming during Skylab missions 2 and 3	86
Figure D-3.	Index map showing NASA aircraft coverage of Wyoming as of October, 1973	87

LIST OF FIGURES (cont'd) PAGE

Figure D-4	Map of Precambrian terrane of the southern Wind River Mountains and Granite Mountains.	90
Figure D-5	Reconnaissance geologic map of rocks of Precambrian age in the Granite Mountains and adjacent areas of Wyoming compiled by use of U-2 and C-130 air photographs and from geologic mapping in T.32 N. Rs. 87 and 88 W.	94
Figure D-6	Reconnaissance geologic map of rocks of Precambrian age in the Granite Mountains of Wyoming compiled by use of U-2 air photographs.	95
Figure D-7	Images of the southeastern Wind River Mountains of Wyoming showing contrasts between Precambrian metasedimentary/ metavolcanic rock and granite/granite gneiss.	92
Figure D-8	Reconnaissance geologic map of rocks of Precambrian age in the Granite Mountains and adjacent areas of Wyoming compiled by use C-130 air photographs...	96
Figure D-9	Reconnaissance photogeologic map of the Barlow Gap area, Natrona County, Wyoming. Compiled from interpretations of C-130 aerial photography.	98
Figure E-1	Comparisons of reflectance and emissivity spectra for acidic and mafic rocks.	102
Figure E-2	Spectral response curves for a group of rocks from Wyoming determined on a Carey 90 reflectance spectrometer. . .	105
Figure E-3	Details of the southeast ¼ of the ERTS Arminto map compared with the same area of the state geologic Map of Wyoming.	107
Figure F-1	Index map of volcanics in northwestern Wyoming.	110
Figure F-2	ERTS-1 MSS-T Mosaic of northwestern Wyoming.	112
Figure F-3	Structural features interpreted from ERTS-1 imagery.	113
Figure F-4	Major rock types mapped from ERTS-1 imagery.	116
Figure F-5	Multiband photography of the Wood River test site.	120
Figure F-6	Intrusives in the Yellowstone-Absaroka provinces.	121

LIST OF FIGURES (cont'd)

		PAGE
Figure G-1	Index map of the Carbon County study area.	124
Figure G-2	Stratigraphic nomenclature chart for south-central Wyoming.	126
Figure I-1	ERTS MSS-5 mosaic of northwestern Wyoming.	139
Figure I-2	Glaciation map of northwestern Wyoming.	141
Figure J-1	An ERTS scene of the Wind River Mountains, northern Thrust Belt, and Absaroka range.	144
Figure J-2	May 3 snow cover map of the upper Green River drainage.	146
Figure J-3	May 21 snow cover map of the upper Green River drainage.	147
Figure J-4	June 8 snow cover map of the upper Green River drainage.	148
Figure K-1	Map of sand dune fields shows migration directions of stabilized and active dunes.	155
Figure M-1	ERTS image No. 1066-17242-4 covering Carbon County and adjacent areas.	159
Figure M-2	Geologic map showing structural features and lithologic relation between Medicine Bow, Lewis, and Mesa Verde formations in the Carbon County Area.	160
Figure M-3	Geologic map showing relation between Medicine Bow, Lewis, and Mesaverde formations in Carbon County.	161
Figure N-1	ERTS-1 image 1014-17352-5 of the Wind River Mountains.	165
Figure N-2	Principal mapped faults, shear zones, and dikes also observed on ERTS-1 imagery.	168
Figure O-1	Major linear elements of the Pryor and Big Horn Mountains.	170
Figure O-2a	Rose diagram showing trends and orientations of observed linear elements.	173
Figure O-2b	Rose diagram showing the orientations of fold axis in the Big Horn Basin.	173
Figure P-1	General distribution of rock types in the Laramie Range.	175
Figure P-2	Lineations in the Laramie Range.	176

LIST OF FIGURES (cont'd) PAGE

Figure P-3a Rose diagram showing dominant orientations of photo linear elements of the southern Laramie Range. 177

Figure P-3b Rose diagram showing dominant orientations of photo linear elements of the northern Laramie Range. 177

Figure P-4 Composite rose diagram of photo linear elements located on aircraft imagery. . . . 180

Figure Q-1 Major linear features of the Great Divide Basin. 183

Figure Q-2 Major structural elements of the Great Divide Basin, Wyoming. 184

Figure R-1 Major tectonic elements of southwestern Wyoming interpreted from ERTS-1 imagery. 189

Figure S-1 Map showing all lineations detected on ERTS images of the Wind River Mountains. . . 194

Figure S-2 Map showing all lineations detected on Skylab S-190A photography of the Wind River Mountains. 195

Figure S-3 Comparison of linear features mapped using ERTS images and Skylab S-190B photographs of a part of the Wind River Mountains showing sun-azimuth bias. . .196

Figure U-1 A 50X density contour map of the study area from ERTS-1 image 1334-17133-5, 22 June, 1973. 206

Figure U-2 A 50X density contour map of the study area from ERTS-1 image 1353-17132-5, 10 July, 1973. 207

Figure U-3 A 50X density contour map of the study area from ERTS-1 image 1388-17128-5, 15 August, 1973. 208

Figure V-1 Index map of Wyoming. 212

Figure V-2 Map I; a vegetation map of Wyoming showing zone 1 (alpine) and zone 2 (timbered mountain slopes). 213

Figure V-3 Map II; a vegetation map of Wyoming showing zone 3 (foothills scrub) and zone 5 (desert and basin). 214

Figure V-4 Map III; a vegetation map of Wyoming showing zone 6 (major river bottoms and irrigated croplands). 215

LIST OF FIGURES (cont'd)

		PAGE
Figure V-5	Map IV; A general map defining agricultural areas of Wyoming.	215
Figure V-6	ERTS-1 image 1015-17404-4, 5, 7, 7 August 1972, showing the Yellowstone Park and Columbia Plateau areas of Wyoming.	218
Figure V-7	A detailed map of zones 1 and 2 taken from the original of Figure V-6.	219
Figure V-8	ERTS-1 image 1013-17294-4, 5, 7, 5 August 1972, showing the Wind River Mountains and Wind River Basin of central Wyoming. . .	220
Figure V-9	A detailed map of zones 1 and 2 taken from the original of figure V-8.	221
Figure V-10	A detailed map of zones 3, 4, 5, and 6 taken from the original of figure V-8. . . .	222
Figure V-11	ERTS-1 image 1047-17175-4, 5, 7, 8 September, 1972, showing the Black Hills and northern Powder River Basin of Wyoming, South Dakota, and Montana. . . .	223
Figure V-12	A detailed map of zone 1 (Black Hills element of timbered mountain slopes) and zones 3,4, and 6 taken from the original of figure V-11.	224
Figure V-13	ERTS-1 image 1013-17300-4, 5, 7 5 August, 1972, showing the Great Basin and Red Desert areas of Wyoming, Utah, and colorado.	225
Figure W-1	Range vegetation map compiled from low-level aerial photography supplemented with ground reconnaissance. (a=east area, b=west area).	233-234
Figure W-2	Range vegetation map interpreted from Skylab photographs (a-east area, b=west area).	235-236
Figure W-3	Range vegetation map developed from ERTS-1 imagery (a=east area, b=West area).	237
Figure W-4	Graphs of log transmittance versus above-ground green biomass.	238

LIST OF TABLES

		PAGE
Table 1	Subdivisions of vegetation discriminable from ERTS-1 imagery.	30
Table D-1	Iron, titanium, and chromium content of samples of iron formation from Barlow Gap, Wyoming.	99
Table F-1	Filtered photometer readings from major lithologies of the Yellowstone/Absaroka test site.	118
Table J-1	Snow-cover and snow-depth estimates made from ERTS-1 imagery.	145
Table J-2	Daily discharge records for the upper Green River drainage.	149
Table J-3	Surface water runoff forecasts for the Green River at Warren Bridge--April to September, 1973.	151
Table J-4	Snow depth and water content measurements.	151

LIST OF PLATES

Plate G-1	Photogeologic map of Carbon County, Wyoming.	(in pocket)

INTRODUCTION

The Wyoming ERTS investigation, originally designated as proposal 364, was combined with EREP investigation (No. 434) and was made part of a single coordinated study involving acquisition and interpretation of data resulting from both the ERTS and EREP experiments. The test site was the state of Wyoming (figure 1). Initial funding requests were reduced substantially as a result of the coordination and also due to modification of original objectives. Basically, geologic and vegetation studies were retained and certain environmental and wildlife studies were eliminated. In keeping with NASA requests a sincere effort was made to make the results of studies available early in the form of special reports. Summaries of these special reports are appended as a part of this final report.

LABORATORY AND OPERATIONAL RESEARCH

In addition to the research projects, other functions of the University of Wyoming Remote Sensing Laboratory include maintainance of a library of remotely sensed data for the State of Wyoming, and demonstrations to other potential users the advantages or disadvantages of remote sensing for their applied research. The following results were achieved:

1. A data library has been established which comprises NASA ERTS-1 imagery, Skylab photography and other EREP data, and aerial photography obtained from the Air Force, Army, Soil Conservation Service, and private firms. The depository also has a catalog of existing maps on such subjects as land use, vegetation, soils, etc. where available. Maintenance of this data file requires about twenty hours per week and is a University contribution. The data and the technical assistance available at the Remote Sensing Laboratory is used weekly by the public. Thus, it gives the NASA program wide circulation to individuals who may see for themselves the utility of the data.

Figure 1. ERTS-1 false-color infrared mosaic of Wyoming (compiled by General Electric Photographic Engineering Laboratories, Beltsville, Maryland).

ORIGINAL PAGE IS
OF POOR QUALITY

2. Meetings with individuals and groups in State and Federal agencies have been held to discuss the the possible utility of remotely sensed data for agency use. A formal meeting was held in September, 1972 in the state capitol with Dr. Short of Goddard in attendance and the meeting resulted in joint studies and use by individuals of several agencies, as follows:

   a. The Department of Economic Planning and Development commissioned a pilot study (emphasis on land-use maps) for the Powder River Basin of Wyoming (appendix A). This study led to a joint proposal submitted as an ERTS-B proposal for a more detailed demonstration project in this area and elsewhere in the state. The program was not approved by NASA, but the United States Geological Survey has recently (September, 1974) indicated a desire to fund parts of the program in the Powder River Basin of Wyoming and Montana.

   b. Wyoming Game and Fish Commission researchers have made use of ERTS color infrared images and aircraft infrared images for vegetation mapping related to game control programs.

   c. The State Highway Department has indicated a willingness to allow use of their aircraft for programs in remote sensing. These programs are pending, but will involve use of the highway department Zeiss aerial camera plus the three-camera Hasselblad unit designed by the remote sensing laboratory for various geologic and earth resource studies.

   d. The Soil Conservation Service has cooperated with the Remote Sensing Laboratory by furnishing new and unpublished soils maps of various areas in the state to see if ERTS,

aircraft, and EREP images can be used to generate soils maps. The maps prepared to date (appendix A, p. 72) are satisfactory general soils maps, but the units mapped do not relate directly to the detailed soils classification schemes in current use. The Soil Conservation Service has also supplied the laboratory with a vast collection of enlarged black and white air photographs that are extremely useful in determining such factors as changing land use from the 1940's to the present.

e. The Wyoming Geological Survey has cooperated in the remote sensing studies by supplying geologic data and information on current and proposed mineral developments. The Geological Survey hired the first individual trained by the Remote Sensing Laboratory and is currently using the data in the Remote Sensing Laboratory on an operational basis. Examples of maps prepared by the State Geological Survey in Cooperation with the Remote Sensing Laboratory are in appendices B and C.

f. The United States Geological Survey uses remotely sensed data in many of its programs, and maintains a file at the Denver Federal Center that contains much of the available imagery for the Rocky Mountain area. But geologists of the Survey have also made some use of Wyoming imagery files; and the U.S.G.S. is currently cooperating with the Wyoming Remote Sensing Laboratory in two projects: 1) Powder River Basin landforms and land-use studies, and 2) in preparation of the new state geologic map. A portion of the geologic mapping done with ERTS imagery has been used to compile the state map where mapping is

out-dated or incomplete. Quaternary rocks and rocks of Precambrian age are generally poorly mapped and the U.S.G.S. has used maps of sand-dune areas prepared by the remote sensing laboratory and has supported mapping of other deposits of Quaternary age using ERTS imagery and Skylab photographs.

g. Research scientists at the University are aware of remote sensing and use is being made of imagery by engineers, agricultural scientists, and plant scientists. Perhaps the major use of remote sensing has been in the preparation of environmental impact statements. The remotely-sensed data serves as a tool by which researchers in many disciplines can obtain physical and environmental data in areas of proposed development. This information can then be applied to planning and impact estimation. The data available prior to development also represents a set of baseline data for change assessments.

The development of these programs in this relatively short period of time show that it is possible to move directly from a successful demonstration program to an operational information system. Such a system must have broad application and be readily accessible to a large number of users.

DISSEMINATION OF DATA

Public

An effort has been made to acquaint the general public with the potential of NASA-acquired remote sensing data through talks to civic groups, news releases, and through an exhibit at the Wyoming State Fair in August, 1974. Non-technical presentations dealing with the ERTS-1 program include:

1. Marrs, R. W., Lecture on remote-sensing and ERTS applications; Laramie Civitans, April, 1974.

2. Marrs, R. W., and others, Remote Sensing applied to problems in energy and the environment; Wyoming State Fair; August 19 - 25, 1974 (program previewed in several news releases).
3. Houston, R. S. and others, University research in energy and environment; a program to aquaint Wyoming people with University research programs, presented in 27 Wyoming cities. Several of these sessions emphasized remote-sensing and the ERTS program. June - August, 1974, (accompanied by radio broadcasts and news releases).
4. Marrs, R. W., and Gordon, R. C., Remote-Sensing research at the University of Wyoming; Agriculture Extension Conference, December, 1974.
5. Marrs, R. W., Remote-sensing research at the University of Wyoming; State Legislators Workshop, December, 1974, (this same presentation was given at the State Fire Meeting, Gillette, December 6, 1973.

Scientific

Presentations dealing in greater depth with remote sensing and the ERTS program were given before scientific and professional audiences:

1. Houston, R. S., and Short, N. M., 1972, Geologic interpretation of ERTS imagery of western Wyoming; First ERTS-1 Symposium, September 29, 1972, Report X-650-73-10, NASA Scientific and Technical Information Office, Washington, D. C., p. 58 - 77.
2. Breckenridge, R. M., 1973, Glaciation of northwestern Wyoming interpreted from ERTS-1, Symposium on Significant Results Obtained From ERTS-1, March 5 - 9, 1973, Report NASA-SP-327, NASA Scientific and Technical Information Office, Washington, D. C., p. 363 - 370.
3. Breckenridge, R. M., Marrs, R. W., and Murphy, D. J., 1973, Remote sensing applied to land-use studies in Wyoming; Symposium on Significant Results from ERTS-1

March 5 - 9, 1973, Report NASA SP-327, NASA Scientific and Technical Information Office, Washington, D. C., p. 981 - 990.

4. Parker, R. B., 1973, Regional Fractures in the Wind River Mountains Precambrian from ERTS-1 Imagery; 26th Annual Meeting of the Geological Society of America, Rocky Mountain Section, (abs.), p. 1520.
5. Houston, R. S., 1973, Application of remote sensing to assessment of Wyoming's natural resources, Wyoming Geological Society Meeting, May 11, 1973, Laramie, Wyoming.
6. Houston, R. S. and others, 1973; Application of the ERTS system to the study of Wyoming resources - with emphasis on the use of basic data products; Third ERTS-1 Symposium, December 10 - 14, Report NASA-SP-351, NASA Scientific and Technical Information Office, Washington, D. C., p. 595 - 620.
7. Houston, R. S. and Marrs, R. W., 1974, Some preliminary results of the use of S-190A and S-190B Skylab sensors for photogeologic studies; 55th Annual Meeting of the American Geophysical Union, Washington, D. C., (abs.), EOS p. 344.
8. Marrs, R. W., 1974, Remote sensing in mineral exploration; 17th Mineral Symposium of the Eastern Wyoming Subsection of the Society of Mining Engineers/AIME, May 11, 1973, 15 p.
9. Marrs, R. W., 1974, Summary of remote-sensing research in Wyoming; Soil Survey Work Planning Conference, Laramie, Wyoming, May 21, 1974.
10. Marrs, R. W., 1974, Interpretation Techniques in remote sensing; Wyoming Geological Society Meeting, May 19, 1974, Laramie, Wyoming.
11. Houston, R. S. and Marrs, R. W., Examples of the use of standard data products of the NASA, ERTS, Skylab, and aircraft programs in the study of Wyoming surface resources, American Association of Petroleum Geologists,

Rocky Mountain Section Meeting, June, 1974, Casper, Wyoming.

12. Marrs, R. W., 1974, Interpretation techniques in remote sensing; American Association of Petroleum Geologists, Rocky Mountain Section, June, 1974, Casper, Wyoming.
13. Houston, R. S., and Marrs, R. W., Use of Skylab S-190A and S-190B photographs in Wyoming earth resource studies; 20th Annual Meeting of the American Astronautical Society, August 20 - 22, Los Angeles, California.

OBJECTIVES

The primary objectives of the 434 project were to set up a laboratory of remote sensing and to use the laboratory to interpret data obtained from both ERTS and EREP experiments. The objectives as modified, by the negotiations that resulted in combination of the ERTS and EREP studies are as follows:

Monitoring	1.	Collect field data to document micrometeorological parameters and spectral signatures, for selected ERTS, EREP, and aircraft passes.
Geology	2.	Evaluate sensor data for application to regional mapping, tectonic analyses, stratigraphic studies, and mineral exploration. This work will include an effort to distinguish major rock units, study of regional fracture systems, and attempts to distinguish mineralized zones from unmineralized zones.
Geothermal	3.	Utilize the thermal channel of the S-192 imager to determine to what extent hot springs and other active areas can be identified and mapped from spacecraft. (ERTS-1 did not have a thermal channel, so thermal studies have been confined to the study of snow scenes and vegetation anomalies as related to thermal areas).

Agriculture-Forestry	4.	Determine the spectral reflectance characteristics of various forest and grassland communities in Wyoming, map major vegetation types and attempt to identify and map seasonal changes in vegetation communities. This would include an evaluation of the usefulness of spacecraft imagery for determining the effects of grazing on plant communities, and evaluate the EREP data as a tool for mapping indicator plants and toxic soils.
Environmental Quality	5.	Prepare a base map showing current environmental conditions in areas containing potential coal strip mines and the fly ash distribution from planned coal-fired power plants, and map density and extent of emission plumes using spacecraft imagery.
Ecology	6.	Attempt to relate the seasonal distribution of wildlife to seasonal changes in plant communities and ground temperature as determined for EREP imagery.

PERSONNEL

The original ERTS proposal was a cooperative proposal with Dr. N. Short of Goddard as principal investigator. The modified ERTS-EREP proposal placed the responsibility of the combined investigation at the University of Wyoming and R. S. Houston as principal investigator. Dr. Short, however, remained as co-investigator and contributed significantly to the study. Individuals who have contributed to the ERTS study are, as follows:

Name and Title	Affiliation	Contribution to ERTS research
R. Houston, P. I. - Geology	Univ. of Wyo.	Administration plus geologic mapping studies and mineral exploration

Name and Title	Affiliation	Contribution to ERTS research
R. Marrs, Co-I. - remote sensing geology	Univ. of Wyo.	Administration and geologic studies plus land-use and monitoring
R. Parker, Co-I. - structure	Univ. of Wyo.	Lineation and field studies
D. Blackstone, Co-I. - structure	Univ. of Wyo.	Regional structure and field studies
R. Breckenridge, Co-I. - geomorphology	Univ. of Wyo.	Glacial geology and environmental geology
E. Decker, Co-I. - heat flow	Univ. of Wyo.	Geothermal and computer processing
L. Borgman, Co-I. - statistics	Univ. of Wyo.	Statistical methods of data processing
D. Knight, Co-I. - botany	Univ. of Wyo.	Vegetation mapping
H. Fisser, Co-I. - plant science	Univ. of Wyo.	Range management
D. Lane, Consultant - petroleum geology	Wyo. Geol. Survey	Petroleum geology

Name and Title	Affiliation	Contribution to ERTS research
G. Glass, Consultant - coal geology	Wyo. Geol. Survey	Coal geology
B. Mears, Consultant - geomorphology	Univ. of Wyo.	Regional geomorphology
R. Surdam, Consultant - Geochemistry	Univ. of Wyo.	Evaporite lakes
P. Huntoon, Consultant - hydrology	Univ. of Wyo.	Groundwater prospecting
D. Love, Consultant - geology	U. S. Geol. Survey	Geologic mapping
K. Diem, Consultant - wildlife management	Univ. of Wyo.	Wildlife management
D. Strickland, Consultant - wildlife management	Univ. of Wyo.	Wildlife management
R. Gordon, Research Asst. - plant science	Univ. of Wyo.	Range management
K. Kolm, Research Asst. - geomorphology	Univ. of Wyo.	Aeolian deposits and soils

Name and Title	Affiliation	Contribution to ERTS research
B. Tomes, Research Asst. - geology	Univ. of Wyo.	Structure and hydrology
J. Earle, Research Asst. - structure	Univ. of Wyo.	Tectonics
M. Evans, Research Asst. - botany	Univ. of Wyo.	Vegetation mapping
F. Redfern, Research Asst. - botany	Univ. of Wyo.	Vegetation spectra
W. Lauer, Technical Asst. - photography	Univ. of Wyo.	Photo processing
S. Baskett, Technical Asst. - general	Univ. of Wyo.	Technical assistance
S. Agard, Work/Study - Research Asst.	Univ. of Wyo.	General geology
N. Froman, Work/Study - Research Asst.	Univ. of Wyo.	General Geology and Computer Applications
K. McCarty, Clerical Asst.	Univ. of Wyo.	Film librarian

Name and Title	Affiliation	Contribution to ERTS research
L. Apperson Work/Study - Clerical Asst.	Univ. of Wyo.	Clerical
K. Meister, Clerical Asst.	Univ. of Wyo.	Clerical assistance

RESULTS OF THE INTERPRETATION OF ERTS IMAGERY

Geology

All geologic tasks were accomplished and some were extended to operational procedures that are now applied to other programs.

Geologic Mapping: Neither ERTS or Skylab images provide sufficient information for detailed geologic mapping because of low resolution. ERTS images are also limited in their utility by the lack of stereo-coverage. The ERTS synoptic view is unparalleled however, for regional studies, and in areas where vegetation is relatively sparse it has been possible to make reconnaissance geologic maps by establishing key lithologic units that can be recognized from space (the remote sensing unit) and to use these for mapping purposes. ERTS images can be best utilized where dips of formations are low and outcrops are correspondingly wide, or where lithologic subdivisions can be recognized by contrasts among formation groups. General mapping capability was increased by use of enhancement techniques such as color-additive viewing of selected ERTS bands, isodensity slicing, snow scenes, seasonal vegetation, pseudo-stereo viewing, edge enhancement and image masking.

As part of our proposal we suggested that it should be possible to distinguish major lithologic types in rocks of Precambrian age by use of ERTS imagery. Specifically, we hoped to distinguish terrane of mafic metamorphic rocks (greenstone belts) from that comprising mostly felsic rocks (granite-gneiss). This indeed proves to be a valuable

application of ERTS imagery. Details of the study are reported in Appendices D and E.

Mapping of volcanic terrane using ERTS imagery produced mixed results. Major lithologic units, such as volcanic, sedimentary, and crystalline rocks in the Absaroka area of Wyoming, are distinguishable but most of the pyroclastic rocks have similar reflectance characteristics. Distinctions between the various pyroclastic units could only be made locally. An important contribution was the utilization of ERTS color-composites to identify intrusive bodies within the Absaroka volcanics. Thirty-four of the forty-nine known centers were identified using ERTS imagery. Recognition of structural features such as calderas, major faults and flow structures in the rhyolite plateau area of Yellowstone Park was also a very useful aspect of the ERTS study. Details of this study are in Appendix F.

General geologic mapping has been undertaken in a number of areas in Wyoming, and the success of such mapping is primarily related to the skill of the interpreter and to his experience in a given area. The lithologic section in Wyoming comprises crystalline rocks of Precambrian age, distinctively colored sedimentary formations of Paleozoic and Early Mesozoic age, relatively drab but vegetatively expressed sandstones and shales of Late Mesozoic age, and light colored sedimentary and volcano-sedimentary rocks of Tertiary age. Spectral reflectance measurements were made at the Goddard Space Flight Center for a representitive group of samples from a sedimentary section in Wyoming. Field spectral readings were also taken at several type localities. A general review of the literature on spectral distinction of rock types and comparison of the spectral signatures for Wyoming rocks suggests that unique identifications cannot be made by use of multispectral data except in local areas and under controlled conditions (i. e., a general knowledge of the lithologic section and the field conditions). Geologic mapping from space is best accomplished by recognizing distinctive units on images, identifying these units on the ground, and

using them as guides to mapping. The ERTS color infrared composites are the most useful image product for most geologic mapping. The experienced photo-geologist can use these as well, if not better, than color photographs of the same resolution (Appendix E, p.101).

Examples of regional geologic mapping using ERTS are in Appendices E and G. This mapping has been checked and supplemented by use of color and color infrared aircraft photographs and, in addition, photogeologic maps have been prepared with aircraft products in two key areas (Appendix E and H).

Topical Mapping: The regional or synoptic view of ERTS has made it possible to undertake a number of topical mapping projects. These include mapping of glacial features and sedimentary deposits of glacial origin, mapping of geomorphic landforms and Quaternary deposits, mapping of dune fields, mapping of playa deposits (modern and fossil), and study of regional facies changes.

The detailed work (Appendix I) with glacial features and sedimentary deposits of glacial origin in northwest Wyoming shows that the regional extent of glaciation can be determined through mapping of such features as flow directions, large moraines, outwash fans, terraces, cirques, large "grooves," "U" - shaped valleys, and glacial lakes. In some areas, such as the Yellowstone plateau, remarkable detail of glacial structure can be seen. It was also determined that ERTS band 7 is expecially well suited to mapping the modern ice field, monitoring glaciers, and mapping ablating areas (Appendix J).

General geologic mapping programs accomplished using ERTS imagery also demonstrated that large-scale landforms can be readily mapped with ERTS images. Pediments may be readily identified because the deposits on pediment surfaces are often characterized by vegetation communities that differ from the vegetation of surrounding areas. Mapping of pediments can help reconstruct the history of paleo-rivers and streams. Other major geomorphic features such as large landslides, surfaces, and terrace deposits can also be recognized. ERTS images were utilized to establish a geomorphic province

classification for Wyoming - a first in this area (Appendix C).

In windy, semi-arid regions such as Wyoming, sand dunes cover large areas. Wyoming dune fields were partially known from mapping of small areas, but the regional extent of stabilized and active dunes had never been determined. The ERTS-1 imagery provided an ideal base for mapping the large dune belts and many of the smaller dune fields in Wyoming (Appendix K). In addition, basic new scientific information of regional mapping of dune deposits using ERTS has a number of direct economic applications. For example, ancient dunes form shallow water aquifers in much of Wyoming, they affect land use because they support a characteristic vegetation and active dune fields are not stable areas. Active and stabilized dunes also yield information on long term wind patterns.

Evaporite minerals (gypsum, anhydrite, halite, trona, etc.) and rocks rich in these minerals are highly reflective. Thus, it is relatively easy to locate and map playa lakes that are entirely or partially dry and that have partially-to fully developed salt pans. In Wyoming a number of these lakes have been or are being mined for magnesium and sodium salts so an inventory of these lakes is of economic significance. These lakes are seasonal and are best mapped in late fall illustrating the advantage of a repetitive mapping system in geologic studies.

One of the surprises of our initial ERTS study was the determination that fossil playa lakes could be mapped if exposed in a sedimentary succession. We have been able to map the trona-bearing playa lake Wilkins Peak member of the Green River Formation in the Green River and Washakie Basins. In one area the interpreter was familiar with the outcrop; in the other he was not. In both areas interpretation corresponds closely to a field map of the Wilkins Peak as recently mapped by the U.S. Geological Survey.

One of the investigation goals was to evaluate ERTS images as an aid in mapping regional facies changes. Mapping

of the Wilkins Peak Member of the Green River Formation discussed above is one example of this. The playa lake facies (Wilkins Peak Member) was distinguished from other lake beds of the Green River Formation mostly on the basis of tonal contrast. Topographic changes along strike of a formation can also be an aid in recognizing regional facies changes. Such changes may be recognized by using ERTS images with side lap or using a summer image that shows a formation by tone in conjunction with a snow-image that has a pseudo-topographic expression. An example of change in facies expressed topographically is the change from resistant limestones to non-resistant siltstones and shales in the Casper Formation on the west flank of the Laramie Mountains (ERTS-1 image 1514-17104). The resistant limestone is marked by a prominent hogback that gradually becomes less well developed as shale and siltstone replacing limestone northward (Fig. 2).

Some lithologic units have characteristic vegetation which is a distinct aid in mapping, especially utilizing color infrared composites. Where these units are continuously exposed over large areas, vegetative change along strike may be related to lithologic or facies changes. For example, in preparation of a regional geologic map from ERTS images in the Arminto area (Appendix E), it was apparent that certain sandstones and siltstones of Cretaceous age developed hogbacks with a characteristic heavy sagebrush growth on the dip slope of the formation. Some of these sandstone units were mapped. A facies change from sandstone to siltstone and to shale was located by use of this characteristic vegetative control.

Red-bed facies of the continental Tertiary of Wyoming can be identified on ERTS images. These units have a distinctive yellowish hue on the standard false-color infrared composites, but they exhibit somewhat higher reflectance than the Permo-Triassic red beds that also appear yellow on the false-color infrared. Mapping in the Arminto area demonstrated that these continental red bed facies could be distinguished from other Tertiary sedimentary rocks.

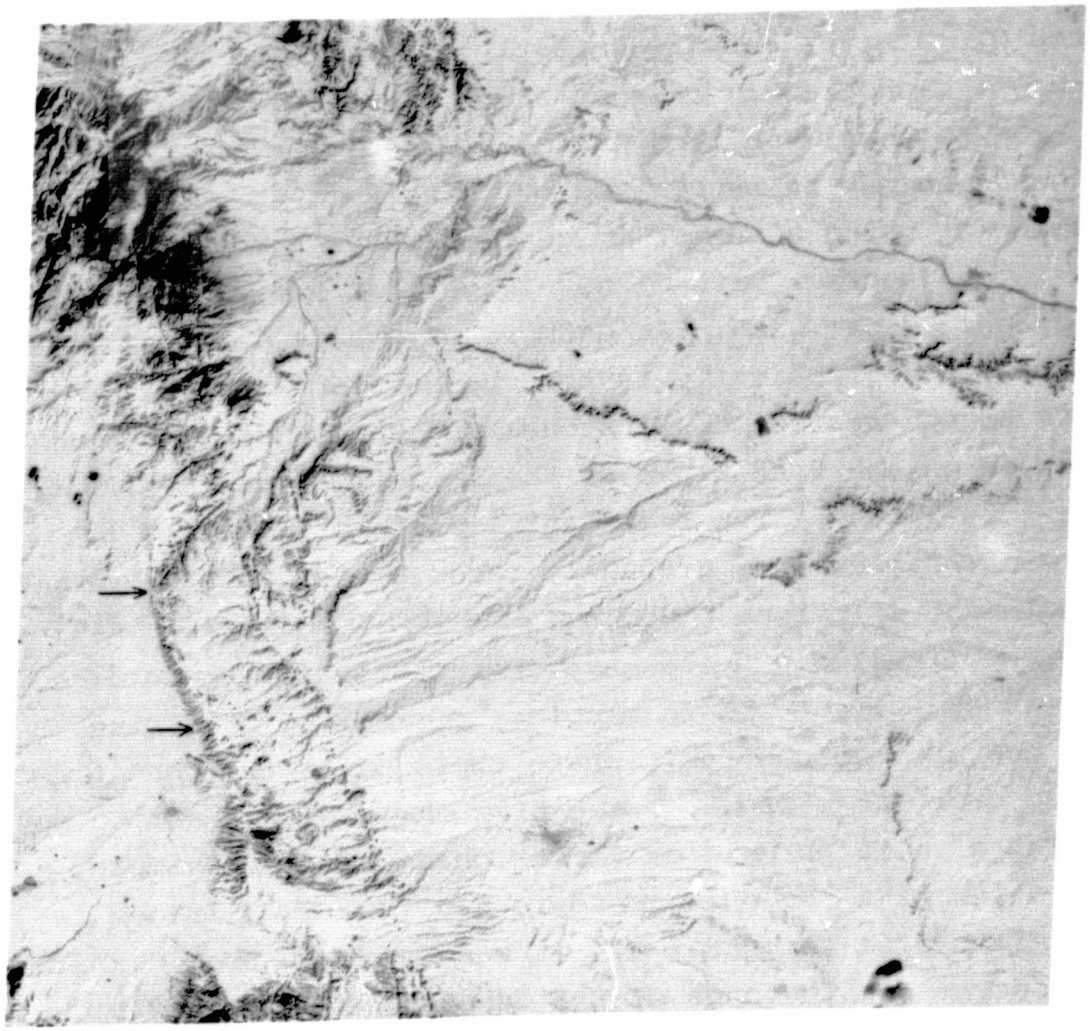


Figure 2. Snow scene of the Laramie Range (Image 1514-17104). Changes in topographic expression of sedimentary units along the west flank of the Laramie Range (arrows) correspond to facies changes.

ORIGINAL PAGE IS
OF POOR QUALITY

Mineral Exploration: Mineral exploration using spacecraft images can be either direct or indirect. Direct exploration might be accomplished through the photointerpretive recognition of some characteristics of a mineral deposit that identifies a specific type of deposit. Indirect exploration techniques might employ a space image to target features such as structure or rock type that may then be studied in detail by use of aircraft images, geophysical techniques, or surface geologic mapping to further isolate economic mineral deposits. This latter technique might also be referred to as multi-level sensing for mineral exploration.

Alteration halos that develop in conjunction with deposition of some types of minerals or through oxidation and hydration of mineral deposits exposed at the surface present a much larger target for exploration than the actual deposit. These alteration halos may be many times the size of the mineral deposit and they may form a "color anomaly." Two types of alteration were studied in Wyoming -- that associated with disseminated copper and molybdenum deposits in igneous intrusive bodies in the Absaroka Mountains, and that associated with uranium deposited in sedimentary rocks of Tertiary age in the Wyoming basins. In the Absaroka Mountains, 35 of the 49 known intrusive centers could be recognized using color infrared ERTS images. These 35 intrusives were studied by several interpreters to determine if altered intrusives (mineralized) could be distinguished. Results were mixed -- some altered intrusives with pronounced alteration were recog- recognized by all interpreters whereas other altered intrusives were variously interpreted and a number of areas were selected by interpreters where altered bodies were not known (Appendix F). It is clear that visual recognition of altered areas is not statistically reliable, but it is also clear that areas of strong alteration can, indeed, be recognized. Therefore, in a given area where the presence of altered intrusions is suspected, recognition of a "color anomaly" by several interpreters may be considered a reliable indication of an exploration target.

In the Wyoming sedimentary basins oxidizing groundwater has moved through and altered arkosic sandstones of Tertiary age and uranium has been concentrated at the interface between altered and unaltered sandstone. Some of these sandstones have been uplifted and exposed at the surface so that now the alteration can be used as a key to exploration for uranium. A study area was selected in the southern part of the Powder River Basin of Wyoming, and several interpreters were asked to examine the imagery of the area to see if altered sandstone could be mapped from space. This attempt met with limited success. The altered areas interpreted from the imagery were poorly defined and did not correspond to alteration zones mapped on the surface. This was essentially the same approach employed in the previous study of alteration resulting from oxidation of sulphide minerals in a desseminated copper deposit. In the areas of copper mineralization the iron oxide and hydrous iron oxides hematite and goethite are common alteration products, and the color anomaly is often strong. The color anomalies associated with the uranium properties are generally faint. This may account for the relatively poor success in using ERTS color infrared images to identify the color anomalies in the areas of uranium mineralization.

Attempts were also made to use the ERTS-1 imagery to identify fossil black sandstone deposits that are present in sandstone of Late Cretaceous age. Color infrared composite images and band-7 images were used to try to identify these deposits because it was expected that the iron absorption band in the near infrared would enhance the contrasts between the iron-rich black sandstone and associated iron-poor quartz sandstone. Unfortunately, the black sand deposits are so small that they are below ERTS resolution limit and could not be satisfactorily identified by visual methods. Larger deposits in northern Montana and large modern deposits on beaches might be recognized by use of ERTS images.

An example of the indirect application of ERTS to mineral exploration is the use of ERTS images in mapping greenstone belts in rocks of Precambrian age. Interpretations of aerial photographs of the greenstone terrane identified several suspicious outcrops that proved to be iron formations. The iron-formation outcrops could not be dectected on the ERTS-1 imagery, but the broad outcrops of greenstone contain in the iron formation are mappable, and can serve as a guide to exploration. This multi-level sensing approach is discussed in detail in Appendix D.

Multi-level sensing techniques can also be used to supplement direct exploration methods. For example, verification of color anomalies by use of aerial photography may be less expensive than field checking. For example, in the rugged Absaroka Mountains of Wyoming an aerial survey would certainly be faster and less expensive than field checking the anomalies located from the ERTS-1 imagery.

To date, structural studies and regional geologic mapping with ERTS and Skylab images has not led to the isolation of an economic prospect in Wyoming, but the regional structural studies already completed or in progress may eventually lead to such discoveries. Oil and mining companies are now using the ERTS imagery in their exploration programs. Some are studying the linear features as an indirect guide in mineral exploration. Interpretation of ERTS-1 imagery of Precambrian-cored uplifts in Wyoming reveals thousands of linear features (Appendix L). Some are faults or fractures. Some can be traced into the basin areas. These may represent basement fractures that have been reactivated and now affect the overlying sedimentary rocks. Such features may control petroleum migration and accumulation, but prospects located by use of these indirect exploration methods may take years to develop. Attempts were made to identify some of the large linear features recognized in the Wyoming basins, but the field studies failed to identify or locate many of the major linear features. Nevertheless, investigators suspect that these may

be faint surface expressions of basement fractures. Their existance should eventually be verified or disproved by explorationists who have access to seismic data or other geophysical information.

It was obvious from a first look that ERTS images could be used to map closed structures such as anticlines, but, in Wyoming, no new closed structures were detected, and some features that appeared to be new closed structures proved to be topographic pseudostructures in flat or homoclinal sedimentary rocks (Appendix M). Stereoscopic coverage would undoubtedly be of considerable value in segregating these pseudostructures from the true closed anticlines and synclines.

Structural Geology: Most structural studies using ERTS imagery have delt largely with the linear features. Lineation study is, indeed, a major aspect of all ERTS structural studies, but these types of studies should be combined with regional geologic mapping and used in conjunction with regional geophysical data to be most effective. In all of these studies the essential field check must be included if the results are to be considered valid.

More linear features can be mapped in a day than can be properly evaluated in several years. We have, in effect, been overwhelmed by linear features. We have determined that linear features seen on ERTS range from joint systems to mega-fractures. In the Precambrian-cored uplifts, abundant linear features include fractures and dike systems ranging in age from Early Precambrian to Recent. In the basins the more recent features are more apparent.

All three major uplifts in Wyoming have been studied (Wind River, Bighorn, and Laramie Mountains). R. B. Parker (Appendix N) has determined that most of the Wind River linear features recognized on ERTS can also be delineated on aerial photos and verified by field check. Many of the larger linear features represent zones of dislocation, cataclases, and metasomatism or alteration. The fractures may or may not be filled by dikes. As yet, many of the major linear features

of the Wind River Mountains have not been verified and are not shown on any published geologic maps.

One approach to analysis of linear features detectable on the ERTS imagery is that of Blackstone (1972; 1973a, 1973b, 1973c) in which the trends of the linear elements in uplifts are compared to trends observed in structures of the adjacent basins to determine possible interrelationships. A study of linear elements in Bighorn and Pryor mountains determined that, in the Bighorns, the trends of 52 linear elements do not correspond to the axial trends of 83 well-defined anticlines and monoclinal features of the flanking basins (Appendix O). The major trend of the fold axes in the basins differs in azimuth from the principal trend of linear elements in the mountain core. This may mean that fractures in the Precambrian uplift did not exert a strong control on the basin structure.

Another study by Blackstone and others of 616 linear elements of the Laramie Mountains of Southeast Wyoming does show a relationship between linear elements of the uplift and folds in the basement (Appendix P). Northeast-trending linear elements in the Laramie range correspond well with the dominant orientation of numerous Laramide folds in areas marginal to the uplift. Blackstone also mapped domains of linear elements within areas of different major lithologies and found that the different lithologies within the Precambrian terrane of the Laramie Range do not influence the orientation of linears.

Subsequent work comparing maps of linear features interpreted from ERTS imagery with those interpreted from Skylab and aerial photography indicates a very strong correlation between dominant trends in linear elements identified from imagery and the sun's azimuth at the time of the overpass (Appendix S). This affect is particularly pronounced in high relief areas.

This complicating factor casts some doubt on the direct correlations drawn by Blackstone in his earlier analyses of

the Bighorn and Laramie Mountains because the ERTS scenes of Wyoming are consistantly illuminated from the southwest -- thus, creating a natural bias toward northeast-trending linear elements. Enhancement of northeast-trending linear features would adversely affect straightforward correlations with northwest-trending features (such as the fold axes of Bighorn Basin structures) and strengthen correlations with northeast-trending features (such as the structures surrounding the Laramie range). Consequently, the possible interrelationships between linear elements and fold axes in these areas should be reconsidered. If possible, the ERTS data should be supplemented with other data obtained under different illumination. A composite map of linear elements interpreted from images having different illumination directions should help to eliminate the bias created by directional illumination.

Linear elements in the basins of southwest Wyoming have also been examined by Houston and Short and by Blackstone (Appendices Q and R). Prominent sets of linears striking north-northeast and northwest are typical of this area. Blackstone has described two major linears which he refers to as the Farson and Red Desert linear elements. He has tentitively interpreted these linear elements as the surface trace of deep-seated structural elements, probably faults, which increase in magnitude of displacement with depth. These linear elements are thought to control the location of volcanic fields and the geometry of major Laramide folds. Blackstone further states that the existence of these and other major subparallel linear elements, extending for tens of miles, suggests a compressional stress field over large areas, present at least in the early stages of regional deformation.

Field checks have shown that some linear features in the Great Divide Basin of western Wyoming represent linear strips of stabilized sand dunes separated by blowouts. These dunes are marked by a distinctive vegetative expression. Other major linear features in this area are probably real but could not be identified in the field, although faults of

minor displacement that parallel these linears have been mapped in this area.

One conclusion drawn from this initial study is that the wind created phenomena are far more pervasive than previously considered in this particular region. We thus have a greater appreciation of the geomorphology.

A more comprehensive evaluation of Wind River Mountain linear features has been made by Tomes and others (Appendix S) using ERTS, Skylab and aircraft data. This comparative study shows the value of both the synoptic view and increased resolution in lineation study and also demonstrates clearly that sun azimuth and sun angle play a major role in determining which sets of linear features will be emphasized in mapping.

A regional tectonic analysis of Wyoming is currently in progress (Appendix M). This analysis will consider all major linear features that can be recognized using both ERTS and Skylab images. It will not be possible to field check the Wyoming linear features map, but the linear features will be checked against known faults and fractures. Field evaluations and correlations with geophysical data will be made in key areas.

In summary, we find that spacecraft images can be used to find unmapped fractures and extend known fractures beyond mapped limits. Most fractures recognized in general studies are seen in two-dimensions and are difficult (if not impossible) to date. Therefore, an extensive field study (on a regional basis) is needed before these fractures can be geneticly interpreted or used in models for regional structural analyses.

In areas where rocks are well-exposed or strongly expressed by vegetation, the ERTS image serves as a physiographic map and displays much of the structural detail. The image can either be annotated to show structure or an analysis can be made by comparison with an overlay (Fig. 3). Analyses of the information gained from image study

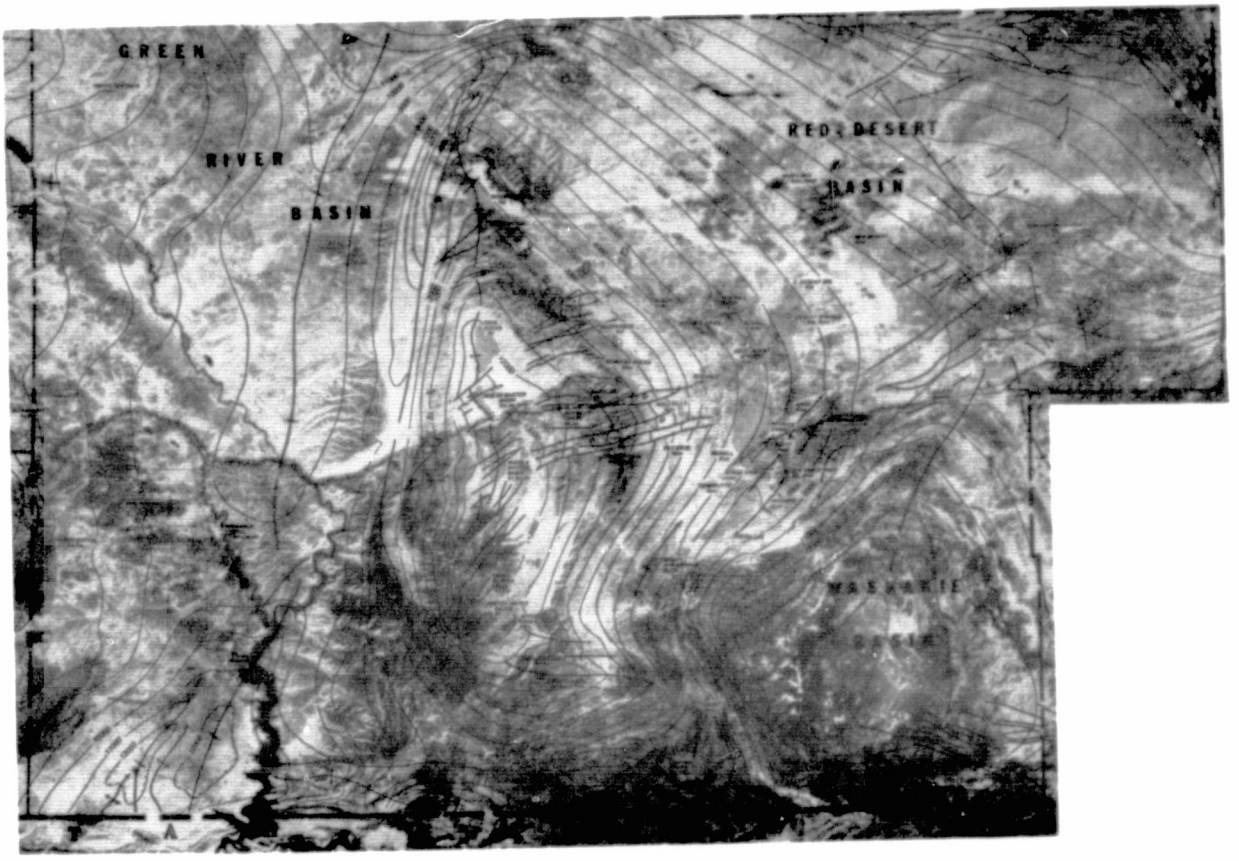


Figure 3. ERTS-1 mosaic of Sweetwater County, Wyoming compared to a structure contour map representing the top of the Cretaceous Dakota formation. Mosaic compiled by U.S. Soil Conservation Service, Regional Technical Service Center, Portland, Oregon. Structure contour map courtesy of Petroleum Ownership Map Company, Casper, Wyoming.

ORIGINAL PAGE IS
OF POOR QUALITY

must include supplementary use of other available data, but the image serves as an excellent base for tectonic map preparation. In Wyoming studies, the imagery has been used as a mapping base while providing the necessary new information to fill gaps in mapping. In areas that are entirely unmapped the ERTS-1 imagery has even greater potential as a mapping tool.

Geothermal

ERTS images are generally useful for regional studies of the earth's surface temperature. An attempt to use ERTS for geothermal studies involved examination of snow scenes in areas of known thermal anomalies to see if melting of light, moderate, or heavy snow-cover might be used as an indicator of thermal anomalies. The two major thermal areas of Wyoming, Yellowstone Park and the Thermopolis hot springs areas, were used as test sites. The light snow-cover was so non-uniform that areas of melting could not be confidently defined from the ERTS-1 imagery. The Yellowstone thermal area was consistently open but the Thermopolis area snow pattern could not be directly related to areas where the surface is known to be anomalously warm. The Yellowstone hot springs and geyser areas remained open even in moderate and heavy snow periods (Fig. 4) suggesting that areas of intense thermal activity could be detected by monitoring snow cover.

These studies suggest that any areas that are consistently open in ERTS snow scenes should be examined as possible thermal areas, and that ERTS snow scenes might therefore be used in the search for intense thermal anomalies in remote areas.

Agriculture and Forestry

Studies in agriculture and forestry have been carried out by botanists, plant scientists, and geologists in a combined attempt to define interrelationships between rock, vegetation, and soil. Early in these studies it was found that there were essentially no vegetation maps of Wyoming, at any scale. Consequently emphasis was placed on vegetation

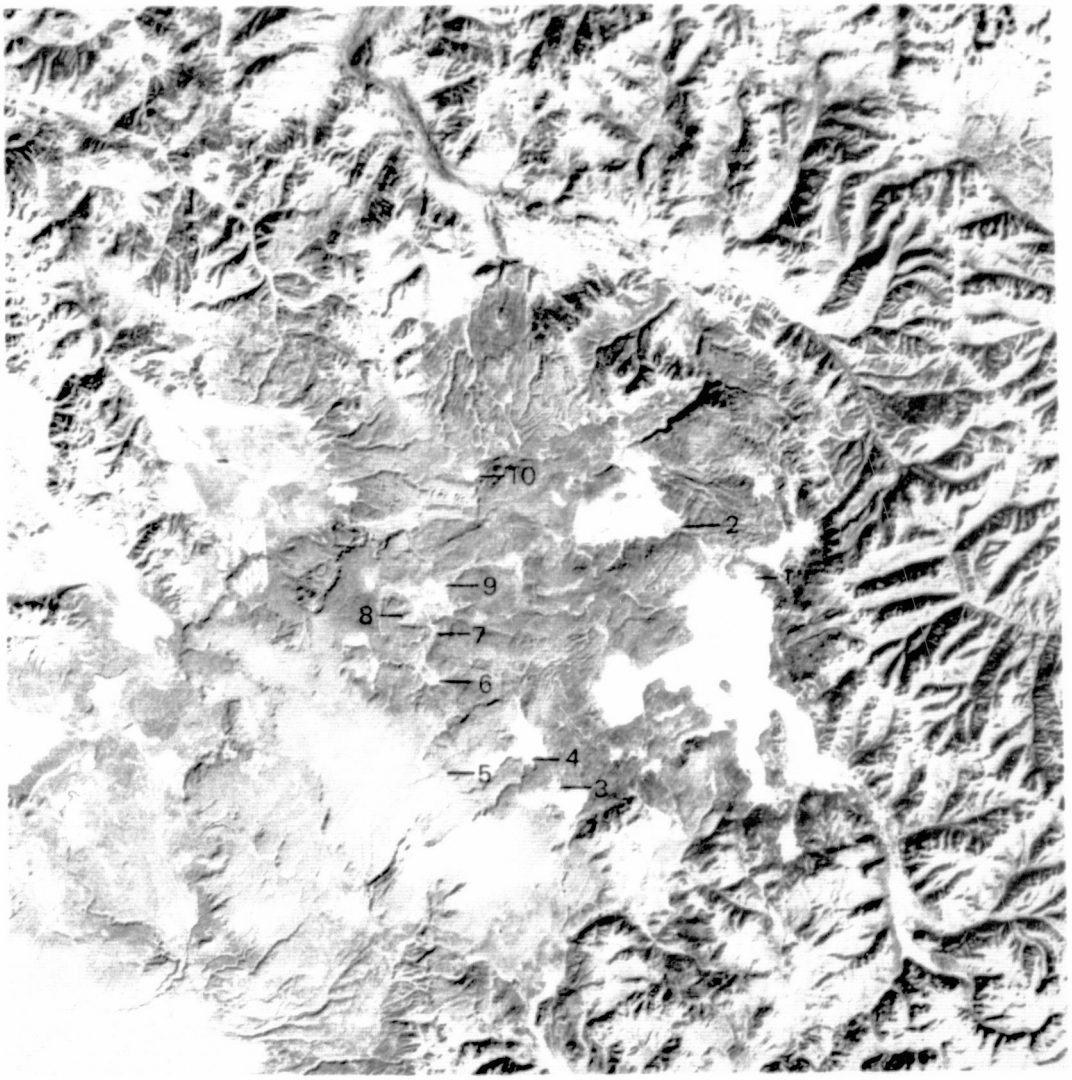


Figure 4. Snow scene of Yellowstone National Park (portion of ERTS-1 image 1213-17475-7). Numbers indicate thermal areas detectable as zones of melted snow or ice.

ORIGINAL PAGE IS
OF POOR QUALITY

mapping. A program was outlined which would use ERTS as a major tool to produce vegetation maps for use in land planning and in preparation of environmental impact statements that are essential background for energy development.

Studies undertaken by botanists include the preparation of vegetation maps in basin and mountain areas of southeastern Wyoming and crop calendar studies in irrigated farm districts of eastern Wyoming (Appendices T and U). These studies led ultimately to the preparation of the first state-wide vegetation maps of Wyoming (Appendix V).

The Laramie Basin was selected for pilot vegetation studies because both aircraft and ERTS data are available and because the initial studies could be completed and checked quickly and inexpensively because of the proximity to Laramie. Vegetation in the Laramie Basin test areas was successfully mapped by use of ERTS. The maps were checked against aircraft data and field studies. The original interpretations in this area were done by Mr. R. F. Redfern and the fieldcheck was completed later by Mr. M. A. Evans. Consequently, we believe that the map evaluation of the ERTS-1 data in this application is unbiased.

Field checks of the Laramie Basin vegetation maps showed the interpreter was able to delineate six major vegetation communities in the basin and eight vegetation communities in the mountains (Table 1).

These studies show that ERTS imagery is adequate for regional vegetation mapping and that density slicing is useful for refinement of classification. The results also suggest that the best time for mapping vegetation in this area is early fall and late summer, and that basin and mountain areas should be mapped individually.

Studies by Evans and Marrs of the Wheatland irrigated farm area (Appendix U) show that crop inventories can be successfully accomplished with ERTS provided seasonal data and interpretation aids such as density slicing are utilized.

An initial attempt was also made to use the Lars Programs and thus accomplish vegetation mapping automatically and with

Table 1: Subdivisions of Vegetation Discriminable from ERTS-1 Imagery

Basin Subdivisions

Classification	No. Species	Major Types
I. Alkaline areas	6	greasewood
II. Light grassland (Moderate alkaline)	10	western wheatgrass
III. Grassland of light cover	13	blue gramma
IV. Grassland of light cover with greater moisture	20	blue gramma plus sedges and rushes
V., VI., VII. Flood plains, no separation in early summer when field check was made -- may be possible in fall when gray scale or tonal map was made	20+	lush vegetation
VIII. Water		
IX., X. Conifers and vegetation on Casper formation -- further subdivisions in mountain classification		

Mountain Areas

Classification	No. Species	Major Types
I. Limestone outcropping and bare areas	23	species of grass
II. Scattered brush within grassland of light cover	13	mountain mahogany
III. Moderate to dense brush	13	big sage brush
IV. Dense brush	24	thick sage brush
V. Broadleaf vegetation (moist area)	29	quaking aspen
VI. Wet grasslands	21	grasses, sedges, rushes
VII. Scattered Conifers	32	Limber pine plus zone 5 vegetation
VIII. Mixed pine and aspen (can be separated by isodensitracing		

greater accuracy. A number of tapes were processed at Goddard and print-outs were studied by the Wyoming team. In this first attempt the classification proved difficult to transfer to Wyoming basins and was not as satisfactory as the visual analyses.

The final botanical project was preparation of four state vegetation maps including:

1. Map defining the agricultural areas of Wyoming, three divisions -- native hay meadow, irrigated crops, and dryland crops.
2. Vegetation map of Wyoming showing major river bottoms and irrigated croplands.
3. Vegetation map of Wyoming showing foothills scrub, grasslands and desert and basin.
4. Vegetation map of Wyoming showing alpine vegetation areas and timbered mountain slopes.

These general maps were prepared by use of ERTS infrared mosaic of Wyoming. More detailed vegetation maps were prepared in key areas within each subdivision (Appendix V).

Range studies have been underway in the Baggs area of south-central Wyoming for the past five years. The Baggs test area was, therefore, chosen as a control test site for application of ERTS-1 data to range mapping and biomass estimations. The area supports both domestic and game animals.

Vegetation maps were prepared for this area at a scale of 1:24,000 using ERTS imagery, Skylab photography, and aerial photographs (Appendix W). The maps compiled from interpretations of the aerial photography were field checked and subsequently used as a control base for comparison with interpretations of satellite imagery.

The area was monitored during five ERTS passes and two EREP passes. Field spectral measurements and clippings were taken to determine the reflectance characteristics and above ground biomass (available for forage) in 25 randomly located plots (5' x 4'). These reference values were to be used as a guide for estimation of above ground green biomass from ERTS

scene brightness values, but the field reflectance measurements could not be reduced to real values. Consequently the biomass reflectance dependence was determined by plotting the biomass estimations directly against the ERTS scene brightness values for each of the ERTS data sets. The initial comparisons indicate a direct relationship between biomass and reflectance in areas of high biomass. In areas of sparse vegetation, other factors such as soils and soil moisture influence the scene brightness such that the biomass cannot be estimated directly from the scene brightness. Nevertheless, biomass estimations may be derived for these areas by extrapolating the biomass changes estimated for the more heavily vegetated areas into the sparsely vegetated areas.

Hydrology

Mapping of surface water bodies and drainage networks is straightforward using ERTS Band-7. Mapping techniques vary from visual interpretation of band-7 film positives, density slicing using the isodensitracer, to the generation of gray-level maps by using digital tapes. Small water bodies (> one acre) can be mapped with ERTS Band-7 images; so it is possible to inventory water in small impoundments and lakes. In areas where water is critical to development one may even detect small man-made ponds where small streams have been impounded and water used for local irrigation or stock watering.

1972, 1973, and 1974 were marked by quite different rainfall in Wyoming. 1972 was a year of normal rainfall, snowpack, and runoff, 1973 an unusually wet year, and 1974 a drought year. The ERTS-1 imagery records the changes in vegetation and water supply that occured during this period. One part of a continuing ERTS program (beyond the present contract) is a plan to study the Powder River basin and adjacent mountain uplifts comparing snow pack in the mountain areas, run-off in streams, extent of irrigation, duration of irrigation seasons, and water impoundment levels at different times of the growing season. This hydrologic picture is essential baseline information for regional environmental

impact studies which must be completed prior to developing the mineral resources of the Powder River Basin.

Seasonal water impoundment studies were begun in the Laramie Basin where many of the small and large lakes are dependent on perched water tables or run-off from ephemeral streams fed by melt water from mountain snowpack. A color-additive comparison of these basin lakes for the 1972 (average) and 1973 (wet) seasons shows the striking contrast (Fig. 5). The clear relationship between the water levels in these lakes and climate is graphically shown. Because lakes of this type are a direct reflection the groundwater levels, their aerial extent can be used as an indicator of the groundwater level. Monitoring such lakes may also help determine whether or not water tables are lowered by excess pumping of near surface aquifers for irrigation and/or industrial use.

Shallow lakes can often be distinguished from deep lakes in the Laramie Basin by direct interpretation of green-band images. Shallow lakes (less than 6' deep) usually have a high suspended sediment level that results from wind action disturbing bottom sediments. Figure 6 shows that these lakes can be distinguished simply by study of band-5 images that show this suspended load. The contrast can be further enhanced by use of band-5 and 7 combinations (Fig. 7).

Plant growth in basin lakes can also be monitored from ERTS. Algal plumes that normally develop in late summer in the basin lakes can be detected. This information is useful to algalogists and limnologists, and also to personnel of the Game and Fish Commission who are interested in the deterioration of sport fishing that parallels the algal growth.

Continued use of the ERTS imagery in conjunction with Skylab research has demonstrated a practical application of ERTS, Skylab, and aircraft imagery in prospecting for groundwater. The major aquifer of the Powder River Basin is the Madison Limestone that crops out in four uplift areas, Black Hills, Big Horn Mountains, and Hartville Uplift, that surround the Powder River Basin on three sides. During the Paleozoic eon

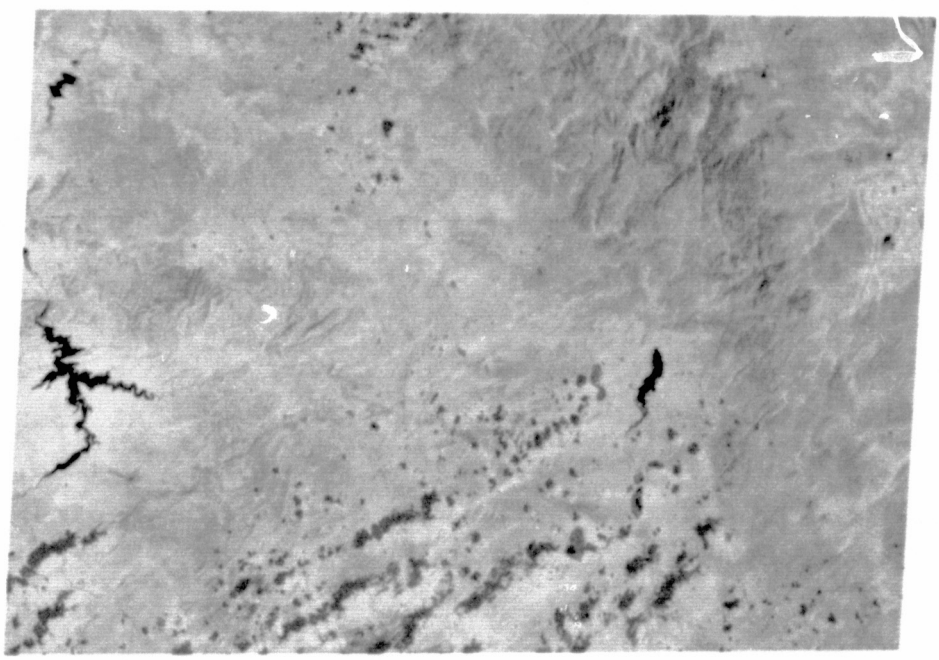


Figure 5. Color-additive comparison of ERTS-1 imagery obtained in autumn, 1972 (1047-17184-7) and in summer, 1973 (1353-17190-7). The striking contrast in surface water distribution is readily apparent on this duotone composite.

ORIGINAL PAGE IS
OF POOR QUALITY

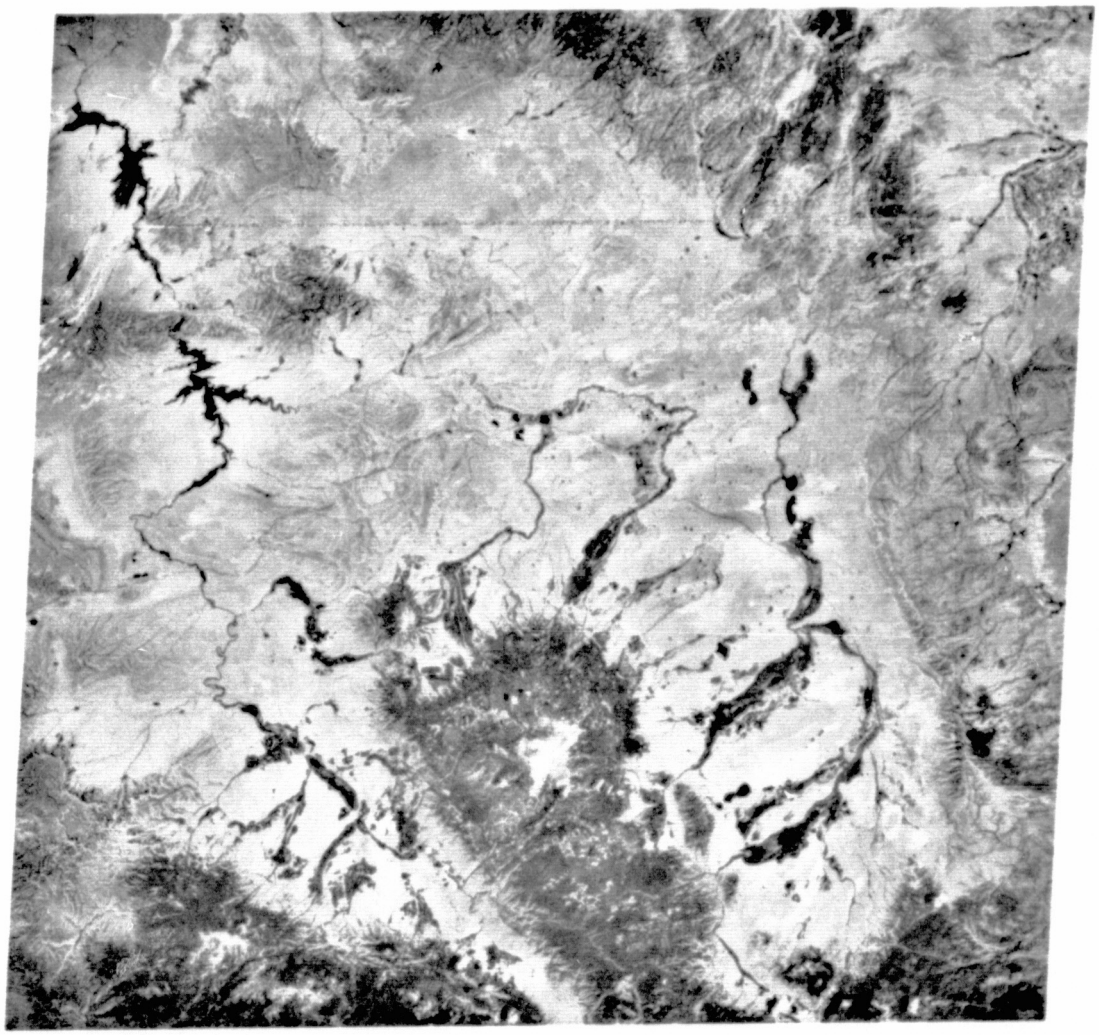


Figure 6. A red-band ERTS-1 image of the Laramie Basin (1353-17190-5) showing contrasts in basin lakes related to water depth and turbidity.

ORIGINAL PAGE IS
OF POOR QUALITY

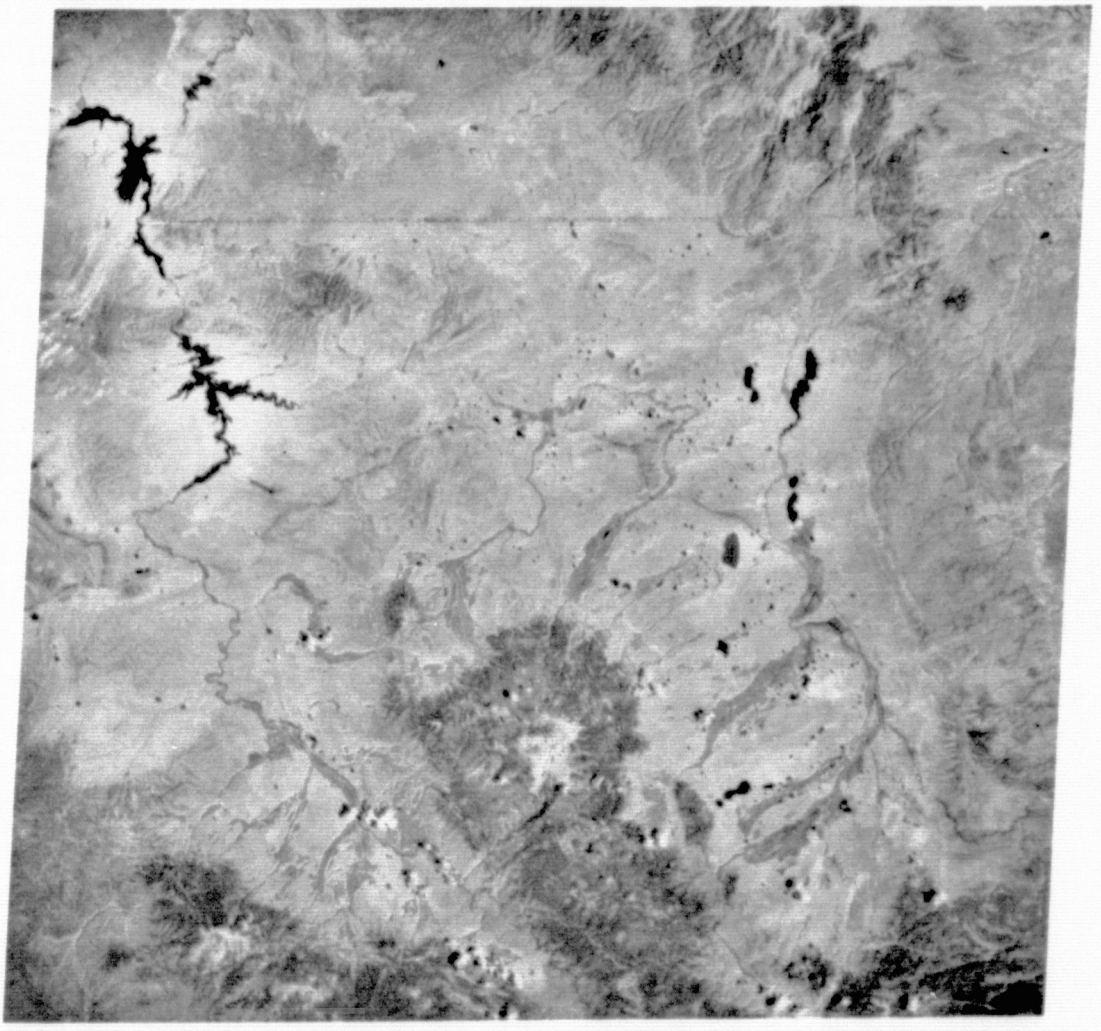


Figure 7. A duo-tone image composite of the Laramie Basin area (ERTS-1 image 1353-17190 bands 5 and 7). This composite shows surface water in contrasting colors which can be interpreted in terms of water depth and turbidity.

ORIGINAL PAGE IS
OF POOR QUALITY

this limestone was exposed to erosion and an extensive karst topography was developed on the upper surface of the Madison formation. The karst was subsequently buried by later sedimentary deposits. This paleo-karst formerly was thought to be an important zone of permeability and porosity for the collection and transmission of ground water. But, recent surface studies of the Madison have shown that this paleo-karst is sealed by relatively impermeable sediment and is not a good source of groundwater. Instead, a recent karst has developed on the presently exposed Madison surface along the basin flanks. Initial studies suggest that water in this less extensive karst system is funnelled towards major fault systems and carried out into the basin. ERTS, Skylab and aircraft images have been employed in the study of these fault systems and associated drainage patterns. Studies of the fault systems in the uplift areas and correlation of these with basin linears should provide better background upon which to base decisions in the search for groundwater in the Madison Formation of the basin.

Environmental Quality

A major problem facing the people of Wyoming today is that of the preservation of environmental quality in the face of major energy developments. Active and proposed developments include coal and uranium strip mines, oil shale developments, and accompanying development of power plants, coal-gasification plants, coal-liquification plants, and new rail and slurry pipeline transportation facilities.

At the time of the initial ERTS proposal submitted to Goddard in 1971, projections indicated limited development of these resources in the 1970's and more extensive development in the 1980's with a large portion of production supporting coal-fired power plants. Consequently, environmental quality was considered a secondary aspect of the ERTS studies when that proposal was written. Interest in the development of the coal resources of Wyoming accelerated enormously as a result of the energy shortages of 1973 and 1974 until

predictions for new strip coal mine developments in the Wyoming Powder River Basin alone range from 10 (announced or committed 1974-1980) to 20, and these new developments will range in size from mines with an annual production of 3 million tons to 20 million tons. The largest active strip coal mine in the United States presently produces less than 8 million tons per year.

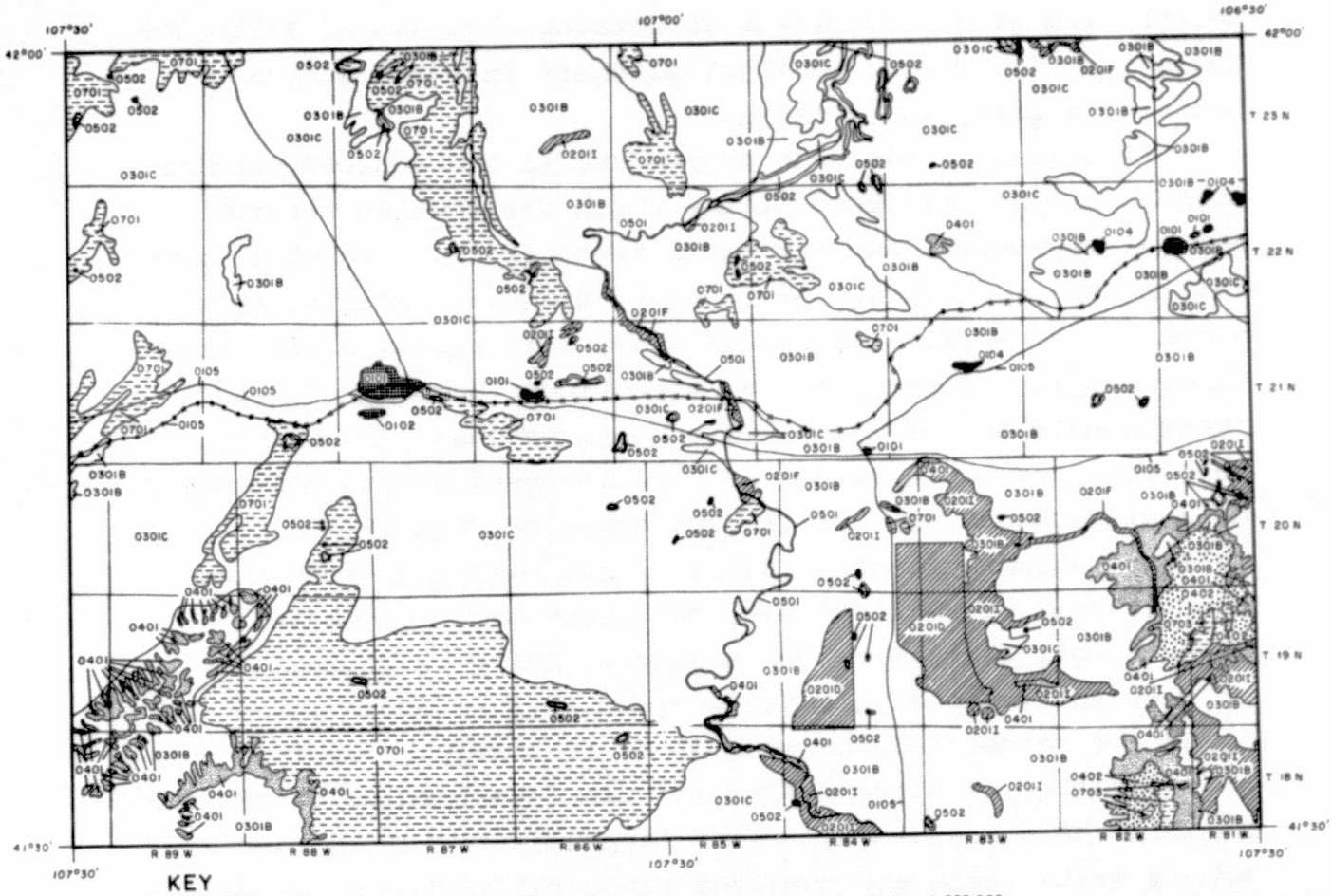
We now recognize that it is essential that we establish baseline environmental information for areas such as the Powder River Basin as soon as possible. The University of Wyoming remote sensing laboratory has therefore undertaken a series of projects designed to demonstrate the potential of repetitive satellite imagery for the preparation of regional baseline maps pertinent to environmental impact and for future monitoring and change detection.

The following pilot studies have been completed:

Land use maps have been prepared for several test areas in Wyoming using ERTS, Skylab, and aircraft products. These maps have been prepared using zoom transfer scopes; or with stereo data, using a Kern PG-2 plotter to transfer information on film positives to topographic and planimetric base maps. The Kern Plotter is ideal for Skylab and aircraft photographs is not effective for ERTS images because of lack of stereocoverage.

An evaluation was also made of the LARS system through a cooperative effort with N.M. Short of Goddard. Print-outs were prepared of selected areas in Wyoming at Goddard and were analyzed by Wyoming investigators. This study suggested that some modification of programs might be required before the LARS programs could be used for land use analyses in Wyoming.

Examples of general land use maps prepared from ERTS imagery are shown in Fig. 8 and Appendix A. It is clearly possible to distinguish major categories such as urban and built-up land, agricultural land, rangeland, forest land, water, and barren land, and, in addition, some 13 subdivisions can be made within these categories. Maps of this type at



KEY

01 URBAN AND BUILT UP LAND
- 0101 RESIDENTIAL
- 0102 COMMERCIAL AND INDUSTRIAL
- 0104 EXTRACTIVE
- 0105 TRANSPORTATION
  - RAILROADS
  - AUTO ROADS

02 AGRICULTURAL LAND
- 0201 I
- 0201 D
- 0201 F

03 RANGELAND
- 0301 A GOOD
- 0301 B FAIR
- 0301 C POOR

04 FOREST LAND
- 0401 DECIDUOUS FOREST
- 0402 CONIFEROUS FOREST

05 WATER
- 0501 STREAMS AND RIVERS
- 0502 LAKES, RESERVOIRS AND STOCK PONDS

07 NONVEGETATED LAND
- 0701 PLAYAS
- 0703 EXPOSED ROCK

N

Scale 1:250,000

5 0 5 10 15 20
Statute Miles

5 0 5 10 15 20 25 30
Kilometers

ERTS IMAGES USED IN INTERPRETATION

URBAN AREAS AND TRANSPORTATION	*1534 - 17214*	*08 JAN 1974*
	1228 - 17253	*08 MAR 1973*
GENERAL	*1030 - 17242cc*	*22 AUG 1972*
GENERAL	*1353 - 17190cc*	*11 JUL 1973*

RAWLINS AREA LAND-USE INTERPRETED FROM ERTS-1 MSS IMAGERY

21 OCT 1974

R.W. MARRS
DEPARTMENT OF GEOLOGY
UNIVERSITY OF WYOMING

Figure 8

ORIGINAL PAGE IS
OF POOR QUALITY

scales of 1:250,000 and 1:500,000 are excellent for regional planning. The Wyoming remote sensing laboratory is currently negotiating with the U. S. G. S. to develop a series of 1:250,000 scale maps for use of regional planners in the Powder River Basin of Wyoming and Montana.

ERTS imagery has also proven useful for topical studies such as mapping of flood plains (with distinction between natural vegetation and irrigated flood plain), regional vegetation maps (previously discussed), rangeland mapping (previously discussed), mapping of major soil types, slope estimation, mapping of strip mining operations, mapping of water impoundments and drainage networks (previously discussed), mapping of potential areas of mineral development, and mapping of small urban areas. Soil maps compiled from ERTS image interpretations closely match regional maps prepared using genetic soil classifications, but these maps do not fit current soil classification schemes. Still these maps can be used for regional planning, especially in areas where soil types are rather related to bedrock lithology.

A method of slope estimation was developed using drainage networks as a measure of relief (Appendix A). This method proved quite rapid and compared favorably with similar determinations made from regional topographic maps, but the method is of little value where good regional topographic maps are available.

ERTS imagery proved to be an excellent tool for mapping of large strip mining operations and associated spoil piles. The imagery should prove equally valuable in monitoring vegetation recovery in these mining areas. Density contouring was used successfully for extracting maximum detail in some of the mined areas (Appendix A).

Imagery obtained with light snow-cover on the ground is very effective in some land use application. Transportation networks are very apparent on this type of imagery and areas of rural activity, such as farm yards are readily detected. Most urban areas in Wyoming are small and difficult

to detect with standard or color-infrared imagery, but these small urban areas were outlined clearly on ERTS snow scenes. Such images, if taken at the proper time, show the level of activity in a small urban area. The business district where human activity is most highly concentrated will appear darker than the residential areas which, in turn, are darker than the rural areas. The snow melts faster where the activity is greatest. Density contouring can be of considerable assistance in defining boundaries of these "activity zones" and sometimes allows further land use subdivisions to be made within some zones (Fig. 9 and 10).

Fortunately emission plumes from industrial activities in Wyoming are seldom large enough to be detected on ERTS imagery. However, a major oil well fire occurred in the southern Powder River Basin in the fall of 1973. The fire burned for several months before it was contained. The smoke plume from this fire can easily be seen on the ERTS-1 imagery Fig. 11a and 11b). In some areas, such as the Green River Basin, industrial emission plumes are visible on the snow-covered imagery (Fig. 12). Study of ERTS imagery confirms that fly ash is being reasonably well controlled at present industrial sites in Wyoming, and the 1972, 1973, and 1974 imagery can be used as a base line for comparison of new plant sites anticipated for this decade.

Further studies of this problem are being undertaken using the higher resolution Skylab photographs.

Ecology

Most of the ecology studies suggested in proposal 434 were eliminated because reviewers believed that the proposed programs could not be effectively completed with low-resolution imagery. For example, it was suggested that selenium rich areas might be mapped either through recognition of a characteristic flora or selenium-bearing rock type or both. The selenium areas present a severe ecological problem because selenium converter plants that grow in these areas are toxic to animals. Preliminary study of Skylab and aircraft

ORIGINAL PAGE IS
OF POOR QUALITY

Figure 9. Snow scene of the Casper area, central Wyoming (ERTS-1 1101-17185-6). The area outlined in black corresponds to the area of the isodensity contour map.

ORIGINAL PAGE IS
OF POOR QUALITY

Figure 10. Isodensity contour map of the Casper area. This map represents a 50X enlargement from the ERTS 70mm transparency. The original map was produced in four colors using a Joyce Loebl/ Tech Ops isodensitracer.



Figure 11A. A portion of ERTS-1 image 1515-17160-4 showing a smoke plume from a fire at the American Quasar #1 Patterson well north of Douglas, Wyoming. The smoke plume is 60 miles long and the fire is large enough to be seen as a bright dot on the ERTS image.



Figure 11b. A ground-level view of the fire at the American Quasar #1 Patterson well. (Photo courtesy of Wyoming Oil & Gas Commission, Casper, Wyoming).

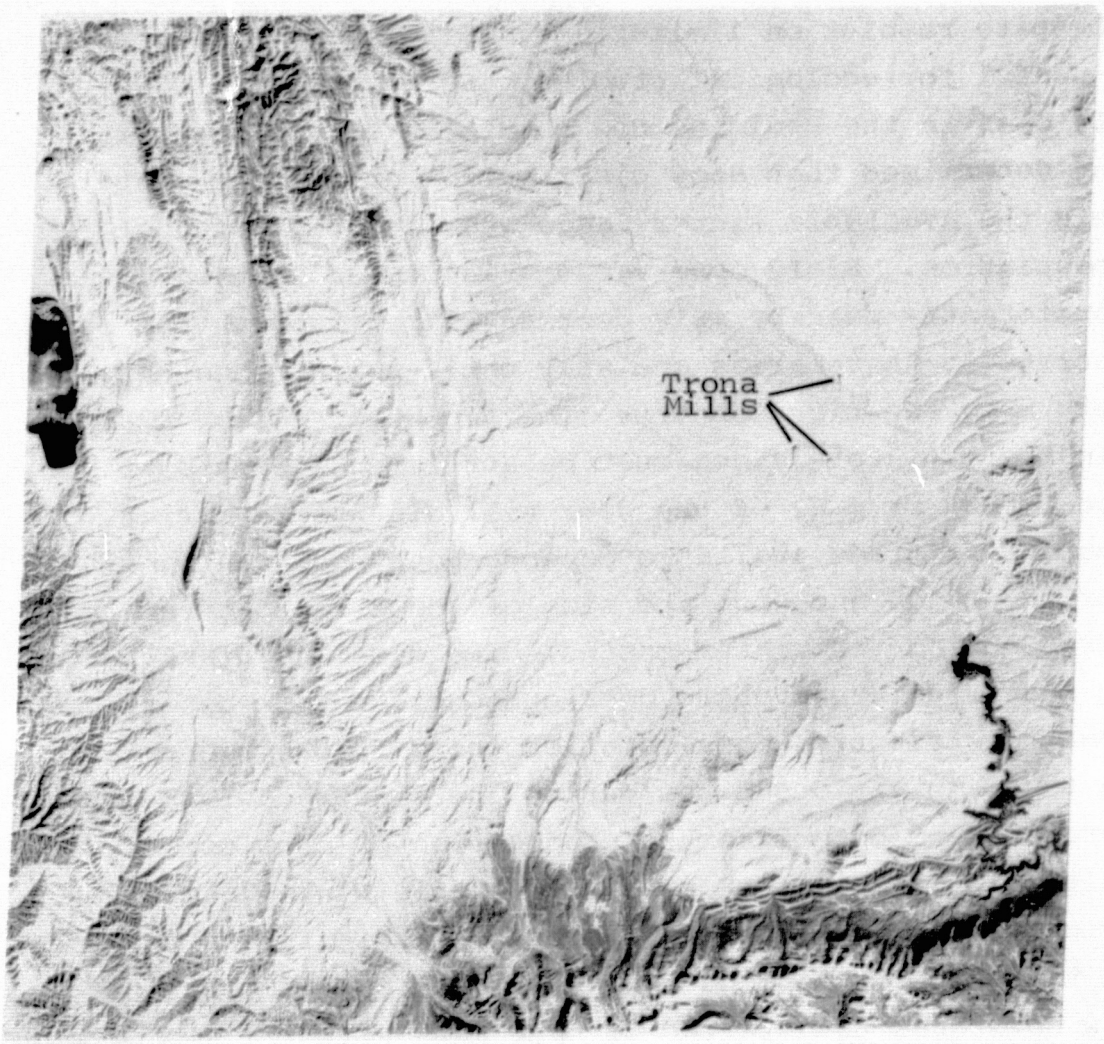


Figure 12. Emission plumes from trona mills and other industrial sites in Wyoming can be seen on this winter ERTS scene (1140-17365-7).

ORIGINAL PAGE IS
OF POOR QUALITY

images in a test area in the Powder River Basin suggests that these areas can indeed be mapped with the higher resolution imagery (Appendix X), but not with ERTS.

Despite resolution limitations, ERTS images have proved to be useful for ecological studies. For example, a study of mule deer in the Medicine Bow Mountains of southeastern Wyoming determined that snow distribution during the winter controls the available winter range and, indirectly, the deer population. Field observations indicated certain areas are consistently used by mule deer as winter range. The deer concentrate in these areas and stay until spring when they can return to the high country. The amount of forage available in these winter-ranges must be sufficient to support the local herd or many of the deer will die before spring. The amount of forage available depends both upon the condition of the range and upon the size of the area that remains snow-free during the winter months. The size and distribution of the snow-free areas where deer concentrate were determined from snow distribution maps compiled using ERTS imagery. Images taken at various dates during the winter of 1972-1973 were examined to determine the progression of snow cover. In addition, maximum snow-cover during this winter and the following winter of 1973-1974 was determined. Images in Band-7 proved the best for mapping snow distribution. An outline of snow cover was transferred to base maps with the aid of a Bausch and Lomb zoom transfer scope. These maps were supplemented with data on snow depth taken at several monitoring stations extablished throughout the area.

The snow distribution maps (Fig. 13) indicated a maximum snow cover around the end of January during both winters. In January 30, 1973 approximately 64.1 square kilometers were without heavy snow cover. In 1974, at about the same time of year, February 12, approximately 285.5 square kilometers were without heavy snow cover. This was an increase of 224.5 per cent in available winter range in 1974. The heavy snow cover in 1972-1973, as can be seen from the map, forced deer from

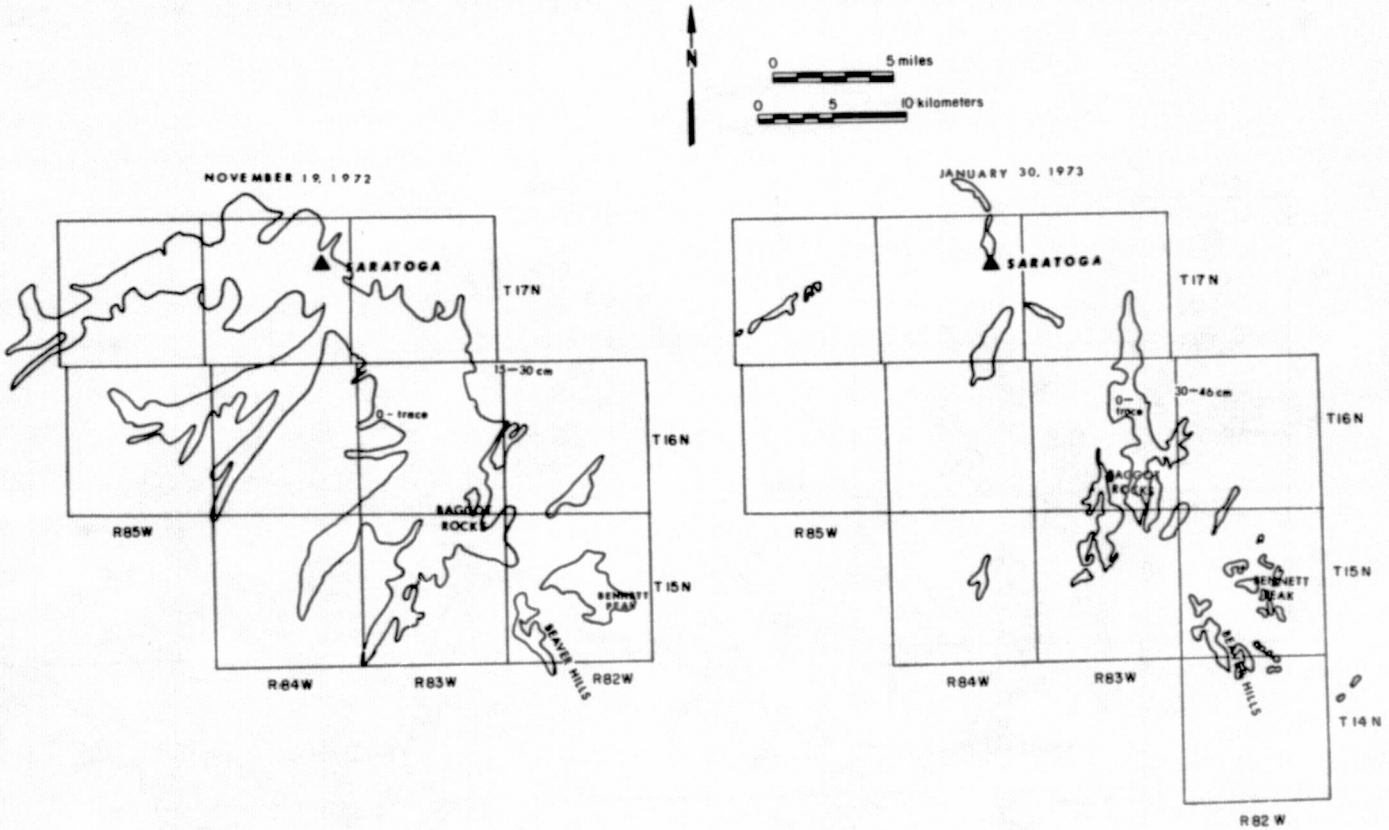


Figure 13a. Snow distribution and area of available winter range in the winter periods November, 1972 and January, 1973.

ORIGINAL PAGE IS
OF POOR QUALITY

ORIGINAL PAGE IS
OF POOR QUALITY

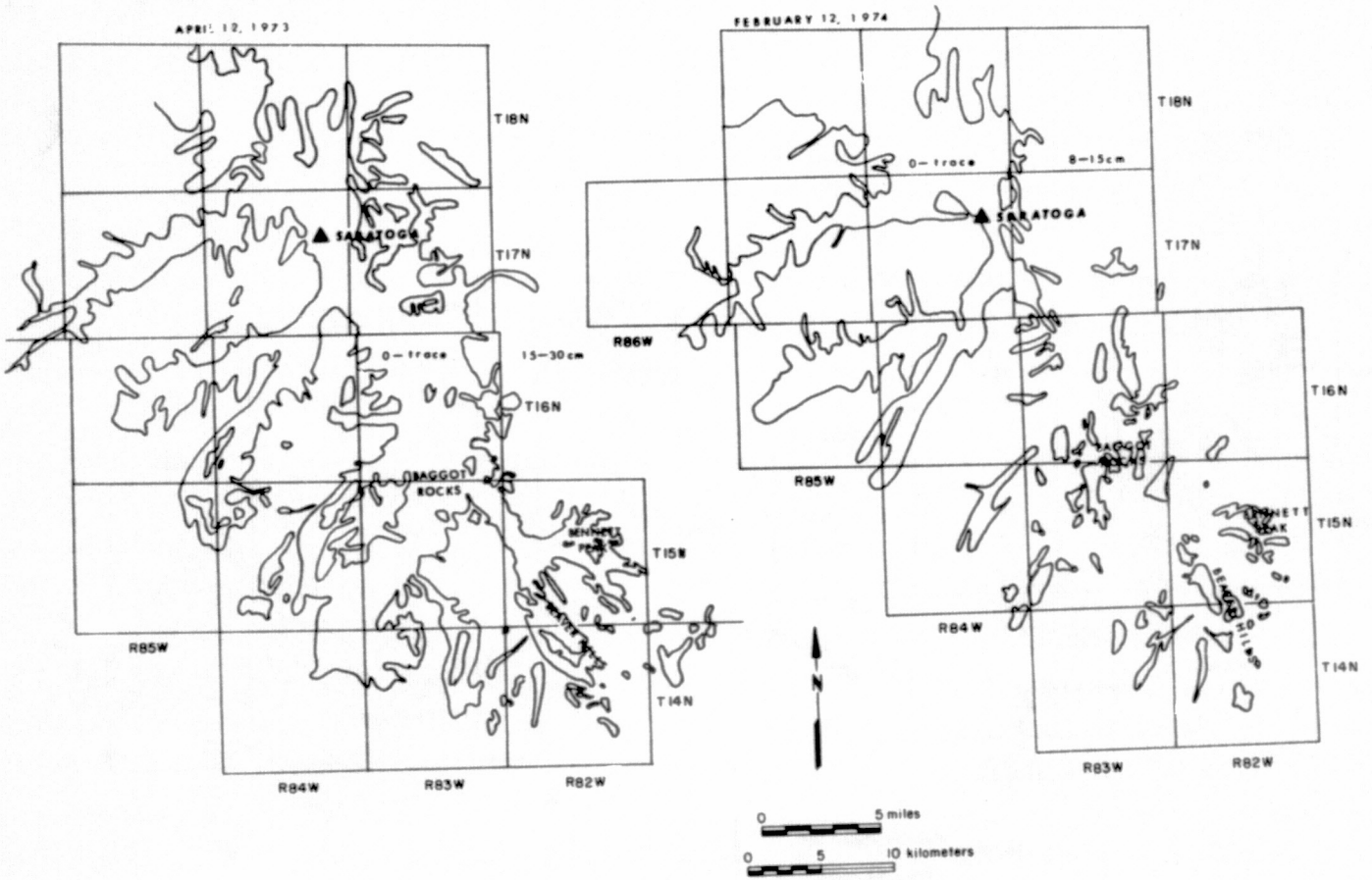


Figure 13b. Snow distribution and area of winter range in the winter periods April, 1973 and February, 1974. Note the relative snow cover for January, 1973, (Figure 13a) as compared to that for February 12, 1974. The unusually severe condition represented by the January 30, 1973 snow cover resulted in a loss of approximately 80% of the resident deer population.

their normal winter range into the Baggott Rocks, Bennett Peak and Beaver Hills areas to winter. This extreme concentration of deer quickly consumed the available forage and resulted in an extreme winter die-off estimated at 80 percent of the herd.

The ERTS photos will allow investigators to determine accurately the minimum critical mule deer winter range in the study area. Similar maps for subsequent winters will provide a measure of the normal fluctuation in snow cover and allow continue correlation with changes in the deer population. Continued monitoring with ERTS will allow game managers to act quickly and provide supplementary feed for the deer herds as the winter range shrinks below a critical size.

Other Applications:

Sand dune maps prepared from ERTS imagery are being used by archeologists in Wyoming as a source of information about dunal trends and possible archeological site locations. The more promising sites may then be excavated in order to find and interpret ancient artifact and bone matter. In addition, landforms, badlands, and aeolian erosional features can be related to specific types of prehistoric food procurement systems, where they were used as trap elements.

Paleontologists note shifts in wind patterns which are recorded in surface or paleo landforms during the Holocene environments.

Similarly, climatic cycles recorded in glacial landforms and in patterns of fluvial deposition or erosion can be interpreted in terms of their effect on ancient man or in terms of paleo environments.

USE OF AIRCRAFT IMAGERY

As a result of the ERTS and Skylab programs plus studies done by the U.S.G.S. for NASA in Wyoming in recent years, some 65 percent of the state has been covered by up-to-date aerial photography. The primary use of this aircraft support has been in checking interpretations of satellite imagery and in adding essential detail in these studies. But the potential

for long term use of aircraft imagery for a variety of studies and the critical environmental baseline information is even greater. Partially because of the potential of the aerial photography and satellite imagery in other applications, the University of Wyoming remote sensing laboratory has developed a color photographic laboratory to process the photographs for research support and for local users. In addition, the laboratory is now a repository for other aircraft photography obtained by State and Federal agencies.

There is nothing really new in the use of aircraft photographs for geologic mapping, but the techniques used today are vastly improved (i.e. Kern PG-2) and the color imagery is far superior to the standard panchromatic prints. Consequently, it is reasonable to assume that geologists will make extensive use of these new data and techniques as a supplement to standard field mapping methods. We anticipate that most students will make an analysis of all available imagery and prepare photogeologic maps prior to beginning their field studies. This will allow each student to study all areas that are well-exposed and to map units readily recognized on the photograph. They will also be able to select key areas where units have to be mapped on the ground and where anomalies require careful field check. The student may then proceed to field studies and finally to a compilation of all data on a topographic base. Completed studies (Appendix H) suggest that geologic maps can often be completed more accurately and in less time using these techniques.

Aerial photography is presently being used in uranium exploration, petroleum exploration, for geologic mapping and for the preparation of environmental impact statements. Most of the several hundred visitors to the Wyoming remote sensing laboratory have shown a major interest in the aircraft imagery.

DEVELOPMENT OF COMPUTER PROCESSING TECHNIQUES

Several approaches have been used to determine the value of computer processing of ERTS magnetic tapes. The most

straight-forward approaches have been ground interpretations of print-outs of LARS programs. In these tests several Wyoming tapes were processed at Goddard. We have also selected certain key mineralized areas to be processed by the GE Image 100 system at the EROS data center and other advanced computer systems, but these analyses are still in progress.

A major effort has been to establish a capability at Wyoming for computer processing of ERTS tapes. Four basic computer processing techniques have been developed and investigated under the sponsorship of the NASA ERTS and EREP projects. These are (1) mini-computer output possibilities, (2) sequented Q-mode factor pattern recognition techniques, (3) frequency space cluster search and alpha mapping procedures, and (4) map feature enhancement with a type of multivariate ratio. Each of these topics will be outlined under a separate heading.

Investigations in the four areas were carried forward until their feasibility was verified and preliminary applications in geology could be made. The conclusions so far are tentative since most of the project time was used in technique development. More complete application testing of the procedures will be carried out in the continuing research of the Remote Sensing Laboratory.

Mini-Computer Output Possibilities

One of the major difficulties of the use of digital computers in geological applications is the necessity of utilizing alphanumeric map plots output from the on-line printer. Maps of this type typically involve north-south scaling distortion as compared with east-west scaling. In addition, site by site mapping from ERTS magnetic tape data of regions large enough to treat typical geological problems involve patching together many line-printer output paper strips and produce maps which are ten feet by ten feet typically. These might be reduced photographically but even so they are difficult and inconvenient to work with.

One alternative to the above output processes is the use of mini-computer-typewriter couplings which communicate with the large digital computer used in the bulk processing of the data. Such devices have the advantage of relatively low price (less than $15,000), greatly improved resolution, avoidance of directional distortion, and full-time dedication to the project studies. The devices have the disadvantage, typically, of being relatively slow.

The Wang 700B mini-computer coupled with a IBM selectric typewriter was used to test the feasibility of preparing high resolution maps. The Wang 700B computer has a 859-step program memory and 120 storage registers. It receives data and programs by cassette tape. Other input options, such as paper tape, disk storage, and punched cards can be used with the Wang 700B although these are not owned by the department.

The IBM selectric typewriter coupled to the Wang 700B has an up-down, left-right carriage motor capable of plotting to 0.01 inch vertically and horizontally. In addition, colored ribbon cassettes can be snapped in or out easily, thus quickly changing colors for colored map preparation.

Unfortunately, the Wang 700B cannot communicate directly with the large campus-wide digital computer. A new slightly more powerful mini-computer, the Wang Model 2200B-1, however, has this capability. It is coupled to essentially the same typewriter-plotter and, in addition, serves as a teletype connection with the large computer.

As a means of evaluating the usefulness of mini-computer output in remote sensing investigations and determining whether it would be desirable co upgrade the Wang equipment to the 2200 level to support the NASA investigations, various mapping feasibility studies were made with the Wang 700B equipment.

A program to prepare a map was written in the Wang language. The map input was coded for storage on a cassette tape which was automatically read line-by-line as needed.

The procedure produced an adequate grey-scale map by plotting asterisks at various spacings. The shades varied from essentially a solid color to a widely-spaced spotted pattern.

The use of colored typewriter tapes was not as effective because the colors available commercially were dark shades of brown, blue, green, and red. Of these, red, blue, and black presented the best map contrast.

A reasonable sized-map (ten inches by ten inches) required several hours output time. Less time was needed if wide grey-scale spacings were permitted for many of the outcrop shadings. More time was required if essentially solid color maps were made. The time was not a big factor, however, since the computer was available for almost full-time use by the project and night runs could easily handle longer jobs.

The study was judged to have demonstrated the feasibility and desirability of mini-computers in remote sensing output mapping and, accordingly, funds for acquiring a Wang model 2200B-1 were included in the project extension proposal submitted to NASA. However, the extension was not funded and the mini-computer investigation was deferred until other funding sources could be located.

Sequential Q-Mode Factor Pattern Recognition Techniques

The use of factor or principle component analysis in geological investigations is becoming more and more widely accepted (Imbrie and Van Andel, 1964; Imbrie and Purdy, 1962; Griffiths and Ondrich, 1969; Klovan, 1966; Davis, 1970). This is a technique in pattern recognition (Andrews, 1972, pp. 24-32) which searches for new linear combinations of the variables which are more sensitive for classification of sites and for geologic source studies.

Let x_{ij} be the (i,j) element in a data matrix where within each column of data are the various measurements at a site. For the ERTS data, the column would consist of four values which are the measured green, red and two infrared reflectance values for each site. If there are

N sites in a region of interest, the data matrix in this case would be four rows by N columns.

Let $\bar{X}_i$ be the arithmetic average over all the sites in the i-th row of the data matrix and let σ_i be the standard deviation of the data values in the i-th row. The row data values can be normed by subtracting the row mean and dividing by the row standard deviation to yield a normed data matrix Z with element Z_{ij} where:

$$Z_{ij} = (X_{ij} - \bar{X}_i) / \sigma_i \quad .$$

The usual statistical correlation matrix, R (for ERTS data), for the data would be the 4 x 4 matrix given by:

$$R = Z\, Z^{\prime} / N \quad .$$

The eigenvectors for R represent the principle components and the corresponding eigenvalues when divided by 4 yield the fractions of the data variance "explained" by each component. Ordinarily only several of the four eigenvectors are needed to "explain" most of the variance and site-by-site alpha maps for the component of the site data values parallel to a particular principle component yield the overall picture of the site loadings on that component. The map giving loadings for the component with the largest eigenvalue will "stretch out" the data to its maximum range of variation.

The above procedure is called R-mode factor analysis in geological statistics because the correlation matrix, R, was the basis for the eigenvectors and eigenvalues. Essentially the principle components were determined by the overall average correlation of one reflectance value with the reflectance value for another color. The computation is trivial, requiring only the storage and manipulation of the R matrix (4 x 4 for the ERTS data).

Geologists have found another type of factor analysis more useful in many applications. This is called Q-mode because the Q or cosine matrix is the basis for the eigenvector computations. Each column of data matrix is regarded as a vector with length:

$$L_j = \sqrt{\Sigma_i x_{ij}^2} \quad .$$

The cosine of the multidimensional angle between the data vectors for sites j and j* is given by:

$$Q_{j\,j*} = \cos(\text{site } j, \text{site } j*) = (\Sigma_i X_{ij} X_{ij*}) / L_j L_{j*} \quad .$$

The cosine matrix Q with elements Q_{jj*} is a N x N matrix where N is the number of sites. The eigenvectors and eigenvalues of Q form the basis for Q-mode factor analysis.

Two points need to be made. Sites with very similar reflectances in the several bands or which keep about the same ratio relations between reflectance components will give cosines close to 1.0. This is because all the site data vectors are normed to unit length initially (by division by L_j) and so intensity is essentially removed. The cosine matrix, thus, forms a natural basis for cluster search. Similar sites have nearly unit cosines with one another.

The second point is that in the context of remote sensing, where N, the number of sites, is extremely large, the N x N matrix is so large it is impossible to store it in even the largest computer. Hence, the advantages of Q-mode are difficult to attain except in small problems where the N x N cosine matrix is not too big for computer manipulations.

Statistical research was carried out under the ERTS contract in the search for a sequential Q-mode factor procedure which would allow the analysis of many sites by Q-mode methods. Under the direction of the ERTS project

statistician, a master's thesis entitled "Sequential Q-mode Factor Analysis," by Mr. Albert J. Wolff was completed in May, 1974. This research established the mathematical foundations for the sequential procedure.

The procedure groups the sites into groups of a hundred or so and completes the ($\simeq$100 x 100) cosine matrix for each group. The eigenvalues and eigenvectors are computed for each matrix and processed together with the data to find a parsimonious set of data vectors which span the data vector space. The (typically) small sets of spanning vectors from each cosine matrix is combined to form a new "data" matrix which is then Q-mode factor analyzed to reduce these vectors to a set of overall spanning vectors. This recombination and summarization for larger and larger groups of sites continues until the complete map area is covered.

In addition to the development of the basic method for sequential Q-mode factor analysis, the master's thesis also included a study of percentage of the original data information retained at each recombination step. Various measures of the information retention were studied and compared. Fortunately, a relatively simple measure based on the trace of one of the analysis matrices was found to be a good index of information retention in the sequential analysis.

During the summer of 1974, a complete set of computer programs were developed and tested to achieve practical use of the Q-mode factor analysis. These programs are listed in Appendix Y. Various applications in map analysis and other geological problems are now underway and the programs are subject to continuing modification to make them more useful in geological studies.

Frequency Space Cluster Search

As an empirical check against the factor analysis, computer subroutines were prepared for making one-, two-, three-, and four- dimensional frequency histograms for the various reflectance intensities versus each other. These were displayed in alpha-numeric patterns for the two or more

dimensional cases. Slice patterns were displayed for the three- and four- dimensional histograms.

The two-dimensional histogram, particularly that for red versus the second infra-red band proved to be the most useful in delineating groupings or clusters of sites into mapping units. Alpha geographic maps based on the Red-IR2 two-dimensional frequency histograms were prepared for an area near Greybull, Wyoming. The maps were compared with area photographs and most features shown in the alpha map were identified. It appeared that many of the features were delineated more precisely on the alpha map than could be outlined by eye on the photographic representations. However this is a subjective judgement which is difficult to validate numerically.

Comparisons of the 2-D histogram with the results of R-mode factor analysis yielded an interesting result for test area used in the study. The direction of the principle eigenvector was aligned along a very characteristic streak of frequencies which dominated the histogram. The streak stretched along a line extending from the origin out along a fixed ratio of one band's intensity to the other. The second eigenvector then represented the next main direction of scatter perpendicular to the principle direction or frequency streak. Thus, mapping data components site-by-site on the first eigenvector direction is equivalent to mapping intensities along a fixed ratio. Similarly, mapping data components on the second eigenvector direction is equivalent, at least in the best area, to mapping by ratio. It follows that the empirical histogram cluster method and the R-mode factor approach both lead to mathematical extensions of a type of ratio mapping.

Similar results are anticipated where Q-mode factor methods have been similarly compared with the frequency histograms. However these studies are still in progress and will have to be reported later.

Multivariate Ratio Techniques

The success of preliminary applications of the above suggested that a study of various multidimensional versions

of ratio procedures deserved study. Consider for example, the ratio of:

$$X = \text{red reflectance intensity}$$
$$Y = \text{infra-red reflectance intensity} \quad .$$

Ratio mapping could be based on values of Y/X or, alternately, on values of θ = arc tan (Y/X). In the two-dimensional of the X and V values, this turns out to be the same as a conversion to polar coordinates where:

$$X = r \cos \theta$$
$$Y = r \sin \theta$$

and

$$r = \sqrt{X^2 + Y^2}, \quad \theta = \text{arc tan } (Y/X) \quad .$$

The concept can be extended to four-dimensions by conversion to generalized spherical coordinates. Let U, V, X, and Y be the intensities of the four reflectance bands. Then generalized spherical transformation relates these to four new variables θ, ψ_1, ψ_2, and by the relations:

$$U = r \cos \psi_1$$
$$V = r \sin \psi_1 \cos \psi_2$$
$$X = r \sin \psi_1 \sin \psi_2 \cos$$
$$Y = r \sin \psi_1 \sin \psi_2 \sin \quad .$$

The reverse relations are:

$$r = U^2 + V^2 + X^2 + Y^2$$
$$\theta = \text{arc tan } (Y/X)$$
$$\psi = \text{arc tan } (X/V \cos\theta)$$
$$\psi = \text{arc tan } (V/U \cos \psi_2) \quad .$$

Thus, mapping on the vector (θ, ψ_2, ψ_1) represents a multivariate generalization of ratio mapping.

The choice is not unique. The ordering of the reflectance bands smong U, V, X, and Y produce apparent differences in θ, Ψ_2, and Ψ_1. In a spherical sense these are equivalent and merely represent different four-dimensional choices corresponding to the selection poles, equator and longitude origin in three-dimensional space. There are, however, more subtle choices in that the listed equations are not the only generalized spherical transformation possible (Miller, 1964, p. 9 - 12; Shelupsky, 1962).

A test area near Pumpkin Buttes, which is geologically interesting in that surface coloration indicates uranium deposits, was selected for study relative to map enhancement by generalized spherical transformations. The techniques of factor analysis and frequency histogram cluster analysis were also applied to this same area so that the relative advantages and disadvantages of the various techniques could be compared. This study is still in progress.

COST BENEFIT ESTIMATES

Accurate cost/benefit analyses cannot be made for most applications of the ERTS data to natural resource studies because most of the benefits are not immediately realized. General geologic mapping, tectonic studies, and mineral exploration may eventually lead to the discovery of mineral deposits. Likewise, sound planning for resource development may save millions of dollars worth of resources that might otherwise be wasted or minimize damage to the environment. Such benefits will only be realized over a period of many years and are largely dependent upon acceptance of the ERTS data as a standard tool by industry, governmental agencies, and the public. Such acceptance will probably be very gradual because the use of the ERTS data often necessitates considerable change in standard procedures.

Nevertheless, some rough cost benefit estimates can be made for general mapping projects by estimating the improvement in mapping efficiency resulting from the use of the

ERTS-1 imagery. Unfortunately, even these estimates consider only the immediate benefit resulting from increased speed and accuracy of the mapping program. The estimates do not provide a measure of the long-term benefits or those benefits resulting from the applications that could not be accomplished without ERTS.

An estimate was made of the cost effectiveness of ERTS in the regional land-use mapping program conducted in the Rawlins area (Fig. 8). Comparing the initial cost of the ERTS imagery to the cost of aerial coverage of the same area a 10-fold (or greater) savings was realized. This estimate does not consider the initial cost of the ERTS launch and its subsequent operation nor does it take into the account the actual cost of flying and aircraft mission. In terms of time saved in compiling the 1:250,000-scale land-use map, a 4-fold reduction in interpretation time was estimated using the ERTS imagery in lieu of high-altitude aerial photography. Some detail that might have been derived from interpretation of the aerial photography was not available from ERTS, but this loss is somewhat compensated by the additional understanding of regional relationships gained from the synoptic view.

A similar time/cost saving can be achieved by using ERTS imagery for regional geologic mapping or land-form studies. Typically, a compilation/mapping program covering an area of some 7000 square miles (the area of a 2^{o} AMS map) would require 9 to 15 months and an investment of $ 20,000 to 30,000. Using the ERTS imagery as a mapping base and using published information and field checks to obtain auxilliary control data, the same area might be mapped in 2-3 months and cost less than $ 10,000. The 3-fold savings in cost is only a partial estimate of the benefit because additional benefit is provided by the savings in time and manpower. In some applications the time factor may be crucial. Certainly, the timelyness of ERTS-assisted mapping programs enhances the value of the products and adds to the indirect benefits by making the information available earlier.

SUMMARY

The ERTS-1 satellite data have proven extremely effective in a number of resource applications. Regional repetitive coverage is a major asset in general geologic mapping, vegetation mapping, land-use studies, and tectonic analyses. The spectral information provided by ERTS is particularly valuable in vegetation studies, mineral exploration, and other applications involving surface geochemistry or soil moisture. The ERTS data were of very limited value in geothermal studies, because only the large and relatively intense thermal anomalies are detectable with ERTS, and even this capability is dependent upon having the proper surface conditions during the overpass.

The most severe limitations of the ERTS-1 data were found to be the lack of stereoscopic coverage (an inherant limitation of the scanner) and the relatively low ground-resolution of the system. Comparisons of ERTS image interpretations and interpretations of Skylab photographic data show that the additional resolution provided by the Skylab data is valuable in many resource studies. Yet, the greater resolution is of little advantage if complete and repetitive coverage must be sacrificed to achieve the increase in resolution.

The computer compatibility of the ERTS multispectral scanner data lends greater flexibility to the ERTS-1 data by providing a means of performing complex spectral or spatial pattern recognition or by allowing rapid classification of some features. However, most resource studies require that the interpreter emphasize certain aspects of the data while ignoring other features which he considers "noise." The interpreter relies upon complex reasoning, correlation, and experience to make these decisions and the result is somewhat subjective. It is difficult or impossible to program these complex decision criteria into a computer, so in most resource applications the roll of the computer is limited to providing the data

user with a more interpretable product or to help him in making rapid comparisons.

APPENDICES

(see following pages)

Appendix A: Summary of Applications of ERTS-1 data to regional land-use studies in Wyoming.

from a report compiled for the Wyoming Department of Economic Planning and Development:

Breckenridge, R. M., Marrs, R. W., and Murphy, D. J., 1973, The application of remote-sensing data to planning in Wyoming--A demonstration project.

Results of this study were also reported at the March, 1973 Symposium on Significant Results Obtained from ERTS-1:

Breckenridge, R. M., Marrs, R. W., and Murphy, D. J., 1973, Remote sensing applied to land-use studies in Wyoming, in Proceedings of the Symposium on Significant Results Obtained from ERTS-1; NASA/Scientific and Technical Information Office, Washington, D. C., v. 1, p. 981-989.

Land-use considerations have become critically important in Wyoming where greatly increased development of natural resources is anticipated. Of prime concern at the present is the development of coal resources in the Green River and Powder Basins as fuel for huge generators. The direct impact of mining, the diversion of water, and the effluent from coal-fired electrical generators will be considerable, but the associated increase in population and the necessary urbanization will have far-reaching effects on the environment in Wyoming. The construction and operation of the power plants and supporting mines will result in a substantial increase in the state's population (perhaps as much as 50%). These population increases will, in turn, affect almost every aspect of land-use.

Governmental agencies have recognized the need for thorough land-use planning in order to properly control development and prevent costly or unnecessary damage to the land and its inhabitants but there is very little land-use data available for use as a basis for such planning. As is commonly the case, the problem requires an immediate solution. It is totally impractical to begin a program for gathering detailed land-use data by conventional means because 1) such a program would be too expensive, 2) insufficient time is available, 3) much of the data would be obsolete by the time the program is complete. Consequently, planners must find

a rapid and efficient means of obtaining the necessary land-use information and a way to continually up-date that information.

As soon as it became apparent that the ERTS satellite program offered considerable potential for obtaining much of the needed land-use data, the state planning office of the Department of Economic Planning and Development contracted the University of Wyoming Remote Sensing Laboratory for a pilot study to determine what land-use data might be gained from the ERTS-1 imagery. The pilot program was to be a quick-look study designed to assess the ERTS-1 imagery as a tool for acquisition of land-use data. The Powder River Basin was chosen as a general test area (Fig. A-1) and suitable sub-areas within the basin were selected for testing individual application.

Because the pilot program was time-limited, a suite of tasks was selected as a representative group of ERTS applications which might yield information necessary for land-use planning. Included in this group were:

1. Identification and mapping of water impoundments
2. Detection of potentially unstable areas
3. Mapping of flood plains, irrigated land, and crops
4. Discrimination of coniferous and deciduous trees
5. Range mapping (type and/or quality)
6. Mapping of soil types
7. Slope estimation
8. Mapping of mined areas
9. Mineral resources mapping (actual and potential)
10. Areas having potential for construction materials
11. Mapping of areas of urban and rural development

Application of standard photointerpretation, color-additive viewing, and/or isodensitometry to these tasks provides results which suggest that many of these tasks can be done routinely. Figure A-2 is a land-use classification map for the Powder River Basin test area, Constructed from interpretations of ERTS imagery. In addition to the broad land-use categories represented on this map, there is a great deal of other significant land-use information available from the ERTS data.

Water impoundments can be readily mapped from the infrared (band 7) ERTS imagery. Impoundments covering 5 acres or more

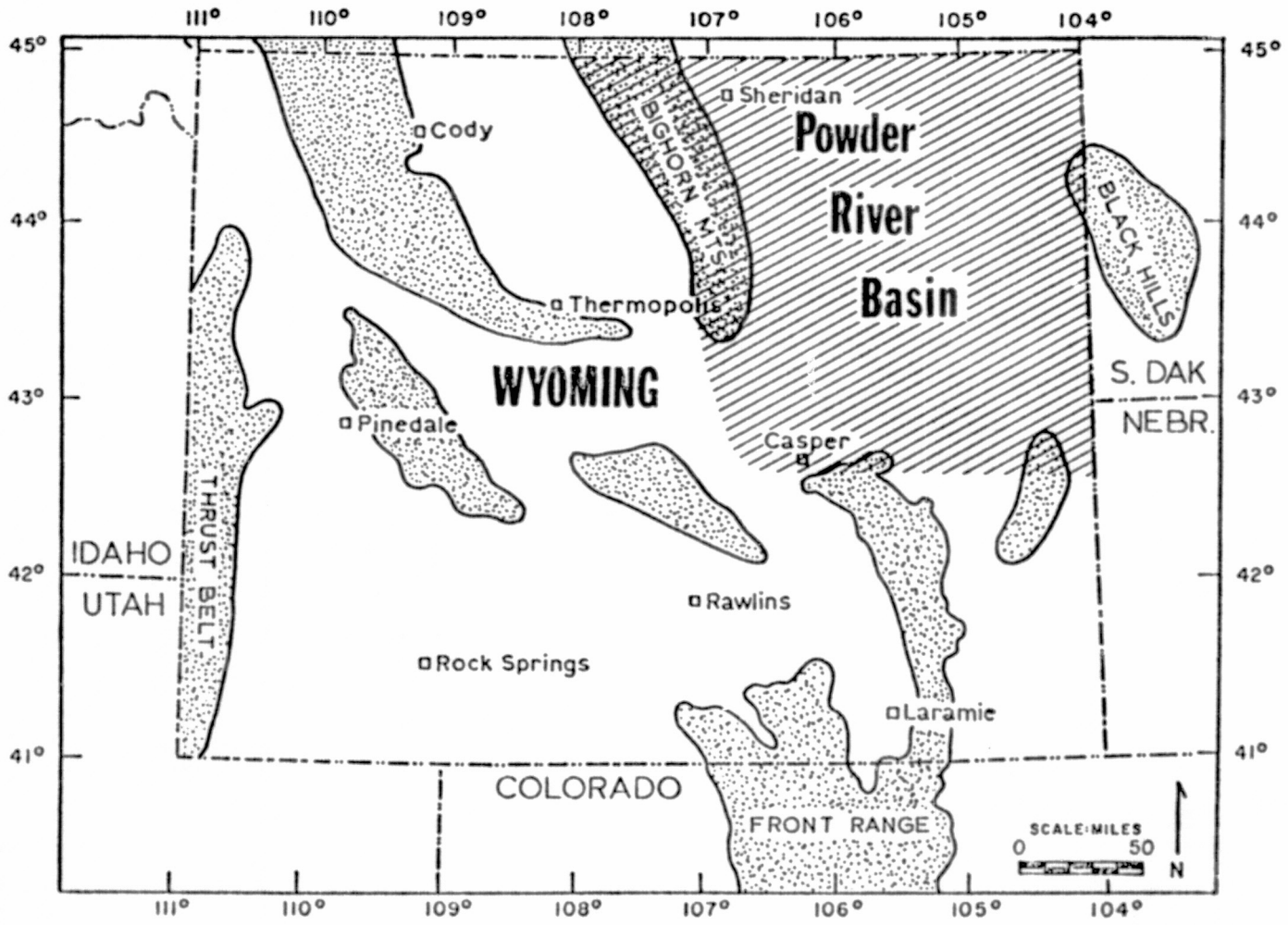


Figure A-1. Index map showing the location of the Powder River Basin test area (cross-hatch).

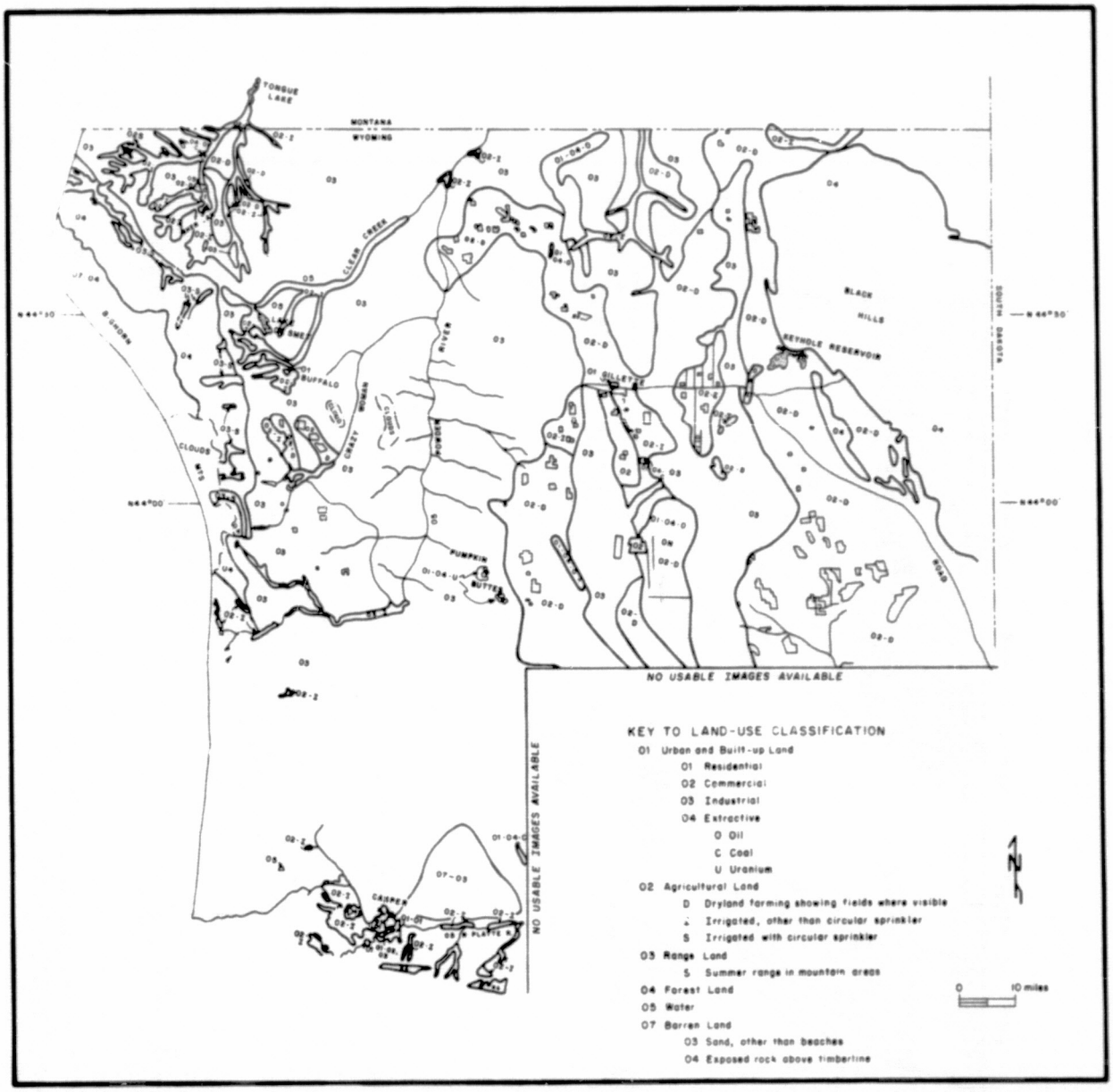


Figure A-2. Land-use classification map for the Powder River Basin, Wyoming constructed from ERTS-1 image interpretations.

ORIGINAL PAGE IS
OF POOR QUALITY

can be mapped reliable and most impoundments larger than 1 acre can be located. However, the actual size of these smaller impoundments cannot be accurately estimated because they are represented by too few scanner resolution elements.

Although in some parts of Wyoming, local unstable areas (landslides, slumps, etc.) have been identified from the ERTS imagery none could be identified in the Powder River Basin test area. Potentially unstable areas were identified on the basis of their regional associations. The potentially unstable areas in the Powder River basin mappable from ERTS include 1) dune fields, 2) flood plains, 3) areas of potential mineral development (coal, oil, uranium), and 4) areas likely to be underlain by clay-bearing soils. Identification of these areas from the ERTS imagery required integrated interpretation of all ERTS bands. Color-additive viewing provided some enhancement of the flood plains and aided in soil and lithologic distinctions.

Color-additive viewing was of considerable utility in mapping of natural flood plain vegetation and irrigated farm land (Fig. A-3). The red and infrared bands (5 and 7) have the greatest utility in distinguishing contrasts within the vegetation. Interpretation of the ERTS-1 imagery provided adequate detail for mapping broad-scale agricultural patterns. Some detail features were recognized in the agricultural pattern. These sometimes allow crop identification if supplemented with other image interpretations showing seasonal variations.

Maps of distribution of conifers and deciduous vegetation were compiled from ERTS-1 interpretations for the Bighorn Mountains (Fig. A-4). These maps are necessarily generalized due to the very small scale of the ERTS images, but they yield a fairly reliable estimate of the distribution of these major forest subdivisions.

Rangeland is readily distinguishable from other agricultural lands and can be subdivided on the basis of tone and texture (Fig. A-5). The resulting map can be correlated

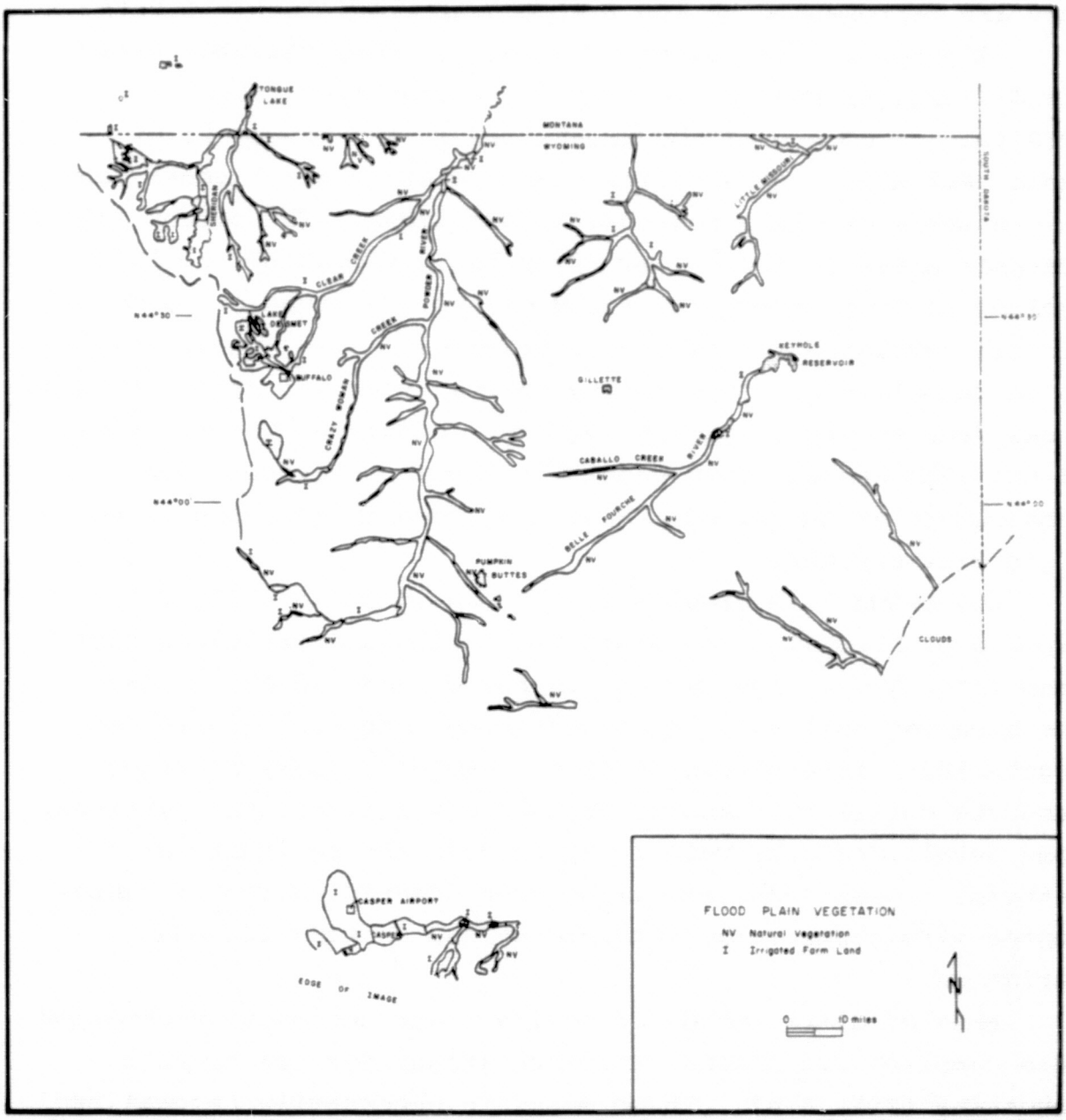


Figure A-3. Flood plains of major streams in the Powder River Basin as mapped from ERTS-1 imagery.

ORIGINAL PAGE IS
OF POOR QUALITY

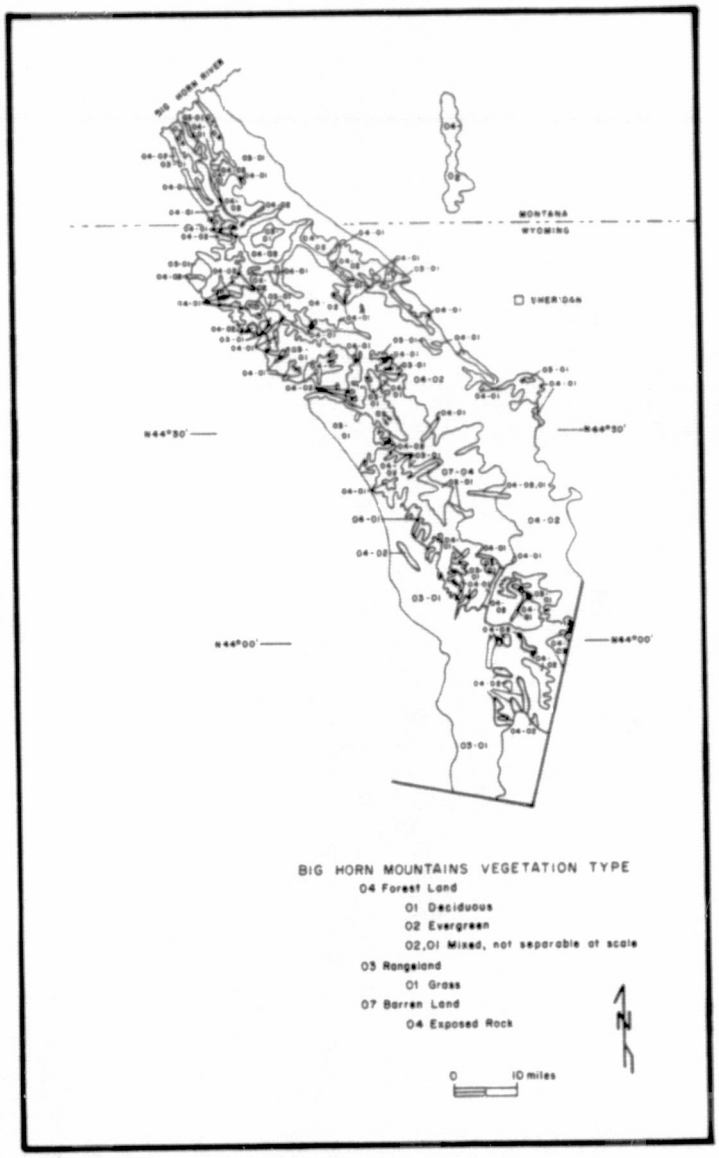


Figure A-4. Map of forest and rangeland in a portion of the Bighorn Mountains (interpreted from ERTS-1 image 1013-17291).

ORIGINAL PAGE IS
OF POOR QUALITY

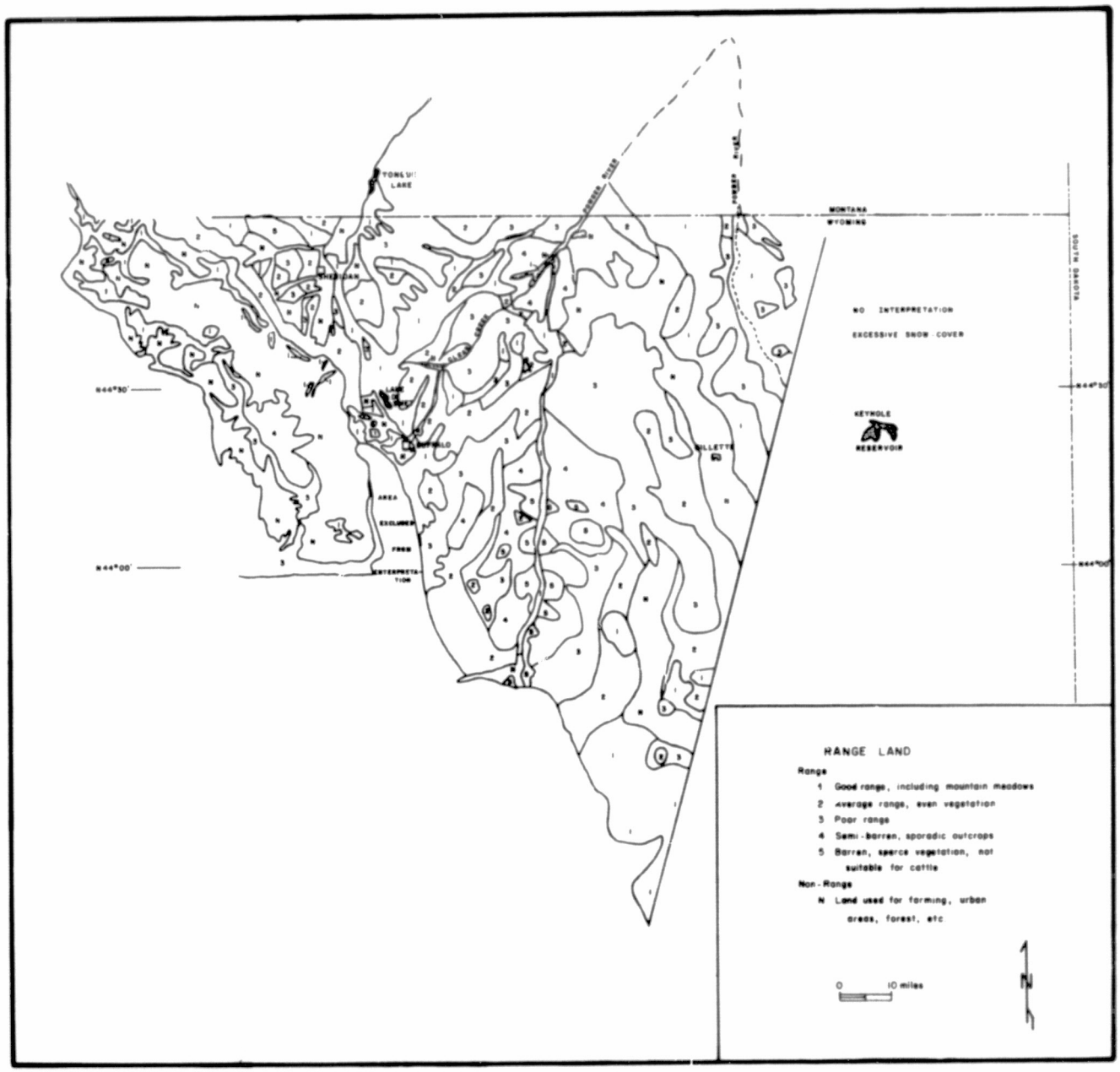


Figure A-5. Range map of part of the powder River Basin test site. (interpreted from ERTS-1 images 1030-17233 and 1030-17235).

ORIGINAL PAGE IS
OF POOR QUALITY

to standing biomass at the time of the satellite overpass, but range type and quality (a time-dependent factor) cannot be established without control data and complementary interpretations from repetitive coverage.

Broad soil classifications can be interpreted from the ERTS imagery on the basis of tone, texture, and regional association (Fig. A-6). The resulting maps show excellent correspondence with available soil maps (Dunnewald, 1957; Thorpe, 1939) which classify soils on the basis of composition (which relates to parent material). Very little correlation is evident between the soil interpretations derived from ERTS and the more detailed soil maps based on the newer Seventh Approximation classification, but similarities may exist between the larger soil groups and the ERTS interpretation.

Slope estimations were based on stream pattern analysis. The frequency and patterns of drainages were used as criteria for subdividing the Powder River Basin into zones of equivalent slope (Fig. A-7). The actual slope values for the various areas were then determined from the topographic maps. This application was particularly successful in the Powder River Basin which has a very intricate system of small drainages that reflect even subtle changes in regional slope.

Abandoned, producing, and developing open-cut coal mines are visible on the ERTS imagery, but small open-cut uranium, bentonite, and gypsum mines and surface evidence of underground mines in the Powder River Basin could not be seen on the ERTS imagery. However the large uranium mines in the Gas Hills district of central Wyoming can be seen on the imagery.

A map of known and potential coal resources was constructed from the combined mine locations and geologic interpretations of the Powder River Basin imagery. This generalized map (Fig. A-8) is useful for defining areas of probable or possible coal mine development for the proposed electrical power installations or other energy needs. Maps of potential areas for the development of other mineral resources were compiled with the favorable locations defined on the basis of geologic

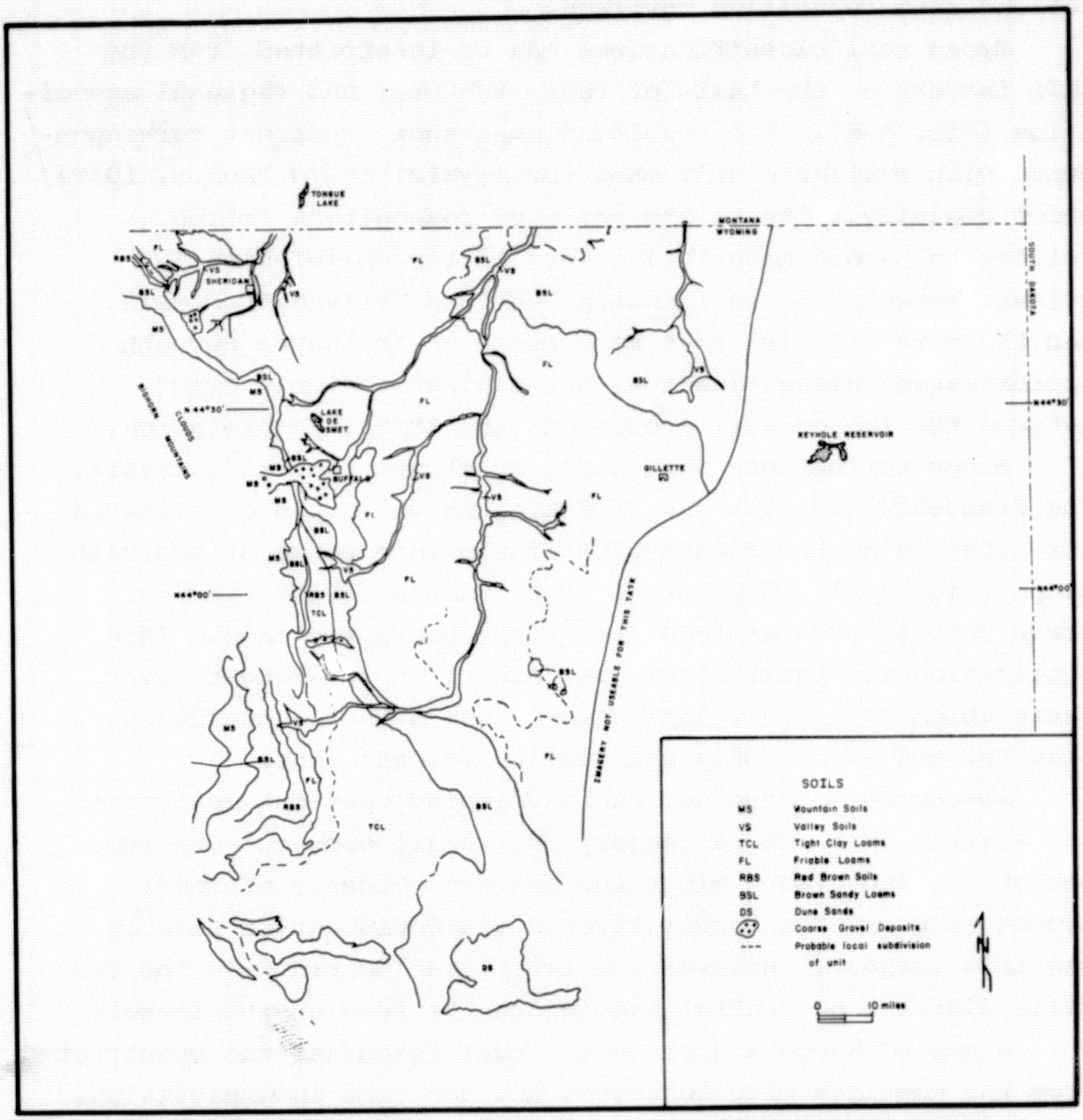


Figure A-6. Soil map of the west-central portion of the Powder River Basin. (interpreted from ERTS-1 images 1030-17233 and 1030-17235).

ORIGINAL PAGE IS
OF POOR QUALITY

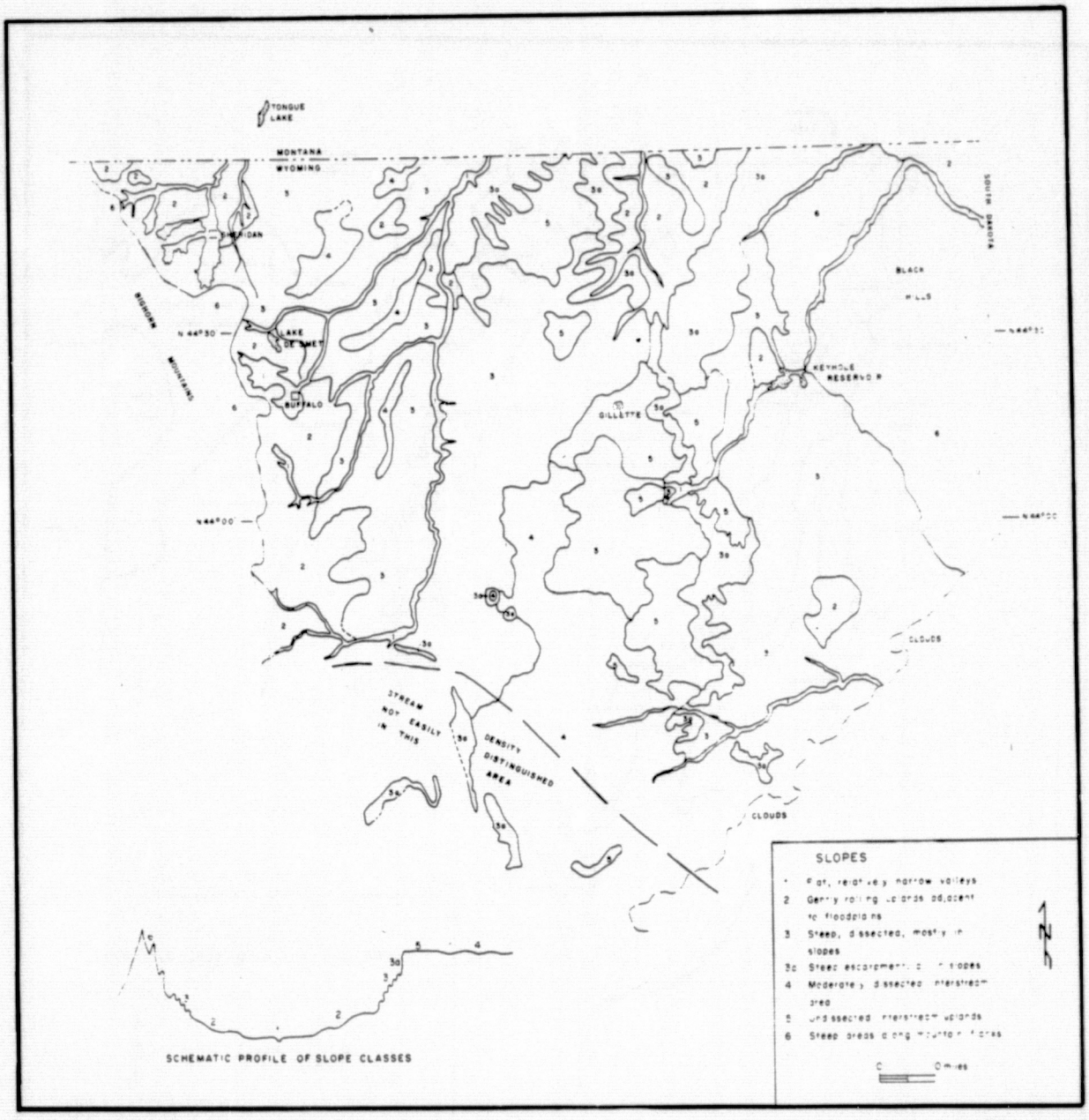


Figure A-7. Areas of equivalent slope estimated from drainage pattern and density.

ORIGINAL PAGE IS
OF POOR QUALITY

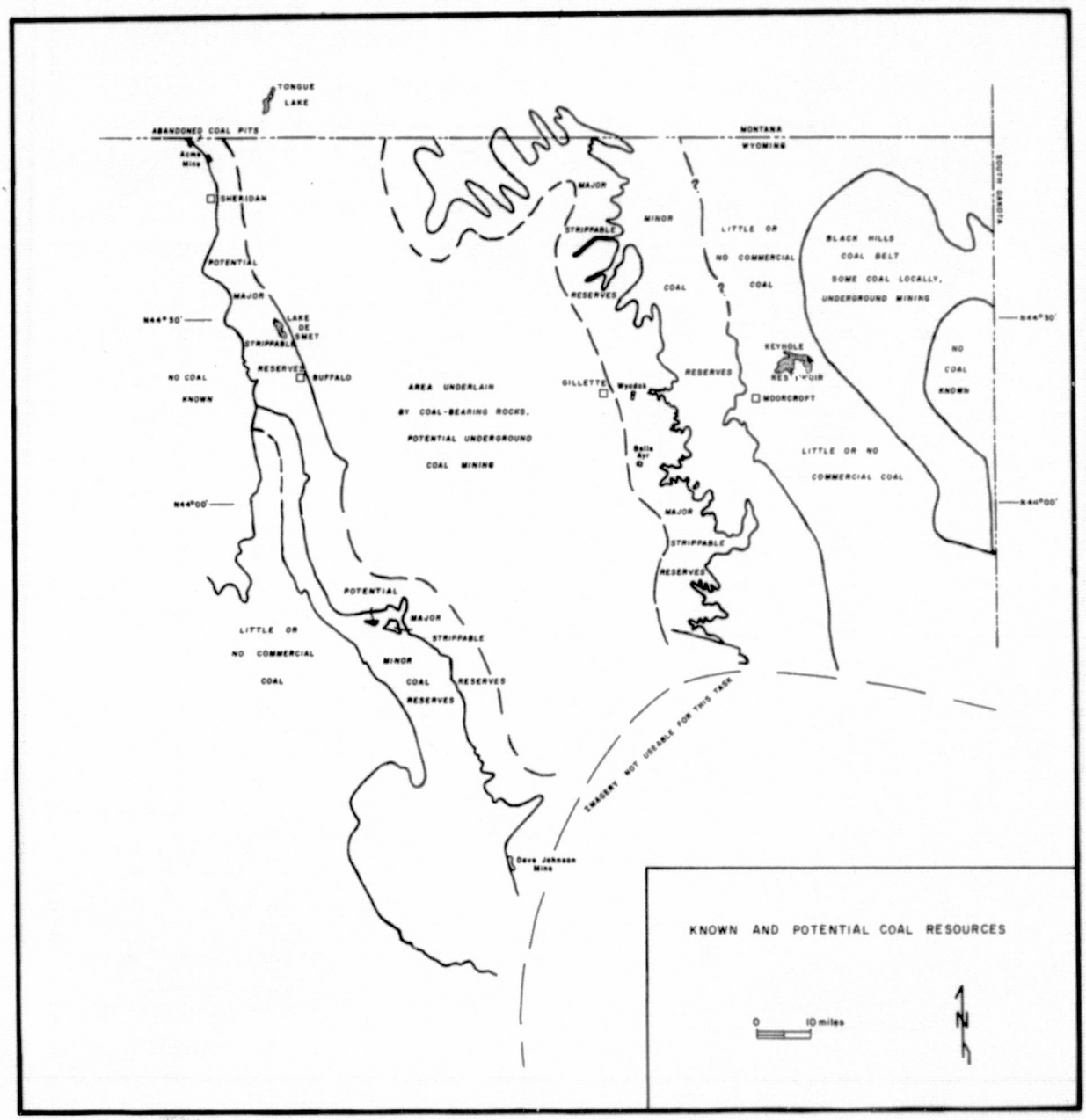


Figure A-8. Coal reserves of the central Powder River Basin. Coal outcrop patterns were interpreted from ERTS-1 data.

ORIGINAL PAGE IS
OF POOR QUALITY

interpretation (Fig. A-9). For example, dunes and terraces were designated as potential sources of sand and gravel, areas of limestone outcrop were mapped as possible sources of lime, and areas of structurally favorable geologic patterns were designated as areas of potential petroleum resources (although virtually all structures visible on the surface have already been tested).

Perhaps the most difficult task attempted was the mapping of urban areas. Cities and towns of Wyoming are relatively small (population 60,000 or less). Early attempts to outline the areas of urban development by standard photointerpretation techniques were unsuccessful. Although the urban areas could generally be located on the imagery, there was often insufficient contrast with the surrounding rural development to allow definition of the urban area. Color-additive viewing was useful in some instances where subtle contrasts on two or more bands could be enhanced by composite display, but it was soon discovered that the ability to discern urban areas was largely dependent on the overall contrast with the surrounding area, and that the urban areas were generally too small to exhibit a characteristic texture or pattern. Even under magnification the urban areas generally appear as fuzzy, grey areas with subtle variations in internal tone and texture. The patterns are too intricate and tonal variations too subtle for visual interpretation.

This problem was circumvented by employing the isodensitracer as a tool for enlarging the images for the urban areas (up to 50x) and enhancing subtle density contrasts. Interpretation of the resulting isodensity contour maps usually allows separation of the urban areas from the surrounding rangeland and natural vegetation but still provides little distinction between urban and agricultural land. A more powerful technique was devised to segregate urban areas from agricultural land. In this technique, four color isodensitracings are prepared for each of the multispectral images and the isodensitracings are then composited to form a color composite map.

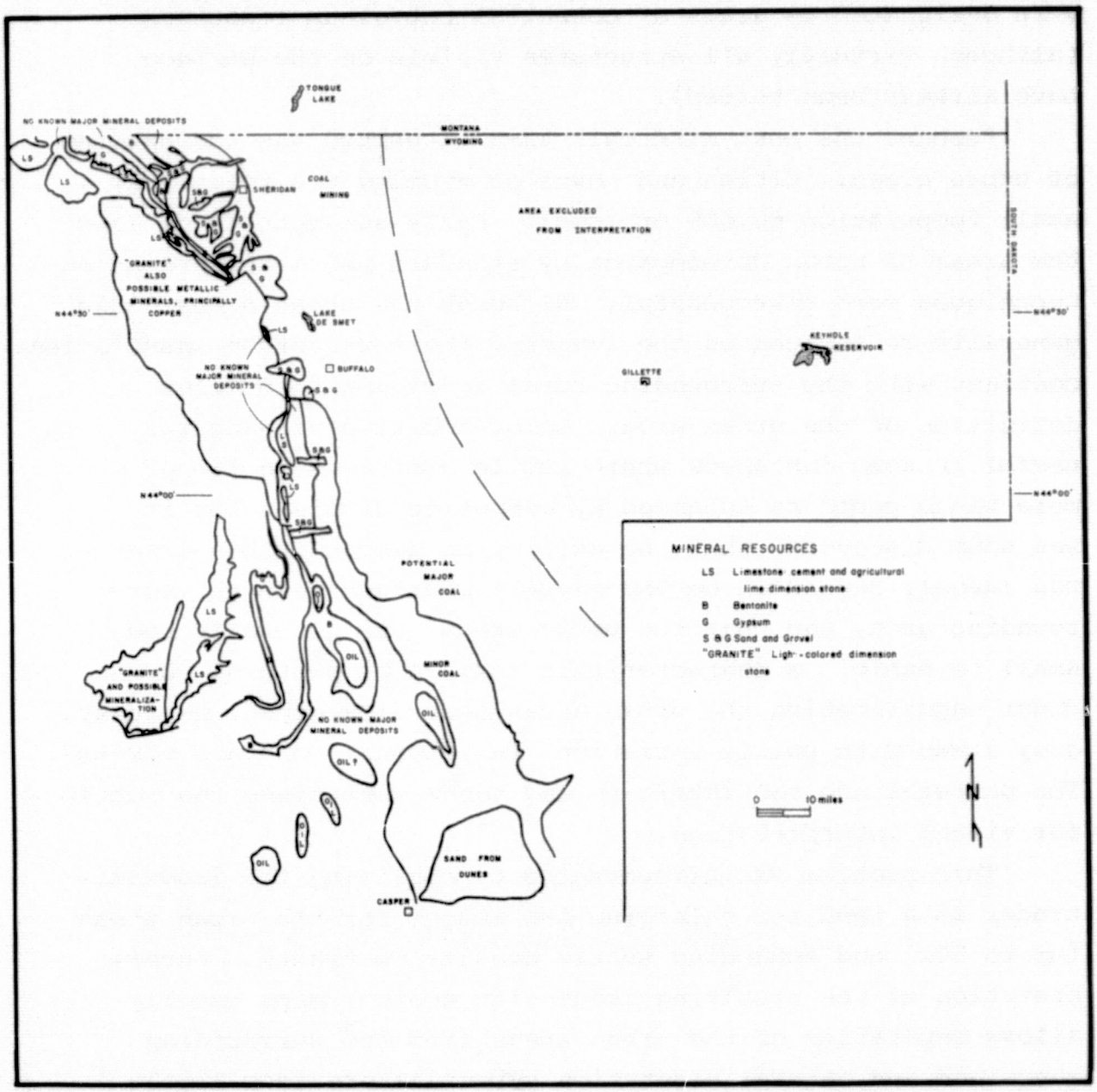


Figure A-9. Areas of potentian mineral resource development along the west fland of the Bighorn Mountains. Areas were identified by interpretation of ERTS-1 imagery.

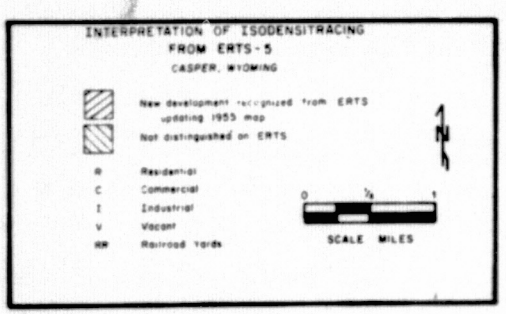
ORIGINAL PAGE IS
OF POOR QUALITY

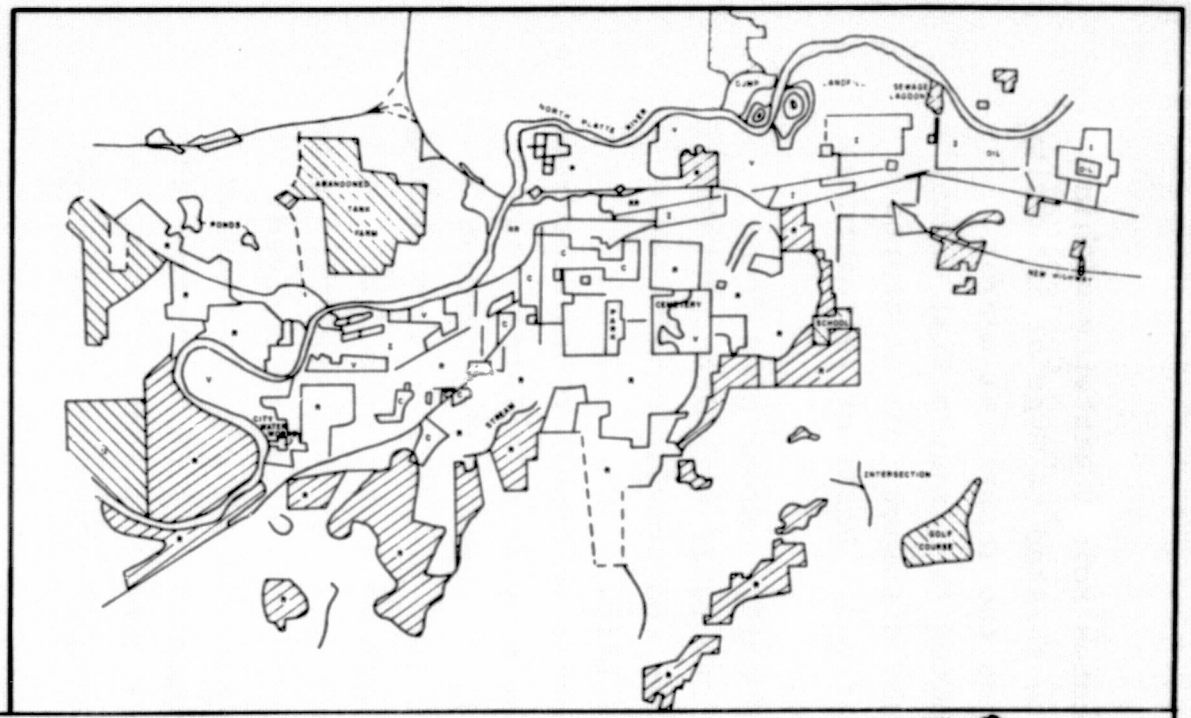
Both isodensitracing techniques reveal patterns within the urban areas that can often be related to type or intensity of development. In some instances the industrial and/or business districts can be segregated from residential areas. New residential areas are commonly distinct from older residential areas which have mature trees. Parks or recreational areas are sometimes identifiable.

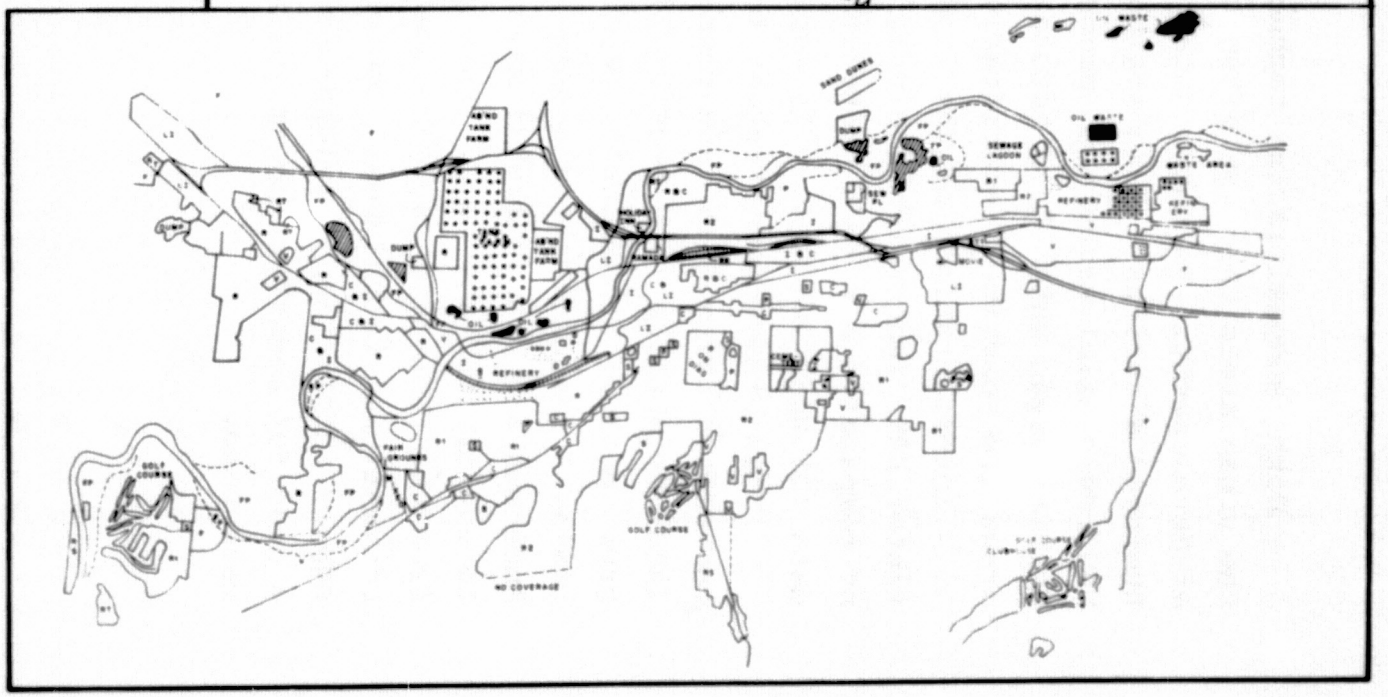
Interpretations of the isodensity contour maps from winter ERTS images compare very favorably with interpretations of comparable aircraft photography and provide considerable data for updating most city maps (Fig. A-10).

This study demonstrates, that even though photointerpretative techniques using ERTS data cannot provide detail that many land-use applications require, it is capable of providing a great deal of broad-scale, basic land-use data on a continuing basis. A classification scheme such as that proposed by Anderson and others (1972) may serve to convert the image data to useful land-use maps. This information can be derived from the ERTS data far more quickly and efficiently than by conventional techniques. Consequently, the ERTS program can supply information for land-use palnning as long as there is a need for constructing or revising the broad-scale land-use data base.

ORIGINAL PAGE IS
OF POOR QUALITY







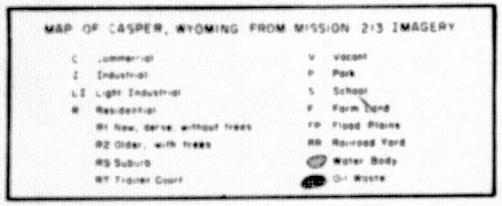


Figure A-10. Land-use maps of Casper, Wyoming.

Appendix B: Application of remote-sensing data to geologic problems encountered by the Wyoming Geological Survey.

summarized from a Wyoming Geological Survey Report:
Breckenridge, R. M., 1973, Geology of the proposed Deer Creek reservoir site, Wyoming Geol. Survey, Laramie, Wyoming.

The proposed dam site is located in the SE¼ of Sec. 11, T. 31 N., R. 77 W. An alternative site is located in the NE¼ of Sec. 13.

The area is located at the northern end of the Laramie Range which was uplifted during the late Cretaceous. Subsequent erosion has removed thousands of feet of Paleozoic and Mesozoic rocks thus exposing the Precambrian core. The northern margin of the uplift is extensively folded and faulted as evidenced by the disturbance of the flanking sediments.

No detailed maps of the area are published. A part of the area was mapped by Sears (1948) before topographic control was available and does not agree with the present-day land survey.

A generalized reconnaissance map of the proposed site was compiled using color aerial photographs of the area (NASA FLT 213, Sept., 1972) from the University of Wyoming, Remote Sensing Laboratory. The immediate area of the dam site was field checked. The proposed location is in a steep canyon cut into Precambrian rocks. Both abutments of the structure would be in bedrock of granite with some mafic dikes and occasional metasediments. The north canyon wall is exposed bedrock while the south side has a mantle of soil and colluvial material.

Major joint sets trend approximately N 50° E in this area. Leakage along joints and fractures could result in percolation through the "gooseneck" or meander.

The alternate location is at the entrance to the canyon near the confluence of Duck and Deer Creeks. The site is also in Precambrian rocks. The west bank exhibits several cut terraces and is probably covered with a mantle of unconsolidated alluvium.

In the case of either dam site, the water impounded would cover an area of low relief called Duck Creek Flats. Several types of geologic materials are present in the area to be covered by the reservoir. Precambrian granites, gneisses and schists form the bedrock and are commonly exposed at the surface. In some places, however, the bedrock is covered by weathered colluvium in addition to Tertiary sediments. Although none of the existing maps of the immediate area show Tertiary rocks, White River or Arikaree sediments have been mapped in the adjacent area of the west fork and probably extend into the reservoir area. The low valley drained by Duck Creek and West Deer Creek is a likely place to find more isolated patches of these Tertiary sediments. A number of springs and seeps are present in the reservoir area which are controlled by factures in the bedrock.

Conclusions

1.) Both the proposed and alternate sites would provide a Precambrian bedrock foundation with minimal excavation of alluvium.

2.) A number of well-developed joint systems are present in the Precambrian rocks. It is recommended that the joints be further evaluated with respect to possible leakage.

3.) The reservoir would cover areas of Precambrian, Tertiary (?), and Quaternary rocks. Some springs are present along fractures in the Precambrian. The Tertiary White River sediments characteristically contain clays which exhibit swelling properties.

4.) No active faults were recognized in the area. Although the area has been tectonically active in the geologic past, it is structurally stable at present.

5.) No other obvious geologic hazards, aside from the joints, were observed in this brief study.

Appendix C: Summary of a study of regional geomorphologic relationships in the Wyoming Basin province.

from a special report by R. M. Breckenridge, Brainard Mears, Jr., and others, Geomorphic Sections of the Wyoming Basin Province (in progress).

The Wyoming Basin geomorphic province (Fenneman, 1931) has never been satisfactorily differentiated into its constituant divisions using geomorphology as the principle criterion. This study attempts to accomplish this subdivision using interpretations of ERTS-1 imagery, aerial photography and field data.

The province was divided into ten basins and associated uplifted regions (Fig. C-1). This delineation was based on distinctions of geomorphic entities apparent from the ERTS-1 color-composite mosaic of Wyoming* and upon available geologic and topographic data. Topography, geologic structure, and stratigraphy were considered along with the geomorphic criteria in defining subdivision boundaries. A description of each of the basin areas was then compiled setting forth its major characteristics and discussing the decision criteria used in selecting each basin boundary. Included in each description is a summary of the geography, size, boundaries, drainage, topography, and general geology of the area. The following description of the Laramie Basin (one of the ten basin subdivisions) presents a typical set of physiographic and boundary conditions upon which the basin subdivisions were made:

> The Laramie Basin of southeastern Wyoming encompasses a north-south trending area 90 miles long and 30 miles wide. It lies between the Laramie Range on the south and east, the Medicine Bow Mountains on the west and the Shirley and Hanna Basins on the north. The northeast-flowing Laramie River is the major drainage for the area, and the basin contains extensive alluvial deposits along the river and its tributaries. Elevations on the basin floor are usually from 7000 to 7500 feet.

*The 1:1,000,000-scale mosaic used in this study was completed by the General Electric Photographic Engineering Laboratories, Beltsville, Maryland.

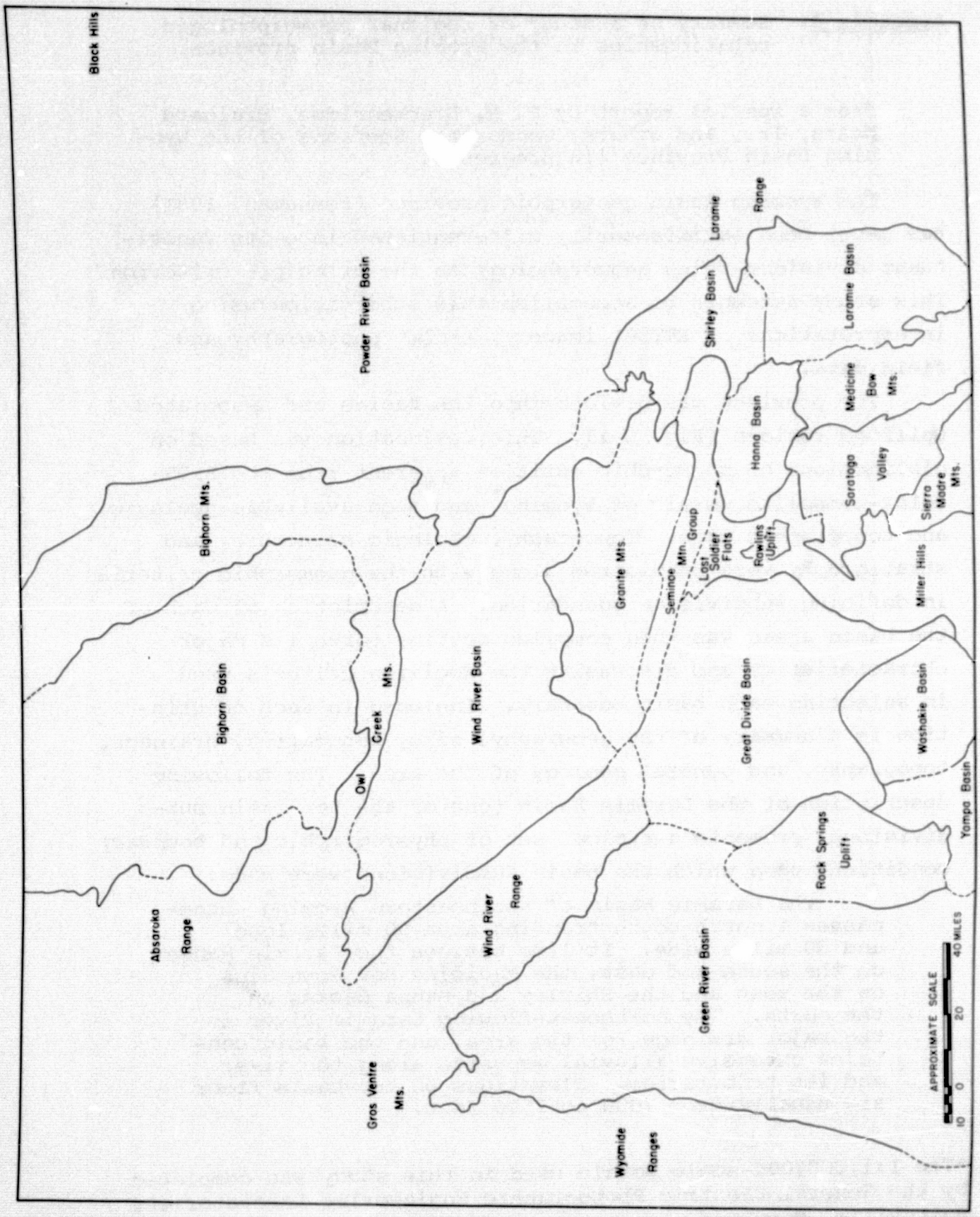


FIGURE C-1. GEOMORPHIC SECTIONS OF THE WYOMING BASIN
as determined from ERTS Imagery

ORIGINAL PAGE IS
OF POOR QUALITY

Structurally the Laramie Basin is a broad north-plunging syncline containing about 8000 feet of late Paleozoic and Mesozoic rocks with some Tertiary rocks in the northwest part of the area. Alluvial deposits and terrace gravels of Pleistocene and later age are also quite abundant. Several smaller anticlines are found on the west and north sides of the basin, but are not prominent topographically as are those of the basins to the north.

The eastern boundary of the Laramie Basin is the top of the Casper Formation and the base of the prominent dip slope developed on the resistant limestones and sandstones of this formation. The southeast boundary, west of Tie Siding, Wyoming, corresponds to the Casper-Precambrian contact and the mountain front of Boulder Ridge. In this area, the base of the Casper dip slope is at a relatively low angle and cannot be shown as a single line. The southern boundary is also arbitrary, as shown by the dashed line, but roughly corresponds to the unconformity between the Precambrian granite and the Fountain Formation.

The western boundary is shown as the break in slope between the relatively flat basin and the steep mountain front of Precambrian from the eastern flank of Bull Mountain to the south, and Jelm Mountain and Sheep Mountain to the north. Centennial Valley is included in the Laramie Basin, the boundary again being the steep mountain form of Precambrian in contact with the Fountain Formation on the east side of Centennial Valley. A fault contact defines the western and northern boundary of Centennial Valley to Corner Mountain.

The north-trending fault-controlled Precambrian front of the Medicine Bow Mountains continues to bound the west side of the Laramie Basin to Arlington. This boundary is dashed northward from Arlington, cutting the center of the Cooper Cove anticline which divides the Laramie Basin from the Hanna Basin. The boundary continues to the north where it intersects the ridges of the Mesaverde Group south of Medicine Bow. The northern boundary of the Laramie Basin is the top of the Cloverly Formation hogback as exposed on Como Bluff anticline. The boundary is dashed eastward from here to the base of the Casper Formation dip slope on the Laramie Range. This northern boundary is somewhat arbitrary, however, it appears best to use the most prominent hogback and the largest feature in the area. In addition, the many minor anticlines and synclines in the northern Laramie Basin appear to be more subdued than those to the north. Como Ridge marks the boundary of this characteristic.

Appendix D: The use of satellite imagery and aerial photography for making lithologic distinctions.

summarized from two special reports submitted under contracts NAS 5-21799 and NAS 9-13298:

Houston, R. S., 1973, Distinguishing major lithologic types in rocks of Precambrian age in central Wyoming using multilevel sensing--with a chapter on possible economic significance of iron formation discovered by use of aircraft images in the Granite Mountains of Wyoming, NTIS, Springfield, Virginia, Report E73-10301, 34p.

Houston, R. S., 1974, Multilevel sensing as an aid in mineral exploration--iron formation example; in Houston and others, 1974, Some illustrations of the advantages of improved resolution in geologic studies; National Technical Information Service, Springfield, Virginia, Report #74-10628, 73p.

NASA coverage of Wyoming includes complete cloud free ERTS imagery (900 meters above the surface, Fig. D-1) on a seasonal basis (18-day cycle, about 1/3 to 1/2 cloud free); greater than 50 percent cloud-free Skylab (270 miles above the surface, Fig. D-2), and greater than 70 percent aircraft coverage (15,000-60,000 feet above the surface, Fig. D-3). Standard products include film positives and prints of multiband images generated from the MSS ERTS multispectral scanner, film positives and prints of six bands from Skylab S190A cameras, high resolution black and white and color positives and prints from the Skylab S190B camera and a variety of products from aircraft sensors including six or more bands from multispectral camera systems, high-resolution color and color infrared prints and film positives from 10-in. aerial cameras and various products from multispectral scanners and spectrophotometers.

Multilevel Sensing

The multilevel sensing approach takes advantage of this material to save time and money in geologic studies. Spacecraft images can be used to target areas of geologic and/or economic interest and images taken at lower (aircraft) elevations can be used to study key areas in greater detail.

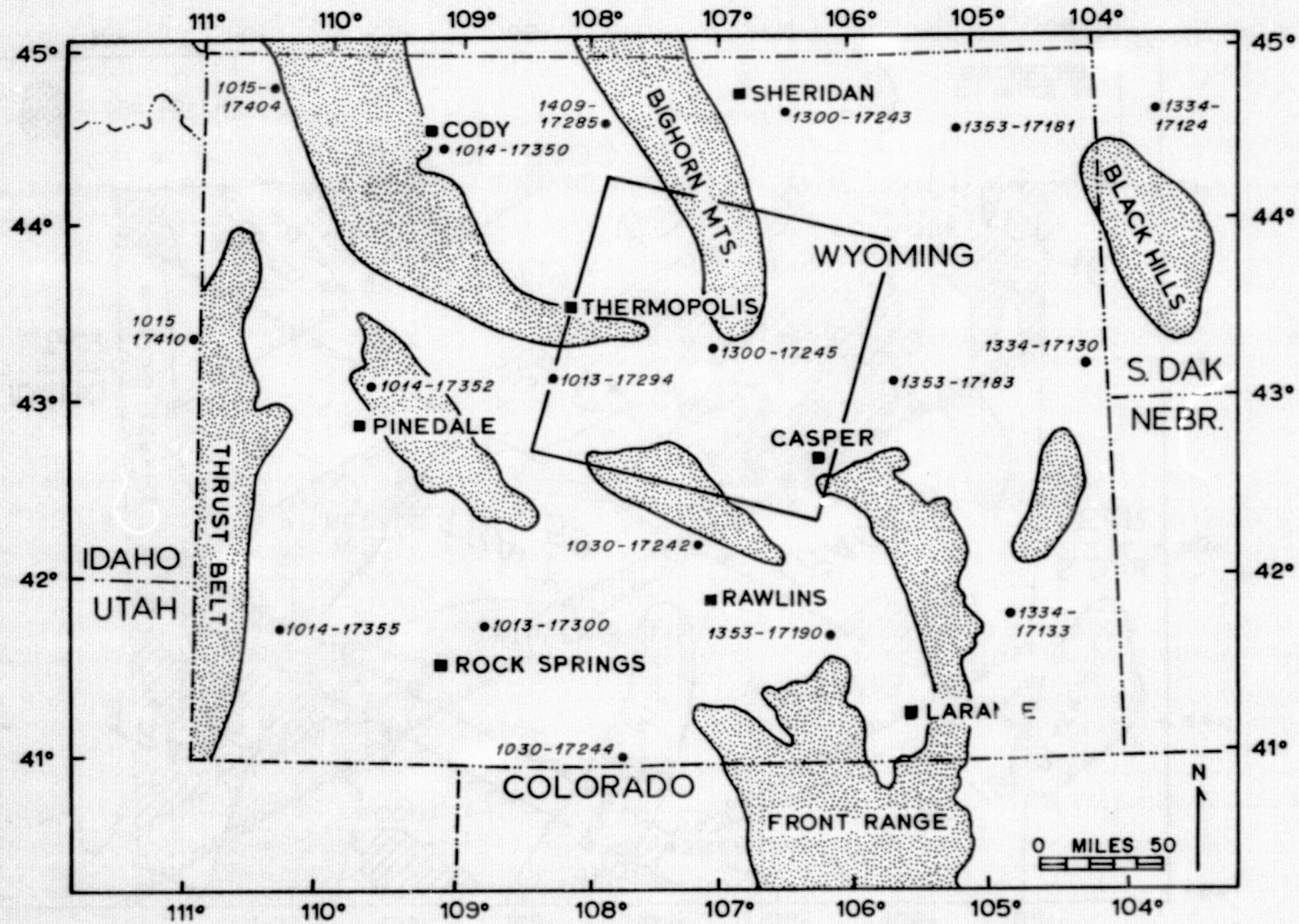


Figure D-1. Map of Wyoming showing identification numbers of best ERTS-1 images generated between July, 1972 and October, 1973.

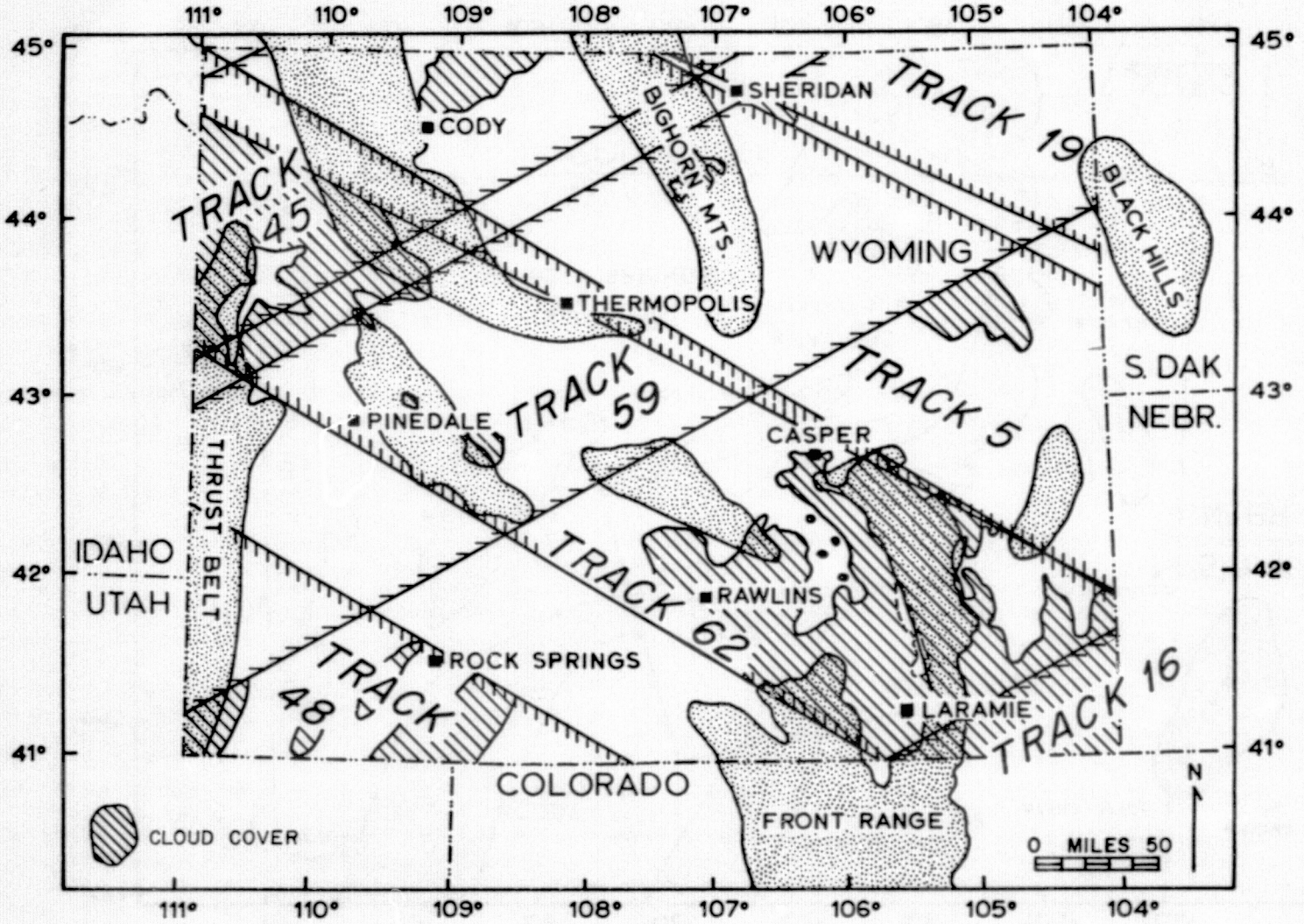


Figure D-2. Index map showing Skylab S-190A coverage of Wyoming during Skylab missions 2 and 3. Cross-hatched area is cloud covered.

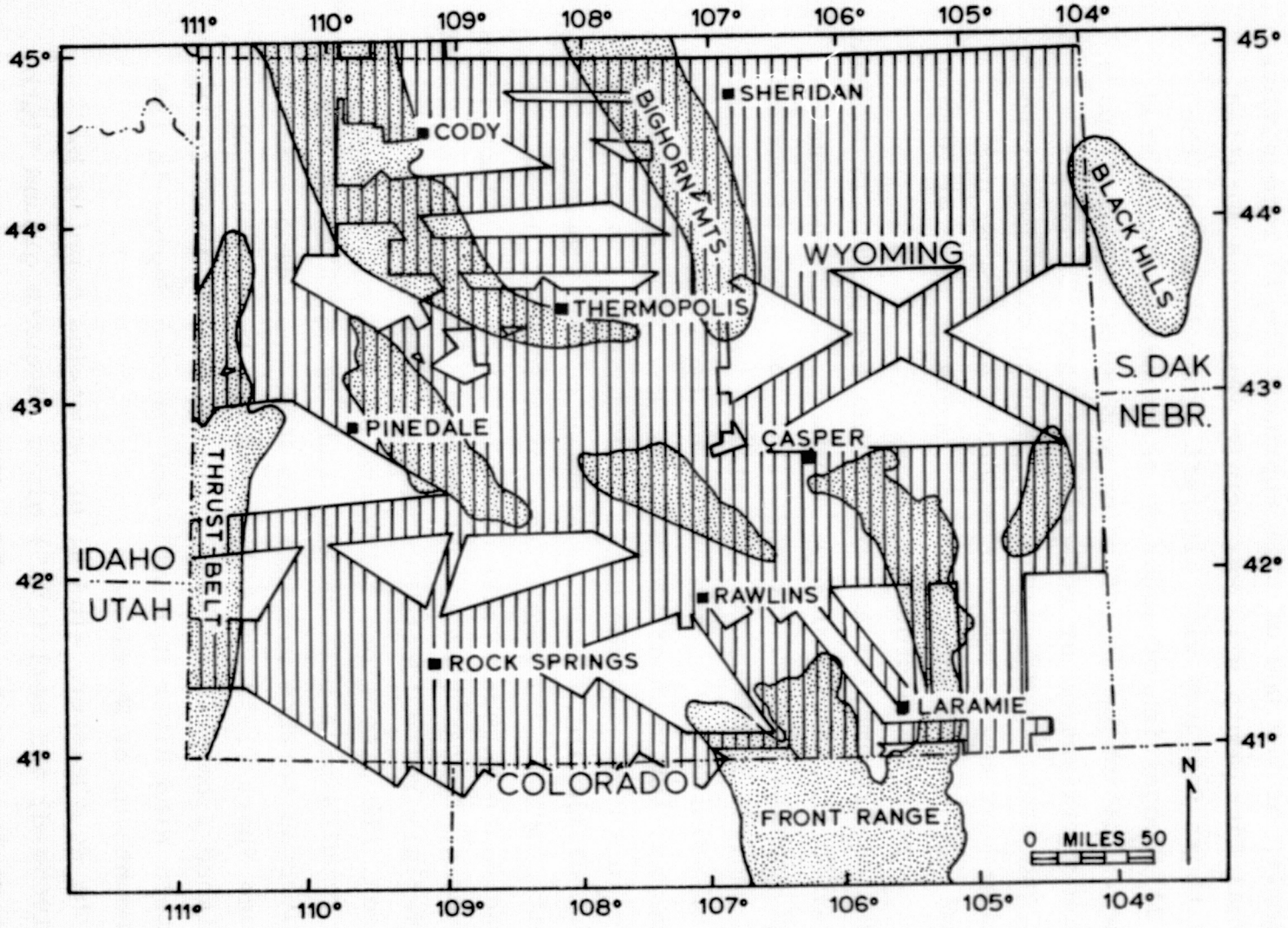


Figure D-3. Index map showing NASA aircraft coverage of Wyoming as of October, 1973.

This approach saves time and money since the user will find the space image can be obtained and analyzed at less cost per unit area.

Examples of the use of this approach are 1) recognition of regional lineaments with spacecraft images and detailed study of these features with aircraft products and on the ground; 2) recognition of major color anomalies associated with mineralization by use of color and color infrared space images and verification or rejection of these by use of aircraft and ground studies; and 3) mapping of major lithologic units that may be host of mineral deposits by use of spacecraft images and study of these units in greater detail by use of aircraft and ground studies.

Rocks of Precambrian age in Wyoming are primarily Archean (2.5 b.y.) in age and consist of two major terranes--greenstone and granite gneiss. The granitic rocks are of economic interest because they may be directly or indirectly one of the sources of uranium now in the sandstone-type uranium deposits of the basins, but most of the mineral deposits in the Archean rocks are in the greenstone belts that make up a relatively small part of the total bulk of Archean rocks. The greenstone belts contain all known iron formations of economic significance and virtually all other metallic mineral deposits in the Wyoming Precambrian except deposits in post-Archean metasedimentary rocks located in southeastern Wyoming. For this reason, the greenstone belts are an economic target.

The results of a preliminary study using ERTS-MSS band-5 for Precambrian terrane distinctions have been discussed by Houston and Short (1972, p. 12) greenstone belts could be distinguished from granite and granite gneiss terrane in the southeastern Wind River Mountains and to some degree in the Granite Mountains of Wyoming.

In the southeastern Wind River Mountains mapping by Bayley (1965a-d) and Bell (1955) gives adequate ground truth to enable us to evaluate the ERTS, MSS-5 interpretation. According to Bayley (1965a) the metasedimentary/metavolcanic

rock terrane (greenstone) consists chiefly of light-brown to black feldspathic and micaceous graywacke, conglomerate and mica schist, and dark-colored mafic lava flows and bodies of gabbro, black graphitic schist, dark brown meta-andesite flows, and lesser amounts of dark quartz-magnetite iron formation and white, gray, or pale green quartzite and pale green mica (fuchsite) schist. The area underlain by these rocks is dark colored and distinctly layered. The granitic terrane (Bayley, 1965c) may be gray quartz diorite and granodiorite or white to pink coarse-grained granite (Bell, 1955, p. 13). The granitic terrane for the most part is light colored and texturally more massive than the metasedimentary/metavolcanic rock terrane. This tonal contrast shows quite well on ERTS MSS-5 imagery with the metasedimentary/metavolcanic terrane indicated as areas of low reflectance and the granitic terrane as areas of higher reflectance.

Although similar distinctions can be made in the Granite Mountains the interpretation from the ERTS image is not as accurate as that of the southeastern Wind River Mountains. The accuracy of the interpretation may be judged by comparing Figure D-4 (the ERTS interpretation) with Figure D-5 which is a geologic compilation from the best available geologic and photogeologic mapping of this area. The major area of metasedimentary/metavolcanic rock in the northeast Granite Mountains can be distinguished but minor granite bodies within this area cannot. In the southwest the general area where metasedimentary/metavolcanic rocks are present can be recognized from the ERTS MSS-5 imagery but an area of metasedimentary rock approximately two miles wide and six miles long was misinterpreted as granite.

The difficulty in making distinctions between rock types in the Granite Mountains is probably the result of several factors. The Granite Mountains are interpreted (Love, 1970) as a once great mountain area like the Wind River Mountains that collapsed to form a graben. The mountains were partially exhumed so that today we see isolated masses of rocks of

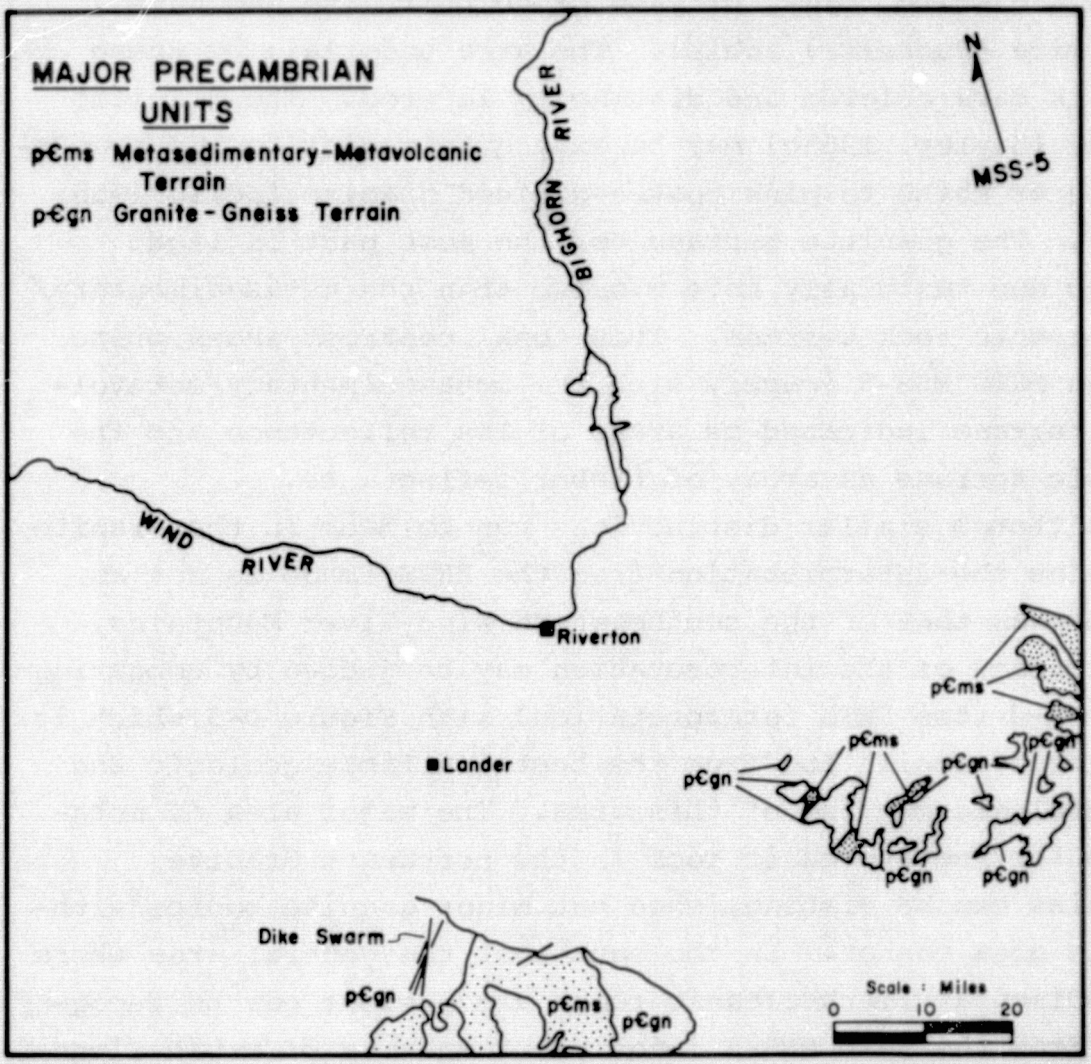


Figure D-4. Map of Precambrian terrane of the southern Wind River Mountains (bottom center) and Granite Mountains (lower right) showing greenstone belts pCms mappable from ERTS imagery.

Precambrian age surrounded by flat-lying sedimentary and volcanic sedimentary rocks of late Tertiary age. Some masses stand well above the Tertiary floor and others are barely exhumed. In general, the granitic rock terrane has higher relief, less soil, and, as stated above, is light colored as compared to the metasedimentary/metavolcanic terrane. The higher reflectance in the red band of granitic terrane is probably a combination of all of these factors rather than a simple expression of rock color alone. In addition, some metasedimentary rock units in the Granite Mountains are more felsic in composition and lighter in color than those of the Wind River Mountains, and are difficult to distinguish from granite even with high-resolution color and color infrared photography. The various factors undoubtedly hinder lithologic distinctions in this area. This conclusion is supported by limited field checks and available ground truth.

Figure D-6 is a geologic map prepared from interpretation of U-2 red band and color infrared 70 mm positive transparencies. Resolution of the U-2 photographs was adequate to distinguish many of the large diabase dikes that cut the granitic rocks of this area so three Precambrian lithologies were mapped; granite-granite gneiss terrane, greenstone belt terrane, and diabase dikes. The distinctions made using U-2 images are good as indicated by a comparison with Figure D-5.

Direct comparison of the U-2 photography with the Mission 184 (C-130) photography shows that only half as many dikes can be resolved on the U-2 photography as on the higher resolution C-130 photography. This is apparently a line-resolution limitation rather than a reflectance difference because the wider dikes are clearly distinguished on the U-2 images.

Figure D-7a and D-7b compare U-2 and ERTS images of a granite-metasedimentary rock contact in the southeastern Wind River Mountains. In this application the U-2 has no advantage over the ERTS images because the contact can be readily mapped with either image.

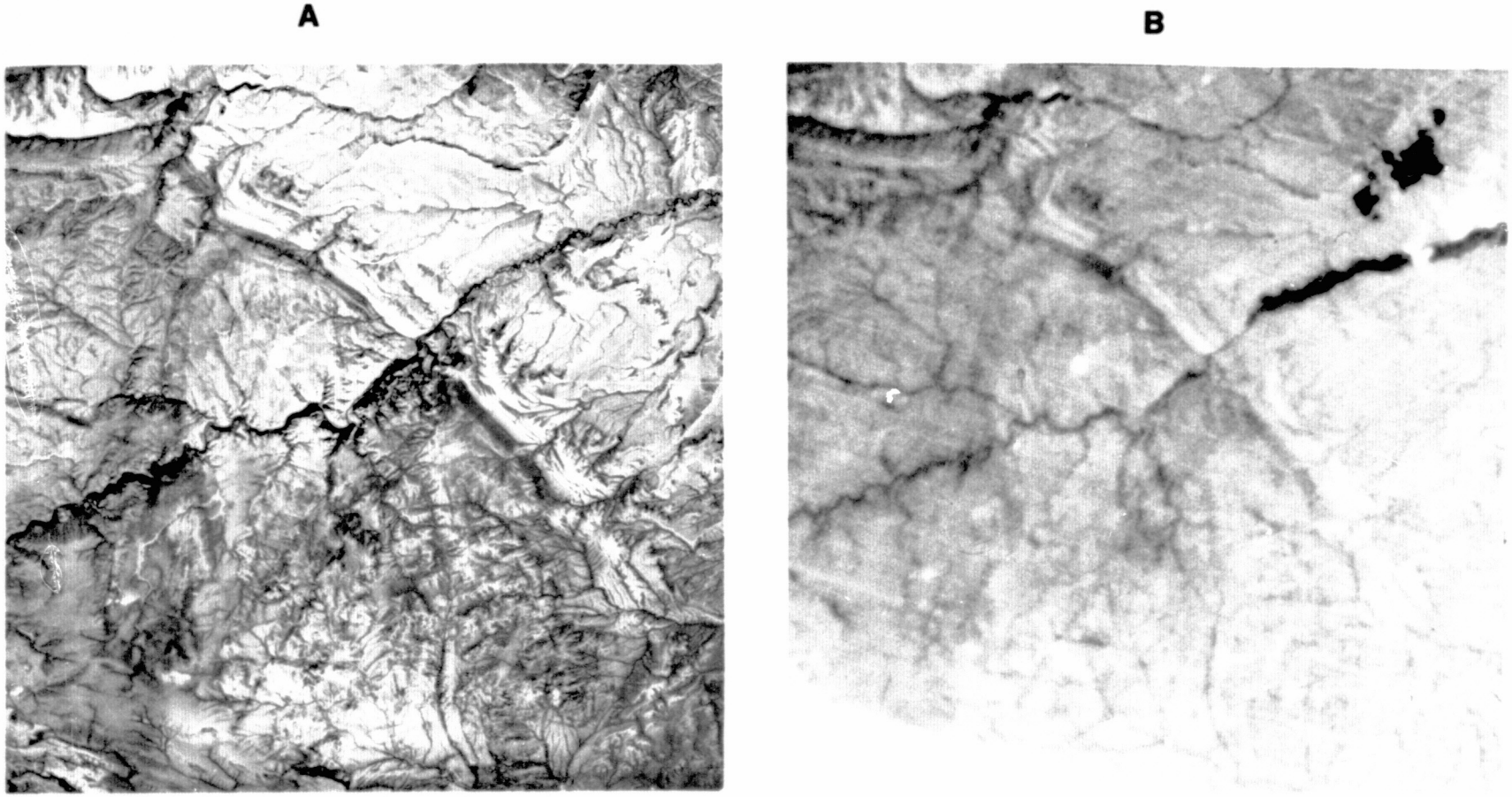
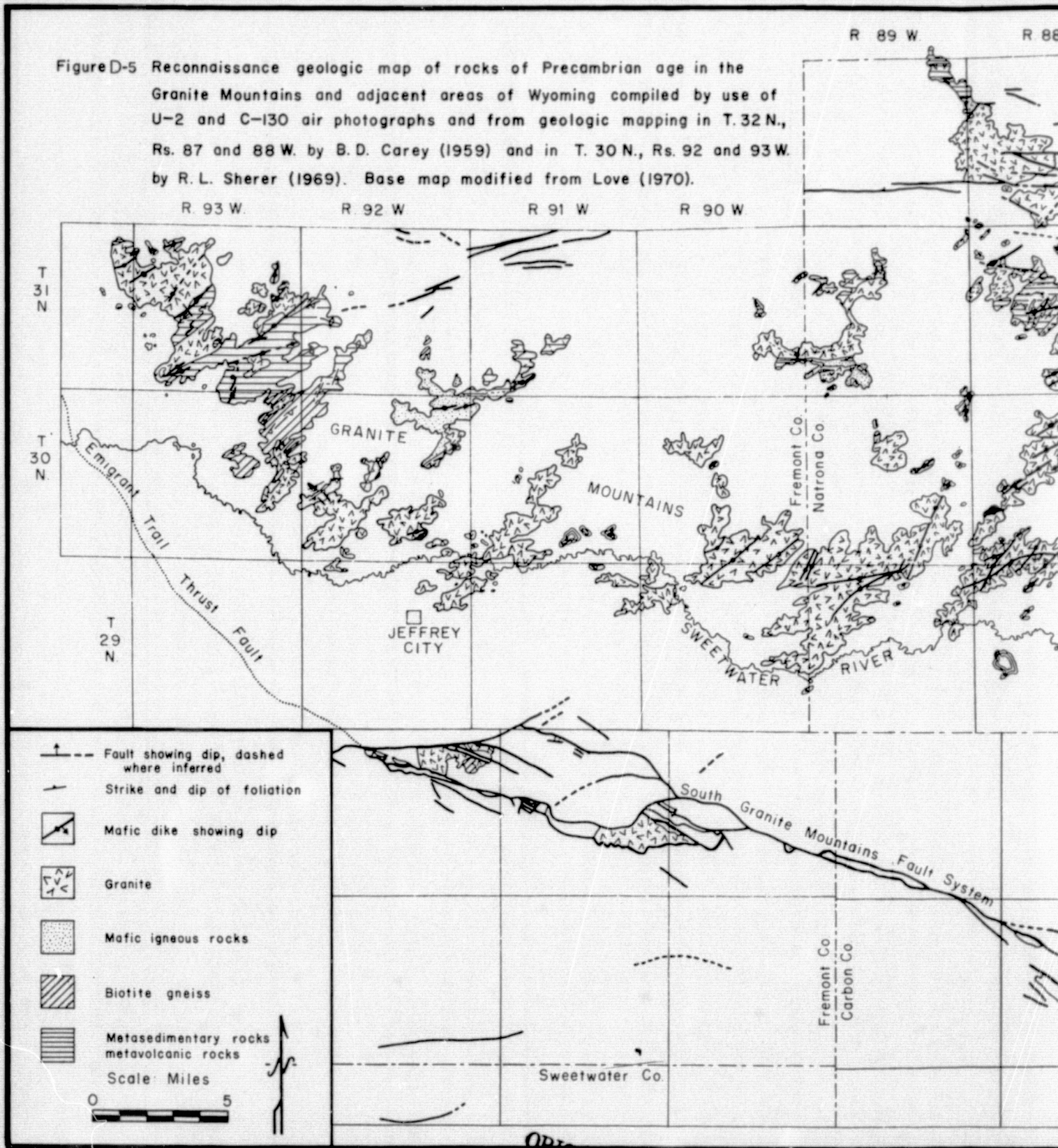


Figure D-7. Images of the southeastern Wind River Mountains of Wyoming showing contact between Precambrian metasedimentary rock - metavolcanic rock (dark mass on left) and granite/granite-gneiss; red band U-2 (A) and MSS-5 (B). The contact strikes approximately north and can be clearly seen in the left center of the images near the fork in the Sweetwater River. A contact between northeast dipping Paleozoic rocks and the Precambrian is in the northeast portion of each image.

Figure D-8 is a geologic map made from interpretation of the C-130 aircraft color and color infrared photography. If this map is compared with Figure D-5, the reader may note that the photogeologic mapping compares favorably with the field-checked geologic maps, but several exceptions are apparent. In T. 30 N., Rs. 92 and 93 W. a series of outcrops of gneissic granite, biotite gneiss, and granite gneiss are exposed in secs. 16, 17, 18, 19, 20, 21, 30, and 31, T. 30 N., R. 92 W., and secs. 1, 2, 11, 12, 13, 14, and 24, T. 30 N., R. 93 W. According to Sherer (1969, p. 7-22), the biotite gneiss is a layered rock with alternating biotite-rich and quartz-feldspar-rich layers and it forms brownish-black to dark-gray outcrops whereas the gneissic granite and granite gneiss (both shown as granite in Figure D-5) have less well developed layering are generally lighter in color than the biotite gneiss. These rocks are mineralogically similar, containing chiefly feldspar, quartz, and biotite with the primary difference being a greater abundance of biotite and better developed layering in the biotite gneiss. They are not easily distinguished in the field because all units have gradational contrasts and are inhomogeneous in mineral percentages. Thus, it is not surprising that these units are not readily distinguished by photogeologic techniques. The biotite gneiss which is probably sedimentary in origin was interpreted as either granite or foliated granite by photogeologic techniques and contacts between the various units are not correct.

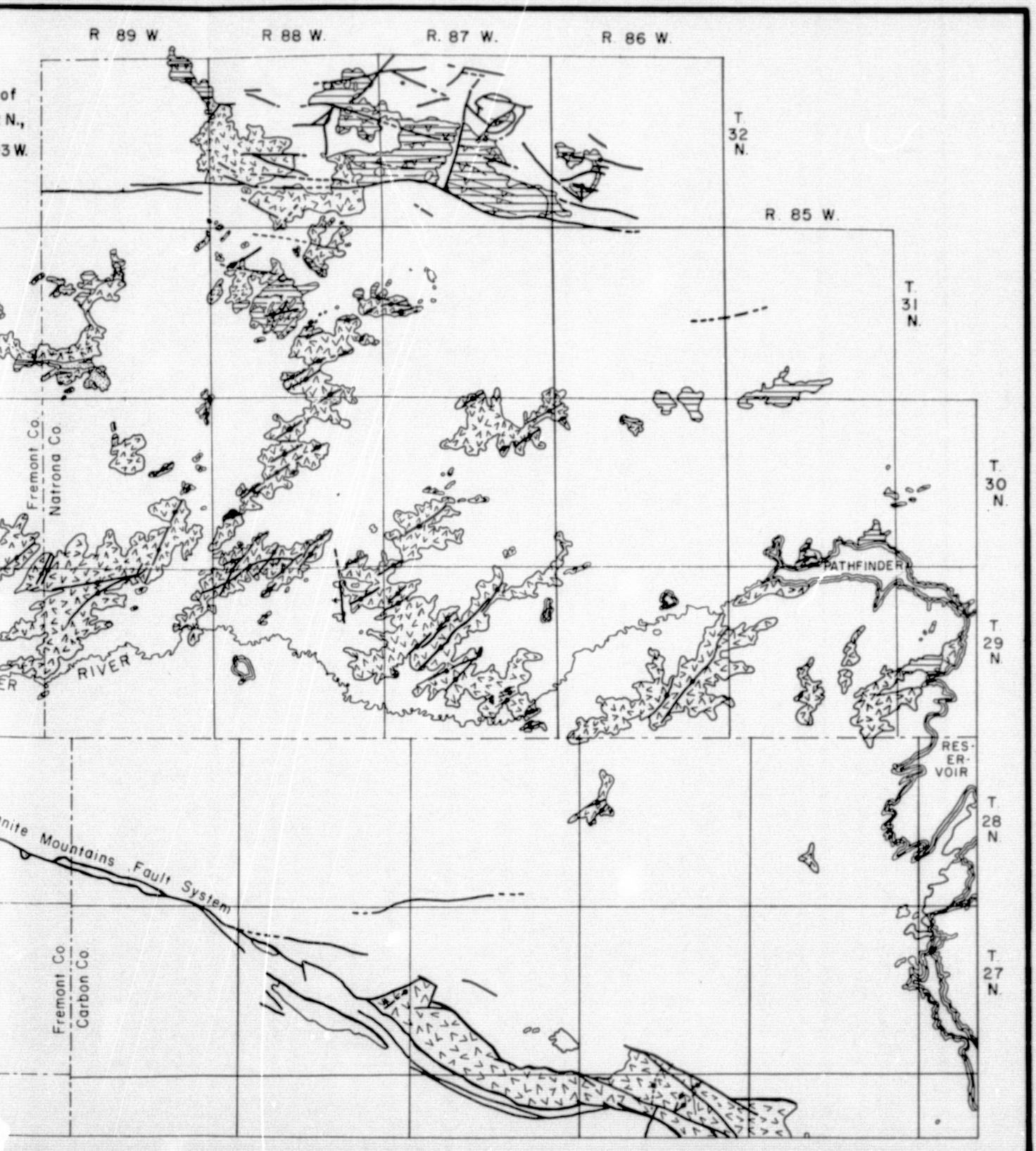
The area in the general vicinity of Barlow Gap is, perhaps, the best for photogeologic mapping in the Granite Mountains. The major rock types show strong color contrasts and lithologies show greater tonal and textural contrast on the film positives than in the field. As noted above, iron formation was discovered in the area during a field check of the photogeologic map in August of 1972. This is the first report of iron formation in the Barlow Gap area, but a small body of iron formation was discovered in an area several miles

Figure D-5 Reconnaissance geologic map of rocks of Precambrian age in the Granite Mountains and adjacent areas of Wyoming compiled by use of U-2 and C-130 air photographs and from geologic mapping in T. 32 N., Rs. 87 and 88 W. by B. D. Carey (1959) and in T. 30 N., Rs. 92 and 93 W. by R. L. Sherer (1969). Base map modified from Love (1970).



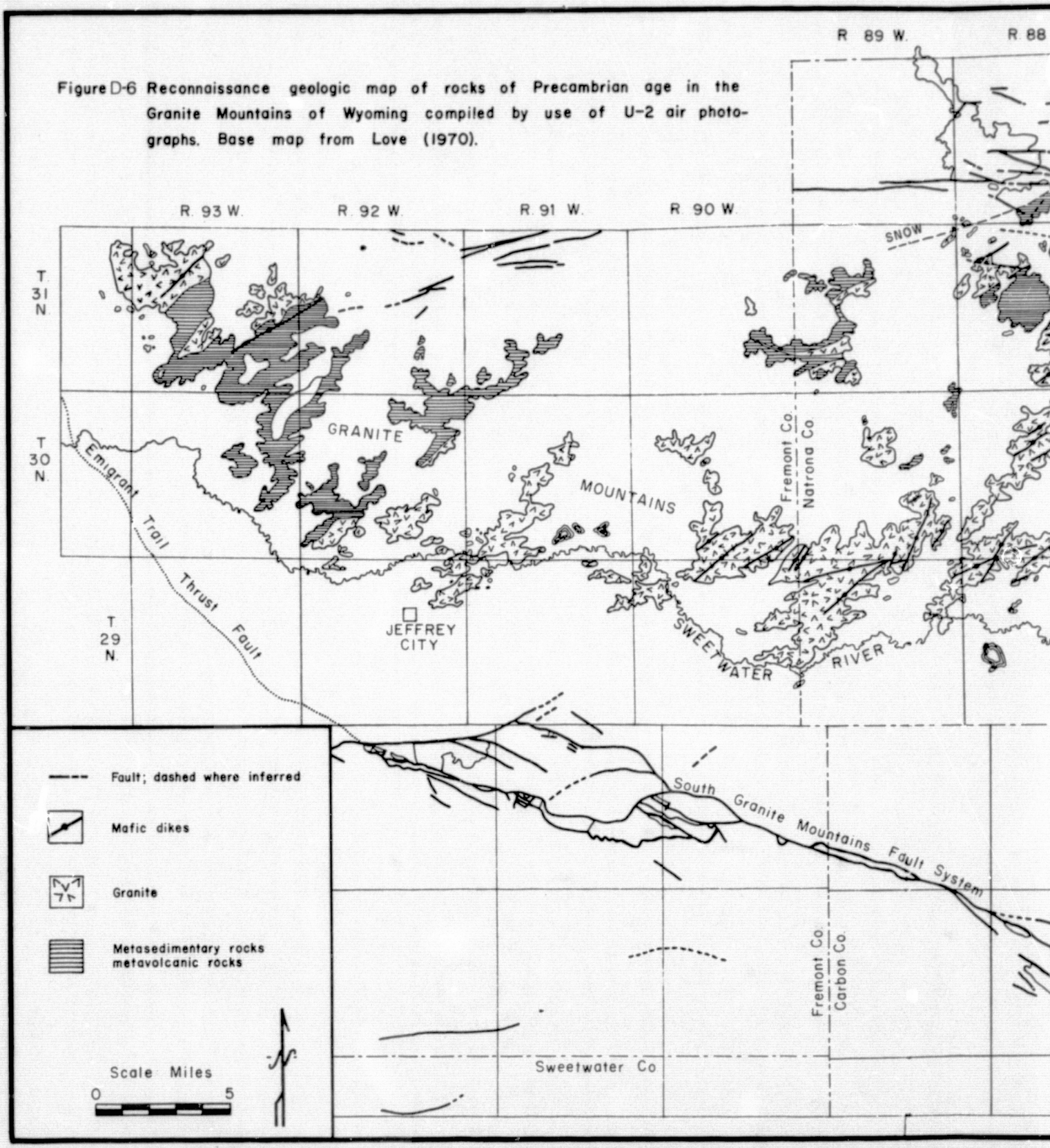
ORIGINAL PAGE IS
OF POOR QUALITY

LDOUT FRAME



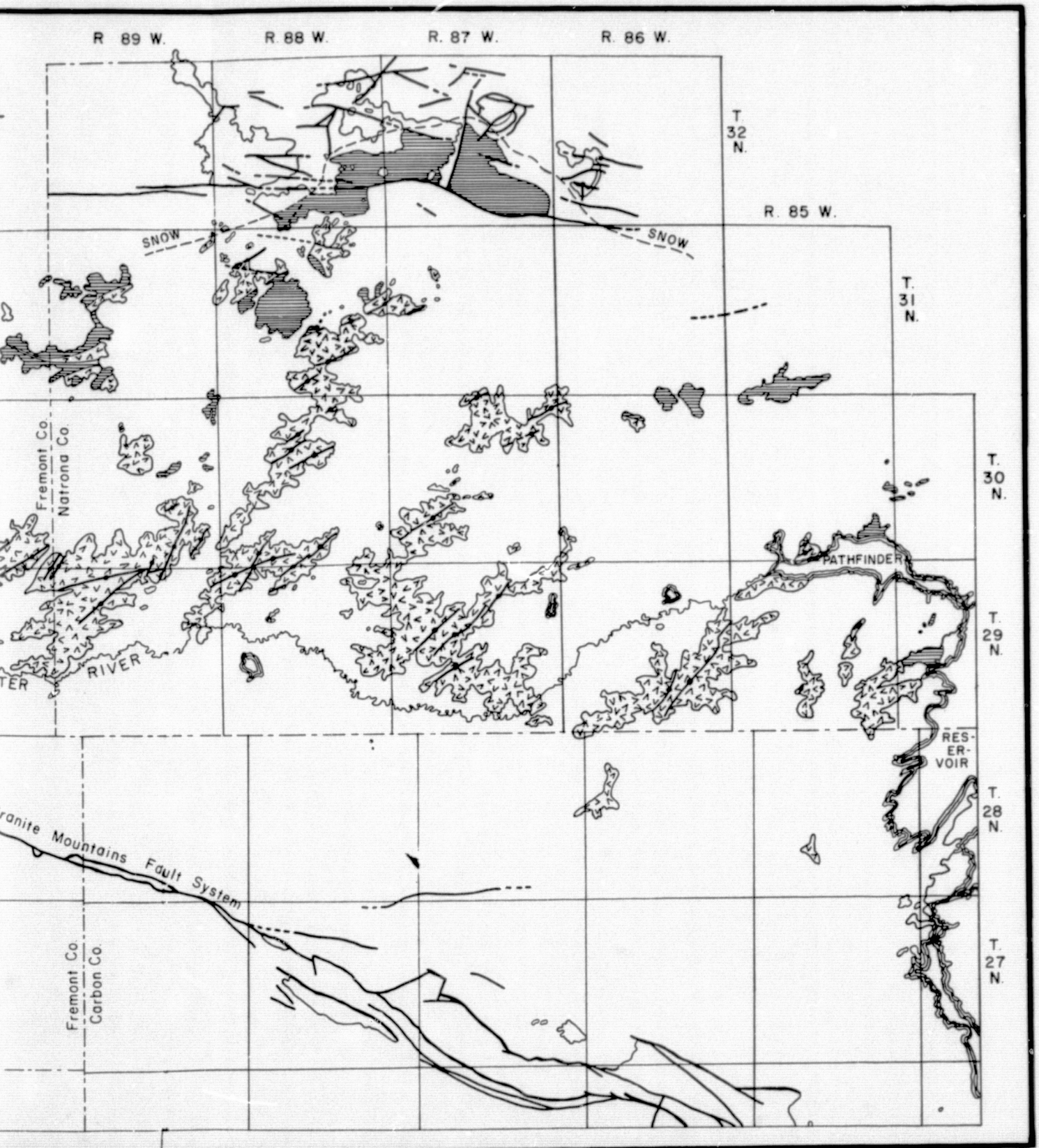
FOLDOUT FRAME 2

Figure D-6 Reconnaissance geologic map of rocks of Precambrian age in the Granite Mountains of Wyoming compiled by use of U-2 air photographs. Base map from Love (1970).



FOLDOUT FRAME /

ORIGINAL PAGE IS
OF POOR QUALITY



FOLDOUT FRAME

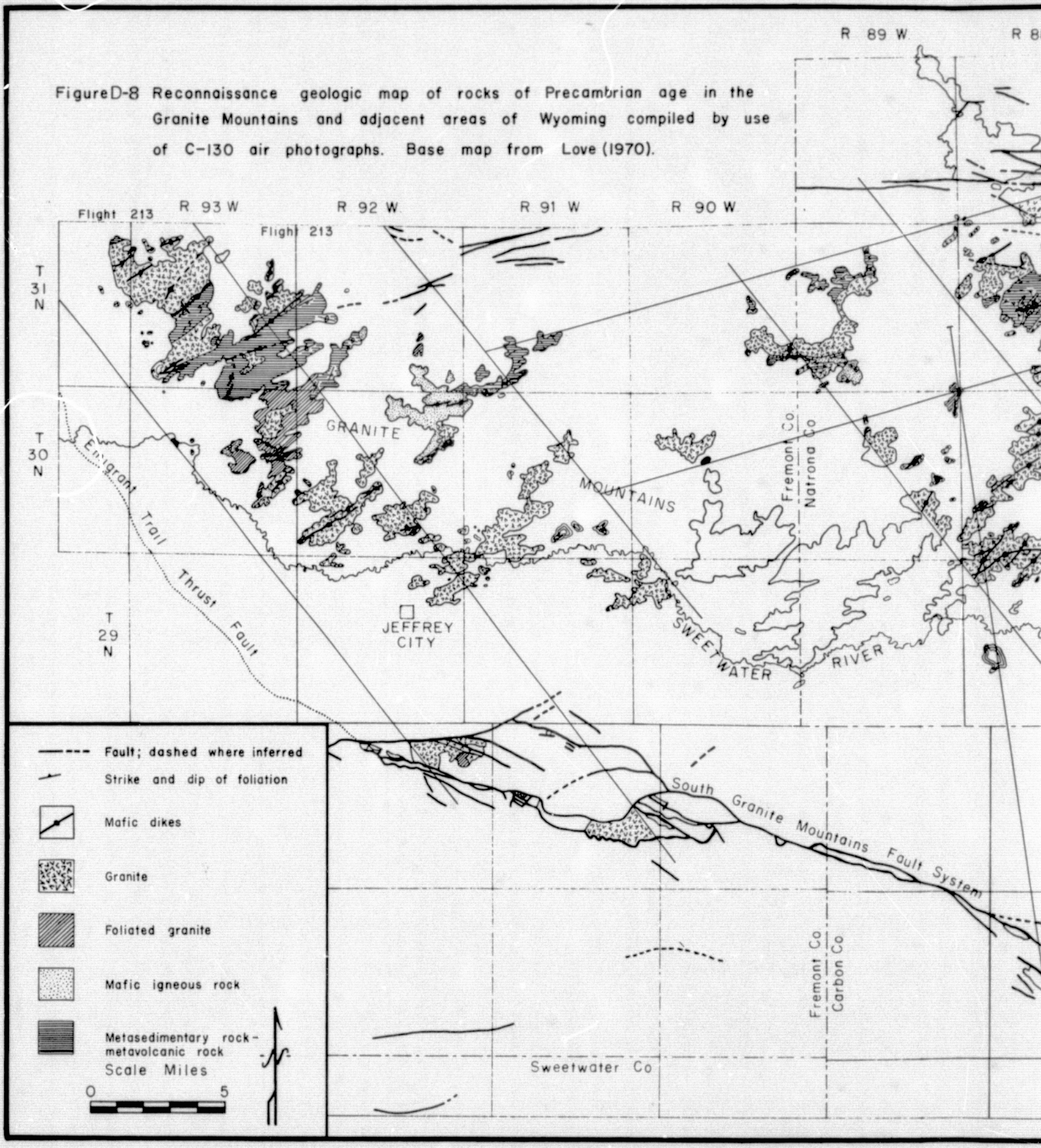
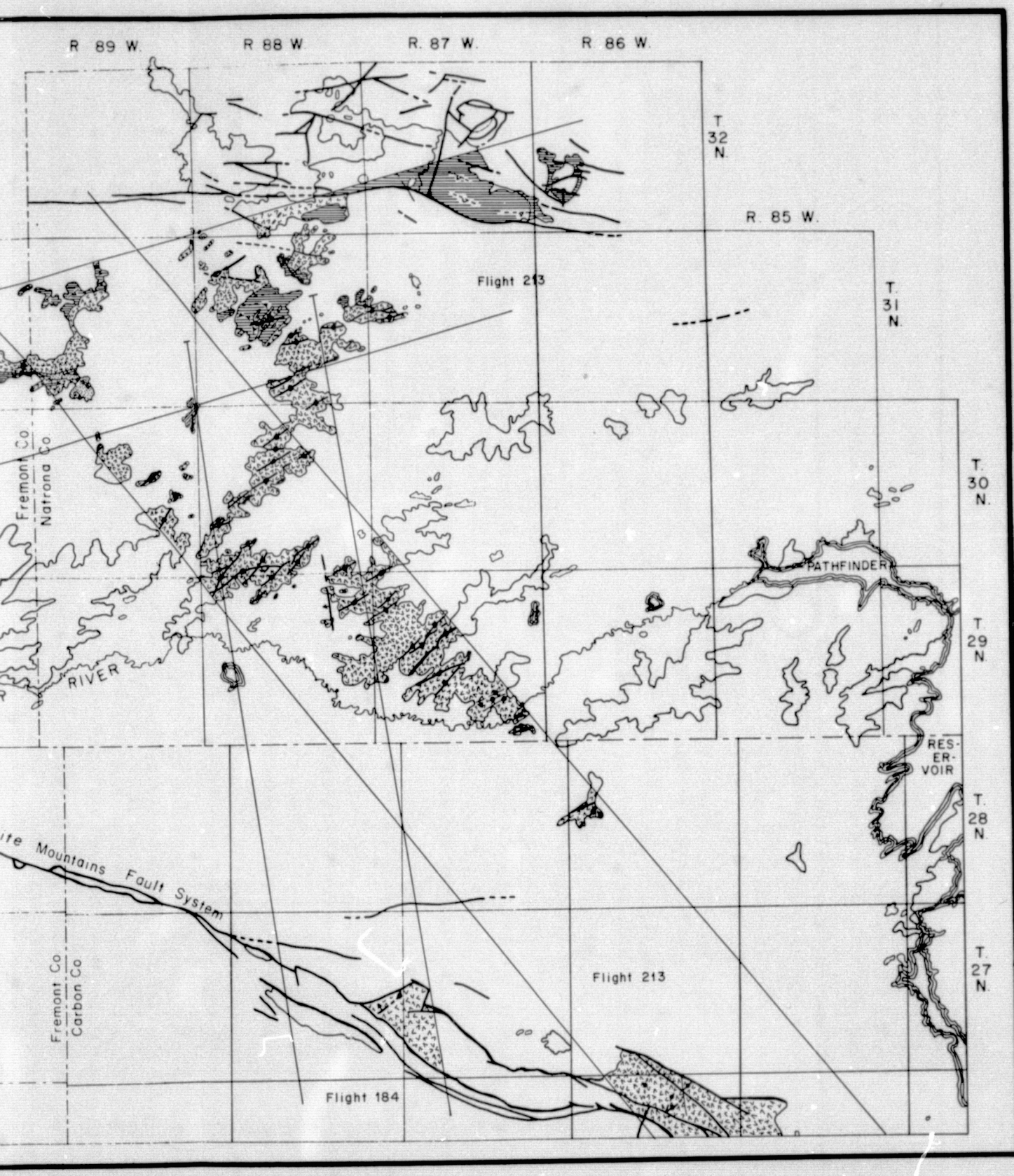


Figure D-8 Reconnaissance geologic map of rocks of Precambrian age in the Granite Mountains and adjacent areas of Wyoming compiled by use of C-130 air photographs. Base map from Love (1970).

FOLDOUT FRAME



FOLDOUT FRAME 2

northeast of Barlow Gap in 1971 by Alfred Pekarek (personal communication, 1971), graduate student at the University of Wyoming.

Three bodies of iron formation (Figure D-9) were noted at Barlow Gap in the one day reconnaissance survey of the area. The largest occurrence is in a small anticline (as indicated by primary structures in sedimentary rock noted in the field) located in SE 1/2, sec. 16, T. 31 N., R. 88 W. (Fig. D-9). Oxide and silicate facies (James, 1954, p. 249) iron formation were recognized. The oxide facies iron formation consists of layers of magnetite alternating with layers of green silicate and brown chert. The silicate facies is a laminated greenish black rock probably composed of minnesotaite and/or iron-rich amphiboles. Thin layers of iron-rich carbonate are also present, but the most abundant iron-bearing rocks are the oxide-facies type with alternating magnetite and green silicate layers. Chemical analyses of these various rock types are in Table D-1. The magnetite layered iron formation ranges from 21 to 29.5 percent less than is typical for this facies as suggested by James (1954, p. 249).

The iron formation at Barlow Gap and that discovered by Alfred Pekarek northeast of Barlow Gap represents a series of small isolated outcrops; none large enough to be of economic value at present and many factors; in addition to tonnage (Ohle, 1972), must be considered before any firm conclusions about the economic value of the iron formation can be made. However, the geologic study of this area is only reconnaissance and the total areas of metasedimentary rocks where iron-formation outcrops are known covers at least 36 square miles. In addition to these outcrops Love (1970, C140) reports results of drilling which brought up numerous fragments of iron formation from the Tertiary Wagon Bed Formation at a depth of 140-160 feet. These fragments of iron formation in the Tertiary beds were probably derived from iron formation in the Precambrian. The well in which they are found is in NW 1/2

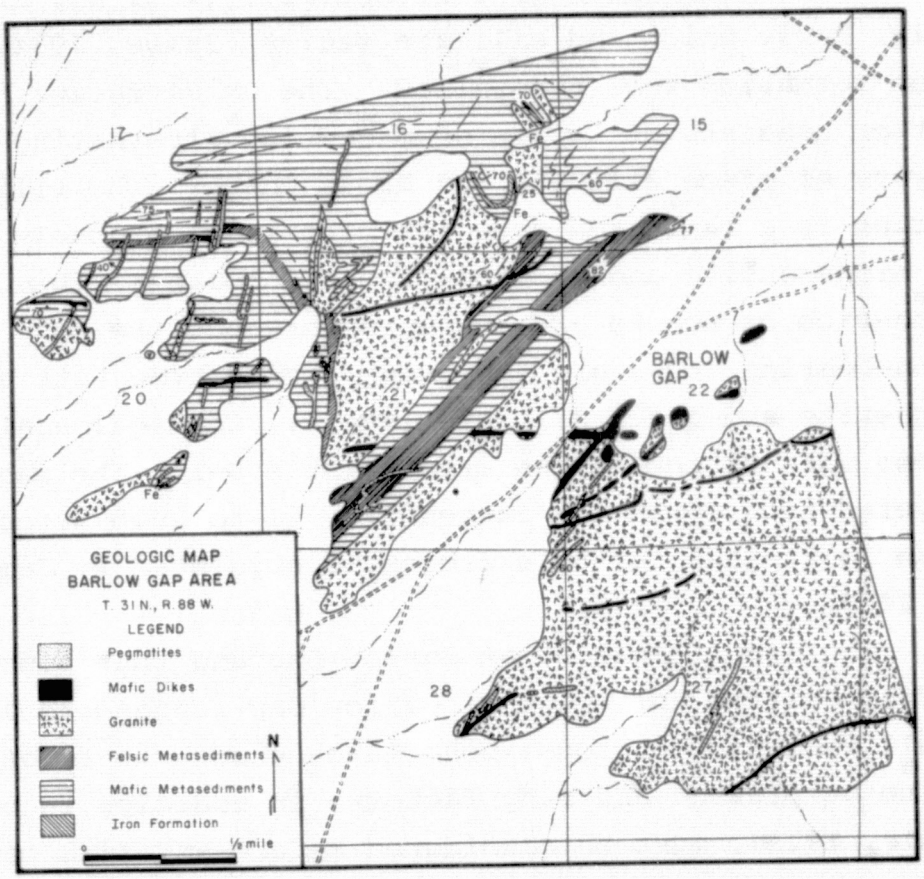


Figure D-9. Reconnaissance photogeologic map of the Barlow Gap area, Natrona County, Wyoming. Compiled from interpretations of C-130 aerial photography.

ORIGINAL PAGE IS
OF POOR QUALITY

Table D-1. Iron, manganese, titanium and chromium content of samples of iron formation from Barlow Gap, Wyoming. (Analyst -- J. W. Murphy, University of Wyoming, Rock Analysis Lab).

Rock Type	Sample No.	%Fe(±0.2)	%Mn(±0.003)	%Ti(±0.1)	%Cr(±0.02)
Silicate	RS72-2A	11.2	0.178	0.5	0.05
Silicate	RS72-2B	31.1	0.198	0.9	0.10
Carbonate	RS72-3A	6.1	0.162	0.9	0.19
Magnitite-Silicate layered	RS72-3B	21.0	0.213	0.9	0.06
Magnetite-Silicate layered	RS72-3C	29.5	0.268	0.9	0.10
Magnetite Silicate layered	RS72-3D	21.0	0.164	0.9	0.06

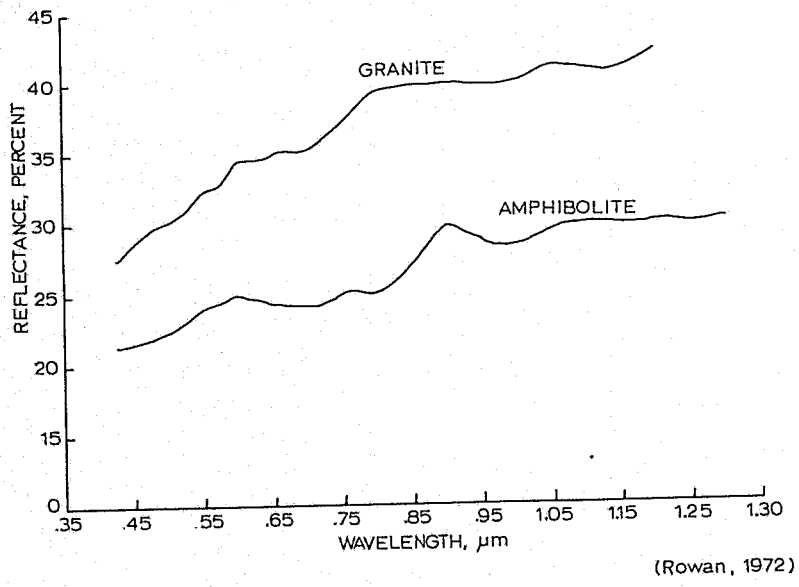
sec. 14, T. 32 N., R. 86 W., 16 miles from the Barlow Gap area. These observations show that iron formation is present in Precambrian metasedimentary rocks in, at least, three townships and Fig. D-5 shows that similar metasedimentary rocks are present throughout much of the northern Granite Mountains. It is the writer's opinion as was Love's (1970, p. C140) that this area should be studied to determine the extent of these iron-bearing units.

Perhaps the most useful and least expensive tool for initial exploration whould be an airborne magnetometer survey. Such a survey might locate iron formation both in surface outcrops and in Precambrian metasedimentary rocks that are buried beneath the relatively thin cover of Tertiary sedimentary rocks.

Appendix E: Geologic mapping from ERTS-1 imagery.

from a special report under contract NAS 5-21799:
R. S. Houston, 1974, Geologic mapping using space images, in Houston and others, 1974, Some illustrations of the advantages of improved resolution in geologic studies; National Technical Information Service, Springfield, Virginia, Report E74-10628, 73p.

Photogeologic mapping using standard black and white products is basically an attempt to map contacts of photo units as expressed by tonal contrasts, texture, and geomorphic features, and to map faults and other structures by use of stereoscopic interpretation. Tonal contrasts expressed on black-and-white prints are useful in mapping lithology, but they can seldom be used to identify rock types. Laboratory determined reflectance spectra for common rocks show differences in the visible and near-infrared regions due primarily to electronic processes in the cation or impurity ions (iron the most common source) and to vibrational processes in hydroxyl groups or molecular water, and in the far infrared (9-12 um) due primarily to silica content (Hunt and Salisbury, 1971). The reflectance spectra also show variation in overall reflectances for rocks depending, in part, on electronic processes which can produce an extremely sharp cutoff in the visible or near-infrared spectrum, or continuous absorption throughout the entire range (Hunt, Salisbury, and Lenoff, 1971, p. 1-3). Thus rock spectra show two main characteristics: narrow absorption bands due mainly to the presence of iron, hydroxyl groups, water and silica, and broad reflectance differences or brightness differences. A granite, for example, has a relatively high spectral reflectance as compared with basalt, basalt may show absorption bands due to iron content not shown by granite, and silica absorption bands in granite are recorded at different wavelengths than those in basalt (Fig. E-1). These spectral differences appear to offer a possibility for remote identification of rocks and a number of studies have been undertaken, primarily using aircraft systems, to determine if rocks can indeed be identified by use of spectral



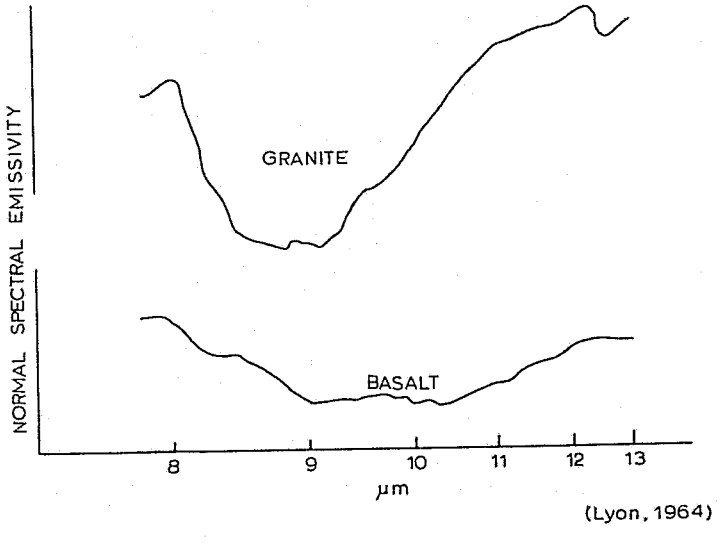


Figure E-1. Comparisons of reflectance and emissivity spectra for acidic and mafic rocks. The reflectance curve for the mafic rock shows a reflectance low (absorption) at about 0.7 μm and 1.0 μm. The thermal emissivity curves show a decided shift in the emissivity low toward shorter wavelength due to the increased silica content of the granitic rock.

differences. One of the most comprehensive studies was that of Lyons (Lyons and Patterson, 1969, p. 527-552) at Stanford who has had some success in identifying rocks by taking advantage of the shift in silica absorption band with silica content in the far infrared. This study made use of an aircraft-mounted spectrometer and radiometer. Characteristic spectra of common rocks were compared with those of the target or unknown as determined by the spectrometer, and under optimum conditions rock types and contacts could be mapped along the straight-line path of the spectrometer. The method is subject to a number of limitations that will be discussed, but for geologic mapping a major limitation is that information is confined to the single narrow path of the spectrometer and is difficult to extrapolate into other areas for mapping. An approach that uses the same silica shift principle in mapping rocks but makes use of a multispectral scanner instead of a spectrometer has been proposed and tested by Vincent (Vincent and Thompson, 1971, p. 247-252). Instead of using the complete rock spectra as was done by Lyons, selected bands of the spectra (i.e. 8.2-10.9 um/9.4-12.1 um) are rationed and ratio images are produced that are useful in distinguishing silica-rich and silica-poor rocks. This method is less specific than that of Lyons, but multispectral scanners produce image data so that maps can be generated from the interpretations and identifications.

The ratio approach has been extended to make use of iron-absorption bands by a number of investigators (Vincent, 1972, p. 1239-1247; Rowan, 1972, p. 60-1-60-18), and because the MSS scanner of ERTS includes near infrared bands the technique has been used to map iron-rich rocks and alteration zones by use of ERTS data (Vincent, 1973; Rowan and others, 1973).

These various techniques plus others using related approaches (Watson, 1972; Pohn, Offield, and Watson, 1972; Watson, Rowan, and Offield, 1971) offer promise for eventual quantitization of geologic mapping, but, as is true for many geologic problems, the number of variables that must be

considered to apply these techniques to actual field problems is very large. Factors that affect rock spectra include grain size, grain orientation, degree of weathering, vegetation cover, sun angle and azimuth, viewing geometry, slope angle, temperature, water saturation, atmospheric conditions and depth of the atmospheric column, shadowing, and such common factors as strike and dip of outcropping beds. No technique has been developed to take all of these factors into account although some are considered in most experiments. Statistical methods that essentially map significant reflectance differences in a given area or use training sets to map a certain tone or density that may characterize a rock in a given area (Anuta and others, 1971; Smedes and others, 1972; Watson and Rowan, 1971) are useful but, again, cannot be applied to general mapping because of variables cited above. The 1974 state-of-the-art suggests that enhancement techniques may be useful for mineral exploration under controlled conditions (i.e. where the method is tailored to a specific area) but general geologic mapping is still best done by the experienced photogeologist using standard photogeologic techniques.

The best approach we have found for geologic mapping using space images is to try to recognize units with distinctive tone or texture that can be used as marker beds in a given region, and to use these beds along with other standard recognition parameters for mapping decisions. Figure E-2 shows laboratory reflectance spectra determined at Goddard Space Flight Center (Short and Lowman, 1973, p. 9) for a typical suite of Wyoming sedimentary rocks. The spectra are not sufficiently distinctive to be diagnostic of rock type, and, as noted by Short and Lowman (1973, p. 18), several individual rocks displayed greater variation between spectra from fresh and weathered surfaces an inch apart than between quite different rock types. Yet it is apparent that one sedimentary rock group, the Cretaceous shales, has exceedingly low reflectance as compared with other units. These beds of the upper Thermopolis Shale and lower Mowry Shale contrast strongly with

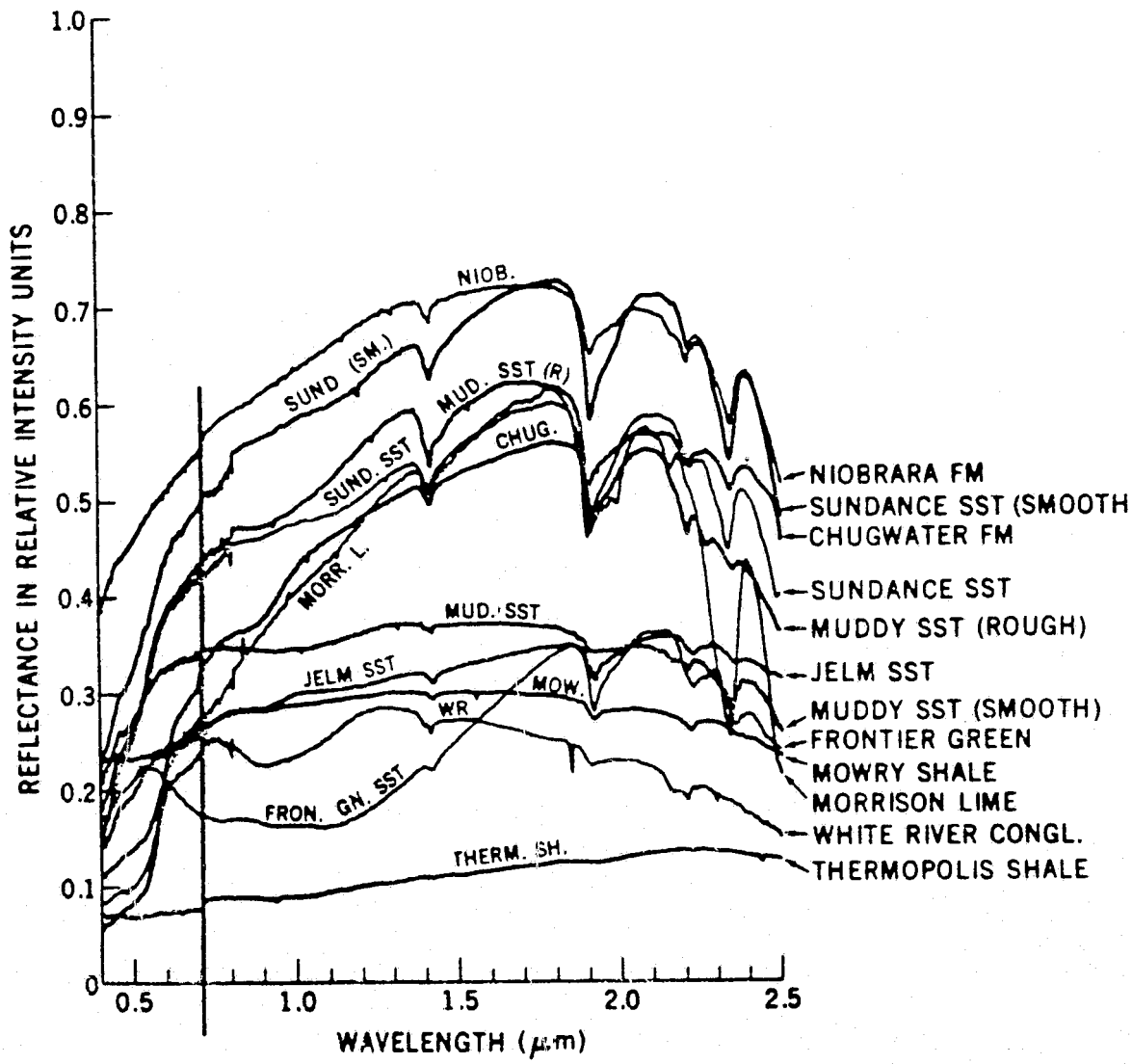
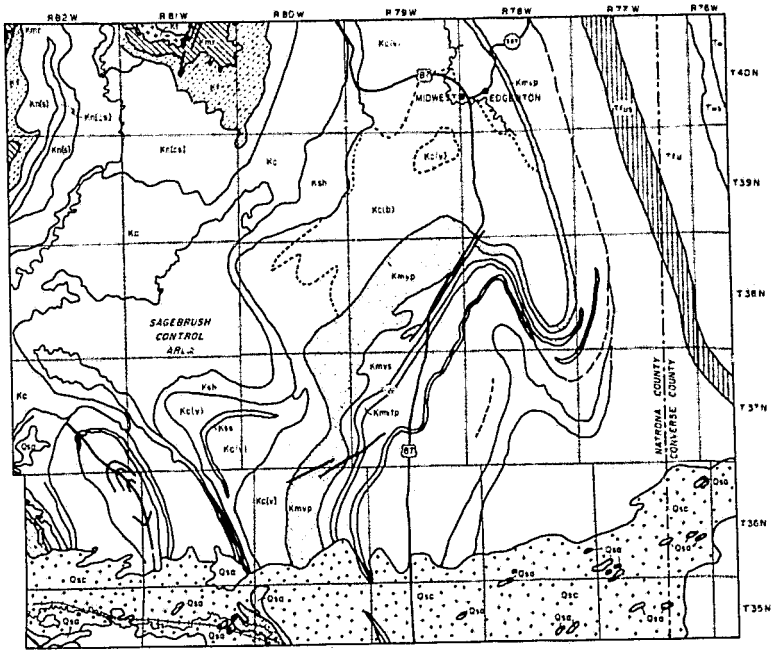


Figure E-2. Spectral response curves for a group of rocks from Wyoming determined on a Carey 90 reflectance spectrometer (from Short and Lowman, 1973, Fig. 30, p. 91).

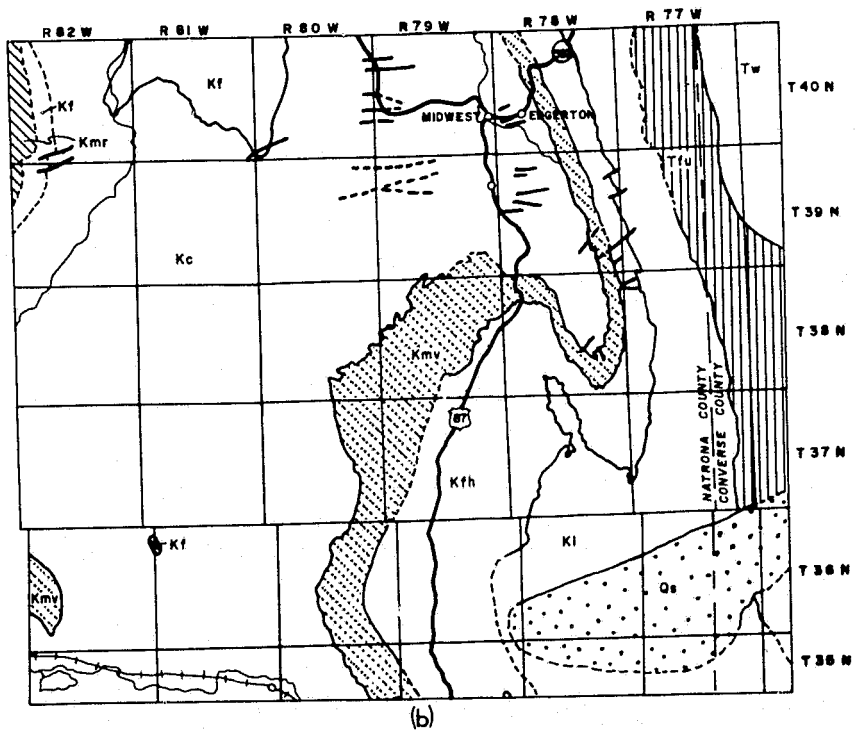
other units as the laboratory spectra predict and can be recognized through most of their outcrop area. Furthermore, with the advantage of color composite images, color can also be used for mapping. Throughout most of Wyoming, Permo-Triassic red beds make excellent marker units.

A geologic map of the Arminto area of central Wyoming was prepared from interpretation of an ERTS infrared color composite using a Bausch and Lomb zoom transfer microscope. When compared with the state geologic map, it was found that units mapped from tonal variations are surprisingly close to those chosen as formations by field geologists -- particularly since most of these major units are rock-vegetation units.

Figure E-3 compares the southeastern quarter of the Arminto AMS map with same area on the geologic map of Wyoming (Love and others, 1955). Much of this area has not been mapped in detail and no mapping is available in published or open-file form. The geologic map shows nine lithologic subidivisions whereas the ERTS photogeologic map shows twenty-five lithologic subdivisions. This area has not been fully field-checked so we cannot be certain that all subdivisions shown on the ERTS photogeologic map correspond to changes in lithology. The large area shown as Cody Shale (Kc) on the geologic map has been subdivided into several units; the areas shown as Kn (cs) and Kn (s) probably correspond to calcareous shales and shales of the Niobrara Formation. The area shown as Kc is typical Cody shale. The area shown as Kstc is the Shannon Sandstone member of the Cody Shale. The area shown as Kc (b) is Cody Shale with irregular vegetative cover. Finally, the lens shown as Kss may be the Sussex Sandstone member of the Cody Shale. The reason for the irregular vegetative cover on the Upper Cody Shale bed has not been determined but it Kc(b) does coincide with the location of a major oil field. The odd-shaped area in T. 38 N., Rs. 81 and 82 W. is an area where the natural vegetation has been disrupted by extensive spraying to kill sagebrush so its significance is probable not lithologic.



(a)



(b)

Figure E-3. Details of the southeast 1/4 of the ERTS Arminto map (A) compared with the same area on the state geologic map of Wyoming (B, after Love and others).

The Mesaverde Formation can also be subdivided into the Parkman Sandstone Member (kmvp), a shale unit (Kmvs), and an upper unit that is probably the Teapot Sandstone member (Kmvtp). Distinctions were also made within the Fox Hills Sandstone (Kfh) and Lance Formation (Kl), but their significance is not known. A unit designated (Tfus) may be a lower, massive sandstone of the Fort Union Formation and a unit designated (Tuss) may be a sandstone of the Wasatch Formation. Finally, stabilized sand dunes (Qsc), active sand dunes (Qsa), and alluvium (Qal) are readily mapped.

The southeastern quarter of the Arminto AMS sheet is particularly well suited for regional geologic mapping with ERTS color infrared because the various formations display good vegetation control, have low dips, and exhibit a fairly broad outcrop area. Other areas are not so suitable for mapping because dips are steeper, structure more complicated, and vegetation tends to mask rock types rather than enhance them.

Appendix F: Geologic applications of ERTS-1 in volcanic terrane.

summarized from a special report under contract NAS 5-21799
Breckenridge, R.M., 1973, Application of ERTS imagery to geologic mapping in the volcanic terrane of northwest Wyoming; National Technical Information Service, Springfield, Virginia, Report E74-10244, 21p.

Two of the largest volcanic provinces in the United States are located in Northwestern Wyoming; the Absaroka volcanic field and the Yellowstone Plateau. The Absaroka Range forms the southern part of the Absaroka field which extends north into the Gallatin Range of Montana (figure F-1). Generally the Absaroka Range consists of a large dissected plateau of layered Eocene volcanic flows, breccias and conglomerates, most of which are andesitic in composition. The Quaternary Yellowstone volcanics adjoin and cover the Absaroka field on the west. Unlike the Eocene eruptions, the Yellowstone volcanism was not violently explosive and accumulated a lava flows and ash flow tuffs. Together the two provinces provide an excellent test area of varied volcanic features.

Purpose and Method of Investigation

The purpose of this study was to evaluate ERTS-1 imagery in interpretation of various geologic features common to this region. Volcanic rocks are notoriously difficult to map. They generally lack sufficient stratigraphic markers and are characterized by rapid facies changes over short distances. Also much of the section is mineralogically homogeneous.

Although parts of the region are well-traveled and familiar to anyone who has visited Yellowstone National Park, most is wilderness area and extremely rugged. For a general discussion of the regional geology, the reader is referred to Keefer (1972); or, for a more detailed discussion, to Smedes and Prostka (1972) and Christiansen and Blank (1972). An ERTS interpretation of the glacial history of this same area was presented in an earlier report, Breckenridge (1973). A first look analysis of the area from ERTS was reported in Houston

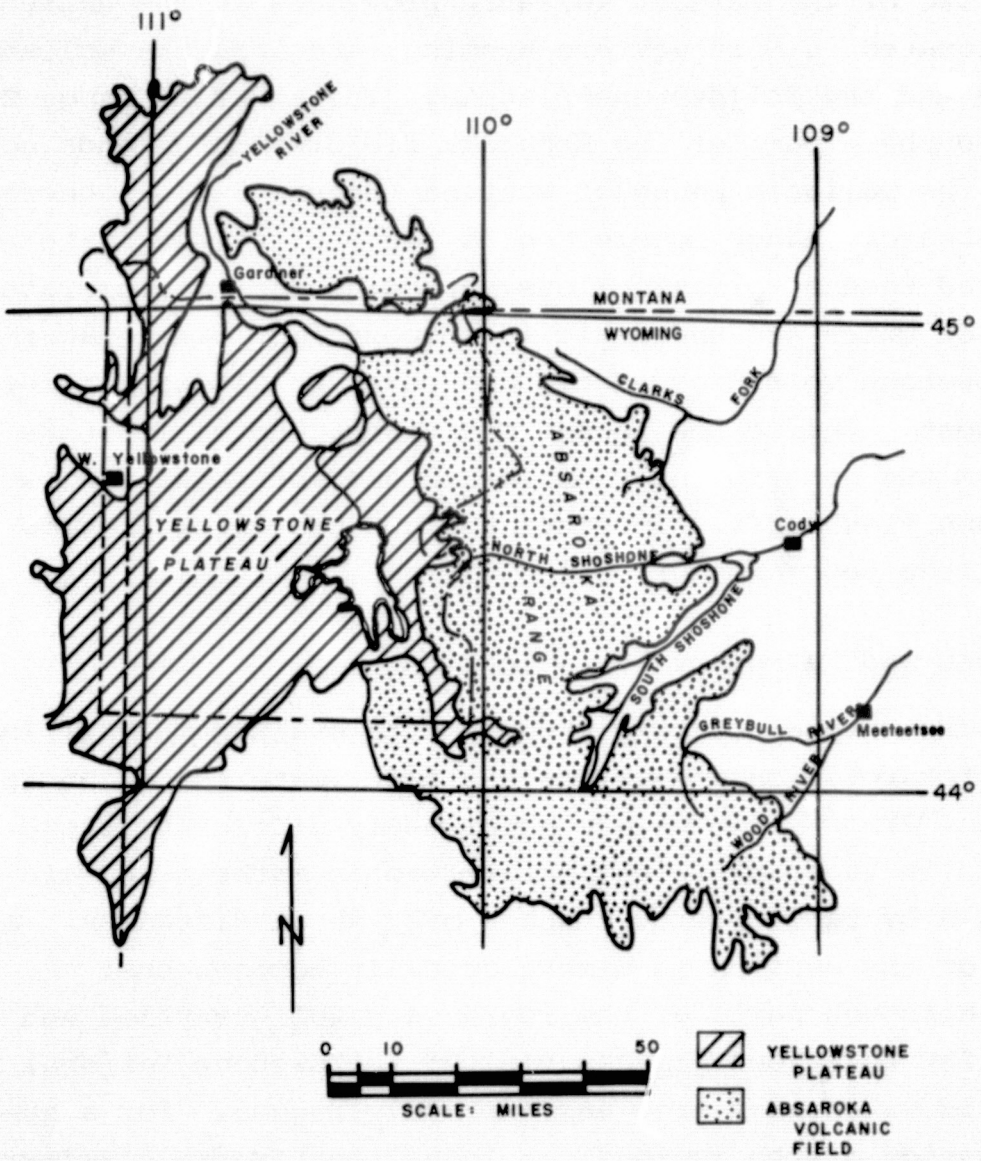


Figure F-1 Index map of volcanics in northwestern Wyoming. (After Renfro and Feray).

and Short (1973). Subsequent receipt of color conposites and application of other interpretive techniques has resulted in improved geologic interpretation.

Laboratory interpretations of the ERTS imagery were made using standard photogeologic techniques augmented by color-additive viewing and isodensity contouring. Several small areas within the main test site were checked in the field in order to confirm the image interpretations. Spectral reflectances of representative rock outcrops were obtained with a multi-channel filtered photometer. Each channel was calibrated by reading a reference grey card at the outcrop. Data were collected in spectral bands corresponding to ERTS bands 4, 5, 6, and 7. Limited time and accessibility permitted field checks of only a small portion of the study area, but it seems reasonable to assume that the interpretation has approximately the same reliability for the entire area as was demonstrated in the areas that were field checked. In some areas aircraft imagery was available as an additional check.

At first an effort was made to restrict the map interpretations to features which any trained photogeologist could recognize, but the author's familiarity with the area precluded an unbiased judgement. However, it is apparent that much extremely useful information could be derived from the ERTS imagery by an interpreter who is more than casually familiar with the area under investigation. For the purpose of this study, all existing knowledge of the region was used to benefit the conclusions.

Structure

An ERTS band-7 mosaic was constructed for the area to facilitate a uniform regional geologic interpretation of the area (figure F-2). Several major structural features and numerous smaller structures were mapped in the ERTS image interpretation. Most of the obvious structural features are in the sedimentary units along the margin of the Bighorn Basin. The largest structural feature noticeable on the imagery is the Yellowstone caldera (figure F-3). The caldera is so large an ill-defined that it cannot be recognized from the ground and, in fact, was not known until the late 1950's

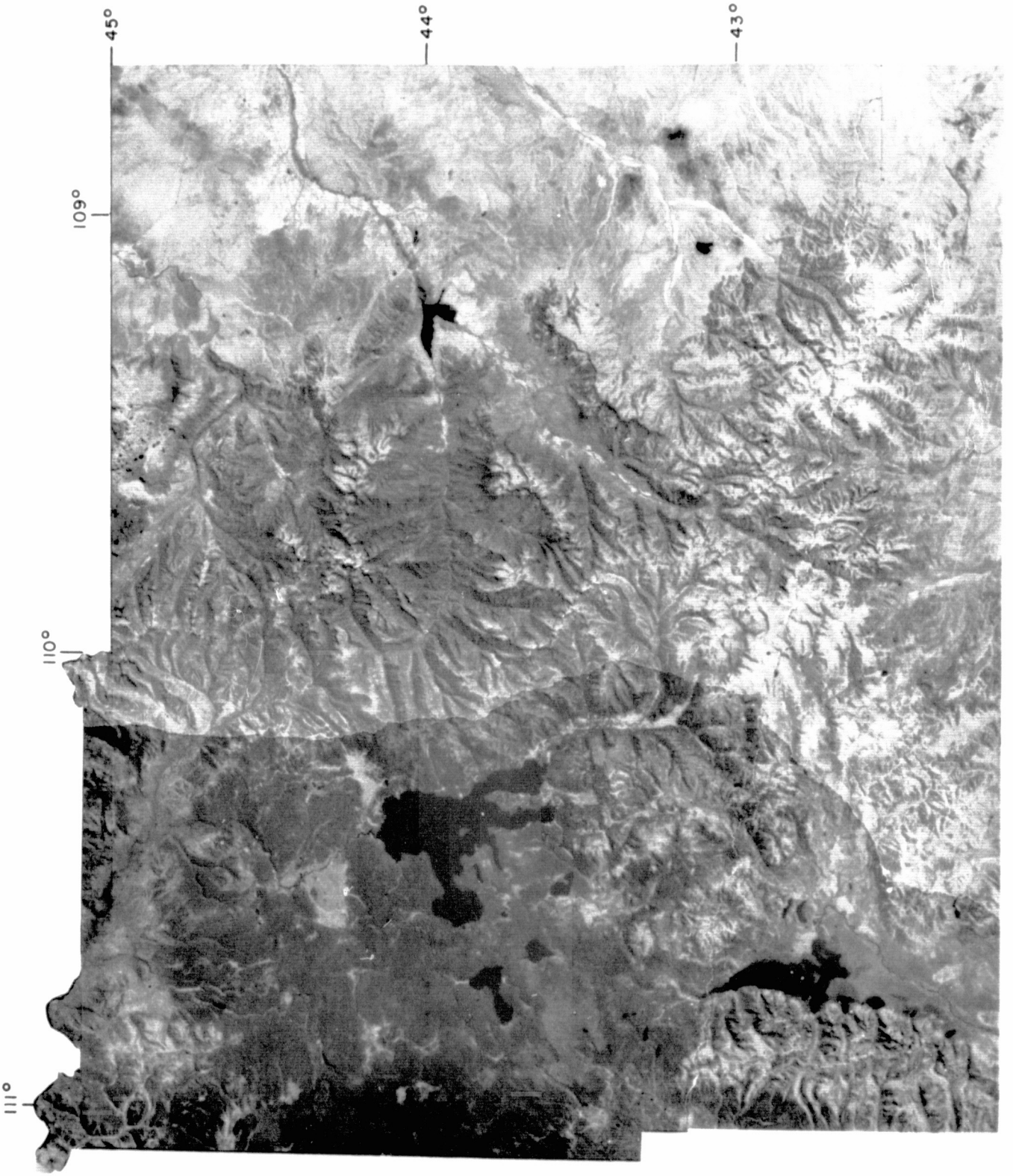


Figure F-2 ERTS-1 MSS-7 Mosaic of northwestern Wyoming

ORIGINAL PAGE IS
OF POOR QUALITY

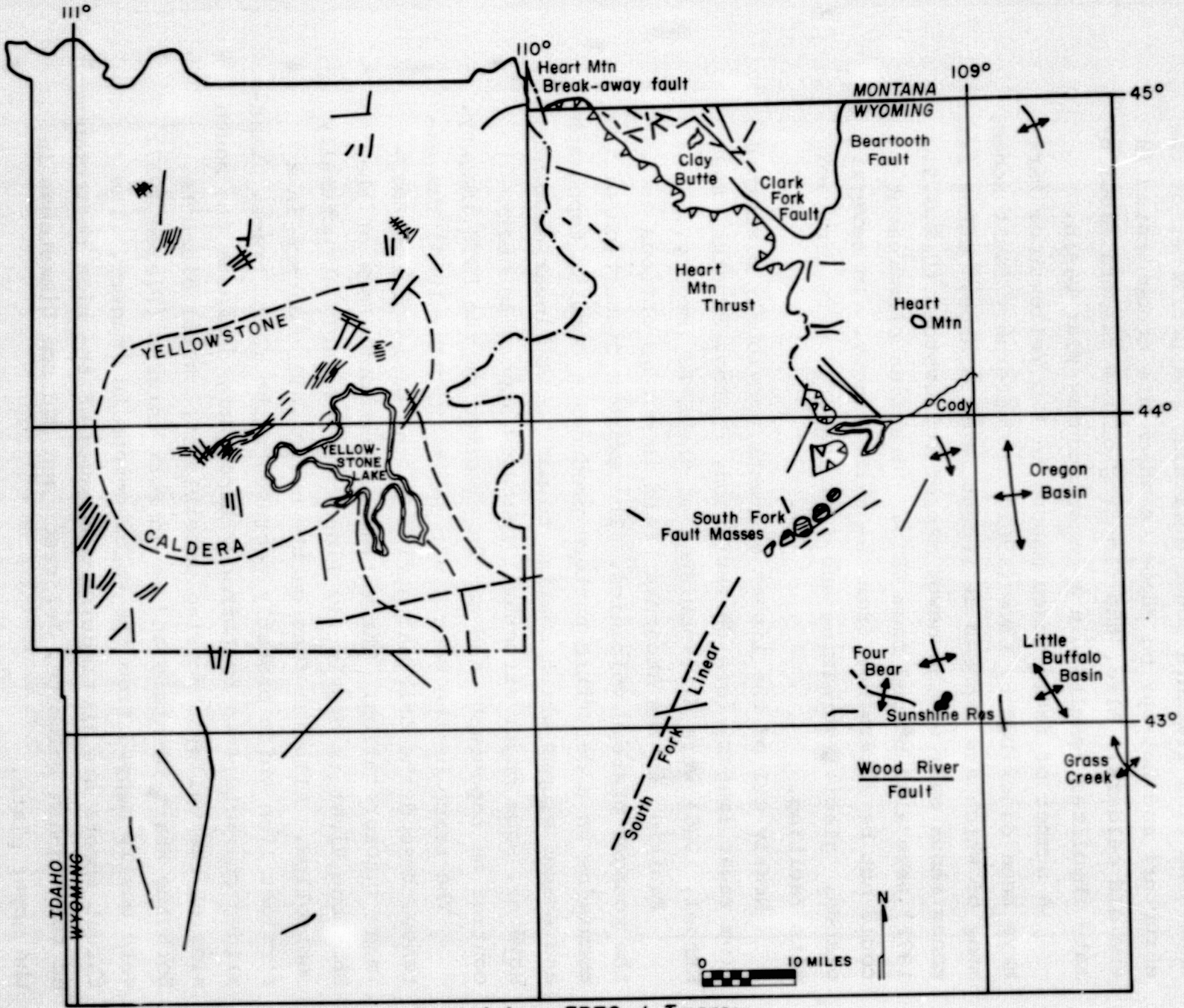


Figure F-3 Structural features interpreted from ERTS-1 Imagery

(Keefer, p. 34-42). Recognition of the feature on the imagery is possible primarily because of the series of topographically expressed ring fracture zones outlining the perimeter of the structure and hot-spring deposits which are concentrated in the old caldera. Also, the flooding of the caldera floor by late rhyolites resulted in a conspicuously flat basin.

A number of fault zones mapped in the Yellowstone Park have been described by Love (1961) as Quaternary fault zones, many of which are exposed as recent fault scarps. Other fault zones shown only on the newer map of Yellowstone (U.S.G.S., 1972) were also mapped from ERTS. Direction of movement could not be determined from the ERTS imagery. In several places, glacial streaming and flow features were confused with faulting.

Nearly all of the linear elements previously discerned from radar imagery (see Christianson, Pierce, Prostka, and Ruppel, 1966) were distinguished of the ERTS imagery.

Faulting in the Absaroka Field is not as obvious as in the younger plateau volcanics. The extreme dissection of the mountains in a dendritic pattern produces a complex topography and shaded slopes which combine to mask most linear elements. However, some major structural features appear to exert control on topography and can be observed on the ERTS imagery.

The trace of the Wood River fault (Wilson, 1964) was extended beyond the original strike on the basis of the ERTS-image interpretation. The valley of the South Fork of the Shoshone River is distinctly linear and probably structurally controlled. Alluvial fans on the north wall coalesce in a straight line which probably represents the fault trace. Landslides characterized by hummocky topography dominate the south side of the valley obscuring possible structural elements. Both the Heart Mountain and South Fork thrusts (Pierce,1957) were easily mapped from the color composite imagery. The thrust sheets are distinguished because of the high reflectance of the Bighorn Dolomite, Jefferson and Madison Limestones in the upper plate.

A number of other "linears", or linear elements suggestive of faulting were recognized and are shown on the map, but were not checked this field season because of difficult access and time limitation.

Lithologic Distinctions

As previously mentioned, the Absaroka volcanic field is a highly dissected plateau of vent- and alluvial volcanic facies. Although compositions vary from andesite to basalt most rocks are andesitic. A wide range of textures occur in the volcanic pile. The stratigraphic nomemclature of the region has a long and complicated history which is treated by Smedes and Prostka (1972).

The stratigraphy of the Yellowstone Plateau volcanics has been recently summarized by Christianson and Blank (1972). The more subdued topography and heavy vegetation of the plateau area combine to limit exposures of the Yellowstone volcanic sequence, but some recent flows can be mapped by recognition of flow-lines, fronts, topographic position, and pressure-ridges.

Differentiation of volcanic, sedimentary, igneous and metamorphic lithologies was best accomplished by using a standard color-composite ERTS image. The Absaroka volcanics have a distinctily dark-brown color and appear much as they do in outcrop. The more mafic units have a characteristic dark blue tone on the color composite ERTS image. Similar drab colors identify the Yellowstone volcanic rocks when they are not obscured by vegetation. The plateau volcanics are most easily differentiated by their flow features, such as pressure ridges and steep fronts. Older crytalline rocks in the Beartooth and Teton Ranges have high reflectance in Band 7 and exhibit numerous joints. The crytalline blocks are often bounded by large faults. Sedimentary rocks in the Bighorn Basin are characterized by bedding, structure, and light tone. Figure F-4 shows the distribution of major rock types in the area. In some cases, the eastern contact of the volcanic rocks was difficult to define because large volcanic-covered pediments lap out over the sedimentary units of the

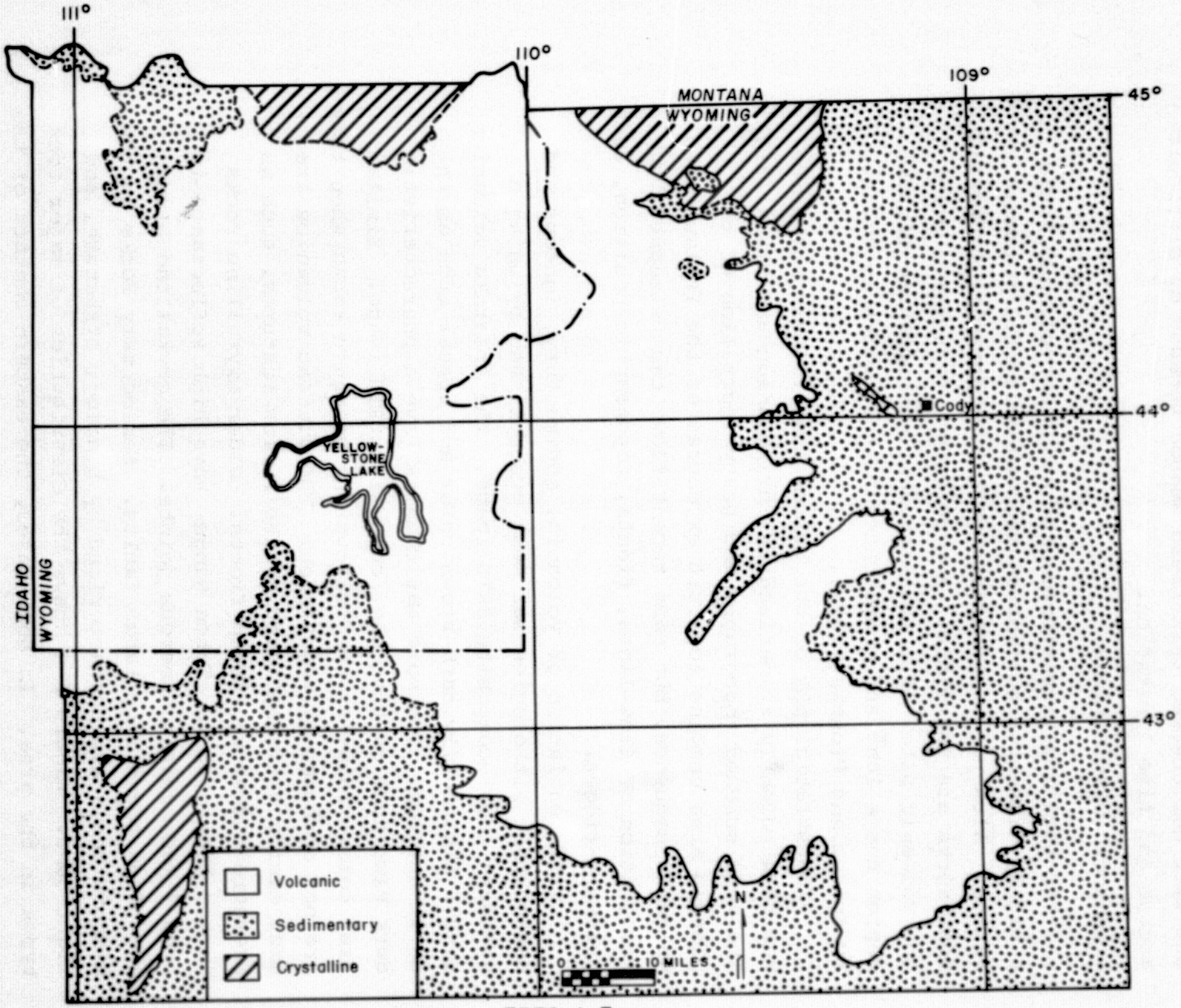


Figure F-4 Major rock types mapped from ERTS-1 Imagery

Lithologic distinctions within the volcanic sequence were best accomplished with band 7 images used in conjunction with a corresponding color composite. Initial field examinations were somewhat disappointing. Units readily recognized in the field could not be distinguished on the imagery. Careful examination of the problem revealed that most of the units were differentiated in the field on the basis of mineralogic texture and outcrop form. For example, some breccias were coarse and massive while others were fine and thinly bedded, and some were chaotic with interbedded lenses while others were uniform. Yet all of the mappable units are similar in composition and spectral response. In addition, many of the better exposures occur in near-vertical walls and are not imaged by vertical-looking sensors. The small-scale textural differences could not be resolved at ERTS scale. However, the cumulative effect of frequent ledges, "hoodoos," lenses, flows, etc. results in large changes that are detectable on the ERTS imagery. After the initial field check the meaningful distinctions reflecting different formation surface textures could be more confidently identified on the imagery and the interpretations improved accordingly.

At the South Fork test site the Wapiti Formation was successfully subdivided into three units similar to those mapped by Pierce and Nelson (1969): 1) an upper series of flows and flow breccias, 2) a middle mafic breccia, and 3) a lower, light-colored volcanic sandstone, siltstone, and conglomerate. Again, the major difference between the flows and breccias is textural or topographic, but the fine-grained volcanic sandstone and siltstone has an anomalously high reflectance and appears light on the image. Spectral response of each rock type was measured in the field for the ERTS and EREP bands (Table F-1). All of the values represent an average of at least 5 readings over a large outcrop. Since the field of view was small (100 sq. ft. or less), these values cannot

	ERTS				EREP		
	4	5	6	7	OC	PP	QQ
INTRUSIVES							
Latite dike (Wood R.)	17.0	18.0	17.5	20.0	17.5	16.5	19.0
Latite dike (N. Fork)	13.0	20.0	20.0	21.0	20.0	21.0	19.0
dike (S. Fork)	21.0	25.0	24.0	22.0	21.0	24.0	23.0
Andesite (Funnel Mtn.)	12.0	9.0	11.0	15.0	11.0	8.0	9.5
BRECCIAS AND FLOWS							
Early Basic Breccia	17.5	18.5	21.0	19.0	20.0	20.5	20.0
Wiggins Fm.	12.0	11.0	11.0	10.0	13.0	13.0	12.0
Crosby Breccia	17.0	18.0	19.0	21.0	18.0	19.5	20.0
Crosby Breccia (green facies)	19.0	21.0	22.0	16.0	24.0	21.0	28.0
Wapiti Fm. (Twb) "breccia"	18.0	20.0	20.0	20.0	16.0	19.0	21.0
Wapiti Fm. (Tws) "flows"	21.5	27.0	26.0	22.0	21.0	25.0	24.0
Wapiti Fm. (Twj) Jim Mtn. Member - Trachyandesite	20.0	24.0	22.0	21.0	19.0	21.0	21.0

Table F-1. Filtered Photometer Readings From Major Lithologies of the Yellowstone-Absaroka Test Site

Note: Values represent uncorrected photometer readings rather than absolute reflectances. Consequently they reflect only qualitative differences between the measured units.

reflect the overall effect of ledge-shadowing or vegetation. Consequently, the field-measurements minimize the weathering characteristics of particular rock types and probably maximize the compositional similarities. They also demonstrate that these rocks have a relatively flat spectral response.

Multiband photography was taken at the outcrop to further evaluate possible enhancement of volcanic lithologic units. Figure F-5 shows a section of pyroclastic rocks in the Wood River test site. To the right of each image is a densitometric curve for that image. As can be seen from the curves, all of the rock units have a relatively uniform reflectance through this part of the spectrum. Consequently, multiband enhancement of the pyroclastic rocks is limited.

Intrusive Rocks

The volcanic flows, breccias and tuffs of the region are intruded by numerous intrusives, ranging from dikes a few feet thick to large plutons. In general, the larger intrusive bodies are much lighter in tone on all ERTS bands than the surrounding pyroclastics. Parsons (1963) recognized seven major vent areas in the Absaroka Range. Figure F-6 shows the intrusives mapped from ERTS. Since some of the intrusions are covered with vegetation or occur on shadowed north sloped, they were not recognized on the ERTS interpretation. A number of intrusions not mapped on black-and-white ERTS images (Houston and Short, 1972) were readily distinguished on the color-composites.

Most of the major vents are centers of extensive dike swarms. Unfortunately, most of the dikes could not be resolved at ERTS scale. Several of the larger dikes in the North Fork Valley were mappable.

Mineralized Zones

Several mining districts in the Absarokas are associated with intrusive activity. The Kirwin-Wood River area was

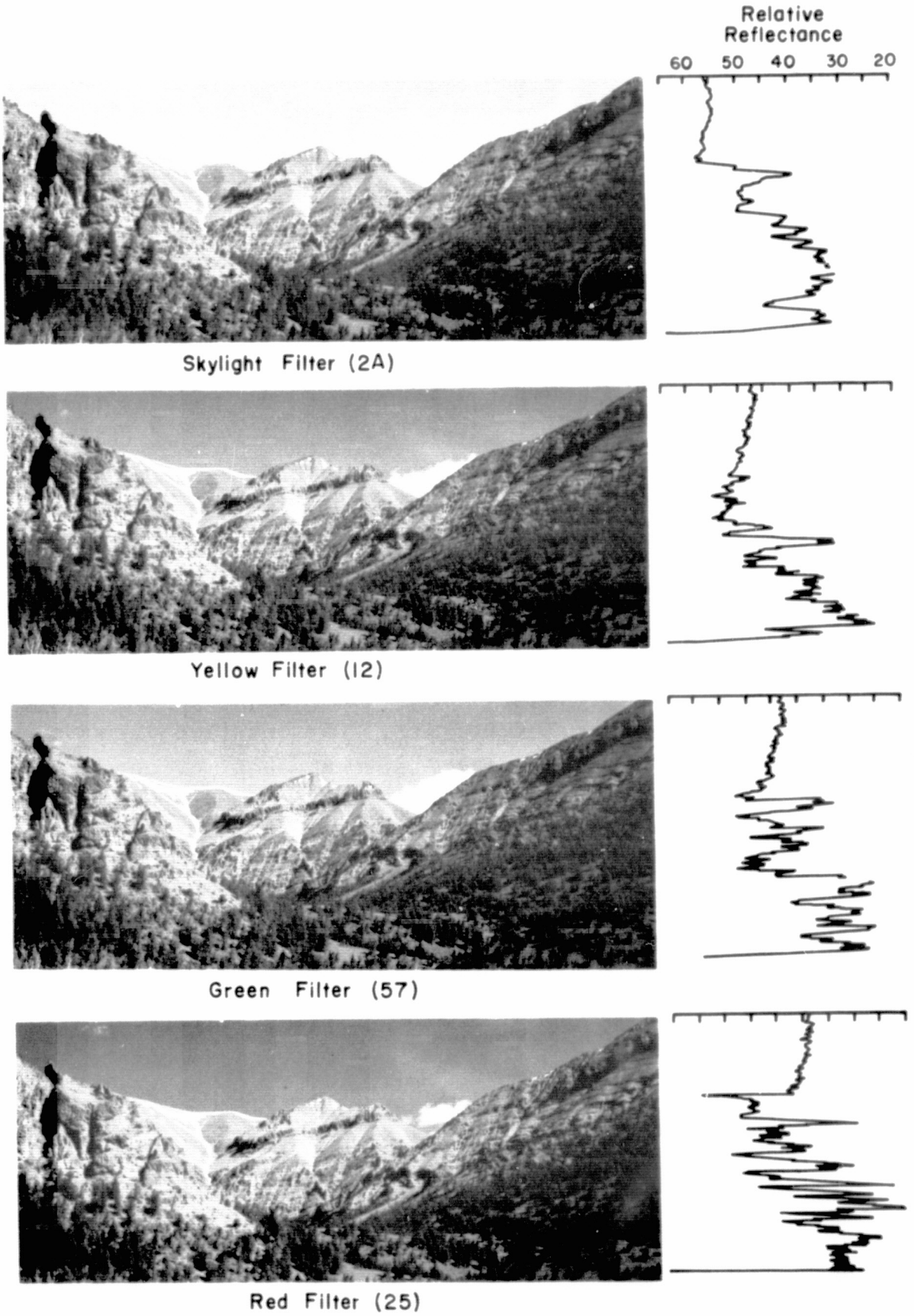


Figure F-5 Multiband photography of Wood River test site

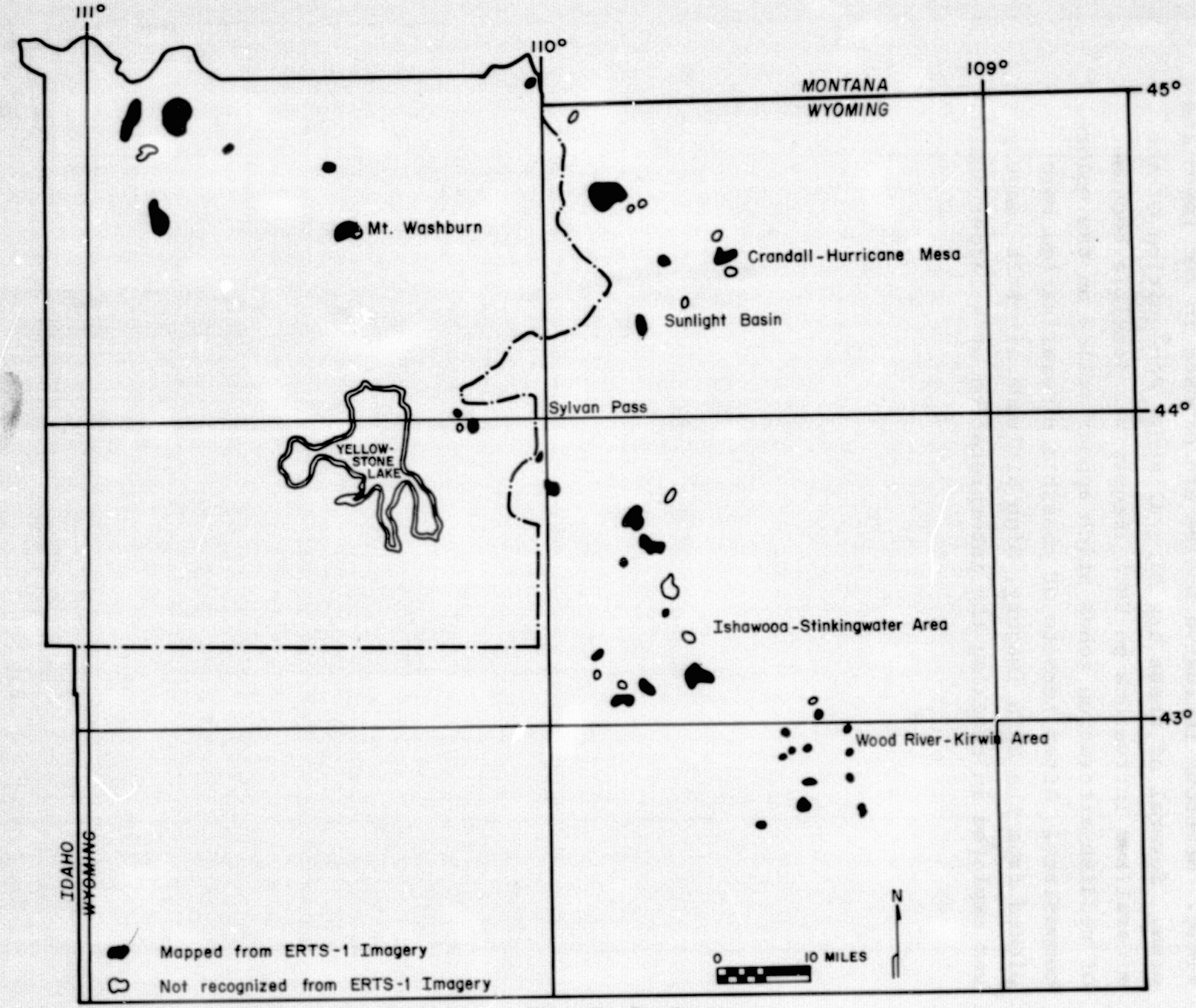


Figure F-6 Intrusives in the Yellowstone - Absaroka Provinces

chosen as a test site for ERTS imagery interpretation. The Kirwin area is one of the major vent centers in the volcanic field. Numerous intrusive bodies are exposed in the immediate area. Several of these are mineralized. Recognition of the mineralized intrusions on ERTS imagery was possible because of reddish alteration zones which appear yellow on the color-composites. After targets of possible mineralization were picked from the ERTS imagery, high altitude aircraft imagery was employed in checking the interpretation at a larger scale.

Appendix G: Geologic map of Carbon County, Wyoming interpreted from ERTS-1 imagery.

from an unpublished report:
Agard, S. S., 1974, Carbon County geologic map interpreted from ERTS-1 imagery; University of Wyoming, Department of Geology, unpublished special project report.

Purpose

The purpose of this study was to map the bedrock and surficial geology of Carbon County, Wyoming, using ERTS-1 imagery, and to determine the accuracy and detail of the information obtained (Plate G-1).

Location

Carbon County encompasses nearly 8,400 square miles of central and southeastern Wyoming (Fig. G-1). It is a geologically diverse area with features ranging from large Precambrian-cored uplifts to small complexely folded structures to large areas of flat-lying Tertiary formations. Regionally, it includes the northernmost part of the Southern Rocky Mountain Province and a major portion of the Wyoming Basin Province. The former is characterized by the broad anticlinal uplifts of the Sierra Madre/Park Range and the Medicine Bow Mountains where large expanses of Precambrian are exposed. The Wyoming Basin in this area consists predominantly of Tertiary-filled basins interrupted and complicated by smaller uplifts such as the Rawlins, Ferris, Seminoe, Shirley and Freezeout Mountains. Older Tertiary formations are often involved in these structural disturbances while younger Cenozoic units are undisturbed. Clastic Quaternary deposits, including large areas of sand dunes, playa lakes, evaporites, glacial drift and alluvium occupy much of the surface area.

Methods

Using a Bausch and Lomb zoom transfer scope (ZT-4) positive 9" by 9" ERTS transparencies were superimposed on

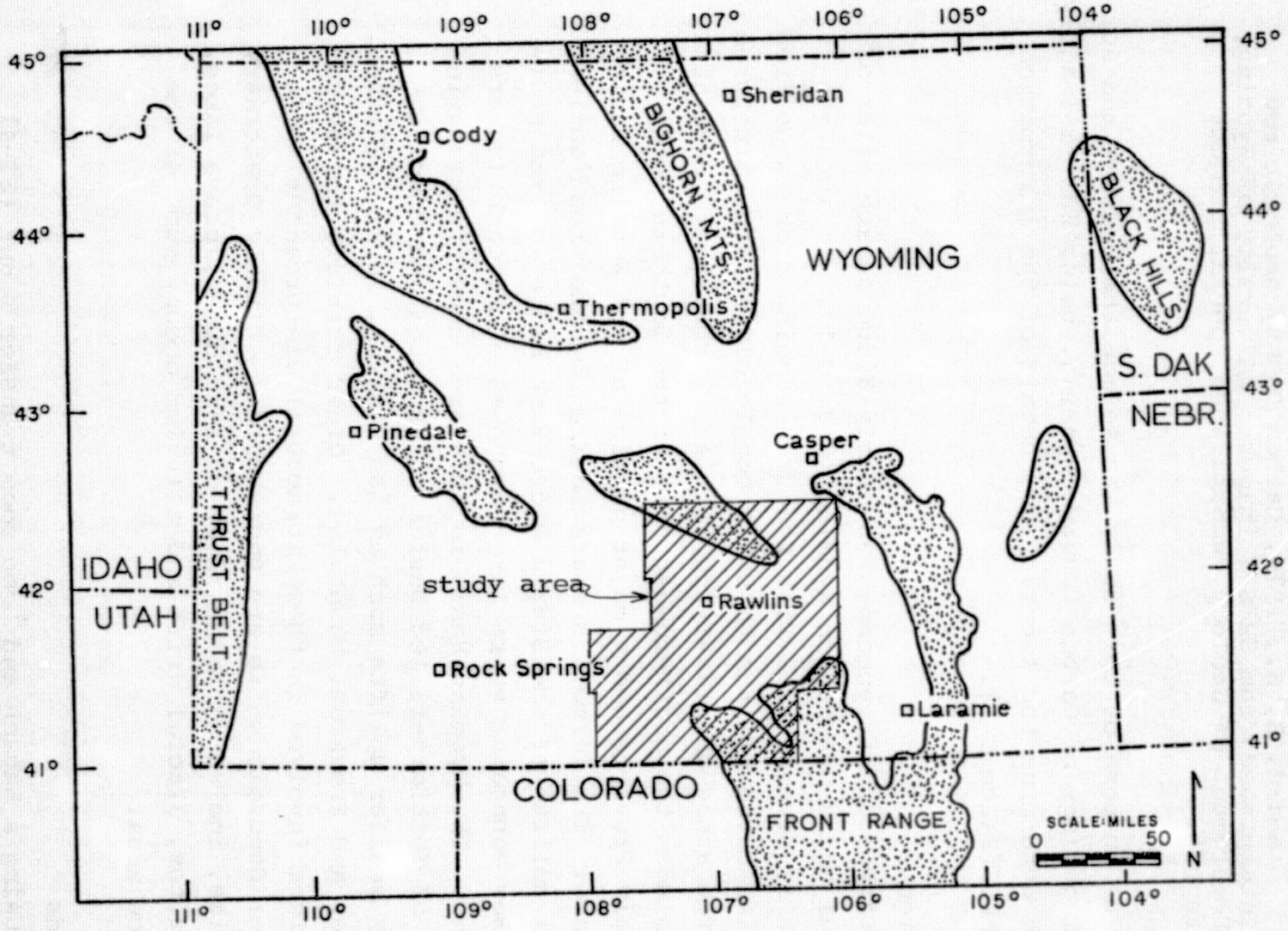


Figure G-1. Index map of the Carbon County Study area.

a base map (scale 1:250,000) compiled from the AMS 2^{o} series. The images used were:

1408 - 17235 4 Sep 73
1353 - 17190 11 Jul 73
1030 - 17242 22 Aug 72 MSS Color Composite
1030 - 17244 22 Aug 72 MSS Color Composite
diazo color composite of 1353 - 17190

Color composites were used when available because the contrasting colors of the units provide the best means for differentiating them. In areas of low color-contrast such as the outcrop areas of Upper Cretaceous and Tertiary units in the western portion of Carbon County, two identical color composite images were superimposed and used as one in order to increase the depth of color and contrast. Black and white images were used for areas in which the color composite coverage was obscured by cloud cover and for the eastern quarter of the county where color composites were not available. Band 5 was used most extensively in these areas since it usually yields the greatest tonal contrast between lithologic units. Band 7 has slightly less contrast but is particularly useful in the heavily vegetated mountain areas which are too dark on the band 5 images. A diazo color composite of the eastern portion of Carbon County yielded good information when used in conjunction with the black and white images. However, the resolution of the diazo composite was too poor for accurate work in geologically complex areas.

Descriptions of Units

The units described below are identified by both their map unit number and the name of the corresponding geologic formation. The photo map units were correlated with the formations using prior knowledge of the geology of the area and by relating the photomap units to the State Geologic Map of Wyoming (Love and others, 1955) and the stratigraphic nomenclature chart (Figure G-2). These correlations are tentative because they have not yet been field checked for

SOUTH CENTRAL WYOMING STRATIGRAPHIC NOMENCLATURE CHART

			WIND RIVER BASIN	RAWLINS UPLIFT, GREAT DIVIDE, WASHAKIE BASIN	LARAMIE-HANNA BASINS
CENOZOIC	TERTIARY	PLIOCENE		NORTH PARK	NORTH PARK
		MIOCENE	UNNAMED BEDS	BROWNS PARK	BROWNS PARK
		OLIGOCENE	WHITE RIVER	WHITE RIVER	
		EOCENE	TEPEE TRAIL AYCROSS	BRIDGER	HANNA
				GREEN RIVER	
			WIND RIVER	WASATCH	
		PALEOCENE	FORT UNION	FORT UNION	FERRIS
MESOZOIC	UPPER CRETACEOUS		LANCE	LANCE	MEDICINE BOW
			MEETEETSE	LEWIS	LEWIS
			MESAVERDE	MESAVERDE	MESAVERDE
			CODY	STEELE	STEELE
				NIOBRARA	NIOBRARA
				CARLILE	CARLILE
			FRONTIER	FRONTIER	FRONTIER
			MOWRY	MOWRY	MOWRY
	LOWER CRETACEOUS		Muddy THERMOPOLIS	Muddy THERMOPOLIS	Muddy THERMOPOLIS
			CLOVERLY, MORRISON UNDIVIDED	CLOVERLY: DAKOTA, FUSON, LAKOTA	CLOVERLY: DAKOTA, FUSON, LAKOTA
	JURASSIC	UPPER		MORRISON	MORRISON
			SUNDANCE	SUNDANCE	SUNDANCE
		MIDDLE	GYPSUM SPRING		
		LOWER	NUGGET SANDSTONE	NUGGET SANDSTONE	JELM
	TRIASSIC		CHUGWATER: POPO AGIE, ALCOVA, RED PEAK	CHUGWATER: JELM, ALCOVA, RED PEAK	CHUGWATER
			"EMBAR": DINWOODY	DINWOODY	
PALEOZOIC	PERMIAN		"EMBAR": PHOSPHORIA	PHOSPHORIA	FORELLE ? SATANKA
	PENNSYLVANIAN		TENSLEEP	TENSLEEP	CASPER
			AMSDEN Darwin	AMSDEN	FOUNTAIN
	MISSISSIPPIAN		MADISON	MADISON	MADISON
	DEVONIAN		DARBY		
	SILURIAN				
	ORDOVICIAN		BIGHORN		
			LANDER SANDSTONE		
	CAMBRIAN	UPPER	GALLATIN	DEADWOOD	DEADWOOD
		MIDDLE	GROS VENTRE, FLATHEAD		
		LOWER			
	PRE-CAMBRIAN		GRANITE	GRANITE	GRANITE

Figure G-2. Stratigraphic nomenclature chart for the Carbon County area (after Brinker and Blackstone, 1951).

ORIGINAL PA

accuracy. The nomenclature used is that of the 1955 Geologic map of Wyoming although some of the units have since been renamed or reclassified.

In general, the Paleozoic and Mesozoic units are exposed only on the flanks of the Precambrian-cored uplifts or in complexly faulted areas nearby. They are consistently thin units and are sometimes difficult to map in detail. They are usually distinct in character and color from adjacent units, but often the characteristics of a unit in one area do not carry through to other areas. The differences are primarily a function of locally different structural attitudes, elevations, vegetal cover, angle to sun, soil moisture and related factors. In such cases, the succession of units may be inferred from the location of a few consistently identifiable units. The Upper Cretaceous and Tertiary units are more uniformly characteristic and could often be directly correlated from one area to another.

The descriptions presented are based purely on the appearance of the units on the images used. Thus, they are tied to the particular times of year that the images were recorded and to the specific color processing used in creating the color composites. Different descriptions and somewhat different results might be obtained using other images.

Unit 1 - Precambrian is exposed in the core of the Sierra Madre, Medicine Bow, Ferris, Seminoe, Shirley, Pedro, and Elk Mountains. The Precambrian rocks generally have a crystalline appearance, exhibit few sedimentary features and are heavily vegetated. They are characteristically deep brownish-red in color. Smaller features, like glacial drift, alluvium or sedimentary remnants within the area, cannot be distinguished against the dark background.

Unit 2 - (Cambrian) is found in contact with Unit 1 on the flanks of the Rawlins, Ferris and Seminoe Mountains. The photomap unit may actually include some thin units of the younger Madison Formation. In the Ferris and Seminoe Mountains the Cambrian rocks have a deep red color (darker than Unit 1) in sharp contrast to lighter colored younger units.

In the Rawlins area, Unit 2 is a lighter, mottled, reddish-brown color. This color seems to reflect sparse tree cover.

Unit 3 - (Carboniferous Madison Fm.) occurs in the Rawlins and Shirley Mountain areas. In the Rawlins region, it is the lightest colored unit in the area as contrasted to Unit 2 and the overlying Tertiary unit. In the complex structure of the Shirley Mountains, Unit 3 forms a relatively barren light colored marker unit contrasting with heavily vegetated Units 1 and Unit 4.

Unit 4 - (Carboniferous Tensleep Fm. and Amsden Fm.) is a marker unit used in correlating the sequence of lower units in different areas. It appears as a prominent, thin, white band in the Rawlins, Ferris and Seminoe Mountains and to the west of Elk Mountain. It is also striking, though somewhat darker in tone, due to vegetation in the Shirley and Freezout Mountains.

Unit 5 - (Carboniferous undifferentiated) includes units 3 and 4 described above where they could not be individually distinguished. These areas, such as the region north of the Medicine Bow Mountains, were heavily vegetated giving a reddish hue to Unit 5.

Unit 6 - (Permian Phosphoria Fm. or Forelle and Satanka Fm.) is located in the Rawlins, Ferris, Seminoe and Freezout Mountains, and near Slate Ridge. In all areas, it has a yellowish-green color which is usually greener than surrounding formations. Variation in actual hue and sharpness of the contact occurs from region to region.

Unit 7 - (Triassic undifferentiated) represents the red-bed sequence of the Rawlins, Ferris and Freezeout Mountains. It has a characteristic yellow color with a slight green tint in some areas. Unit 7 includes the Chugwater, Dinwoody, and some parts of the Phosphoria Formation.

Unit 8 - (Jurassic Undifferentiated) is located in the Ferris, Rawlins, and Slate Ridge uplifts. The light turquoise blue color is fairly even and forms a distinct contact with

other units. The Nugget Sandstone, and the Sundance and Gypsum Springs Formations make up this unit.

Unit 9 - (Jurassic Morrison Fm. and Cretaceous Cloverly Fm.) is found in the same areas as Unit 8. Its color varies from a mottled, light greenish-yellow in the Rawlins area to light, blue-green elsewhere. It is generally lighter than surrounding units.

Unit 10 - (Jurassic-Cretaceous Morrison, Cloverly & Sundance Fms.) includes Units 8 and 9 in areas where they are indistinguishable or too thin to be mappable. Unit 10 was mapped in the Freezeout Mountains and Como Ridge. It appears light turquoise in color.

Unit 11 - (Cretaceous Muddy & Thermopolis Fms.) was mapped as two subunits in the Rawlins-Grenville Dome area. The older unit (11a) is dark blue while unit (11b) is a lighter blue-grey. The two subunits were indistinguishable in the Ferris and Freezeout Mountains and by Slate Ridge and Como Ridge. Here Unit 11 is light green in color.

Unit 12 - (Cretaceous Frontier Fm.) also appears as two units in the Rawlins-Grenville Dome area. Both are fairly consistent light blue with unit 12a being slightly darker. Elsewhere it is mapped as one unit, somewhat more blue in color than Unit 11.

Unit 13 - (Cretaceous Niobrara Fm.) was mapped in the northeast part of the county along the outer flanks of the Shirley Mountains, Slate Ridge and Como Ridge. It is highly mottled with brown, tan, and blue colors, and does not always form a distinct contact with younger units.

Unit 14 - (Cretaceous Cody Fm. or Steele Fm.) forms wide topographic low areas around the outer flanks of the uplifts. It is found throughout the county as a very light colored, sometimes mottled unit. It contrasts sharply with the generally well defined bluish colored older units and the prominent brown ridges of Unit 15.

Unit 15 - (Cretaceous Mesa Verde Fm.) occurs as a prominent ridge system around the major uplifts. It is easily traced from one region to another and so forms a good marker unit

for correlation. In some areas as many as six distinct subunits can be seen (as in the Sheep Mountain-Syverson Flats area). These become less distinct and grade into one another as the local structure changes; steep dips decrease the number of mappable subunits. All subunits of the Mesaverde Formation are different shades of brown and grey. Unit (15c) is generally darkest in color and most continuous in character from region to region. Other subunits are lighter, more mottled, and regionally more variable.

Unit 16 - (Cretaceous Lewis Fm.) is found throughout the region in contact with Unit 15. It forms areas of low relief adjacent to the ridges formed by Unit 15 and is usually very light brown in color.

Unit 17 - (Cretaceous Lance Fm.) was mapped in the western part of the county as a gently dipping hogback extending from near Lamont to Baggs. It is mottled light brown and tan, and is sometimes indistinguishable from surrounding units.

Unit 18 - (Cretaceous Medicine Bow Fm.) is located in the areas surrounding the Hanna Basin. To the east of the Haystack Mountains, it is a light tan color with a slight olive tint. In the Saddleback Hills area, it is a much darker brown-grey and more mottled in appearance.

Unit 19 - (Paleozoic-Mesozoic undifferentiated) groups the above units (2 - 19) in areas too small to show detail or where individual units were not distinguishable.

Unit 20 - (Tertiary Ferris Fm.) flanks the structural depression of the Hanna Basin. Its coloring is similar to that of Unit 19 but is generally darker than the underlying units.

Unit 21 - (Tertiary Ferris Fm.) extends from Separation Flats south towards Baggs. In places as many as three distinct subunits are seen. The lower unit is consistently light grey-brown through the area. The middle and upper units vary from a dark brown in the north to a bluish-green or bluish-brown in the south. The middle unit is usually darker than the upper unit but the distinction is gradational in places.

Unit 22 - (Tertiary Hanna Fm.) is the most prominent unit of the Hanna Basin. Its appearance is highly mottled with blue, green and brown. Variations in color indicate subunits within Unit 22 and were used to trace possible structures within the area. Some of the apparent structures may be related to the local topography rather than true structure. Stereoscopic study of these areas might help solve this ambiguity.

Unit 23a - (Tertiary Wind River Fm.) was mapped in the northeast part of the county around Bates Hole and the Shirley Mountains. It is a mottled blue grey and tan as contrasted with the more even coloration of surrounding units.

Unit 23b - (Tertiary Wasatch Fm.) is located along the flank of the Washakie Basin forming a large flat lying region. It is mostly yellowish brown with several discontinuous units of darker blue and brown which may reflect subtle changes in lithology.

Unit 24 - (Tertiary Green River Fm. - Tipton member) forms the outer unit rimming the Washakie Basin. It is a relatively dark blue grey with even coloring and texture. To the northwest it becomes somewhat lighter in color.

Unit 25 - (Tertiary Wasatch Fm. - Cathedral Bluffs member) is also located on the flanks of Washakie Basin. The prominent bright yellow color is characteristic in the area. To the northwest the ridge appears to show two mappable units, one bluish-grey and the other a mottled bright yellow.

Unit 26a - (Tertiary Green River Fm. - Morrow Member) forms a highly dissected ridge (badlands?) in the Washakie Basin. The comparatively dark brownish-green color appears mottled due to local topography.

Unit 26b - (Tertiary Green River Fm. - Laney member) is a slightly yellowish buff color in contrast to the much darker underlying units. The coloration is more even, suggesting less dissection of this part of the ridge.

Unit 27 - (Tertiary undifferentiated) includes most of the unfolded flat-lying units in the county. In the north unit 27 is dark grey with blue or red hues locally present along the flanks of the Ferris, Seminoe, Pedro, Shirley and Freezeout Mountains. To the south, Unit 27 is a lighter, evenly colored brown where it covers the structure in the lower units near Rawlins, Cedar Ridge and Pass Creek Ridge.

Unit 28 - (Tertiary Browns Park Fm.) covers a large area west and north of the Sierra Madre Mountains. The dark brown to brownish red unit exhibits low dips and covers the underlying structure except where streams have dissected it. It forms a prominent scarp along the north and western edges, particularly in the Miller Hill area. To the east it is overlain by Unit 31 but the contact is not distinct.

Unit 29 - (Tertiary North Park Fm.) is seen in the Saratoga Valley. Its contact with the older units of the Sierra Madre and Medicine Bow Mountains is sometimes sharp and sometimes gradational. It is generally a light brown or blue-grey color contrasting with the very dark red of Unit 1. Where Unit 29 is heavily vegetated the exact contact with Unit 1 is not apparent.

Unit 30 - (Tertiary intrusives) is located west of the Sierra Madre Mountains near Battle Mountain. The intrusive bodies stands out above Unit 28 as darker colored circular buttes.

Unit 31 - (Quaternary glacial drift) is located north of the Medicine Bow Mountains near Kennaday Peak. It is a red and brown mottled color and grades into surrounding units.

Unit 32 - (Quaternary playa deposits) is found near the Rawlins uplift and Haystack Mountains. The playas are bluish-grey or white in color and are often associated with small lakes (also playas?) in the flatland areas of Unit 14 and other Quaternary units.

Unit 33 and 33d - (Quaternary dunes) covers a large area between the Rawlins uplift and the Ferris-Seminoe Mountains. The striped areas on the map denote probable active sand and

wind erosion. The dunes appear very white in color and show a dominant northeasterly trend. Other areas include stabilized dunes with some vegetation. Stabilized dune areas appear pockmarked like a karst surface and are generally dark tan or brown in color.

Unit 34 - (Quaternary alluvium) is associated with modern streams throughout the county. The alluvium appears light tan or bluish-grey in some areas and red (due to vigorous vegetation in others. Where Unit 34 is vegetated it is so designated since it is often impossible to tell from the imagery if cropland areas along streams are actually underlain by bedrock or alluvium. This distinction was particularly difficult in the heavily farmed Saratoga Valley. Field checking is needed to determine which areas are actually alluvium.

Structure

In general, the broad structures apparent on the ERTS imagery were easily mapped. The major uplifts of the Rawlins, Ferris, Seminoe, Shirley and Freezout Mountains along with associated faults and structural complications were mapped in considerable detail. The major unconformities were Tertiary and Quaternary units overlie older units were readily discerned. However, structural detail interpreted from the ERTS imagery is not always consistent with resolution. In some areas, more detail could be seen than could be mapped at 1:250,000 (i.e. the small area west of Elk Mountain). In other areas, very little structural detail could be seen (i.e. the blank area on the map east of Rock Mountain). In the latter area, the color variations were discontinuous and the structure could not be interpreted. In some areas, a single unit could be subdivided many times whereas elsewhere it appeared only as one.

This variation in mappability is controlled by a number of factors, including the attitude of the units, their relation to sun angle, the elevation, vegetation cover and climate. More subunits were generally distinguished in areas of shallow

dip; fewer were apparent in steeply dipping and structurally complex areas. In heavily vegetated areas, all units were characteristically red in color and difficult to distinguish. In areas sloping gently away from the sun azimuth enhancement served to increase the detail somewhat.

Objectivity

There are many built in biases in any geologic interpretation but they are perhaps more prevalent in a photo interpretive map. The factors described above tend to increase the detail interpreted in one area while limiting the interpretable detail in another. The imagery used was not uniform throughout the county. Some areas had the added advantage of color-composite presentation whereas the eastern part was available only black and white. Cloud cover in some areas resulted in piecemeal interpretations compiled from several images.

The order in which the areas were mapped affected the end product. The Rawlins uplift and surrounding area was interpreted first. The interpreter was relatively unfamiliar with the map area, the data, and the interpretive procedures. Consequently, much time was spent mapping this small area. The initial attempt bogged down in detail, necessitating an overall assessment of the area for "mappable units." Also, the criterion and techniques used for interpreting the first areas mapped evolved as the study continued.

Perhaps the greatest bias in the interpretation was the correlation from the state map and the author's previous knowledge as to what should be seen in each area. The sequence of units, their position and role in major structures of the county and their expected topographic expression were all known before the interpretation was begun. In general, the state map was not used for correlation of units until after the interpretation for each region was completed, but the structural style and characteristics of each area checked certainly influence interpretation of subsequent areas.

Future Work

The Carbon County photomap should be carefully checked against all available published data and detailed aerial photography. Areas of major discrepancies should be field-checked to determine the cause of the discrepancies. Until these essential checks are made, the information presented on the photo map and the correlations with geologic formations and structure must be considered tentative.

Conclusions

The ERTS-1 imagery of Carbon County yields good detail for large scale mapping. Photo linear elements that may represent faults and joints are shown in greater detail than on the Geologic Map of Wyoming. The areas of Tertiary outcrop exhibit subtle differences not always evident on the ground. Other areas showed less detail than has already been mapped. A thorough check of the photomap is the next essential step in determining validity of the interpretations and the utility of the ERTS imagery in this application.

Appendix H: Utility of high-altitude color photography for geologic mapping.

from an unpublished master's theses:
Vargas H., Rodrigo, 1973, Photogeologic map of the Jelm Mountain Quadrangle, Albany County, Wyoming; University of Wyoming, Dept. of Geology, M. Sci. thesis, 68p.

Color infrared film positive (scale 1:39600 approx.), color film positive (scale 1:39600 approx.), and black and white panchromatic prints (scale 1:27700 approx.) were used for photogeologic mapping of the Jelm Mountain quadrangle. The color and color infrared films correspond to two flight-lines oriented approximately N 35° W. The black and white prints are part of three N-S trending flight lines. The black and white photography was taken by the United States Geological Survey in July, 1947 and the color photography by the National Aeronautics and Space Administration in September, 1972 (mission 213).

Prints for the color and color infrared photography were available but were not used because they contained less information than the corresponding transparency images, largely because of overexposure and the resulting loss of color contrast. The same lithologic units were differentiated on the three photographic products used. But, it is necessary to keep in mind that: 1) the black and white panchromatic photography was larger scale; 2) the black and white panchromatic film was flown at a different time than the color infrared photography and yields a somewhat different perspective on most slopes; and 3) the determination and delineation of these lithologic units were more quickly and easily made on the color infrared film positive than on either of the other photographic products.

When comparing color and color infrared films with the black and white panchromatic prints, it is observed that the color mode allows an easier determination and delineation of the stratigraphic units present in the studied area. This

color mode is still more valuable on the color infrared film because of its higher contrast.

Because color infrared film presents the greatest tonal and color contrast, it is considered the most valuable (in this particular case) of the three studied photographic types.

The high tonal and color contrast allows faults and some lithologic units (Forelle Limestone, Morrison Formation) to be more readily and precisely delineated on the infrared photography. Color contrast between the different lithologic units allows a ready observation of their offset along the fault line. Quaternary deposits are easily delineated by their geomorphic form, and their color is largely dependent on the color of the parent material from which they were derived. Pediment gravels are characteristically portrayed by a grayish green to dusky, yellow-green color with a spotty pattern due to the vegetation (sagebrush). This spotty pattern could be due to a "patterned ground" which is one of the most conspicuous and characteristic features of periglacial regions (Embleton, and King, 1968, p. 485).

The color infrared photography allows ready identification of key stratigraphic units when used in geologic mapping. The key units in this area are: The red beds that are characteristically portrayed in yellow or yellow-green on the color infrared photography; the black shales which appear darker than any other sedimentary rock, and the light-colored sandstones which are depicted in white on the imagery.

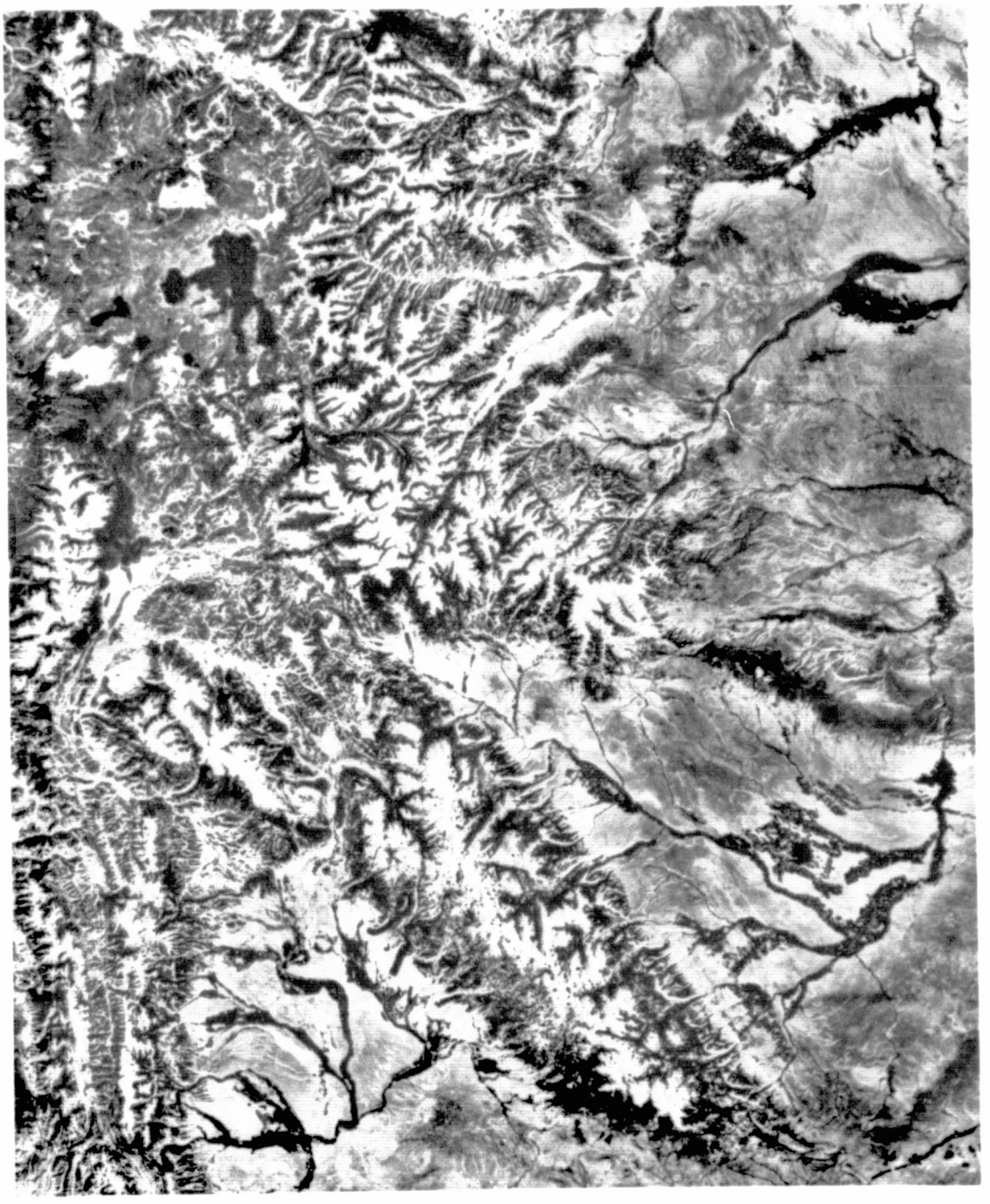
Combining these key units with general stratigraphic knowledge of the area, a geologist can construct a reasonably accurate geologic map in a considerably shorter time than is required for completing the same work using standard photography and field mapping. Nevertheless the utility of the color infrared photography must not be over-emphasized. Its use does not allow the field work to be avoided but rather, increases the overall efficienty of the operation by reducing field work to a minimum.

Appendix I: Mapping of large glacial features using ERTS-1 imagery.

a summary of a paper presented March 5-9, 1973 at the Symposium on Significant Results Obtained from ERTS-1:
Breckenridge, R. M., 1973, Glaciation of northwestern Wyoming interpreted from ERTS-1 imagery; Symposium on significant results obtained from ERTS-1, March 5-9, 1973, Washington, D. C., Report NASA-SP-327, NASA Scientific and Technical Information Office, Washington, D. C., p. 363-370.

During the Pleistocene epoch the largest mass of glacial ice outside of the continuous ice sheet in North America formed in northwestern Wyoming leaving a profound effect on the present day topography and scenery. In addition the sand and gravel deposits formed by glacial erosion are important sources of construction materials as well as being excellent aquifers. Glaciation also provided numerous natural reservoirs in the form of tarns and moraine-dammed lakes. Rocky Mountain glacial chronology is based on type deposits found in the Wind River Mountains of Wyoming. Although glaciation has locally been studied in detail, the region as a whole has not been studied from a glacial standpoint. The large area involved, rugged topography, lack of control and general inaccessibility have discouraged regional investigations. ERTS-1 appeared to provide an excellent base for broad-scale geomorphic studies of this type.

Figure I-1 is a small-scale photomosaic of ERTS-1 MSS-5 imagery in the area studied. The darker area with moderate relief and the prominent lake in the northwest corner of the image is the Yellowstone Plateau. It is bordered on the east by the rugged Absaroka Range and on the south by the Teton and Gros Ventre Mountains. The large northwest-striking structure in the south-center of the mosaic is the Wind River Range. The north-trending ridges and valleys on the southwest margin of the image are the Wyoming Overthrust Belt. All of the images were taken in early fall (1972) and are cloud-free.



0 50 miles

Figure 1-1

ERTS MSS 5 MOSAIC OF NORTHWESTERN WYOMING

ORIGINAL PAGE IS
OF POOR QUALITY

The imagery was analyzed using basic photo interpretive techniques together with color-additive and pseudo-stereoscopic viewing.

Overlay maps were compiled outlining the extent of ice at glacial maximum. A simplified and reduced glacial map is presented in Figure I-2. Glaciated areas as shown are based on the recognition of one or more glacial features. Glacial landforms can be grouped into erosional and depositional features both of which could be recognized on the imagery. Moraines are considered the most diagnostic depositional glacial landform. The Bull Lake and Pinedale type deposits (Wisconsin) were easily outlined on the imagery although they could not be separated where in close contact. These massive looping terminal moraines impound large glacial lakes on the flanks of the Wind River Range.

Terminal and lateral moraines in mountain valleys could neither be reliably distinguished from stratified drift nor from other valleyside surficial deposits except in a few cases where characteristic geomorphic features were recognized. Most of the pre-Wisconsin glacial features have been subsequently destroyed by erosion or covered by later deposits. Remaining exposures are too small to recognize on the imagery. Large gravel-capped mesas or pediments at the mountain flanks and in the basins probably represent erosional cycles of these early glaciations. These pediments or benches appear dark on all bands but are best recognized using a composite of MSS 5 and 7.

Where massive terminal moraines were absent or not recognizable, glaciated areas were outlined on the basis of glacial topography. Alpine glacial erosion is distinctive and stereoscopic viewing of adjacent ERTS passes facilitated the recognition of U-shaped troughs, cirques, horns, aretes, cols and truncated spurs. Ice limits can be located approximately where valleys change from a U to V shape in cross valley profile. Most of the crests of Wyoming mountain ranges culminate in flat uplands often referred to as high-level erosion surfaces which bevel across the rock structure. Glacial dissection of these

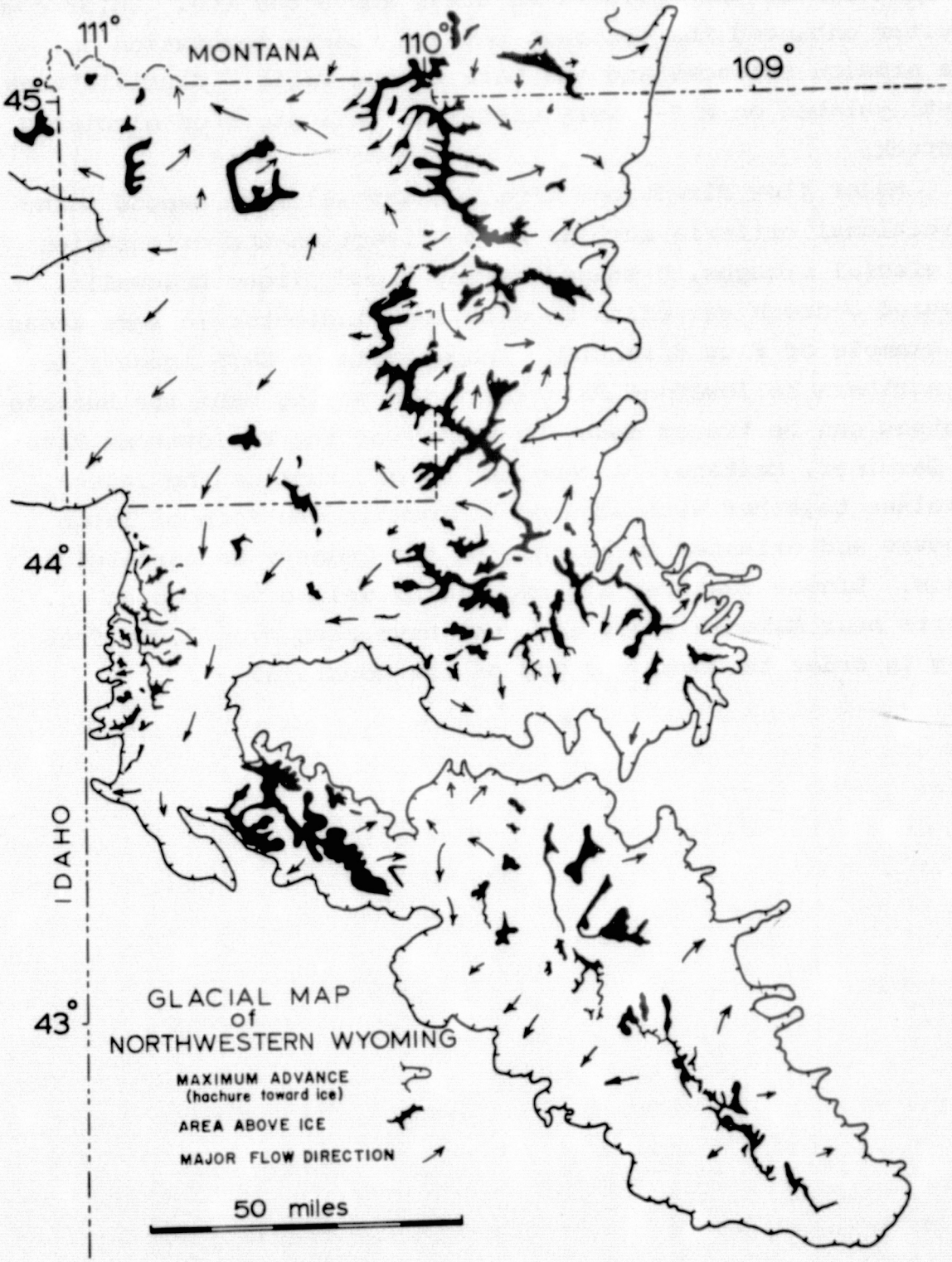

111°
MONTANA
110°
109°
45°
44°
IDAHO
43°
GLACIAL MAP
of
NORTHWESTERN WYOMING
MAXIMUM ADVANCE
(hachure toward ice)
AREA ABOVE ICE
MAJOR FLOW DIRECTION
50 miles

Figure I-2

surfaces results in the classic biscuit-board topography. Morphology and topography recognized using stereo pairs allowed distinction of the unglaciated areas above the ice. Color composites enhanced the contrast between tundra vegetation on the erosion surfaces and the bare cirque walls. Glacial tarns distinguished on MSS-7 were useful as indicators of glaciated bedrock.

Major flow directions (Fig. I-2, arrows) were mapped using directional criteria such as slope direction and orientation of glacial troughs, U-shaped valleys, and cirque headwalls. Scoured bedrock served as an excellent indicator in some areas. An example of flow direction recognizable on ERTS imagery is in northern Yellowstone Park where ice moving from the Buffalo Plateau can be traced down the valley of the Yellowstone River to Gardiner, Montana. A combination of drumlins and lateral moraines together with scoured bedrock in the form of large grooves and oriented tarns show on the imagery as parallel lines. Linear features are especially well developed on Mt. Everts near Mammoth where ice must have been over 2,000 feet deep in order to cover the top of the mountain.

Appendix J: Extimating available water contained in snowpack.

an unpublished class report by:
R. W. Marrs and J. Thompson, University of Wyoming, Water Resource Research Institute.

The May 21, 1973 ERTS scene of the Wind River Range (1302-17362, Fig. J-1) was first interpreted to produce a map of snow-cover at the time of overpass. But the distribution of snow, by itself, is seldom an adequate index of available snowpack and cannot be used directly to estimate runoff. Snow depth and snow water-content data are required in order to make meaningful estimations. Accurate estimates of snow depth and density plus several years correlation between ground measurement of runoff and the snow-cover estimate made from ERTS scenes are needed.

Determination of the areal distribution of snow from the ERTS scenes is straightforward except in scenes with cloud cover. The clouds can usually be distinguished from snow, but they do obscure the boundaries of the snow-covered areas.

Color-additive presentation of snow scenes often allows the interpreter to identify areas where the snow is melting or has exceptionally high moisture content. However, it is not always possible to separate differences due to sun angle and slope variations and from differences reflecting moisture content or partial vegetation cover. Spectral comparisons made by color-additive viewing or by computer analysis can help in making these distinctions. Combinations of ERTS MSS bands 5 (red) and 7 (infrared) are often most useful. Both bands record the area of total snow cover, but the infrared reflectance of the snow seems to vary with moisture content more than does the red-band reflectance. Consequently, a false-color combination of these bands shows variations in color corresponding to varying moisture conditions on the surface of the snow layer.

A series of snow-cover estimates and maps were compiled for the upper Green River drainage (Table J-1, Figs. J-2, J-3,

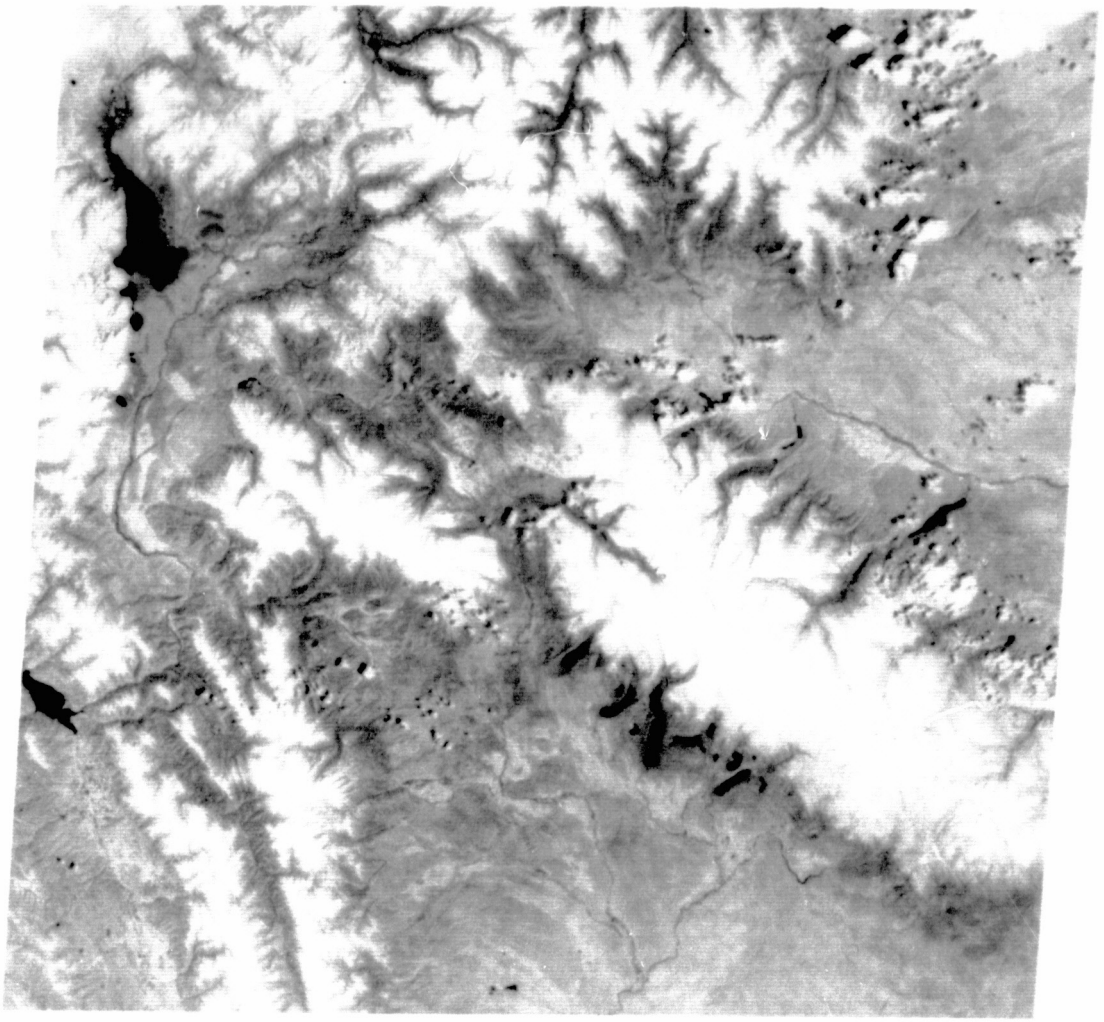


Figure J-1. An ERTS scene of the Wind River Mountains, northern Thrust Belt and Absaroka Range. The upper Green River drainage is in the center of the image.

Table J-1: Snow cover and snow depth estimates made from ERTS-1 imagery

DATE	IMAGE	SNOW COVER (total)	MELTING SNOW	EST. DEPTH.	CLOUDS
15 Jan. '73	1176-17355	100%	0	20"	0
2 Feb. '73	1194-17362	100%	0	25"	0
20 Feb. '73	1212-17363	100%	0	38"	0
10 March '73	1230-17364	100%	?	20-40"	60%
15 April '73	1266-17364	100%	5%	10-40"	0
* 3 May '73	1284-17363	99%	5%	0-40"	15%
*21 May '73	1302-17362	65%	46%	0-30"	0
* 8 June '73	1320-17361	33%	8%	0-10"	0
26 June '73	1338-17360	5%	5%	0-5"	60%
1 Aug. '73	1374-17353	0	0	0	5%

*Estimates made from maps (Figs. J-2, J-3, and J-4).

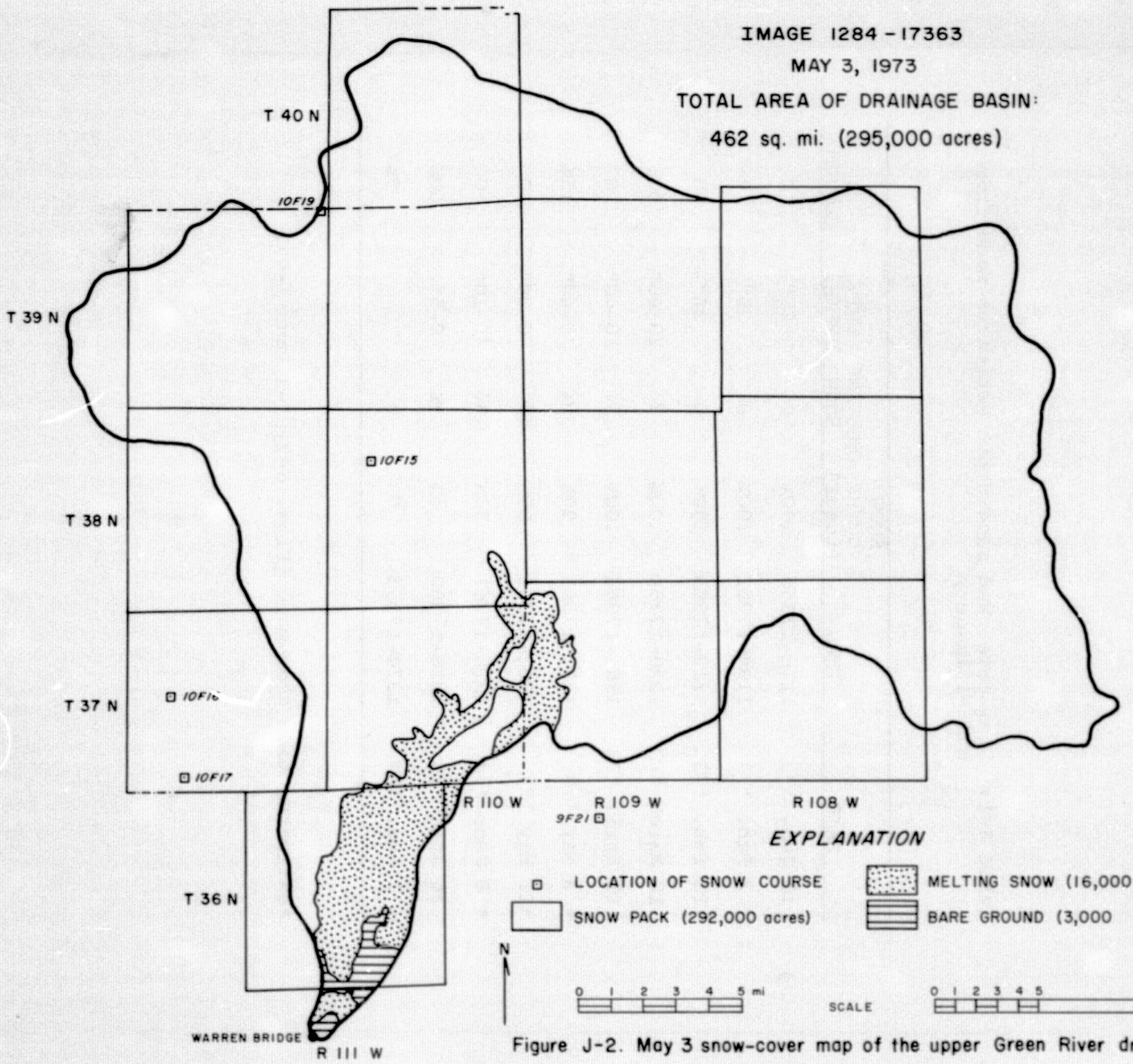


Figure J-2. May 3 snow-cover map of the upper Green River drainage (previous months showed total snow cover.)

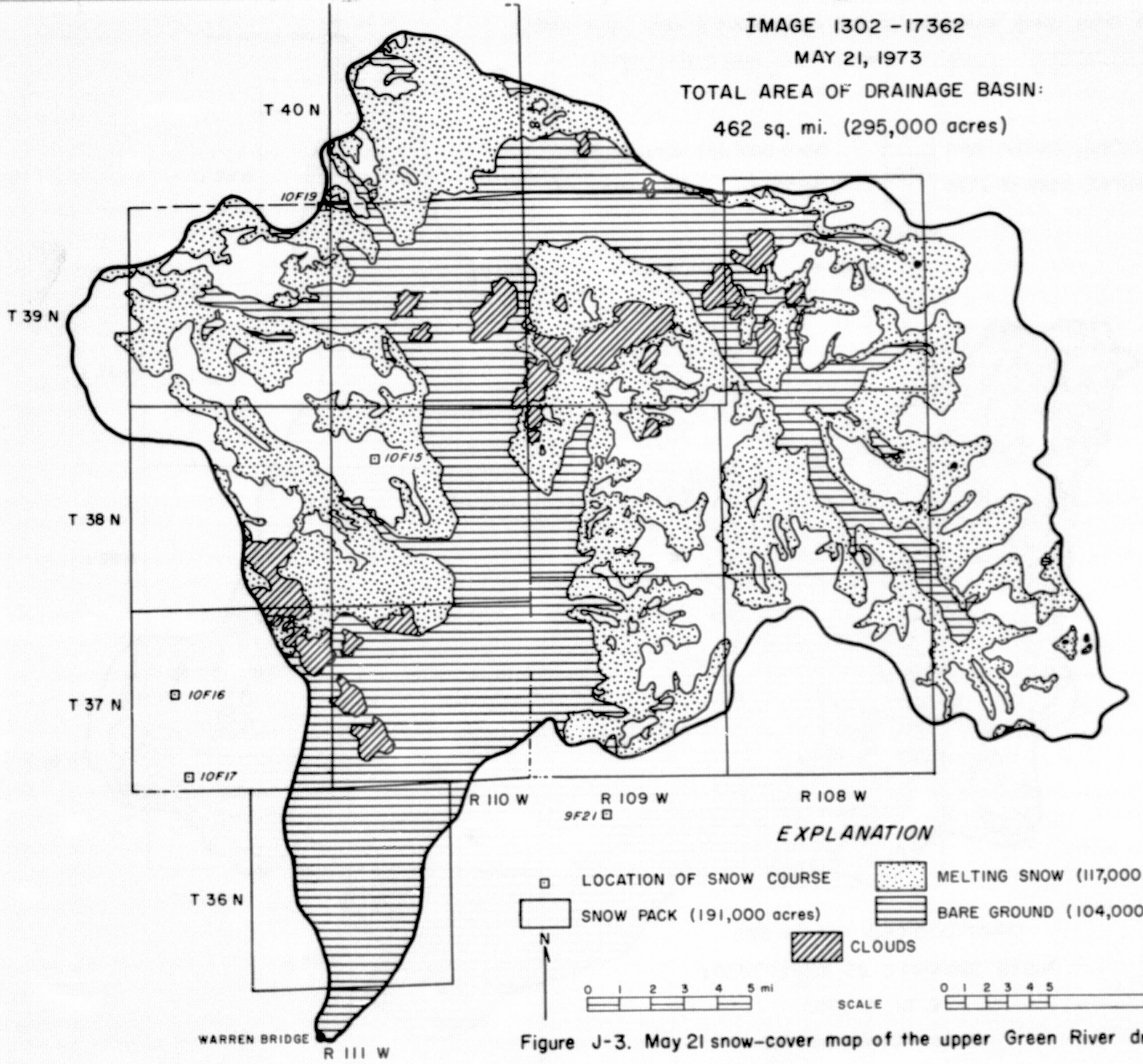


Figure J-3. May 21 snow-cover map of the upper Green River drainage

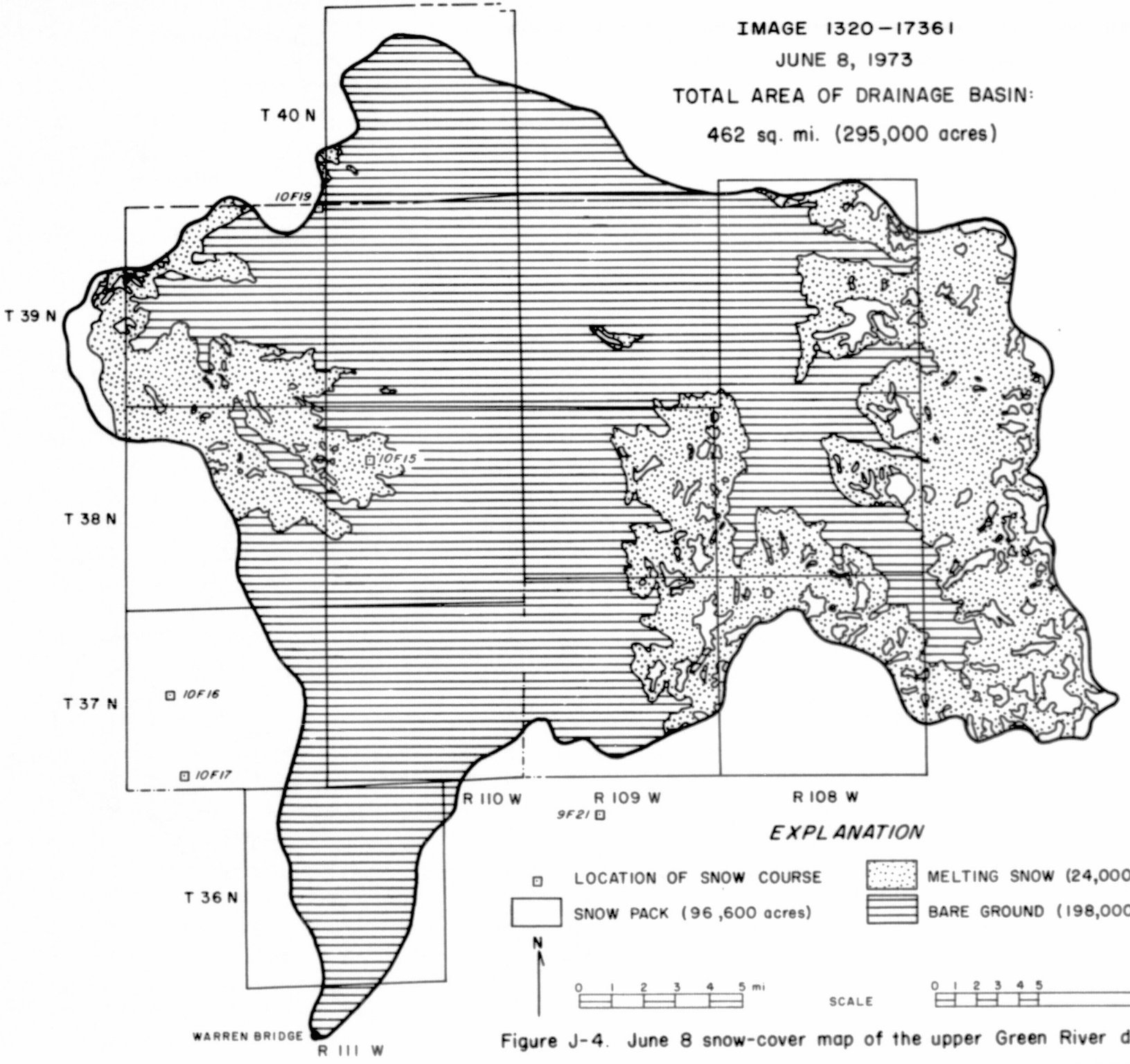


Figure J-4. June 8 snow-cover map of the upper Green River drainage

Table J-2. Daily discharge records for the upper Green River drainage (from the Warren Bridge gage station)*, (January-September 1973, discharge in cubic feet per second).

DAY	JAN	FEB	MAR	APR	MAY	JUN	JUL	AUG	SEP
1	108	101	135	108	242	824	1,840	604	271
2	105	105	132	110	222	1,080	1,680	568	299
3	100	110	130	115	214	1,070	1,440	562	306
4	97	113	128	120	284	944	1,190	616	302
5	95	115	128	130	400	796	1,130	664	292
6	90	115	132	135	687	775	1,140	712	284
7	100	114	130	130	1,010	936	1,170	705	285
8	120	110	125	125	960	-1,290	1,190	659	308
9	130	108	120	120	568	1,640	1,150	592	363
10	140	107	125	114	430	1,930	1,080	538	383
11	150	110	130	139	445	2,120	984	508	447
12	150	115	132	139	475	2,150	920	490	600
13	154	118	125	147	586	1,400	1,010	483	719
14	158	115	120	139	747	1,640	1,080	469	664
15	155	115	122	-147	976	1,780	1,010	451	556
16	143	117	122	155	1,360	1,680	866	435	483
17	140	120	121	134	1,760	1,390	747	430	425
18	138	122	118	144	2,310	1,060	691	461	375
19	133	124	114	142	2,460	838	691	461	336
20	130	125	110	114	2,490	700	775	468	308
21	129	123	115	110	-2,550	617	1,000	450	292
22	128	121	115	110	2,000	635	1,240	450	276

Table J-2 (cont.)

DAY	JAN	FEB	MAR	APR	MAY	JUN	JUL	AUG	SEP
23	128	121	111	119	1,580	778	1,200	465	272
24	125	125	107	132	1,460	997	968	440	284
25	123	120	103	169	1,660	1,210	810	411	292
26	120	125	104	187	1,690	1,340	691	410	280
27	113	130	105	194	1,330	1,510	646	380	268
28	108	135	104	250	1,030	1,670	622	350	256
29	104	-----	100	264	904	1,770	628	322	250
30	102	-----	98	250	838	1,840	640	298	246
31	100	-----	105	-----	789	-----	634	278	-----
TOTAL	3,821	3,279	3,666	4,392	34,457	38,910	30,843	15,130	10,721
MEAN	123	117	118	146	1,112	1,297	995	488	357
MAX	158	135	135	264	2,550	2,150	1,840	712	719
MIN	90	101	98	108	214	617	622	278	246
AC-FT	7,580	6,500	7,270	8,710	68,350	77,180	61,180	30,010	21,270

CAL YR 1972 TOTAL 248,615 MEAN 679 MAX 4,760 MIN 91 AC-FT 493,100

WTR YR 1973 TOTAL 164,648 MEAN 451 MAX 2,550 MIN 90 AC-FT 326,600

NOTE.--No gage-height record Dec. 14 to Mar. 29.

*Records taken from U. S. Geological Survey, Water Resources Data for Wyoming, Part 1, Surface Water Records, 1973.

Table J-3. Surface water runoff forecasts for the Green River at Warren Bridge-April to September, 1973 (1000 acre feet), (from U.S.G.S., 1973).

MONTH	FORECAST 1973	% OF ACREAGE	FLOW 1972	1953-67 AVERAGE	FLOW 1973	DIFFERENCE FROM ACTUAL
Feb.	277	86	431	323	267	+10
March	270	84	431	323	267	+ 3
April	252	78	431	323	267	-15
May	238	74	431	323	267	-29

Table J-4. Snow depth and water content measurements, (from U.S.D.A., 1973).

	1973				1972	
MONTH	SNOW COURSE	SURVEY DATE	SNOW DEPTH (in)	WATER CONTENT (in)	WATER CONTENT 1972 AVG.	
Feb.	9F21	1/29	30	7.0	13.9	
	10F15	1/28	26	6.2	15.8	
	10F16	1/30	34	7.2	19.4	12.0
	10F17	1/29	29	6.8	14.1	
	10F19	1/28	29	5.7	11.6	8.6
March	9F21	2/26	35	8.7	16.9	
	10F15	2/25	34	7.4	19.6	
	10F16	2/26	41	9.2	23.5	
	10F17	2/26	36	8.3	19.5	
	10F19	2/25	32	6.1	14.4	10.8

Avg. depth 29.6 in.
Avg. moisture 6.58 in.
Avg. depth 35.6 in.
Avg. moisture 7.94 in.

Table J-4 (cont.)

MONTH	SNOW COURSE	1973 SURVEY DATE	1973 SNOW DEPTH (in)	1973 WATER CONTENT (in)		1972 WATER CONTENT	1972 AVG.
April	9F21	3/30	43	10.1		19.3	
	10F15	3/28	36	7.8	Avg. depth 42.2 in.	19.5	
	10F16	3/27	46	11.8		27.1	
	10F17	3/30	46	10.5	Avg. moisture 9.76 in.	21.4	
	10F19	3/30	40	8.6		16.9	12.6
May	9F21	4/27	32	10.5		15.6	
	10F15	4/28	23	8.8	Avg. depth 31.6 in.	13.5	
	10F16	4/27	41	12.0		26.8	
	10F17	4/29	29	9.5	Avg. moisture 9.68 in.	16.5	
	10F19	4/28	33	7.6		14.4	11.8

and J-4) using both the band 5 and band 7 ERTS images. These estimates were then compared to surface water runoff records (Table J-2) and runoff forecasts (Table J-3) to determine the potential for using snow-cover estimates interpreted from ERTS with snow co rse measurements (Table J-4) to estimate runnoff or available water in snowpack. A direct correlation could not be made in either of these applications. The surface water runoff measurements include contributions from snowmelt, rain, and from springs. Conversely, some of the meltwater evaporates and some sinks into the ground, so that only a portion of the water from melting snow goes directly into the surface system and is measured at the gage. Comparisons of the ERTS derived data with surface measurements indicate a very complex relationship.

Work is presently underway to better define these relationships through consideration of other factors such as temperature and precipitation and through correlations of ERTS image for 1972 and 1974 with appropriate records. Continued correlation of the repetitive ERTS data with seasonal and daily surface measurements may eventually reveal key relationships that are not immediately apparent in the results from a single season.

Appendix K: ERTS imagery applied to mapping of sand dunes.

A detailed discussion of this study is presented in a special report under contract NAS 5-21799 and as part of a Geologic Survey of Wyoming report

Kolm, K. E., 1974, ERTS MSS imagery applied to mapping and economic evaluation of sand dunes in Wyoming, National Technical Information Service, Springfield, Virginia, 31 p.

Kolm, K. E., 1974, ERTS MSS imagery applied to mapping of sand dunes in Wyoming; Geol. Survey of Wyoming, Report of Investigation 10, p. 34-38.

Active and stabilized dune fields of regional extent were mapped using Earth Resources Technology Satellite (ERTS) imagery (Fig. K-1). Previously mapped dune fields (Ahlbrandt, 1973; Houston, 1974; Love, Weitz, and Hose, 1955; Toehler, 1969) were confirmed by the ERTS image study, and some new dune fields were discovered. Additional confirmation was provided by field work and high-altitude aerial photographs which were available for some areas.

Results indicate that color composite ERTS images are most helpful in locating active dune fields. This is attributed to subtle color differentiation between active dunes, clouds, sandy alluvium, pediments, alkali flats, snowfields, and light-colored rock formations. The color composite images were also employed in mapping stabilized dune fields which usually exhibited a brown-green coloration characteristic of sparse and relatively dormant vegetation. The contrast between both stable and active dunes and the surroundings was most apparent on the image transparencies because the transparencies have higher resolution and greater flexibility in the intensity of illumination than do the prints. Color prints were most convenient for field use. Another general advantage of ERTS imagery is the display of regional linear patterns and topographic features. Crosscut relations between dune fields and surrounding rock formations were also recognized.

The disadvantages of ERTS imagery are: 1) the imagery is of a small scale, and small dune fields were sometimes

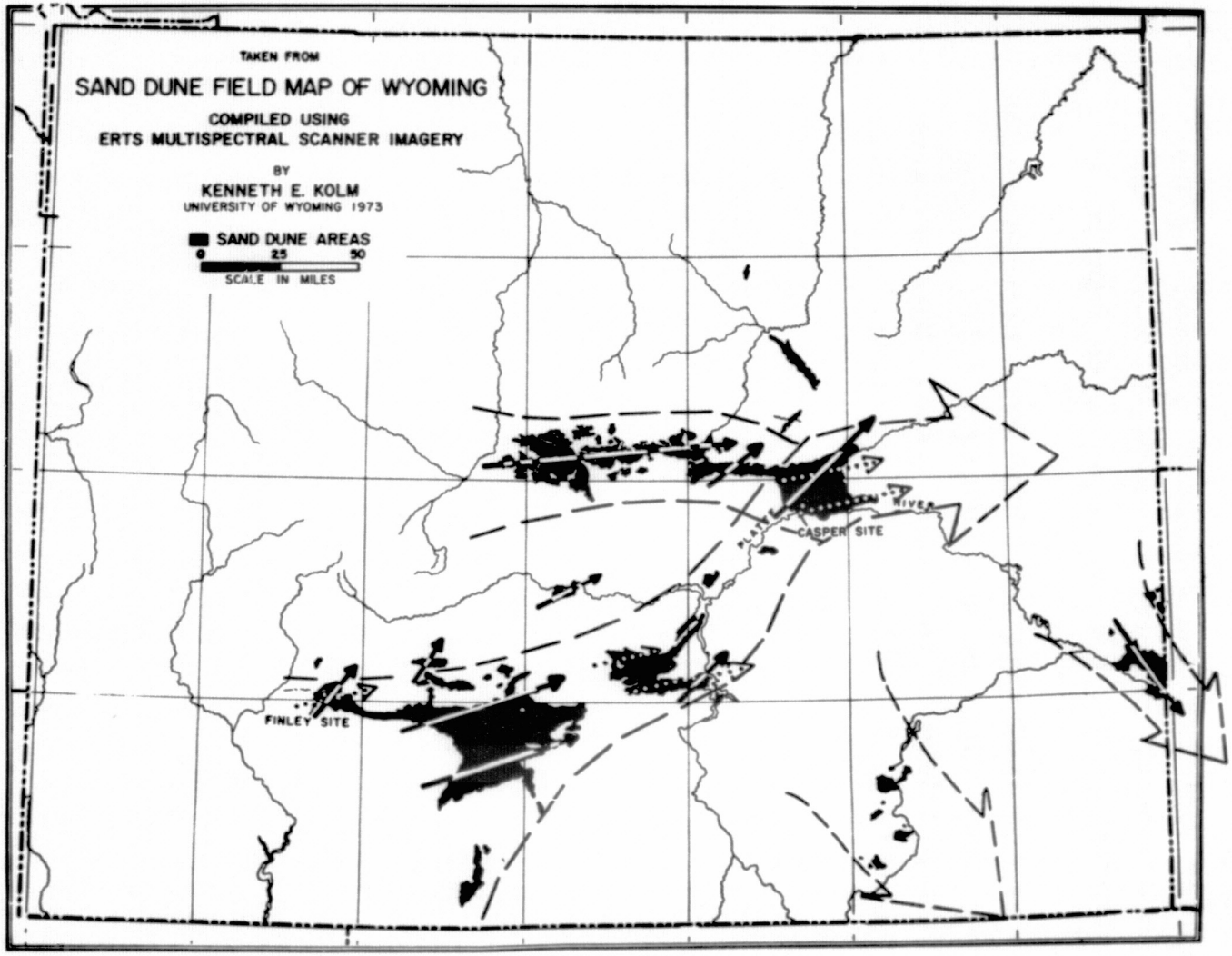


Figure K-1. Map of sand-dune fields shows migration directions of stabilized (solid arrows) and active (dotted arrows) dunes. Apparent wind directions are indicated by large, dashed arrows.

missed; and 2) there is sometimes a lack of distinct color and tonal contrast between a stabilized dune field and its surroundings.

The mapping with ERTS was evaluated by comparing the ERTS map with a similar map prepared using high-altitude aircraft photography. The comparison shows an impressive similarity.

It was hypothesized that the differences between active and stabilized dunes might be a record of a shift in wind directions from prehistoric to recent times. More research is needed to determine when this shift occurred.

Appendix L: Tectonics and linear elements interpreted from ERTS.

A progress report summarizing applications of ERTS imagery to regional tectonic analysis, from a report in preparation by J. Earle.

Several fracture pattern analyses have been done on the Wyoming Province (Sales, 1968; Stone, 1969) and have been correlated with Moody and Hill's (1956) wrench fault fracture pattern study. A tectonic study of ERTS photo linear elements is being compiled for comparison with these published fracture-pattern and tectonic analyses. The linear features are compiled on a mosaic of black-and-white winter imagery, covering the region extending from latitudes 40^{o}N to 45^{o}N and longitudes 104^{o}W to 112^{o}W.

The linears were first mapped on black-and-white transparency images and then transferred to a mylar overlay of the mosaic. Large linears that traverse more than one image were mapped directly on the overlay. The azimuth and length of each linear was measured and rose diagrams of directional data are being compiled for interpretation and correlation of each province. A separate rose diagram will be prepared for each major area of Precambrian outcrop, each major basin, the Absaroka volcanic plateau, and the Wyoming Thrust Belt. The linear trends in each area will be compared with the linear trends in other areas (Precambrian with Precambrian, basin with basin, Precambrian with basin, etc.). A second overlay of the mosaic showing general or inferred linear trends obtained visually from previously compiled mosaics (summer imagery) has also been prepared. Linears on this mosaic will also be considered in the final interpretation.

From a preliminary examination of the data, it appears that a valid correlation between linear trends mapped on ERTS imagery and empirically-derived tectonic trends is highly possible. Comparison of ERTS photo linear trends with those found on Skylab imagery, aircraft imagery, and geologic and topographic maps is planned.

Appendix M: Structural geology of south-central Wyoming.

from a special report under contract NAS 5-21799.

Barton, R., and Marrs, R. W., 1974, Location of geologic structures from interpretation of ERTS-1 imagery, Carbon County, Wyoming; National Technical Information Service, Springfield, Virginia, Report E74-10333, 8 p.

ERTS image 1066-17242 (Fig. M-1) covering Carbon County and adjacent areas was studied with a primary view to mapping structures in the sedimentary rocks of the Hanna Basin.

A color-composite image was available for the area, so the interpretation was made both on the basis of tonal and textural contrast seen on the black-and-white ERTS-1 image and color information available from the color composite. The overlay map (Fig. M-2) depicts structural and lithologic relations interpreted from the image set. After the interpretation was completed, the Geologic Map of Wyoming (Love and others, 1952) was used as a guide in naming the major lithologic units identified in the image interpretation. Direct comparison was then made of the image interpretation and the geologic map (generalized for the Hanna Basin area in Fig. M-3). The units mapped on the interpretation were readily correlated with major units on the state map. Several features (numbered 1 through 6 on the image interpretation were not indicated on the geologic map, but were marked by the interpreter as significant geologic features warranting further investigation. The numbered features described below are found on the photogeologic map (Fig. M-2) at the locations indicated by the corresponding numbers.

1. Although emphasis in the study was placed on lithologic relationships, some of the more prominant linear features were also noted. The east-west lineation west of Seminoe Reservoir, interpreted as a fault from the image, does not appear on the state geologic map.

2. To the northeast of the Washakie Basin the ERTS image indicates a structure, possibly domal, in the Lewis

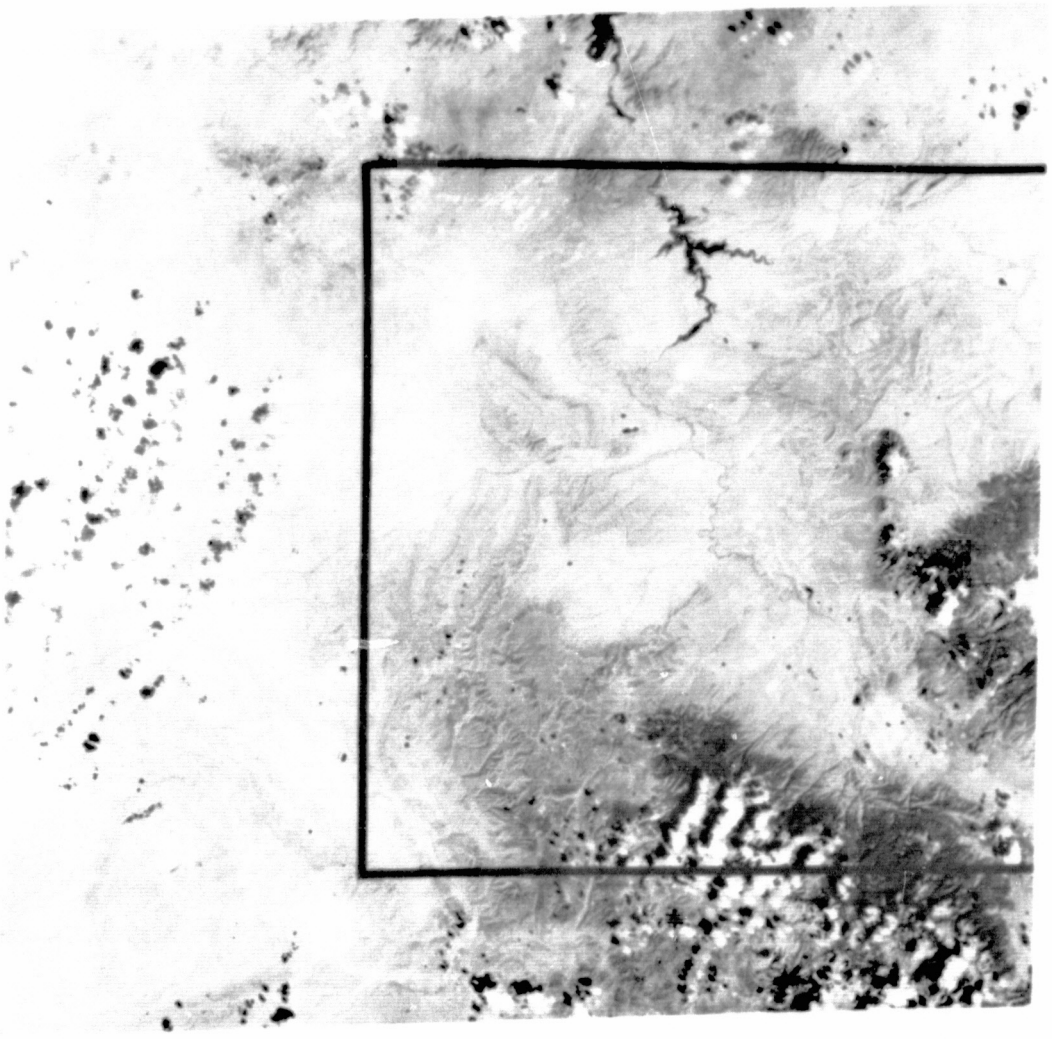


Figure M-1. ERTS Image No. 1066-17242-6 covering Carbon County and adjacent areas. The present study was concerned with the eastern portion of the image, which consists mostly of folded sedimentary rocks of the Hanna Basin. The basin is bounded to the north by the Sweetwater Uplift, to the west by the Rawlins Uplift, and to the southeast by Medicine Bow Mountains. The Sierra Madre Mountains occupy much of the southeastern part of the image. The Washakie Basin lies in the southwest corner of the image area.

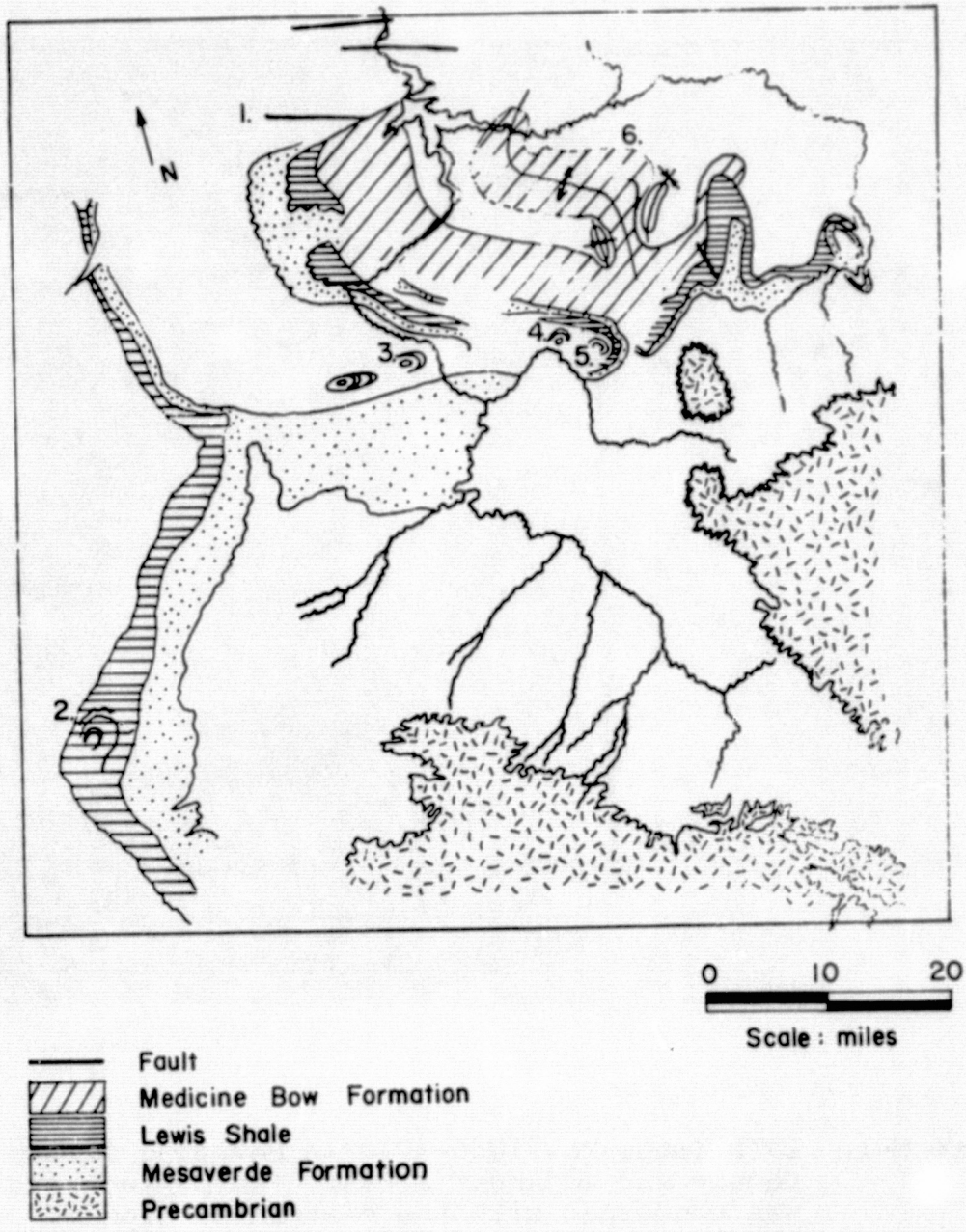


Figure M-2. Geologic map showing structural features and lithologic relation between Medicine Bow, Lewis, and Mesaverde formations in the Carbon County area. Prepared from a portion of ERTS image 1066-17242 and colour composite 1066-17242.

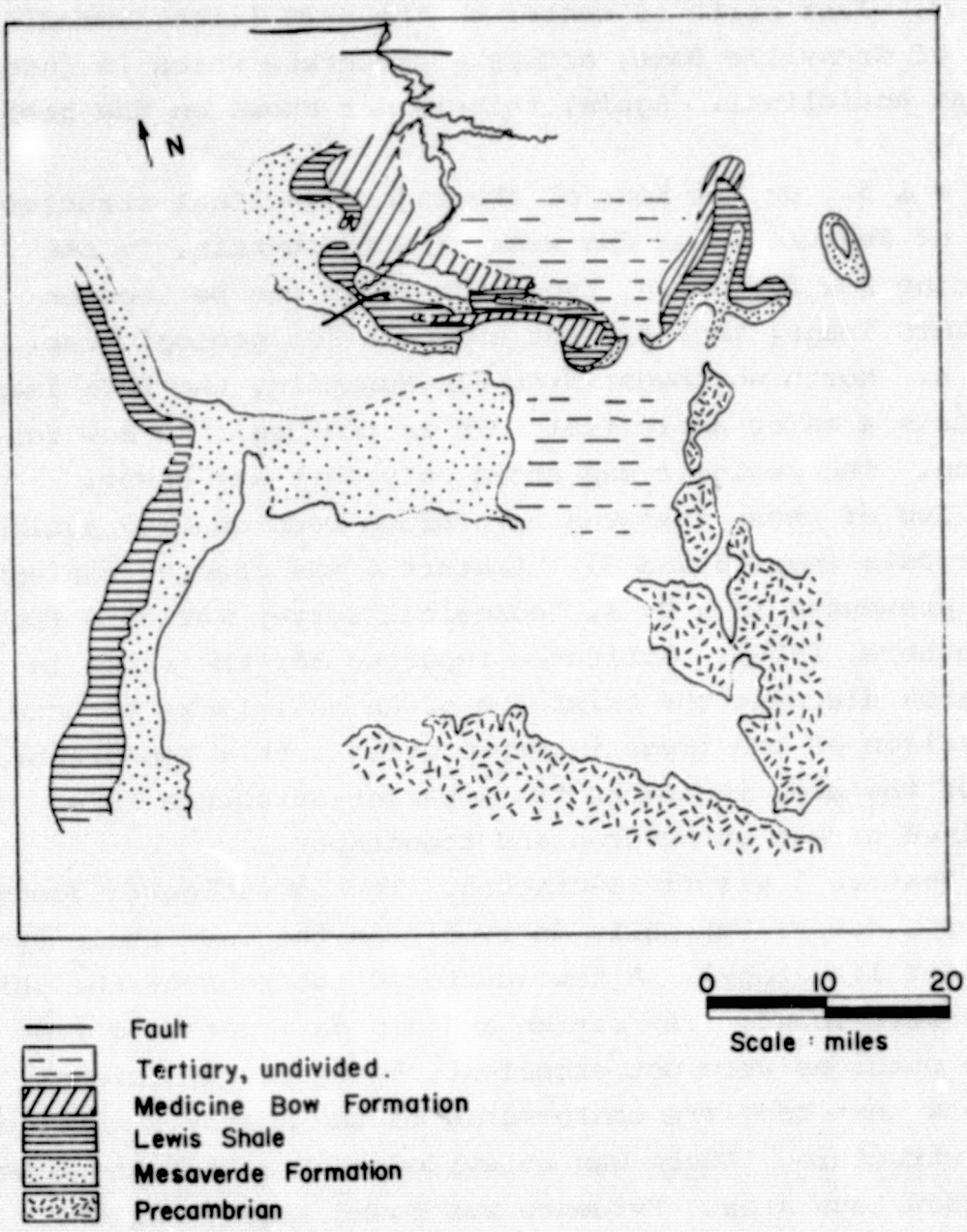


Figure M-3. Geologic map showing relation between Medicine Bow, Lewis, and Mesaverde formations in Carbon County by J. L. Weitz and J. D. Love, 1952 (Covers the same area as fig. M-2).

shale. There is no evidence of this on the geologic map.

3. Just north of center on the ERTS image, immediately east of Grenville Dome, occurs a structure which is interpreted as anticlinal. Again, this is not shown on the geologic map.

4 & 5. On the nose of the major synclinal structure east of Feature 3 and due west of Elk Mountain, in the Medicine Bow formation, two minor folds can be seen on the ERTS image; they are not shown on the geologic map.

6. North northwest from Elk Mountain, the ERTS image suggests a major anticlinal fold in the Medicine Bow formation. The geologic map shows only Tertiary cover.

Two of these features have since been checked against other data (nos. 6 and 3). Feature 6 was checked against work presented in a U. S. Geological Survey Bulletin (Dobbin and others, 1929). Attitudes reported for the rocks in the area discount the existence of an anticlinal structure. Comparison of the image interpretation with a topographic map of the area indicates the apparent structure is a combined effect of outcrop and topography.

Feature 3 was field-checked. The investigator found the area covered by soils derived from the Cody shale (the dominant lithology). A few scattered outcrops of the thin sands were found. The strike and dip data gathered from these outcrops were not excellent, but were sufficient to show that beds are conformable to the nearby Grenville Dome structure. There was no evidence of a separate dome in the anomalous area. Evidence was found suggesting that the anomalous area is sometimes covered by standing water--that it is a playa lake. The anomalous light-covered spot, interpreted as a circular outcrop pattern, corresponds to the relatively saline soil of the playa.

The other four features have not yet been field checked.

Generally favorable comparison of the Geologic Map and the ERTS-1 image interpretation demonstrates that the

ERTS-1 imagery serves very well as reconnaissance mapping base. Topographically controlled outcrop patterns or soil anomalies can easily be misinterpreted as structure. Stereoscopic coverage would eliminate much of the ambiguity that leads to such misinterpretation. Similar mapping efforts in other parts of Wyoming have demonstrated that color-composite imagery, and low-altitude aircraft photography greatly augment contruction of an accurate geologic reconnaisance map. The experience of the interpreter is also a very important factor. The experienced geologist/interpreter can use his knowledge of the regional structure and stratigraphy and his refined interpretive ability to maximize the information gained from the image interpretation and construct a more complete and accurate geologic map.

Appendix N: Mapping of major fractures with ERTS-1 imagery.

from a special report on research under contract NAS 5-21799.

Parker, R. B., 1972, An evaluation of ERTS-1 imagery for mapping major Earth fractures and related fractures; National Technical Information Service, Springfield, Virginia, Report E72-10349, 7 p.

The primary objective of the study was to evaluate the suitability of ERTS imagery in mapping of regional fracture patterns in Precambrian crystalline rocks. Such large-scale features are commonly difficult to map in the field because of their great extent. The synoptic overview afforded by satellite imagery appeared promising for studying these features. The Wind River Mountains of Wyoming (Fig N-1) are an excellent test site inasmuch as an extensive Precambrian terrane is well exposed over about 6,000 square kilometers in a relatively unweathered condition.

Aircraft imagery (Mission 184) was used for a regional reconnaissance of a strip approximately 6 km wide, crossing the Wind River Mountains from west to east. Broad distinctions were made among a group of crystalline rocks including gneisses, migmatites, and granites of diverse character. In addition, many linear features were noted which appeared to be fractures or faults of regional extent.

The reconnaissance strip was field checked during August and September of 1972. Access to the area is limited to horseback or foot travel via a limited network of trails. All portions of the test strip could not be examined because of difficulty of access, but sufficient localities were visited to generally confirm the conclusion made from the aircraft imagery.

The linears interpreted from the aircraft images proved to be major zones of dislocation, cataclasis, and metasomatism is equally varied and ranges from weak recrystallization mostly accompanied by epidotization to more completely altered rocks composed almost entirely of epidote. In two cases, replacement by pink potassium feldspar is complete

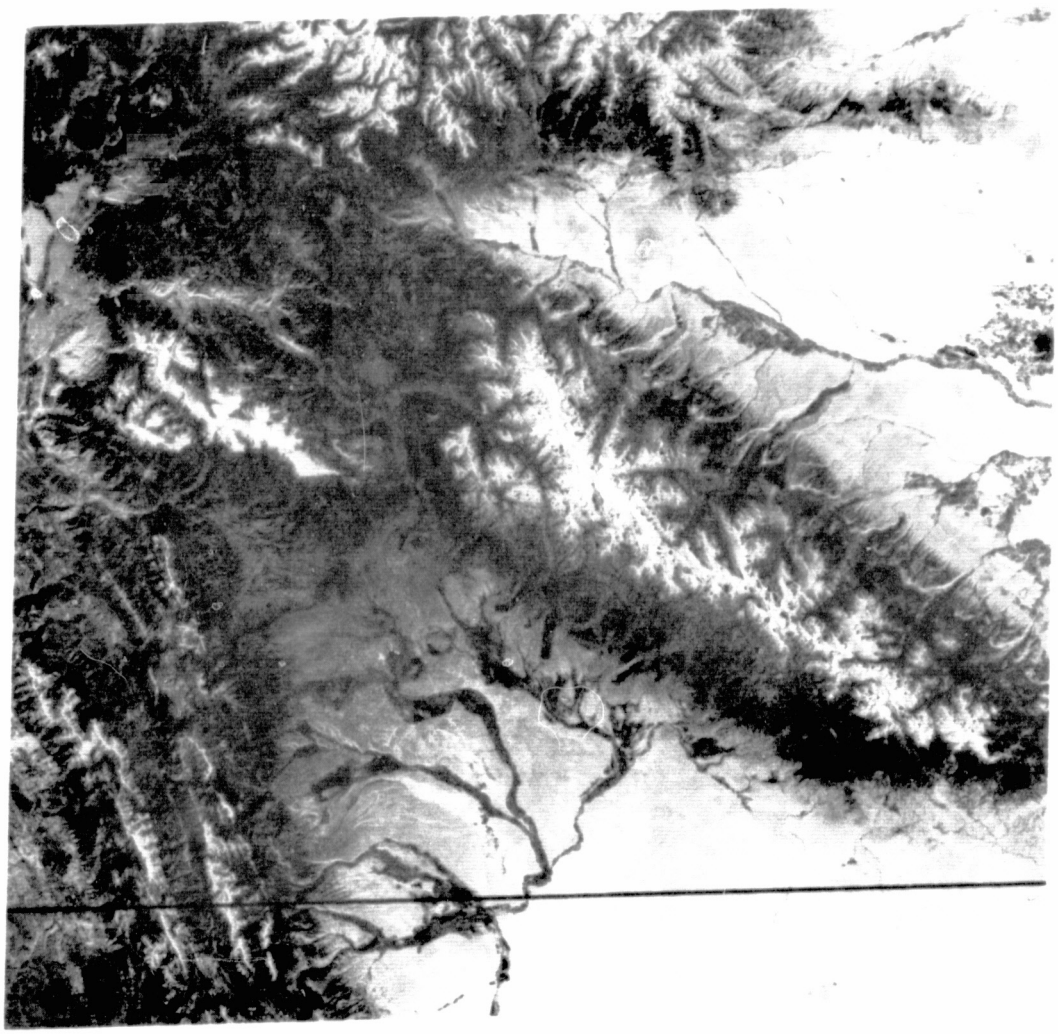


Figure N-1. ERTS-1 image 1014-17352-5 of the Wind River Mountains. Linear features were interpreted from this and other ERTS images of the same area.

with local development of rocks composed entirely of that mineral.

The origin of these fractures is not clear at this point. Certainly movement has taken place along the fractures as evidenced by the cataclastic rocks in the fracture zones. They are not merely major joints. However, the existence of major faults cannot be demonstrated because there are no rock units obviously displaced by the fractures. A more detailed study of the fractures should resolve this question.

Figure N-2 shows the fracture pattern as mapped from the ERTS-1 imagery. For comparison, fractures mapped by previous workers which were confirmed by the ERTS-1 imagery are shown in Figure N-3. A number of fractures and dikes mapped by Granger and others (1971) could not be found on the satellite imagery. Conversely, their work did not indicate some very prominent linears observed on the ERTS-1 imagery. The large linear indicated by the arrow in Figure N-1 is the most striking feature in the entire range on the ERTS-1 imagery, yet is of uncertain significance at this time because it is neither a fault nor a lithologic contact on the map of Granger and others (1971). That area could not be visited in 1972 because of extreme inaccessibility, but a ground study is planned for 1973.

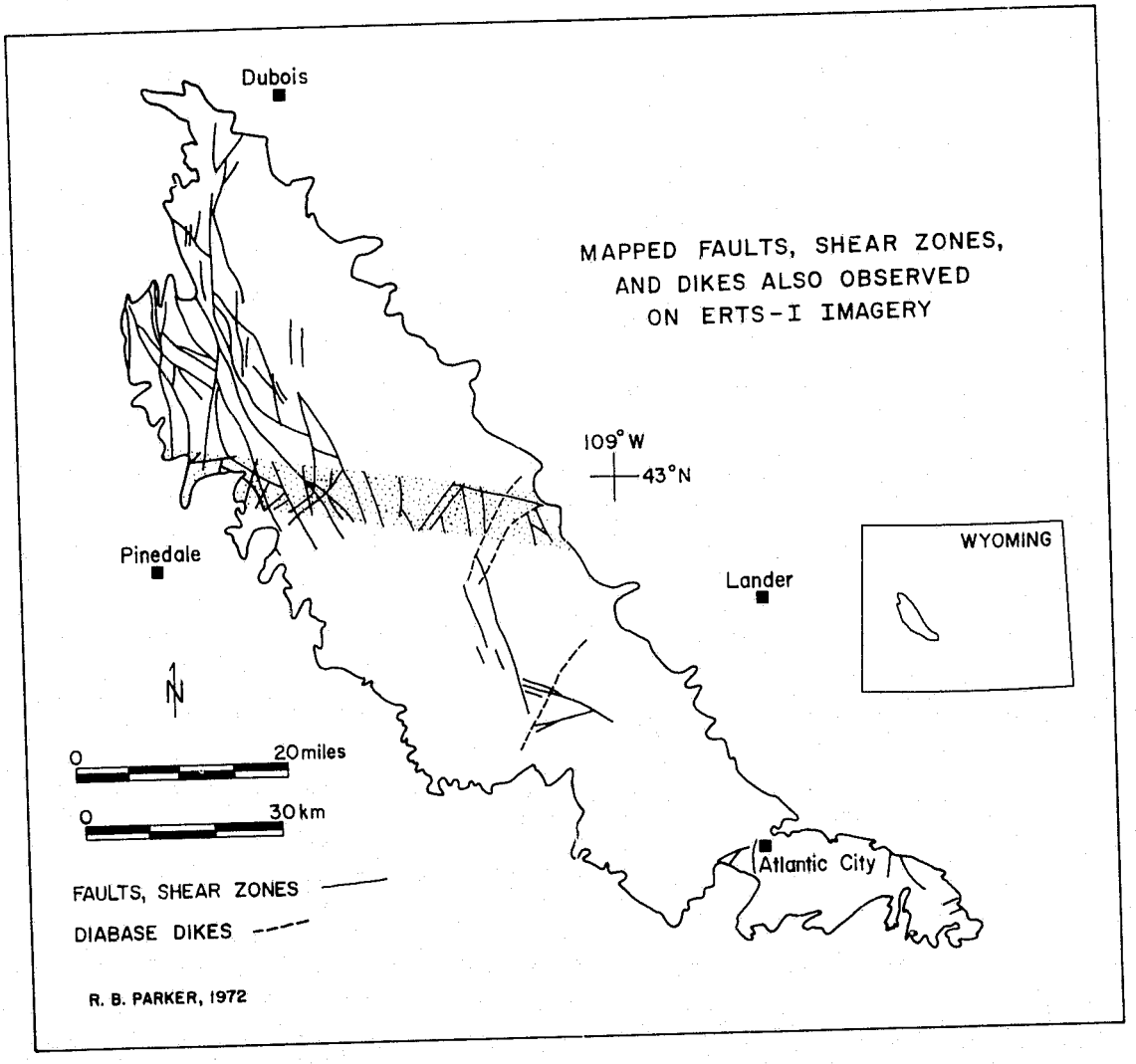


Figure N-2. Principal mapped faults, shear zones, and dikes also observed on ERTS-1 imagery (from Parker, 1972, Figure 1).

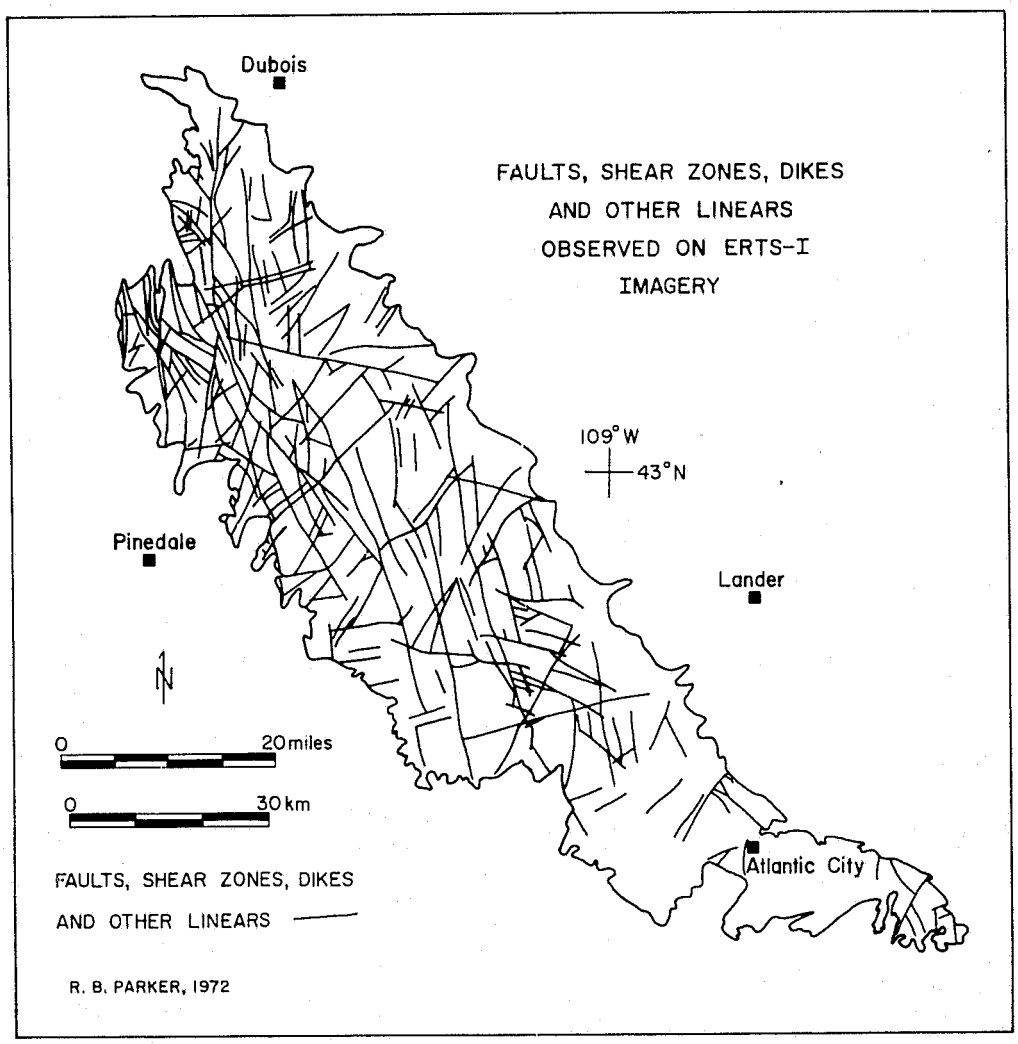


Figure N-3. Principal faults, shear zones, and other linear features observed on ERTS-1 imagery from (Parker, 1972, Figure 2).

Appendix O: Analysis of photo linear elements, Bighorn-Pryor Mountains, Montana and Wyoming.

from a special report on research under contract NAS 5-21799.

Blackstone, D. L., 1973, Analysis of photo linear elements, Bighorn-Pryor Mountains, Montana and Wyoming; National Technical Information Service, Springfield, Virginia, Report E73-10704, 15 p.

In a continuing study of photo linear elements* in the exposed Precambrian rocks on the core of several Wyoming mountain ranges the following ERTS images were examined:

1013 - 17291 - 5	5 August, 1972	(Fig. 2)
1030 - 17235 - 5	22 August, 1972	(Fig. 3)
1211 - 17302 - 5	19 February, 1973	(Fig. 4)
1013 - 17291 - 4, 5, 7	Color Composite	

All well defined linear photo elements were plotted on overlay sheets at the same scale as the imagery (approximately 1:1,000,000). The elements observed range from a few miles to tens of miles in length. The August imagery is essentially free of cloud cover whereas the February imagery has complete snow cover. Certain elements were accentuated by the snow cover.

Fifty-two major linear elements were located on a map with some geographic data (Fig. O-1). Included in the plots were monoclinal features involving the Lower Paleozoic sedimentary rocks on the assumption that they reflect basement features, as has been demonstrated by previous ground-mapping in both the Pryor and Bighorn Mountains.

No data were taken from the folded sediments in the Bighorn Basin proper. No ground check has been made subsequent to the examination of the ERTS imagery. However, the writer has had extensive field experience in these areas.

*Note: The term photo linear element is used here to describe any markedly linear element observable on the imagery irregardless of cause. In this particular situation the linear features have a geomorphic expression.

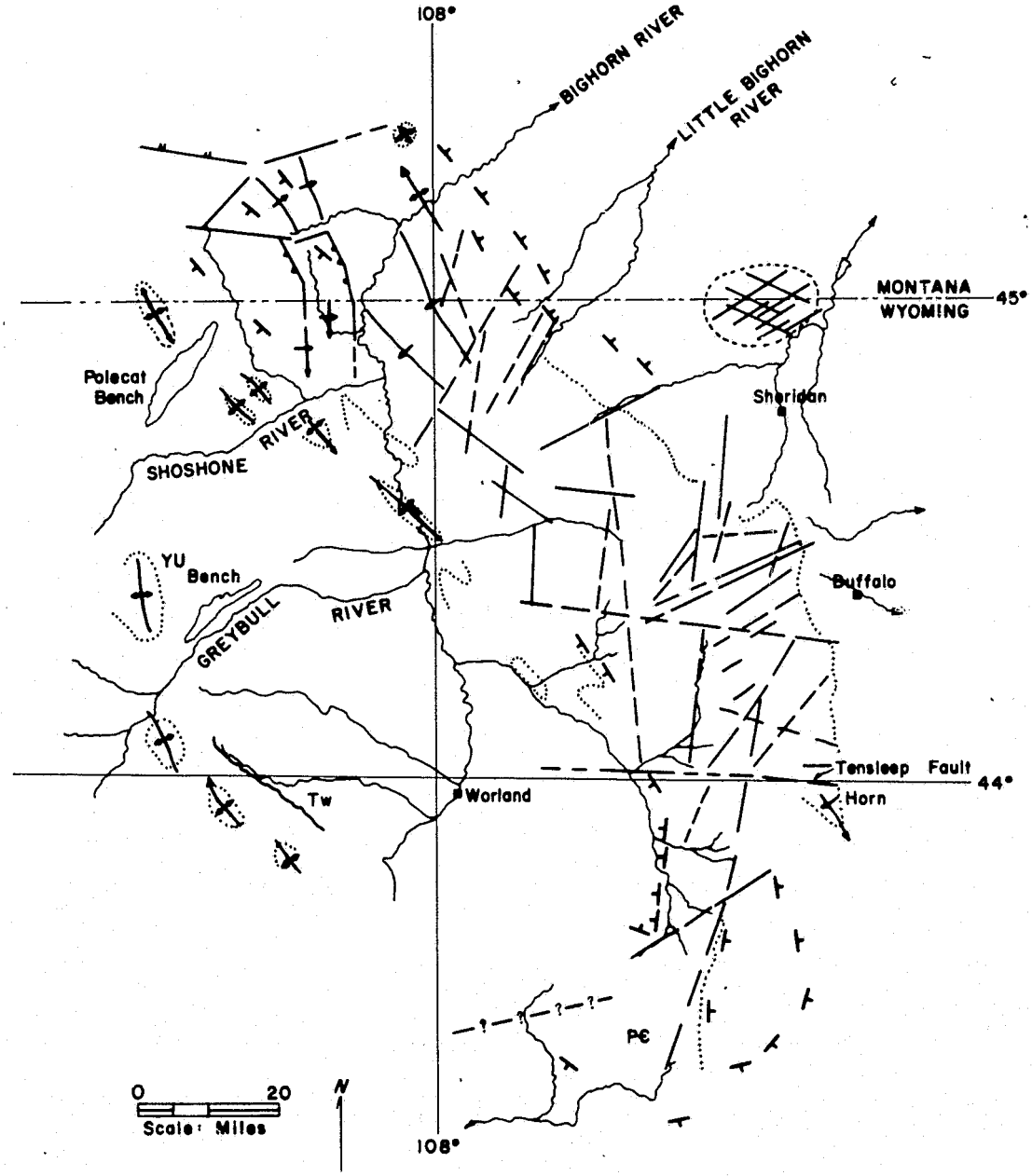


Figure O-1. Major linear elements of the Pryor and Bighorn Mountains.

ORIGINAL PAGE IS
OF POOR QUALITY

The azimuth of fifty-two (52) linear photo elements were plotted on a rose diagram in order to visually portray the concentration and orientation of the elements. A scale of 1 cm equals two (2) percent of the total population was used. Figure O-2a is the final plot.

The plot indicates that the majority of the observed linear elements have a northeast-southwest orientation with a bimodal distribution. One concentration of azimuths lies between longitudes N 55° E and N 65° E and the other concentration centers near N 25° E. The two sets thus intersect at an acute angle of approximately 45 degrees.

A lesser concentration of linear elements has a northwest-southeast orientation with the azimuths concentrated between N 10° W and N 30° W.

Many investigators have studied the problem of basement control upon the overlying sedimentary succession during the Laramide orogeny. Chamberlin (1945), in a classical paper, discussed the problem as it applies to the Bighorn Basin region. One facet of this problem is the role that fractures, shear zones, etc. in the Precambrian basement rocks might have played in Laramide deformation by being reactivated.

If the observed photo linear elements are ancient Precambrian features, and if the pattern, in the basement rocks continues westward beneath the sedimentary rocks of the Bighorn Basin, then the possibility exists of testing the relationship between basement control and orientation of Laramide folds.

The writer utilized two maps prepared by the U. S. Geological Survey:

Oil and Gas Investigations Preliminary Map No. 3. "Structure contour map of the Big Horn basin, Wyoming and Montana" by David A. Andrews, William G. Pierce and Jewell J. Kirby, 1944

Oil and Gas Investigations Map OM 182. "Structure and contour map of the Tensleep Sandstone in the Bighorn Basin, Wyoming and Montana" by A. D. Zapp, 1956.

From these maps the trend (azimuth) of 83 known and well defined anticlines in the Bighorn Basin was determined, and then plotted on a rose diagram in the same fashion that data concerning the photo linear elements were plotted.

The plot of the azimuth of the axes of the folds is presented in Figure O-2b. The dominant trend direction is northwest-southeast with a strong maximum (24%) concentrated between N 40° W and N 50° W.

By comparison with Figure O-2a, it is readily apparent that the trend of the anticlinal axes lies at an angle of about 80° to the principal concentration of trends of the photo linear elements. The only coincidence of trends is at a bearing of about + or - five degrees from true north. Approximately 7% of the photo linear elements and approximately 9.6% of the fold axes have this trend.

The preliminary conclusion is that the photo linear elements reflect major fracture systems in the Precambrian age basement rocks, but that they do not directly control the orientation of folds in the sedimentary rocks overlying the basement in the Bighorn Basin.

A further conclusion is that the folds in the Bighorn Basin have a remarkably consistent trend of the anticlinal axes, that is related in some as yet undetermined fashion to the Laramide downfolding of the basin as a whole.

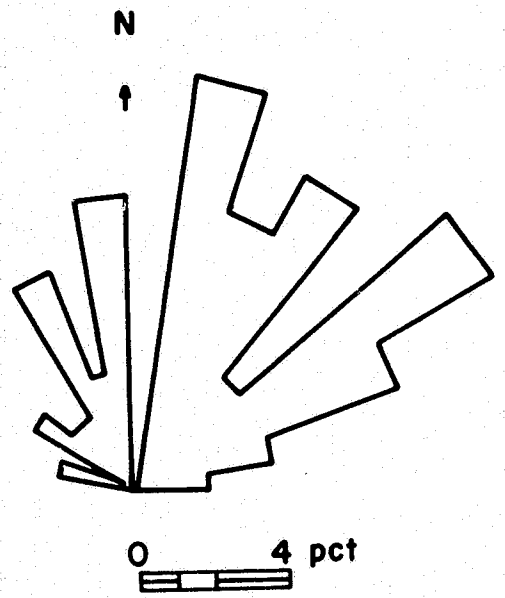


Figure 0-2a Rose diagram showing trends and orientations of observed linear elements.

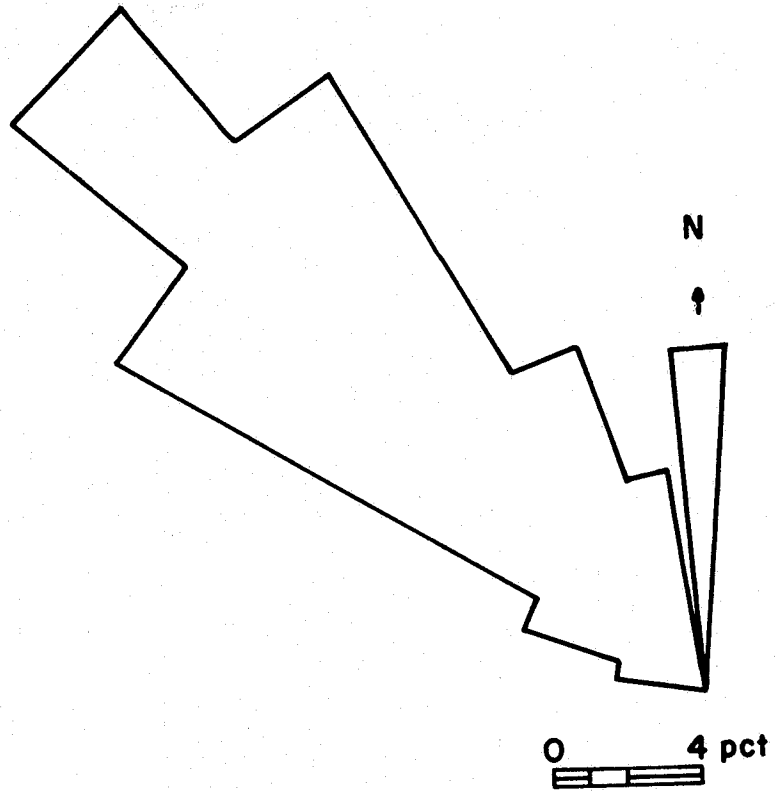


Figure 0-2b Rose diagram showing the orientations of fold axis in the Bighorn Basin.

Appendix P: Analysis of photo linear elements, Laramie Mountains, Wyoming.

from a special report prepared under contract NAS 5-21799.

Blackstone, D. L., 1973, Analysis of photo linear elements, Laramie Mountains, Wyoming; National Technical Information Service, Springfield, Virginia, Report E73-10663, 16 p.

The essentially north-south trending Laramie Mountains developed during the Laramide orogeny, but have many associated northeast trending folds of considerable magnitude. The relationship of the strongly divergent structural trends is not readily apparent and is the subject of this study.

Using both satellite and aircraft imagery the terrane was examined for linear structural features. The linear features are, for the most part, expressions of rock fractures rather than layering within the rock bodies. Recognition of linears was greatly facilitated by light snow cover.

All such features were plotted on acetate overlay sheets, the strike (azimuth) determined, the features counted and the results displayed in rose diagrams as frequency of occurrence. No field check has been made to date. Correspondingly, the results must be considered as first order reconnaissance, subject to further check.

The general distribution of lithologies of the Laramie Mountains is shown on Fig. P-1, modified from Condie (1969), Newhouse and Hagner (1957) and Darton, Blackwelder and Siebenthal (1910). All linear features taken from ERTS images are shown on Fig. P-2. Comparison of Figures P-1 and P-2 indicates that the underlying rock type does not control the distribution nor the trend of the linear features.

The rose diagram plots of the azimuths of 720 linear features of the southern Laramie Range imagery is shown on Fig. P-3a. The plot defines three principal trend

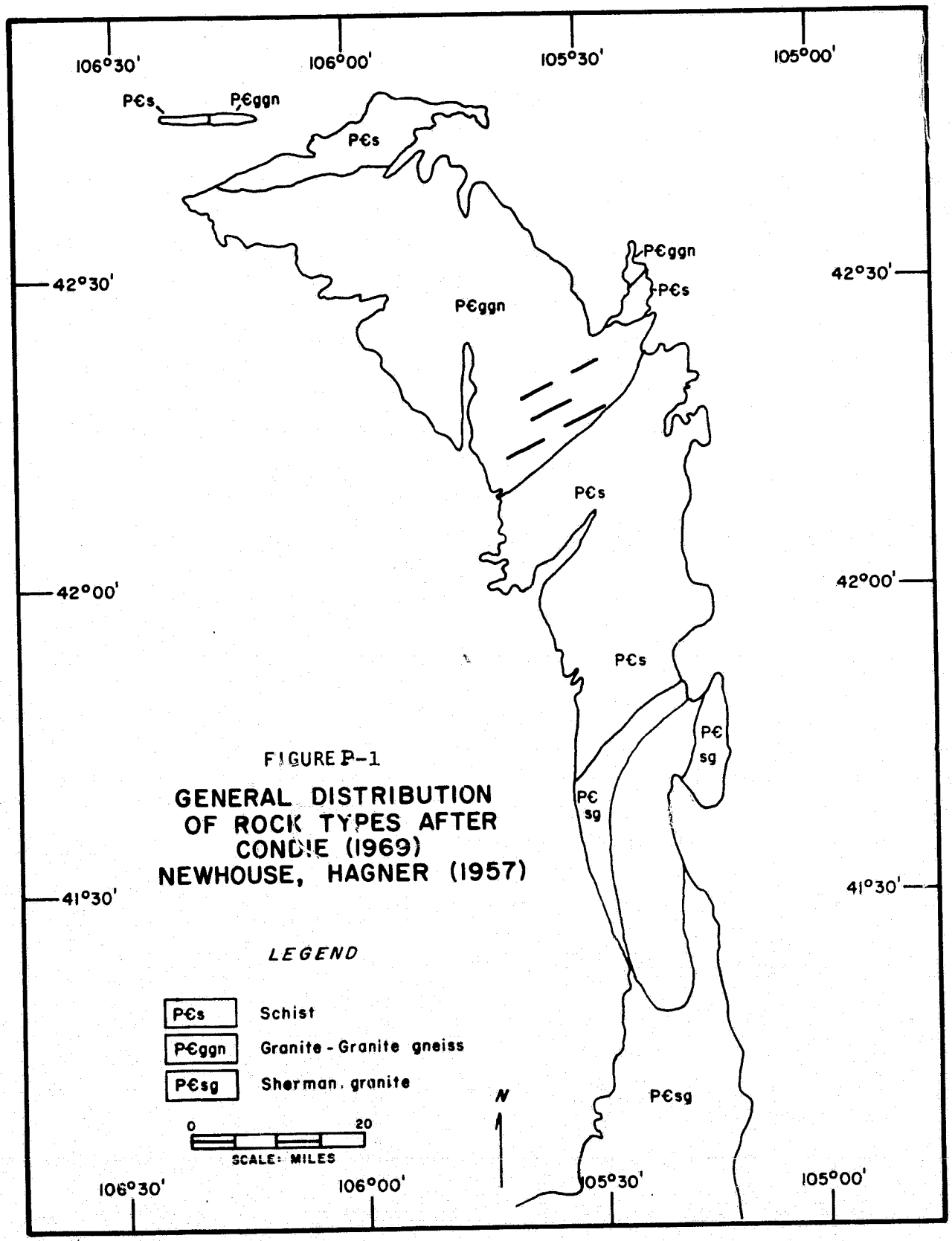


FIGURE P-1

GENERAL DISTRIBUTION OF ROCK TYPES AFTER CONDIE (1969) NEWHOUSE, HAGNER (1957)

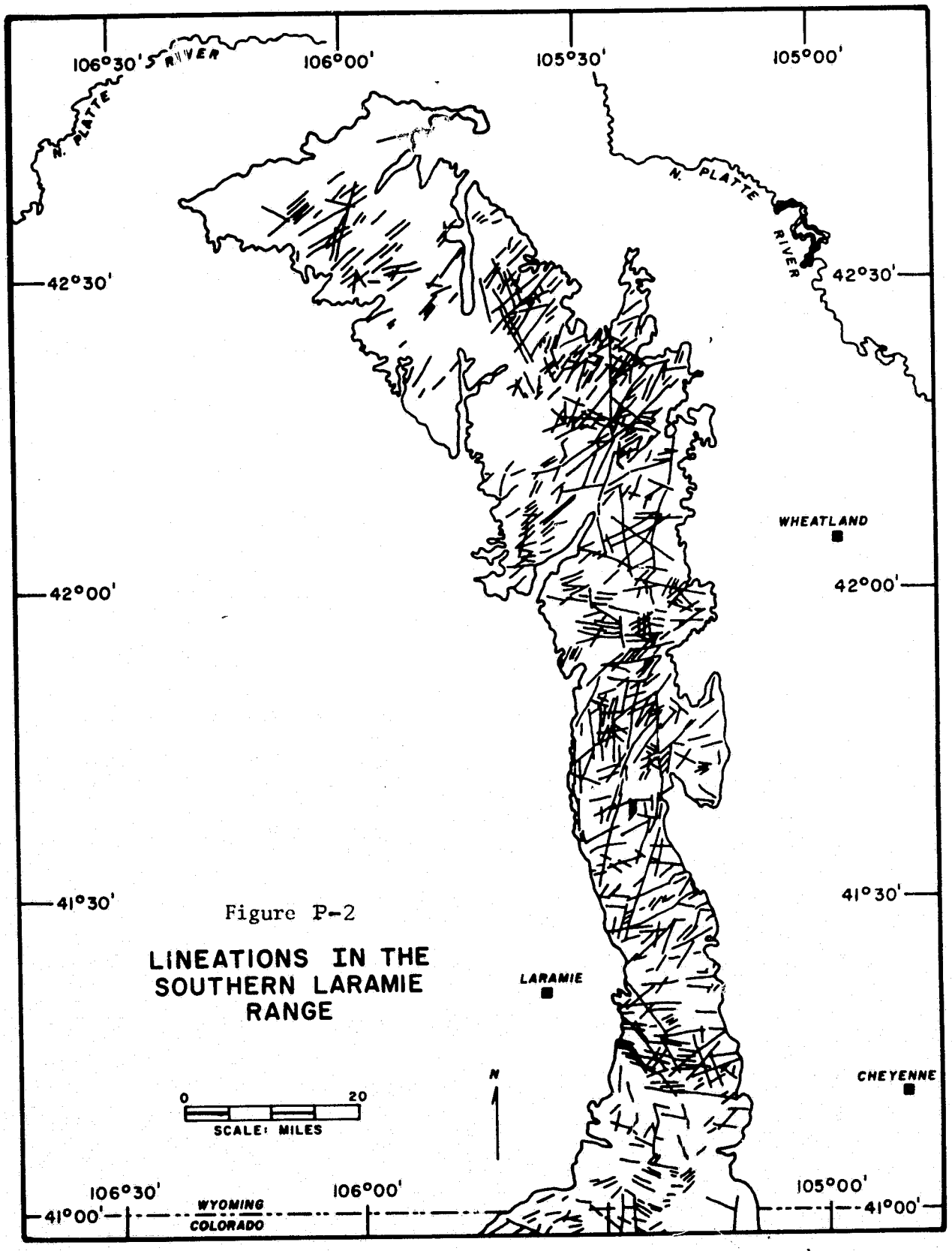


Figure P-2

LINEATIONS IN THE SOUTHERN LARAMIE RANGE

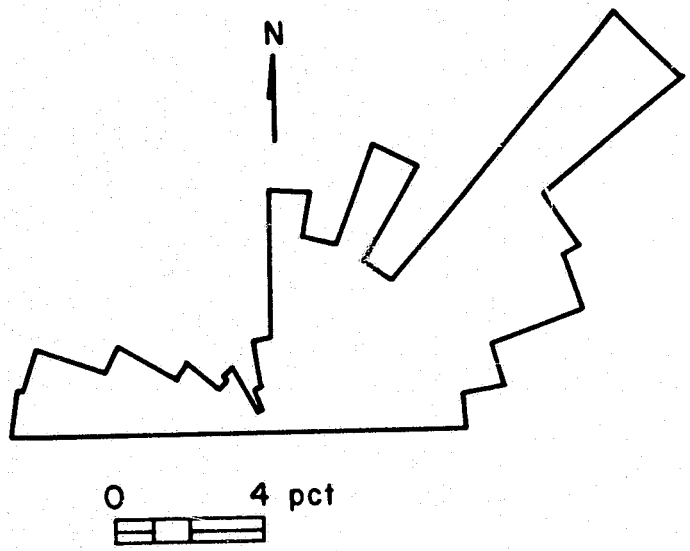


Figure P-3a. Rose diagram showing dominant orientations of photo linear elements of the southern Laramie Range.

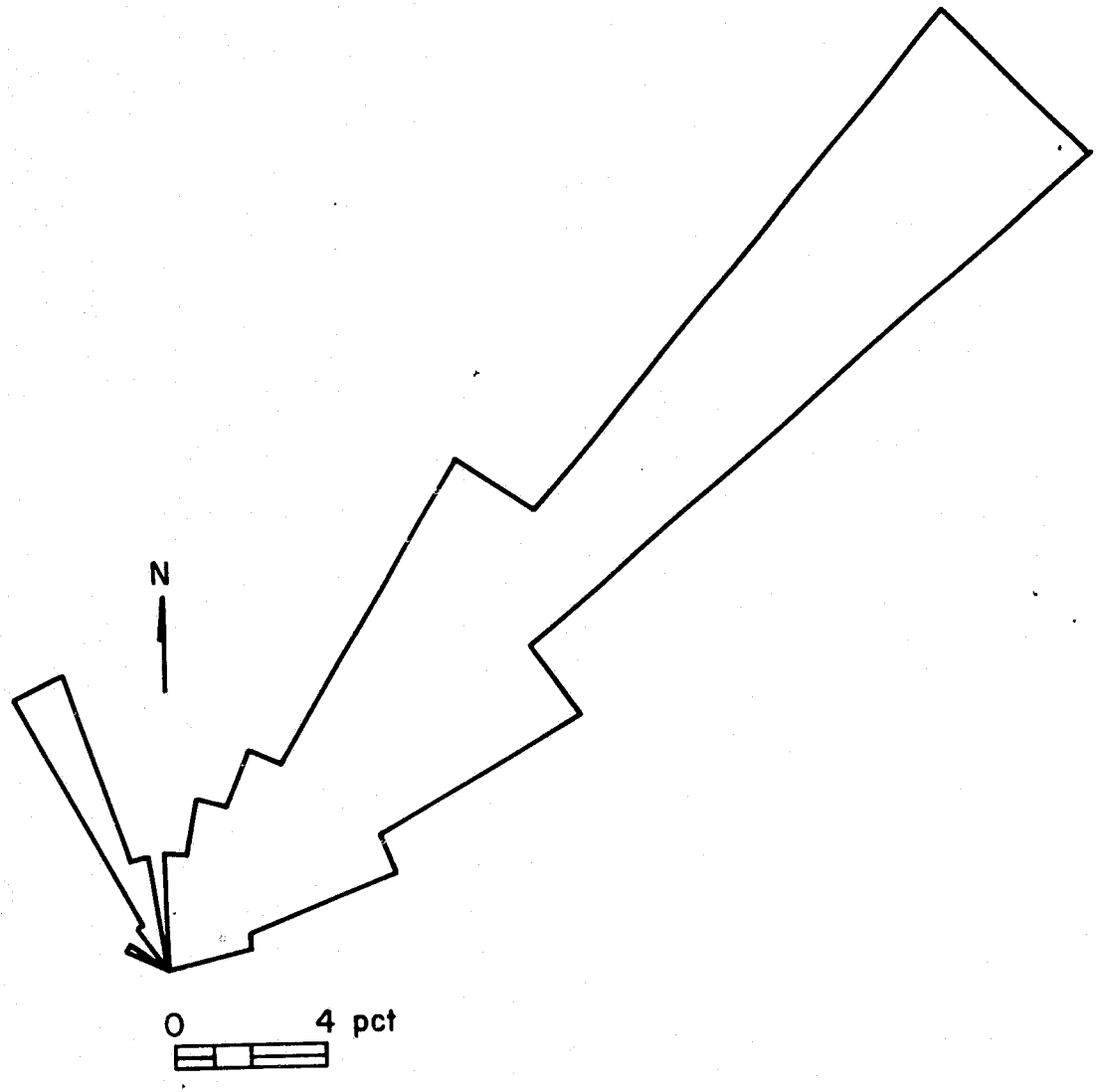


Figure P-3b. Rose diagram showing dominant orientations of photo linear elements of the northern Laramie Range.

directions of the linear features which are believed to be fractures. The three dominant directions are:

Quadrant	Concentration	Azimuth
N. 20 E.	8.2%	20^{o}
N. 40 to 50 E.	14.5%	40^{o} to 50^{o}
N. 70 to 80 W.	13.7%	280^{o} to 290^{o}

Granite and granite gneiss terranes totally dominate the northern Laramie Range, consequently there was no opportunity to establish any relationship between rock type and variation in orientation of linear features.

The rose diagram plot of 160 linear features of the northern Laramie Range shown on Figure P-3b reveals a pronounced northeast orientation. The principal orientation is:

Quadrant	Concentration	Azimuth
N. 40 to 50 E.	31.8%	40^{o} to 50^{o}

With a limited number of linear features having an orientation of:

Quadrant	Concentration	Azimuth
N. 20 W.	6.3%	340^{o}

In addition to the measurements described above, and made from interpretations of ERTS satellite imagery at an approximate scale of 1:000,000, a similar set of measurements was made from interpretations of aerial photography (color) at a scale of approximately 1:16,000. To accomplish this comparison, three small areas were selected to be analyzed through interpretation of the aerial photography.

Data from the three small domains follows.

Domain A - T. 17 N., Rs. 71 and 72 W.
167 Readings

Domain B - T. 26 N., R. 72 W.
169 Readings
Area of granite and granitic gneiss

Domain C - T. 30 N., R. 75 W.
280 Readings
Area of granite and granitic gneiss

No domain entirely within an area of schistose rocks was studied.

In Domain A the observed data is summarized below.

Quadrant	Concentration	Azimuth of Trends
N. 45 E.	7.2%	45°
N. 80 E.	10.1%	80°
N. 60 W.	11.4%	300°

Data from Domain B is summarized below.

Quadrant	Concentration	Azimuth of Trends
N. 5 E.	2.9%	5°
N. 50 E.	26.6%	50°
N. 85 E.	4.1%	85°
N. 65 W.	5.3%	295°

Data from Domain C are summarized below.

Quadrant	Concentration	Azimuth of Trends
N. 15 E.	7.1%	15°
N. 50 E.	17.5%	50°
N. 85 W.	5.0%	275°
N. 60 W.	11.1%	300°

Figure P-4 is a composite rose diagram of 616 readings in the restricted domains.

A comparison of the data from the two sets of imagery (satellite and underflight) shows very little variation. The number of observations from the restricted domains is greater, indicating that smaller scale features can be seen from the underflight that are not detectable from the satellite imagery. It is also apparent that the minor fractures agree will in orientation with the major ones.

Hamed Bekkar (1973) compared the orientation of the imagery features with the orientation of folds and faults for the entire Laramie Basin, and demonstrated the close agreement of the two sets of observations. Therefore, it is concluded that the northeast trending linear elements control the orientation of numerous Laramide folds in the areas marginal to the Laramie Mountain uplift. Examples of such folds are Como Bluff anticline, McGill anticline, and Flat Top anticline.

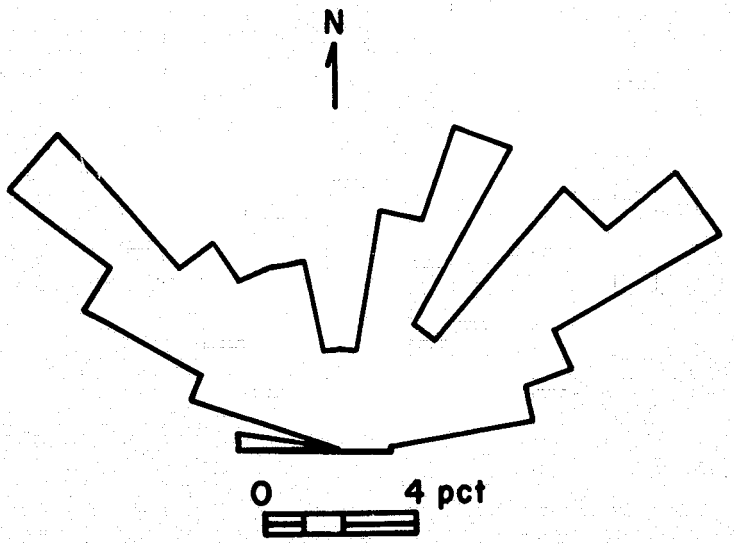


Figure P-4. Composite rose diagram of photo linear elements located on aircraft imagery.

The type of rock within the Precambrian terrane does not appear to influence the orientation of the fractures (assuming that the photo linear features are the expression of bedrock fracturing).

Appendix Q: Geology of photo linear elements, Great Divide Basin, Wyoming.

from a special report for contract NAS 5-21799.
Blackstone, D. L., 1973, Geology of photo linear elements, Great Divide Basin, Wyoming, National Technical Information Service, Springfield, Virginia, Report E73-10958/WR, 14 p.

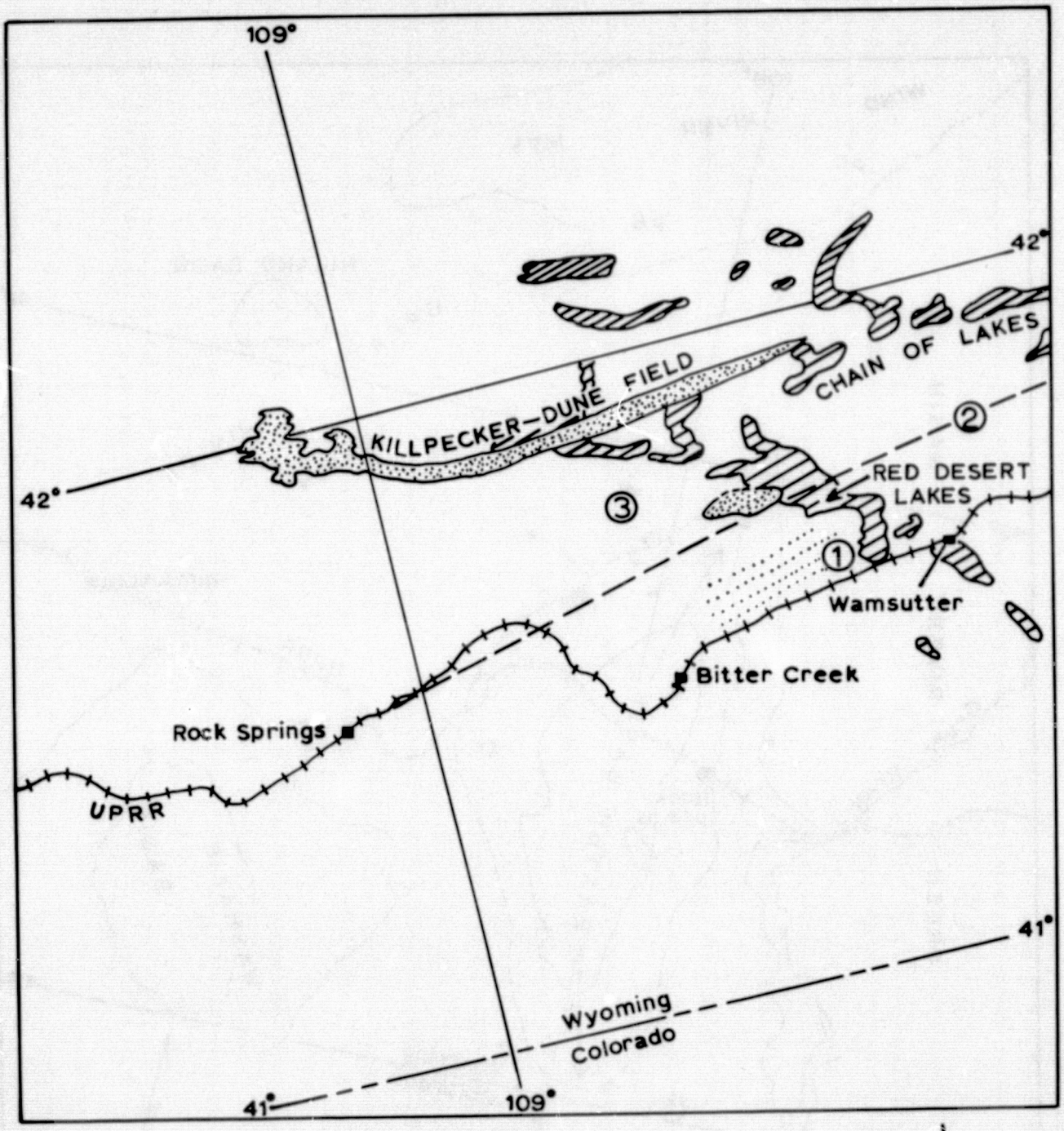
The Great Divide basin is a broad structural depression lying east of the Rock Springs Uplift, south of the Wind River Mountains, and Sweetwater Uplift, and east of the Rawlins Uplift. The southern boundary is the poorly defined Wamsutter Arch.

The structural basin does not fully coincide with the area of interior drainage that includes what has been called the Red Desert, Great Divide depression, etc. The Continental Divide separates into two strands in T. 27 N., R. 101 W., which diverge widely and enclose an area of about 4000 square miles before rejoining into a single divide near Divide Mountain in T. 18 N., R. 81 W. The area of internal drainage is characterized by extensive playa lake deposits, sand dunes, silt and clay dunes, saline lakes, and very few permanent streams. In part this area of internal drainage may result from the blocking of eastward-flowing drainage by sand dune migration in the eastern part of the area. The features examined appear on ERTS images:

1013-17300 (bands 4, 5, 7 and color composite) and
1030-17242 (bands 4, 5, 7 and color composite).

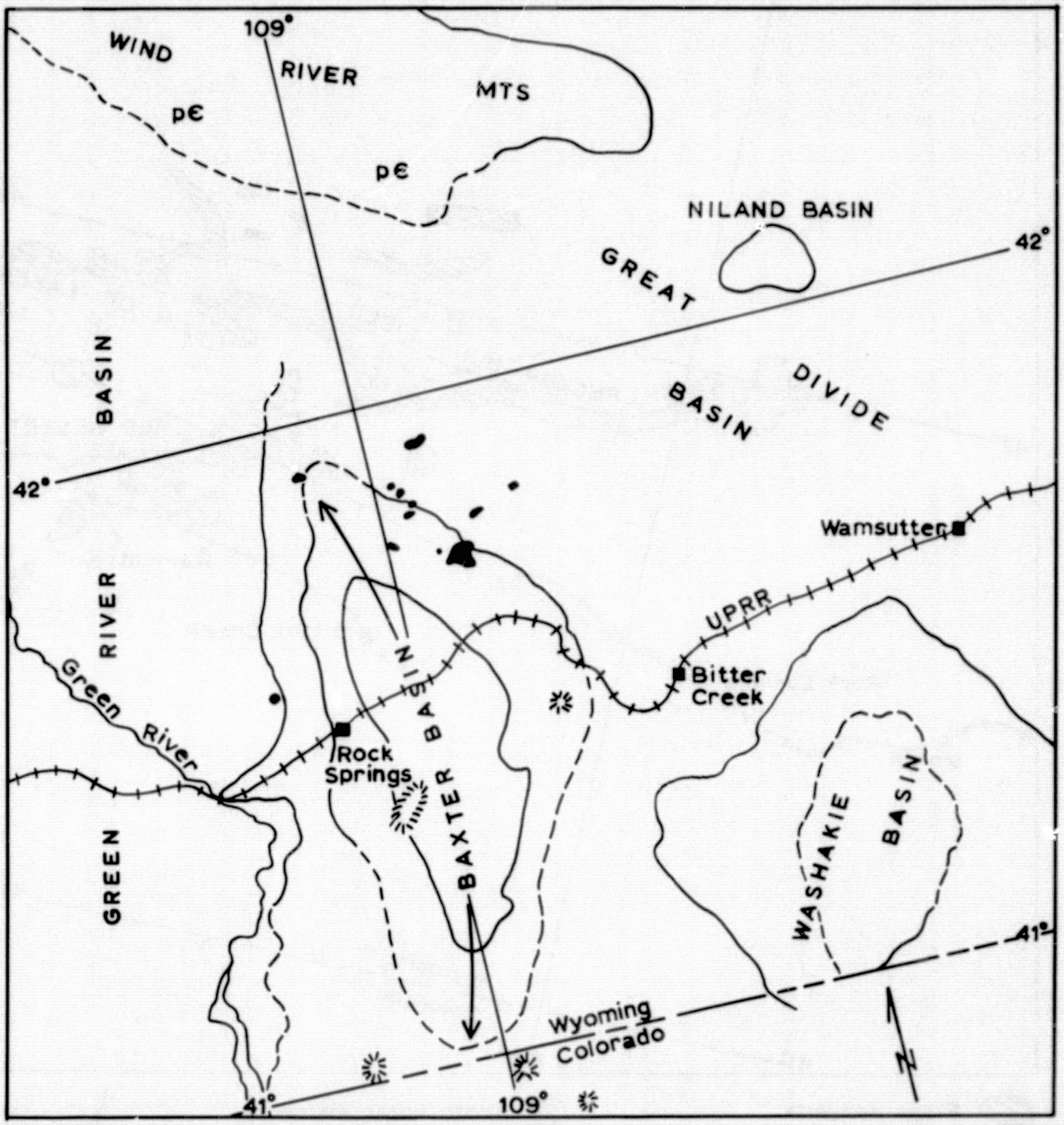
Figure Q-1 outlines the major photo linear elements and can be compared with Fig. Q-2 to see the relationship to the major tectonic elements.

Immediately north of U. S. Highway 1-80 (U. S. 30), at Tipton Siding, the imagery shows an area of strongly striped ground. The area is about 20 miles in length and about 10 miles in width. First examination of the imagery suggests some type of fault control, but ground elevation examination reveals that the striped ground is the site of linear



Major linear features of the Great Divide Basin (from ERTS-1 image interpretation).

Figure Q-1



Major structural elements of the Great Divide Basin, Wyoming.

Figure Q-2

strips of stabilized sand dunes of moderate relief. Within each dune belt strip are blowouts and short transverse dunes.

The dunes are stabilized by greasewood (Sarcobatus sp.) rabbit brush (Chrysothamus sp.) and other minor species which have a contrasting color, and also are markedly different in color value from the sagebrush (Artemesia sp.) which is the common shrubbery cover of the region. A more detailed treatment of the relationship between Wyoming sand dunes and the stabilizing vegetation is presented in separate ERTS-1 special report (Kolm, 1974).

The alignment of the dunes is about N. 75 E. This trend is more northeasterly than the prominent and presently active Killpecker dune field in the northern part of the basin. The distribution of the dunes is limited on the east by the rising series of escarpments encircling the northern flank of the Washakie Basin. The dune area essentially terminates along the eastern end in the Red Desert playa.

A second, more subtle, photo linear feature (location 12, Fig. Q-1) crosses the area in a N. 80 E. direction beginning near Point of Rocks siding and continuing northeasterly to a point about due north of Creston, Wyoming. The linear element appears on the color positive transparency image as a faint line which at times appears lighter than the surrounding terrain and at other places appears darker.

Several traverses were made in a north-south direction across the linear element in the area between Table Rock and Creston Junction, north of U. S. Highway 1-80. Specific ground control was sought to establish the nature of the linear elements.

Particular attention was given to geomorphic form, stream alignment, observable bedrock geology which might reveal faulting, vegetational changes, distribution of playa deposits, and aeolian features.

The result of the traverses was negative with regard to critically defining the nature of the Point of Rocks

photo linear element. No positive faulting was found. Minor faulting with a trend of approximately N. 65 E. has been reported by Pipiringos (1961) and by Masursky (1962) in the Great Divide basin. These faults are reported to have displacements up to 70 feet. Unfortunately this system of fractures does not coincide in position with the feature under consideration. The low relief and widespread Quaternary deposits made detailed examination of the bedrock very difficult. Previous mapping is undoubtedly detailed enough to define the bedrock structure.

The Great Divide basin area is characterized by internal drainage and the phenomena associated with such drainage situations. To date, no single paper has discussed geomorphology and origin of the internal drainage in this basin. In fact, only in 1864 did the topographic base map of Wyoming reflect the dual divide. The most complete presentation of the geology is that in the Hydrologic Atlas (Welder and McGreevy, 1966). The geomorphic history is complex, and warrants study as to its origin.

The playa-lake flats are the site of a limited amount of lacustrine deposition, but the depressions in which the playas exist must be due in part to an earlier cycle of deflation. The material removed from these sites must be accounted for even if transported considerable distances.

The total effects of wind action, both deflational and depositional are very large in this region. The extensive Killpecker dune field is still partially active, and is perhaps the most striking example; though there are extensive areas of active dunes in the eastern part of Separation Flats. The results of wind action in other parts of the Great Divide basin are less pronounced though several areas of stabilized dunes are present (location 1, Fig. Q-1).

In many areas thin strands of completely stabilized linear dunes can be seen. These appear on the ground as low ridges covered by sagebrush (Artemesia sp.); though other plants, such as rabbit brush (Chrysothamus sp.), favor this environment. The ridges are from two to ten feet in hieght and, 10 to 30 feet in width. The dune ridges vary in length from tens to hundreds of feet. The dunes are unobtrusive on first

inspection, and become evident only as the observer learns to discriminate these forms from the bedrock vegetation association.

The total effect of the distribution of these smaller, finer linear dunes is to give a northeast trending grain to certain areas of topography which might be interpreted as a bedrock structural grain.

The scale of the imagery precludes final judgment as to how much of the photo linear aspect is due to aeolian action, rather than bedrock control. This investigator believes that wind created phenomena are far more pervasive than previously considered.

Appendix R: Tectonic analysis of southwestern Wyoming from ERTS-1 imagery.

from a special report on work performed under contract NAS 5-21799:

Blackstone, D. L., 1972, Tectonic analysis of southwestern Wyoming from ERTS-1 imagery; National Technical Information Service, Springfield, Virginia, Report E72-10377, 8p.

Examination of the positive transparency no. 1013-17300-5, August 5, 1972, Rock Springs Uplift area, Wyoming and those immediately adjacent reveals two previously unreported tectonic features (Figure R-1).

1. A linear element trends about N. 40° W. (320°) and passes approximately through the common corner of Townships 25 - 26, N., and Ranges 105-106 W., 6th Principal Meridian, Wyoming. The element passes approximately 4 miles northeast of the community of Farson, Sweetwater County, Wyoming and will be referred to by the name Farson element.
2. A linear element trending N. 65° E. (65°) and aligned northeastward from the town of Rock Springs, Sweetwater County, Wyoming, and thence across the Red Desert to a point near Lamont, Carbon County, Wyoming, will be called by the name Red Desert element.

The two linear elements are inferred at this time to represent the surface trace of deep seated structural elements, probably faults, which increase in magnitude of displacement with depth. The element passing near Farson is subparallel to the zone of normal faulting previously mapped at Tabernacle Butte (McGrew & Berman, 1955). The linear element continues southeastward into the area of the Leucite Hills volcanic field (Kemp & Knight, 1903). The northeast flank of the Rock Springs Uplift as far south as the Black Buttes station on the U.P.R.R. is also aligned with this trend.

Two interpretations of the data are made:

a. The Leucite Hills volcanic vents are associated with and possibly controlled by the Farson linear element,

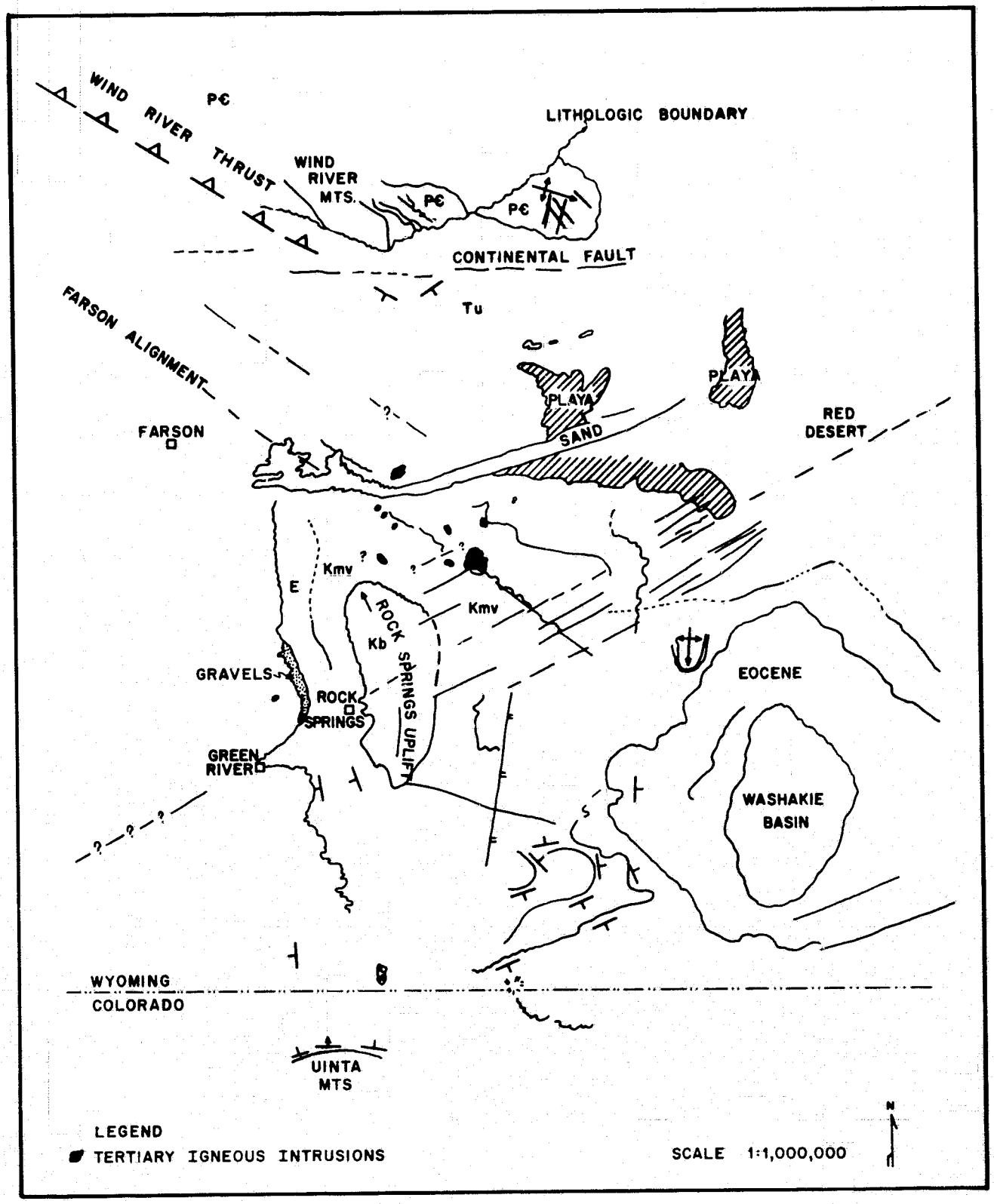


Figure R-1. Major tectonic elements of southwestern Wyoming interpreted from ERTS-1 imagery.

b. The Farson structural element was active in Laramide time delimiting the northeast flank of the Rock Springs Uplift; and must have continued active until the eruption of the Leucite Hills volcanic products in Pliocene time. The volcanic rocks are dated as 1.25 m. y. by Bradley (1961).

The second structural element trends northeastward from Rock Springs, crosses the Rock Springs Uplift and extends across the Red Desert/Great Divide Basin to the east. The east flank of the Rock Springs Uplift is ruptured by numerous high-angle reverse faults (Schultz, 1909) with northeast strikes. It should be noted that previously mapped and documented structural elements having the same structural trends exist in southeast Wyoming. The Como Bluff (Dunbar, 1944) to Pinto Creek faulted anticlinal trend (Kaabar, 1971) is a very prominent feature displacing the Precambrian basement rocks along its eastern extent in the Laramie Mountains. The Mullen Creek part of the Mullen Creek - Nash Fork shear zone (Houston, 1968) in the northern Medicine Bow Mountains, Wyoming, also has the same orientation. The rather poorly defined Wyoming lineament (Ransome, 1915, Blackstone, 1951) is a zone of structural discontinuity that is also roughly parallel to the Rock Springs element.

The Precambrian rock exposures of the northern Laramie Mountains terminate along a faulted syncline at Deer Creek southeast of Casper, Wyoming which is exactly on the northeastward extension of the Rock Springs - Red Desert linear element. There is no evidence of structural disturbance where the projected alignment crosses the Ferris - Seminoe Mountains in central Wyoming.

The significance of the Rock Springs - Red Desert element is that it further documents a system of northeast trending structural elements in SE Wyoming which have had a profound effect upon the delineation of the tectonic pattern.

In terms of interpreting the Laramide tectonic pattern of Wyoming the new data reinforces the concept that the pattern is best compared to a mosaic of blocks; and that the blocks are

bounded by structural elements which have a limited number of orientations, probably not more than six.

Regional tectonic implications for origins of the tectonic patterns in Wyoming have been suggested by several investigators (Blackstone, 1963; Malahoff and Moberly, 1968; Sales, 1968). The basic question to be resolved is whether the major tectonic elevations and depressions of the crust in the Rocky Mountain foreland are due to a compressive, horizontally directed stress field or a stress field reflecting dominantly vertical motion.

The existence of major subparallel linear elements, extendind for tens of miles suggests a compressive stress field over large areas, at least in the early stages of the regional deformation.

Appendix S: Comparison of ERTS imagery with Skylab S-190A, S-190B, and aerial photographs for lineation mapping.

from a special report under contracts NAS 5-21799 and Nas 9-13298:

Houston, R. S., Marrs, R. W., and Tomes, B. J., 1974, Some illustrations of the advantage of improved resolution in geologic studies; National Technical Information Service, Springfield, Virginia, Report E74-10628, p. 56-67.

A portion of the Wind River Mountains of Wyoming has been studied by use of ERTS images, Skylab 190A and 190B photographs, aircraft photographs, and on the ground. The Wind River Mountains are a northwest striking, Precambrian cored, major uplift located in west central Wyoming. The uplift is approximately 100 miles long and over 30 miles wide at its greatest width. The uplift has the form of an assymetric anticline with steep overturned and faulted limb on the southwest and great gently dipping northwest striking hogbacks of Paleozoic and Mesozoic sedimentary rocks on the northeast (Berg, 1962). The Precambrian rocks of the core of the structure are primarily Early Precambrian felsic gneisses and schists and various types of foliated granite cut by basalt dikes of different Precambrian ages. In the extreme southeast part of the uplift (Bayley, 1965a), a major greenstone belt cuts through the range.

The Precambrian core of the Wind River Mountains is cut by numerous fractures ranging from major faults and shear zones to minor faults and joints. These fractures have been mapped in a small part of the uplift (Barrus, 1968; Granger and others, 1971; Parker, 1972; Pearson and others, 1971; and Richmond, 1945) and they range from shear zones with extensive catalysis and mylonization that probably developed during Precambrian episodes of high-rank metamorphism to discrete fractures of Tertiary age. Many of the Precambrian fractures were filled with basaltic magma and are now expressed as basalt and diabase dikes that cut the gneisses and granitic terrane.

The most striking aspect of ERTS and Skylab images of the Wind River Mountains is the multitude of lineations that are

primarily expressions of the fractures and dikes, that show on the images. The initial study of the Wind River lineations was made by Parker (1972, Appendix N) who mapped the major fractures of the mountains using ERTS MSS-5 and 7 images and compared these lineations seen on aircraft images and recognized on the ground by a field survey.

Figures S-1 and S-2 show lineations mapped from ERTS images and Skylab 190A photographs of the western part of the Wind River Mountains. In this study all lineations were mapped that could be recognized, rather than simply the major lineations that were mapped by Parker. Three factors affected the mapping -- resolution, sun angle, and sun azimuth. ERTS is sun synchronous so that images are ordinarily generated in the morning with a sun azimuth that established a bias towards northeast-striking linear features; whereas Skylab passes give different perspectives and may result in the emphasis of a completely different set of lineations as shown in Figure S-3. Rose diagrams in Figure S-3 show that there are not only more lineations recognized on the Skylab 190A photograph but that the major set strikes north-northwest rather than northeast as is the case for ERTS. This is a sun azimuth effect because the major linear features are approximately perpendicular to the sun azimuth in both examples. It is primarily due to the fact that many lineations are expressed topographically and sun shadowing due to topography is more pronounced at right angles to the direction of illumination. Sun elevation will also play a role in lineation mapping because low sun elevations cause distinct shadowing where lineations are topographically expressed. Therefore, a few more lineations might have been mapped at the 42^{o} sun elevation of ERTS than at the 49^{o} sun elevation of Skylab, but this cannot be quantitized because of the variation in azimuth.

A judgment of the affect of resolution cannot be made directly because of the role played by sun azimuth. For example, Parker's map of major mapped fractures in the Wind River Mountains (Appendix N) suggests that more fractures strike

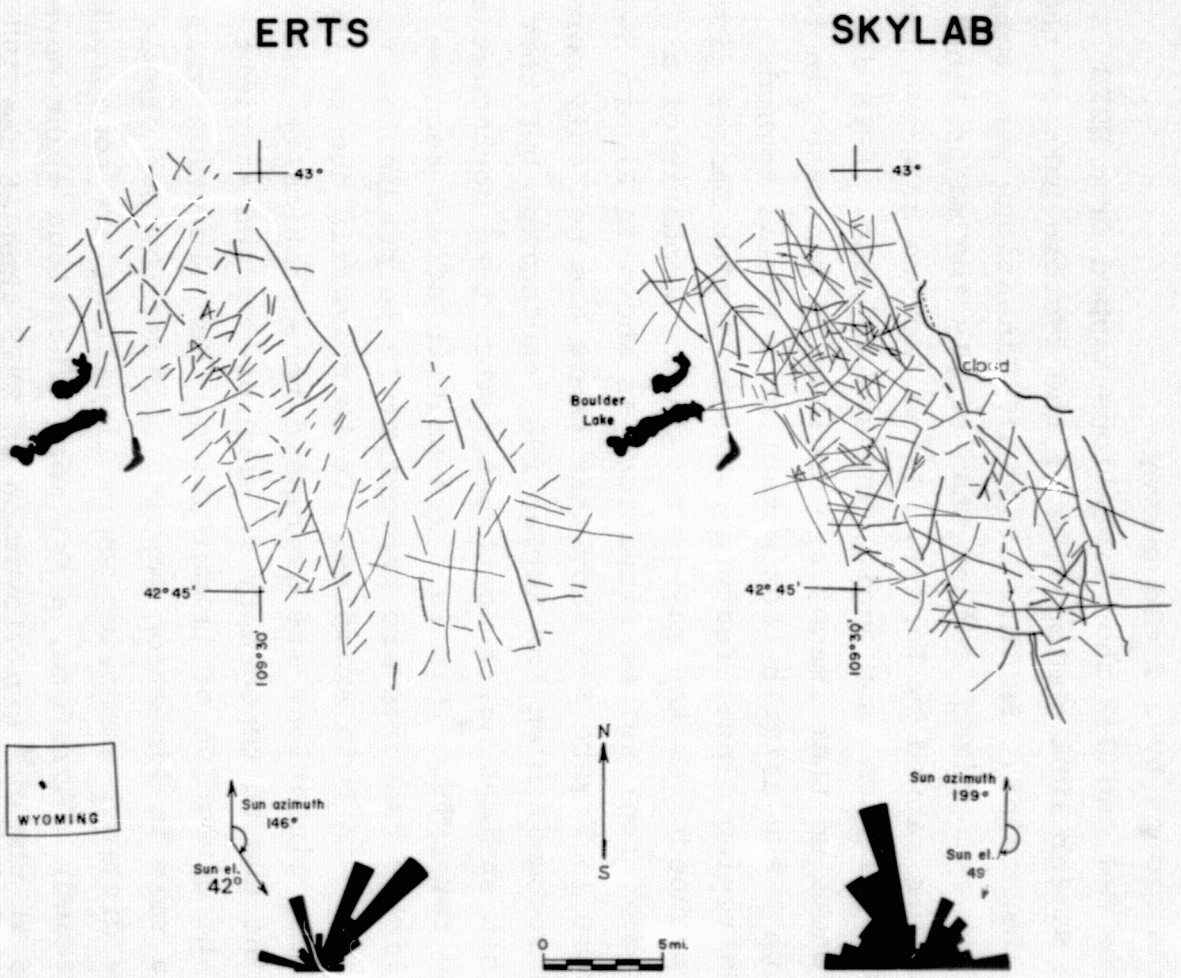


Figure S-3. Comparison of linear features mapped using ERTS images and Skylab S-190 B photographs of a part of the Wind River Mountains showing sun-azimuth bias.

OUT FRAME

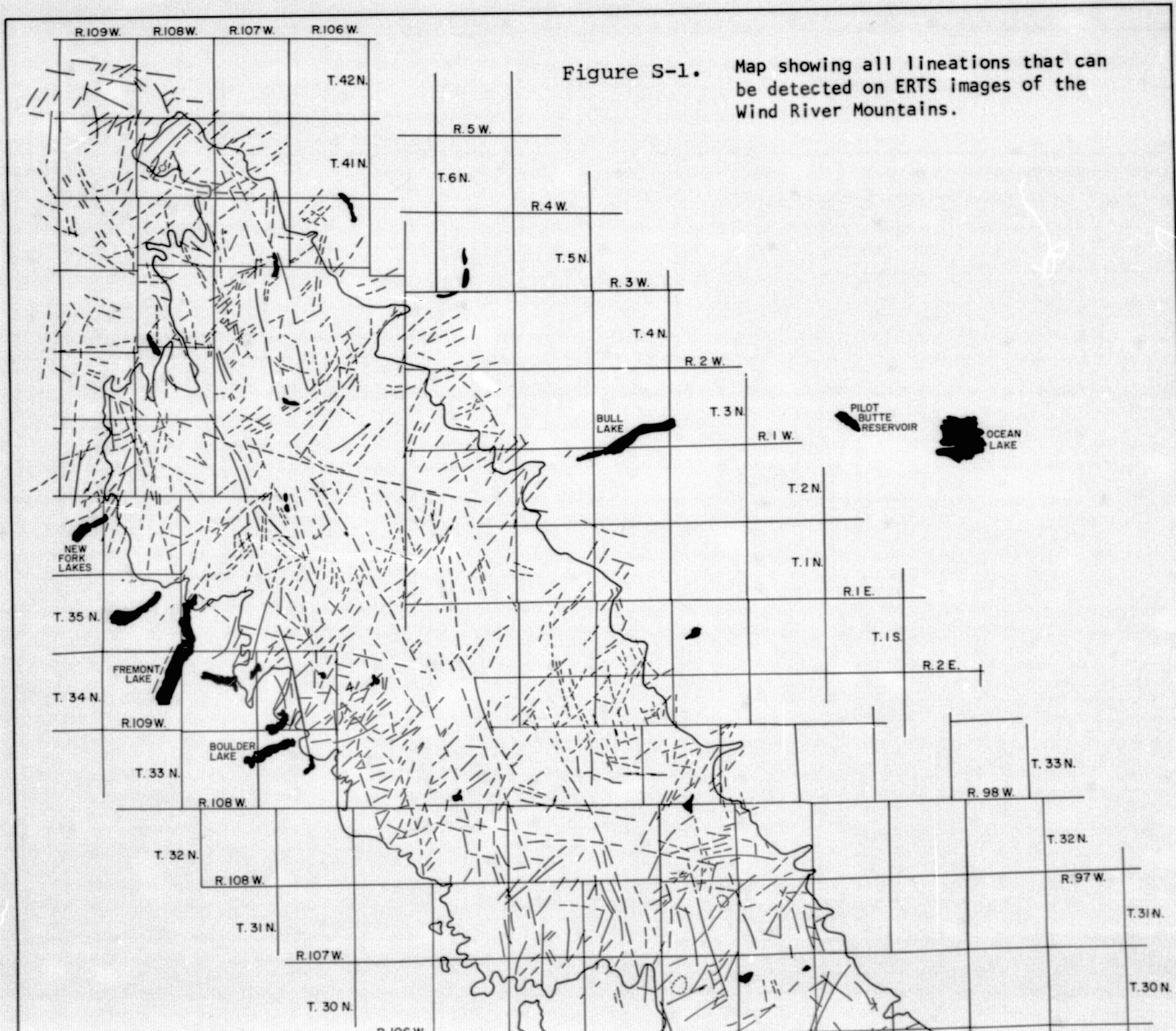
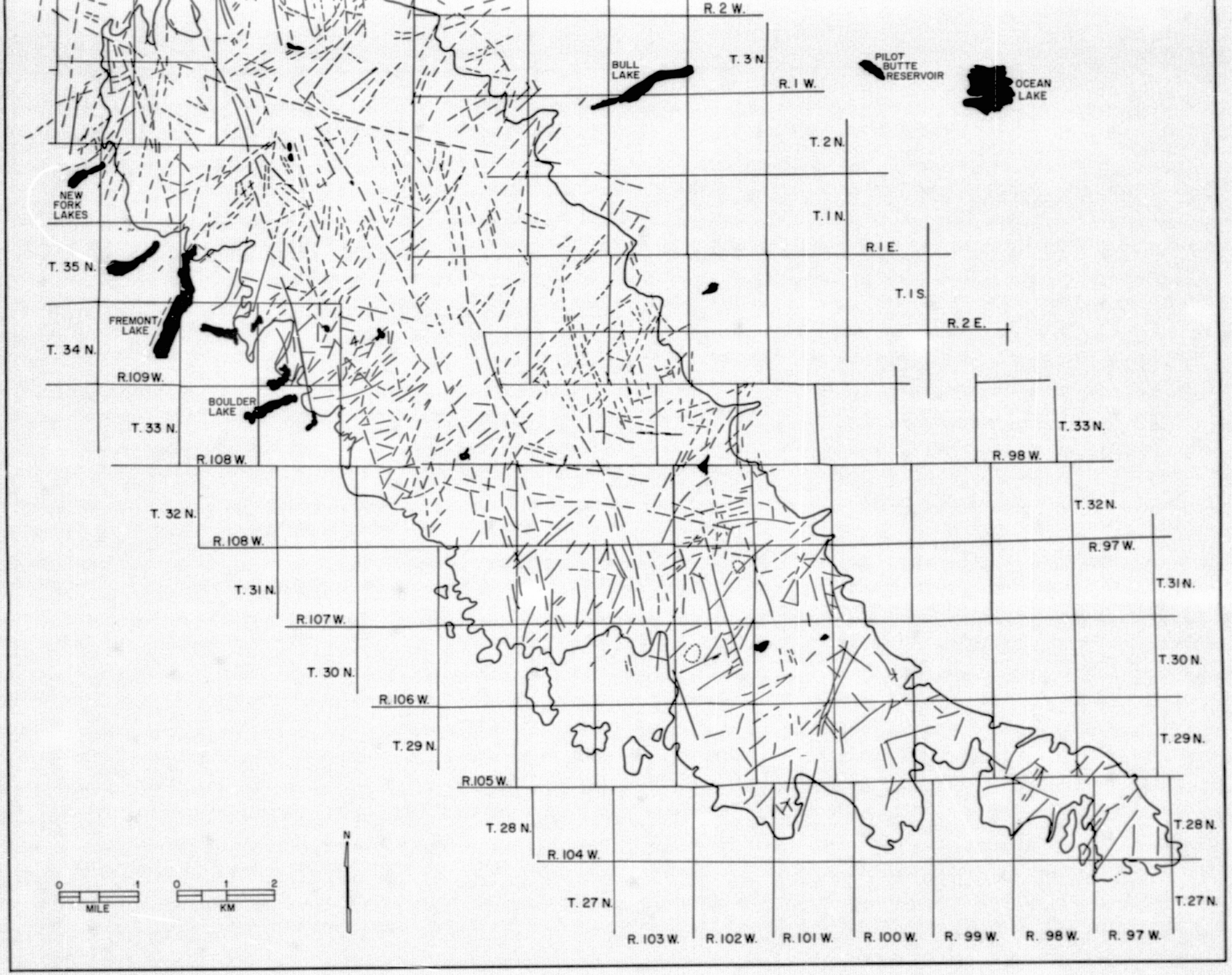
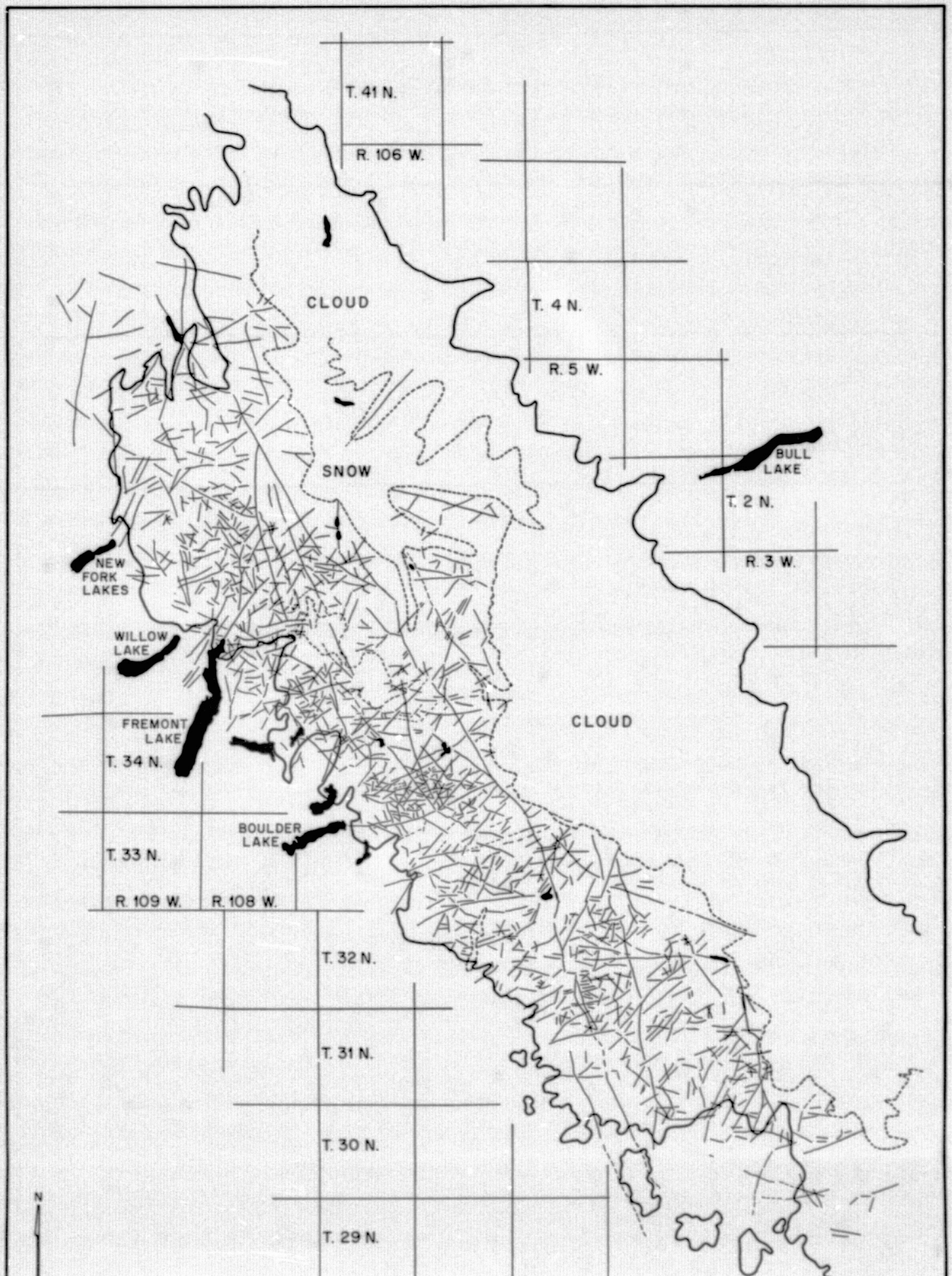


Figure S-1. Map showing all lineations that can be detected on ERTS images of the Wind River Mountains.



FOLDOUT FRAME

CUT FRAME


T. 41 N.
R. 106 W.
CLOUD
T. 4 N.
R. 5 W.
SNOW
BULL LAKE
T. 2 N.
R. 3 W.
NEW FORK LAKES
WILLOW LAKE
FREMONT LAKE
T. 34 N.
CLOUD
BOULDER LAKE
T. 33 N.
R. 109 W.
R. 108 W.
T. 32 N.
T. 31 N.
T. 30 N.
T. 29 N.
N

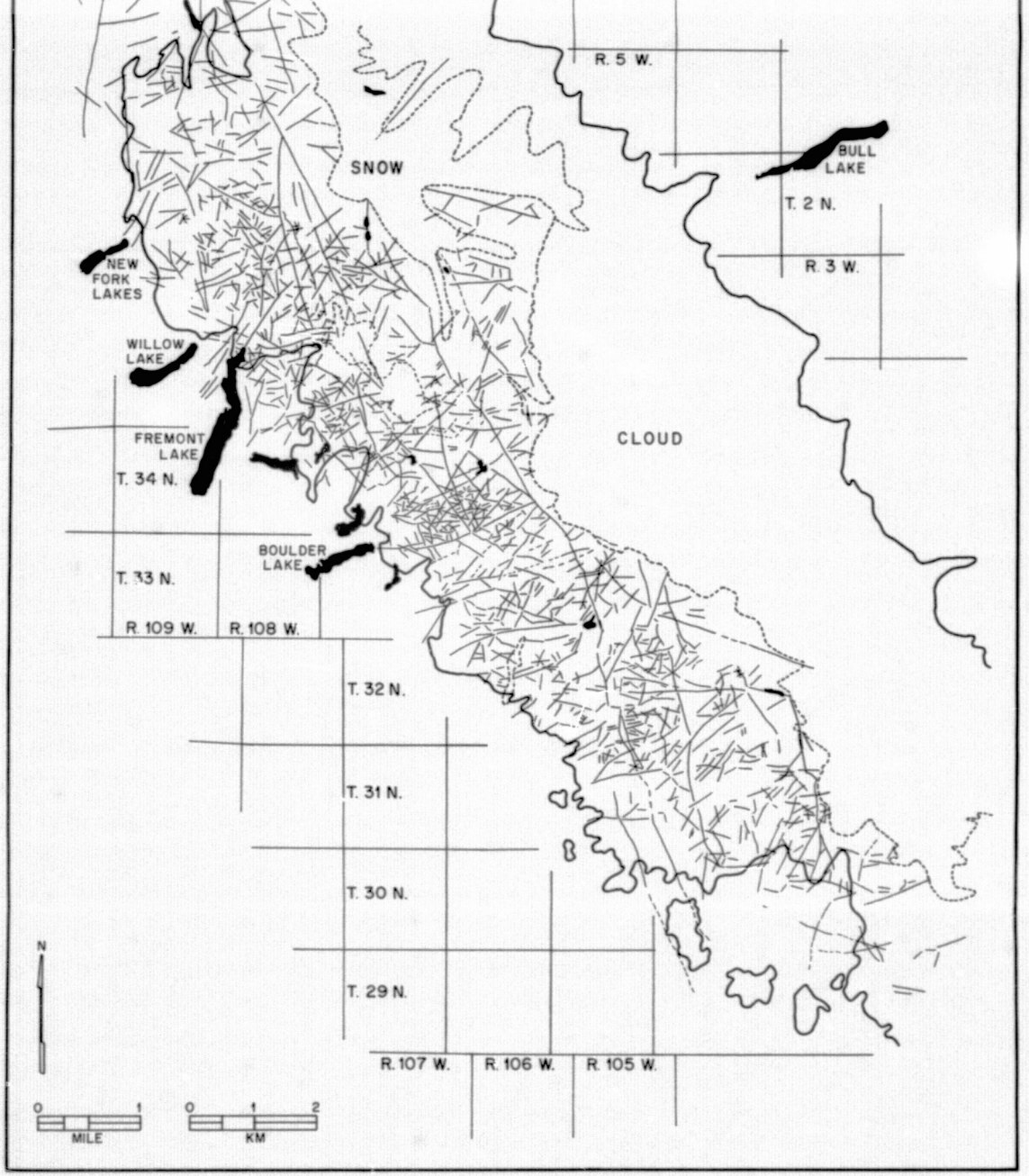


Figure S-2. Map showing all lineations that can be detected on Skylab S-190A photography of the Wind River Mountains.

FOLDOUT FRAME 2

northwest than northeast. If this is true throughout the range, the sun azimuth of Skylab would tend to bring out lineations that result from these fractures better than that of ERTS so that more lineations should show on Skylab photographs regardless of resolution. However, if we select a lineation direction such as east-west that should not be biased by sun azimuth the number of lineations mapped on a Skylab photograph is about three times that of ERTS for the area shown in Figure S-3. This cannot be taken as a quantitative measure of the exact resolution difference for lineation measurements because the total number of lineations measured by use of Skylab photographs is only an order of magnitude greater than ERTS for this area (Fig. S-3), but it is clear, nonetheless, that more lineations can be recognized on the higher resolution Skylab 190B photograph.

If we compare known faults (as mapped by field geologists) with linears mapped using Skylab and ERTS, we find a similar correspondence. In the northwestern part of the Wind River Mountains Richmond (1945) mapped a series of faults and shear zones and this mapped area is covered by both Skylab and ERTS. Results of study of linears from this area are shown below:

	Skylab (190A)	ERTS
Total number of linears	202	104
Total length of linears	600 kilometers	520 (kilometers)
Total number of linears that correspond to mapped faults and shear zones	17	13
Total length of corresponding linears	95 kilometers	95 (kilometers).
Total number of corresponding linears unbiased by sun azimuth		

Appendix T: Vegetation analysis in the Laramie Basin, Wyoming from ERTS-1 imagery.

from a special report on research conducted under contract NAS 5-21799:

Evans, M. A., and Redfern, R. F., 1973, Vegetation analysis in the Laramie Basin, Wyoming from ERTS-1 imagery; National Technical Information Service, Springfield, Virginia, Report E74-10145, 54p.

A vegetation map of the Laramie Basin test area was constructed from ERTS image interpretations in order to test the utility of the ERTS imagery for mapping and analysis of range vegetation. Image 1029-17148, bands 5 and 7, was used in the interpretation. The image interpretation was supplemented by an isodensity contour map of the band 5 image.

Some vegetation types can be discriminated from the red band alone. Heavily vegetated floodplains are easily separated from drier areas supporting other vegetation types. Floodplain vegetation shows a variety of contrasting radiance patterns on both bands 5 and 7. These patterns are readily interpreted by comparison of density contour maps derived from ERTS bands 5 and 7. Ligh-toned areas surrounded by floodplain vegetation may be elevated grassland areas or simply alkaline flats devoid of heavy vegetation cover. Alkaline areas show up distinctly on band 5 but are easily confused with dense mesic vegetation on the infrared bands.

The Laramie Basin is predominantly a shortgrass prairie. This grassland exhibits a mottled appearance on the ERTS imagery. In some areas slightly alkaline conditions produce light-toned regions on the band 5 imagery. Straight-line tone changes often represent fence lines and corresponding differences in grazing intensities. Some of the tonal contrasts may reflect differences in species composition of the grassland, especially where grazing pressure affects species composition and vegetative biomass.

Reflectance characteristics of various range vegetation types were observed qualitatively. Plant absorption in the visible spectrum is due primarily to quantum absorption which is a function of the density of pigments. Thus, absorption in

the green and blue bands indicates the amount of pigments present, especially chlorophyll. The chlorophyll content, in turn, can be related to vegetation type, cover, biomass, water availability, leaf area index, available nutrients, etc. Infrared reflectance, which is substantial in many species, is closely related to development of the leaf structure, particularly in the mesophyll layer, as well as to leaf area index and cover, (Gates et al, 1965; Hoffer and Johannsen, 1969; Gates, 1970; and Meyers, 1970). Thus, broad-leaf vegetation in mesic environments, with profuse and well-developed leaves, should exhibit considerable absorption of the visible energy and have high infrared reflectance. This holds true for the Laramie Basin. Drier vegetation shows less visible absorption and less infrared reflectance. Xeric plains vegetation, with its poorer leaf structure development and sparse cover, shows little difference in visible and infrared reflectance.

The effect of water on leaf structure and quantity of vegetation is apparent when comparing crops in dry and irrigated fields and dry plains with wet hay meadows. For example, irrigated crops appear very dark in the visible ERTS-1 bands and extremely light in the infrared, whereas the effect is less pronounced in dry-land crops. Differences in crop species do not affect reflectance variations as severely as does water availability. Similarly, the leaf structure of the wet meadow vegetation is well developed and with a large leaf area index, thus, much visible radiation is absorbed and infrared is reflected. Dry grasslands show little or no difference between infrared and visible reflectances.

The ERTS images are definitely of value in photogeographical studies. Readily discriminated with a large degree of confidence are deciduous forests, coniferous forests, and floodplain vegetation, irrigated farming, dry-land farming, alkaline areas, and grassland-shrubland.

The two ERTS-1 bands that appear most useful are 5 and 7. Band 4 is similar to band 5 with regard to vegetation reflectance, whereas band 6, being a combination of deep red and

very near infrared, represents a frequency range in which many plants show high absorption in the red and high reflectance in the infrared. As such, band 6 is generally no more effective in vegetation analysis than an average of bands 5 and 7. However, this does not mean that bands 4 and 6 are never important in interpretation. Indeed, their value may be significant in quantitative vegetation analysis.

There are no coniferous forests in the area of the preliminary vegetation map. However, in nearby mountain areas, conifers are readily mapped from the imagery because they are relatively dark in both bands 5 and 7. Clearcut and burned-over areas can be identified and studied quantitatively. Cloud cover is common in high mountain areas and often obscures large areas of coniferous forest. A small test area lying immediately south and east of the main Laramie Plains test area was chosen to evaluate the ERTS data for mapping of vegetation in mountainous areas. The area was mapped both by interpretation of aerial photographs and of ERTS 1 imagery. Again, isodensity contour maps were used as an interpretation aid.

A field check of the vegetation zones mapped from the ERTS imagery was conducted in late June and early July 1973. Both the Laramie Basin and Laramie Range study areas were field checked. In both areas a number of each of the mapped zones were checked, and a species account was made. The dominant species in each area were determined and a list was made of all species encountered in each area.

The ERTS imagery is seen to provide resolution approaching theoretical limits through the clear and dry Wyoming atmosphere. Consequently, comparatively small stands of vegetation can be identified under optimum conditions: they must be somewhat wider than one resolution element. A minimum sized stand should be on the order of .16km by .16km, a size equal to four resolution elements, to obtain a value approaching the actual radiance (less atmospheric attenuation). The larger the stand, the less the worry with edge effects and scattering into the instantaneous field of view, and extensive communities of

the major vegetation types (conifer, brush, grassland, etc.) should be delimitable from ERTS data. Atmospheric scattering, however, does not appear to be an important problem in the Laramie Basin during optimum imaging weather.

Vegetation identification by ERTS imagery is often limited by factors such as sun angle, topography, complexity of the vegetated landscape, and substrate. A scene-radiance which would be correlated to brush on light soils with a tolerable degree of accuracy could not be so correlated on darker soils, where grassland might give the same radiance. Vegetation on slopes sheltered from full sunlight will reflect levels of radiation dissimilar to corresponding vegetation on slopes bathed in full sunlight. Changes in sun angle can alter reflectance as well as radiance due to the effects of shadows and light incidence angle. In view of such dissimilarities, the concept of "signature" in ecological remote sensing is not useful in a strict sense. Thus automatic mapping and monitoring of "natural" vegetation is obviously far more difficult than that of crops, which has had its own share of problems (Hoffer and Goodrick, 1971).

There are several possible solutions to the problems of satellite-based remote sensing of natural vegetation. Clustering techniques (Smedes et al., 1971), which group like radiances for interpretation, can be useful but not sufficient in themselves for identification as indicated by the present study. With computer analysis of several radiation bands, it is possible to effect various mathematical transforms of the radiance data (Smedes, 1971 and Kridgler et al., 1970). Such transformations promise to be particularly useful in mollifying effects of atmosphere and topography. However, if it is deemed useful to map and monitor vegetation from orbit, it appears clear that much low-level and ground-truth data will be needed for vegetation maps of any accuracy. Apparently it will be easier and more accurate to map vegetation by predominantly manual methods rather than automatically if maps amenable to botanists are to be produced. In addition to proximate data,

models which comprehend factors such as topography, sun angle, and substrate are required to automatically monitor vegetation. Of course, the volume of augmentative data is a function of the accuracy desired. It appears possible to map broad vegetation types such as conifers, broad-leafed trees and shrubs, brushland, grassland, desert, etc., with present ERTS imagery alone. Increasing resolution will eventually require more sophisticated imaging coupled with sophisticated techniques of analysis, including modeling.

A rough inverse correlation exists between radiance types and the amount of vegetative biomass present. Pearson and Miller (1972), working in the shortgrass prairie of the Pawnee National Grassland, have found good correlation between the ratio of infrared to red reflectance and green biomass. With a proper model, the estimation of biomass over large areas appears possible.

Certain wavelengths seem to be indicators of potential productivity in vegetation. For example, Odum (1971, p. 62) suggests that the "yellow-green" index of Margalef, which is inversely correlated with the ratio of productivity to respiration, might be used as a remote sensing tool. Myers (1970, p. 264) suggests that reflectance at about .54 um is a function of the chlorophyll concentration and that increased reflectance of this wavelength possibly indicates nutrient deficiencies. In addition such things as the ratio of reflectance in a near infrared band to reflectance in a band on the red might indicate the potential rate of photosynthesis. Also, remote sensing techniques can measure absorption of photosynthetic wavelengths by vegetation, especially when problems of atmospheric scattering are solved. If suitable remote sensing indices of ecological factors can be found, they can be augmented by meteorological and other data and possibly used to extimate productivity and respiration.

A difficult but important ecological parameter to measure is evapotranspiration. Measurement of this parameter can be apprehended by energy budget studies. If such studies can be

done for given elements of terrain from space platforms, this parameter, an important factor in water cycling as well as an indicator of net primary productivity (Rosenzweig, 1968), might be estimated and applied to vegetation analysis.

Appendix U: Identification of irrigated crops.

from a special report on research conducted for contract NAS 5-21799:

Evans, M. A., and Marrs, R. W., 1974, Identification of irrigated crop types from ERTS-1 density contour maps and color infrared photography; National Technical Information Service, Springfield, Virginia, Report E74-10312, 12p.

The use of ERTS-1 imagery for identification and mapping of irrigated and dry-land crops was investigated in an agricultural area north of Wheatland, Wyoming. Initial attempts to identify crop types by direct photointerpretation were only marginally successful. On the other hand, a trained interpreter could readily identify the various crops on 1:120,000-scale color infrared photography of that same area. The contrast apparent from the color infrared aerial photography and the ability of the interpreter to delineate the field patterns on the ERTS imagery suggest that image-enhancement procedures might improve the success of crop-identification from ERTS. The lack of textural information and detail on the ERTS imagery might be compensated by a more accurate estimate of the relative brightness of the fields on the different ERTS bands. Consequently we elected to construct density contour maps of the test area from the ERTS imagery, in an effort to enhance the critical contrasts.

The test area is a mixed dry-land/irrigated agricultural area approximately 2- by 2 1/4-mi. in size and located about 4 miles northeast of Wheatland, Wyoming. The area comprises both irrigated and dry-land farms, rangeland, and heavily-vegetated floodplains. Each of these three major zones is represented by a distinct tone, texture, and pattern which can be readily identified on the ERTS-1 imagery. Further subdivision of the zones is more difficult.

Fourteen crop classes were recognized from the August, 1973 color infrared photography of the test area. They include corn, sugar beets, alfalfa, grains (oats and barley), grain used as a nurse crop for alfalfa, grass/hay and pasture,

beans, plowed ground, natural vegetation, natural vegetation supported by irrigation-water runoff, water (ponds and reservoirs), uncultivated floodplain, cultivated floodplain (alfalfa) and farm yards.

Density contour maps were constructed from the ERTS imagery to give an enlarged presentation of the test area along with absolute film density information. The large-scale (1:19,760) density map permits accurate delineation of the contrasting fields, while the density contours allow the interpreter a means of making objective decisions about contrasts and similarities of various areas. He can also use calibrated density contour maps as a means of comparing various bands and time-sequential images. The interpreter must use these contour maps in much the same way as he would a low-altitude photograph, keeping in mind the mechanical variables as well as the natural variables (irrigation, climatology, etc.).

In this study, three time-sequential ERTS images were selected on the basis of image quality and time distribution. The red-band, 9-in. positive transparencies were chosen for time-comparison density slices. The instrument used was a Joyce Loebel/Tech Ops isodensitracer.

For control, an outline map of the crop types was constructed from the aerial photograph. The crop types were positively identified from field checks and were the same crops throughout the summer. The settings on the microdensitometer were the same for each density contour map.

Figures U-1, U-2, and U-3 are black-and-white duplicates of the red-band isodensitracings (density contour maps). In original form, the various density patterns are displayed in color. A crop map, interpreted from a 1:120,000 color infrared aerial photograph of the area has been superimposed on each of the isodensitracings.

The density contour map shown in Figure U-1 was taken from ERTS-1 image 1334-17134-5, 22 June 1973. This image was taken early in the growing season and the natural vegetation areas show up dark, because of early growth of grasses and sagebrush. The corn, beans and beets are still young and

ORIGINAL PAGE IS
OF POOR QUALITY

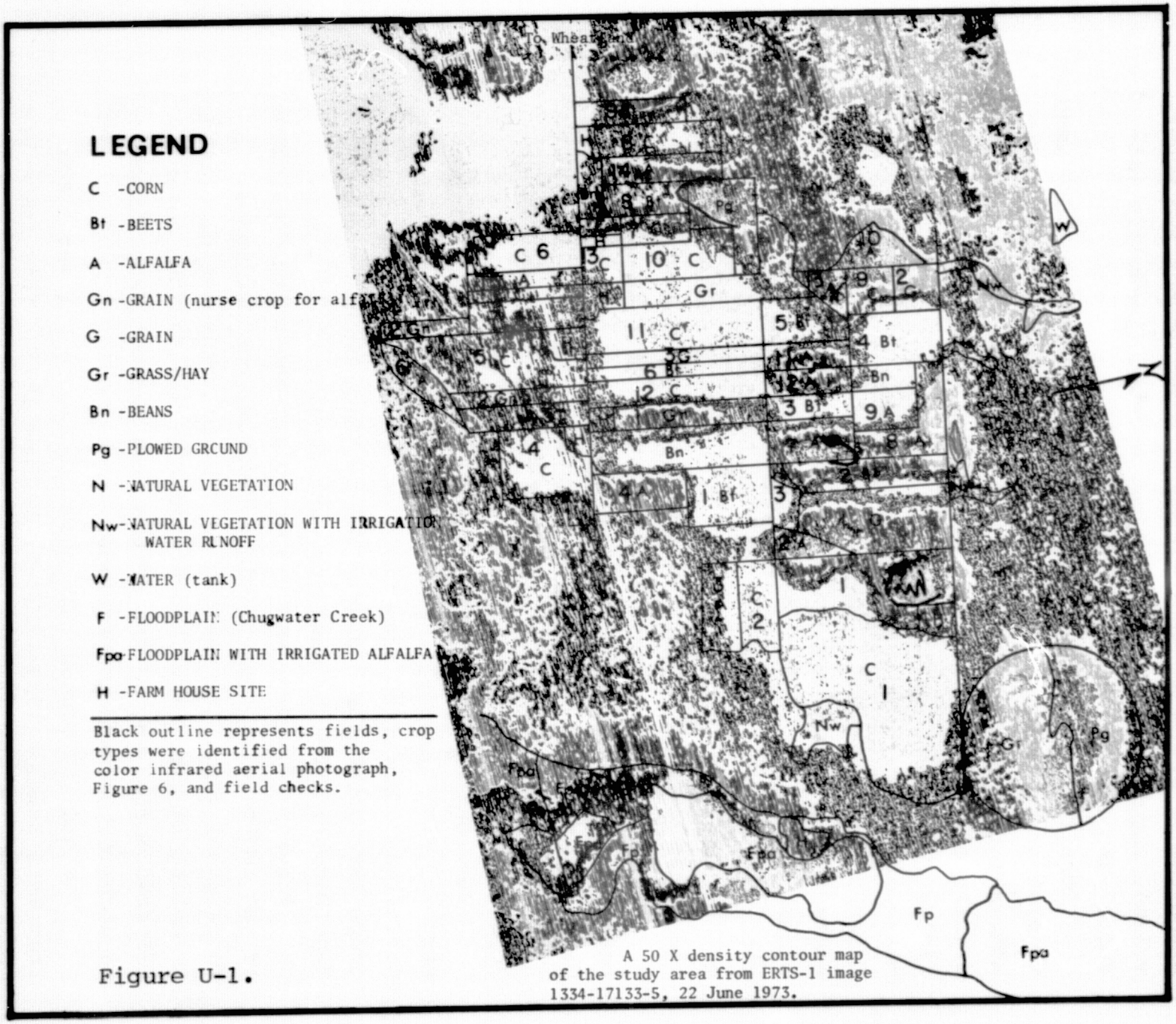


Figure U-1.

A 50 X density contour map of the study area from ERTS-1 image 1334-17133-5, 22 June 1973.

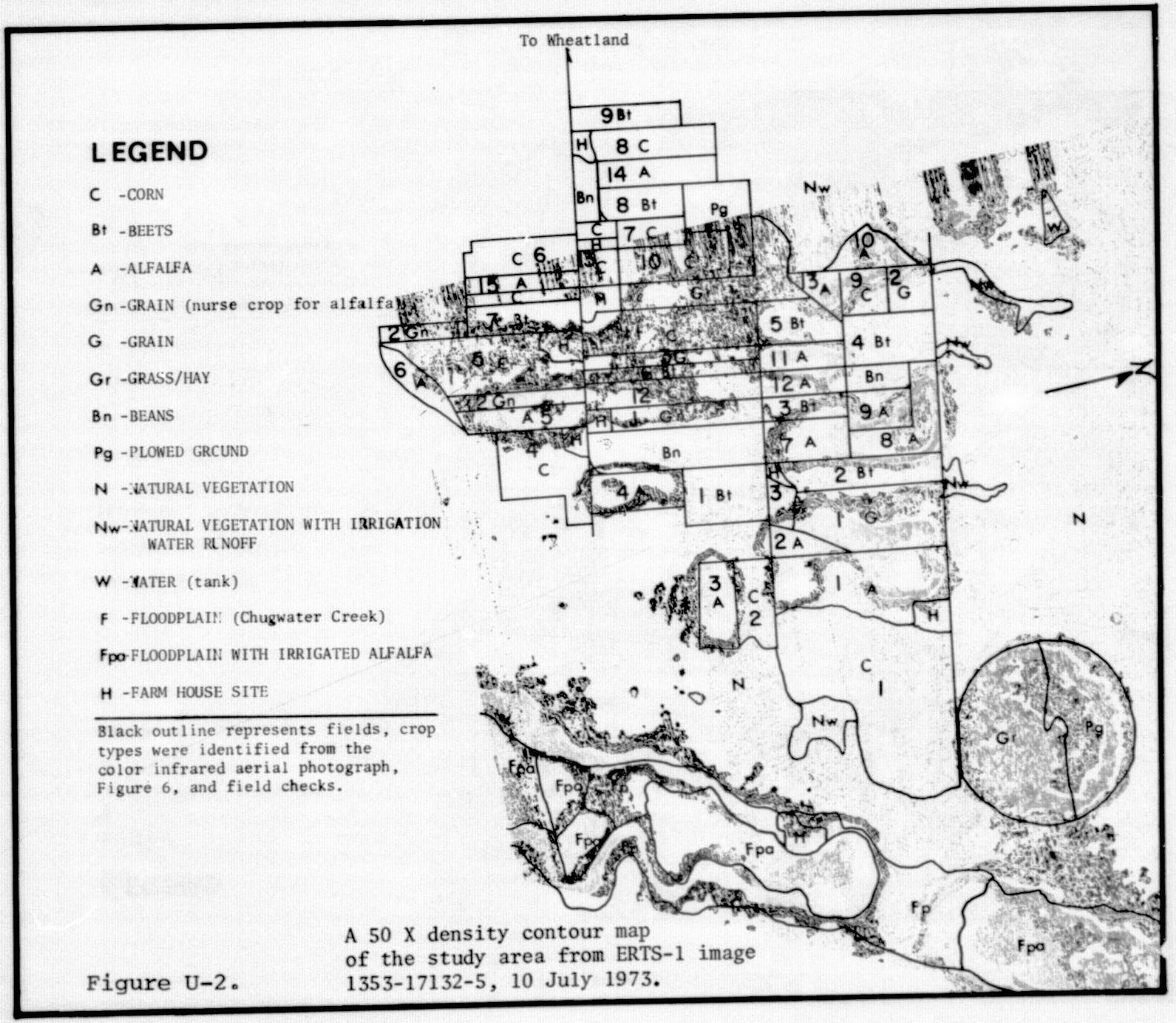


Figure U-2. A 50 X density contour map of the study area from ERTS-1 image 1353-17132-5, 10 July 1973.

ORIGINAL PAGE IS
OF POOR QUALITY

ORIGINAL PAGE IS
OF POOR QUALITY

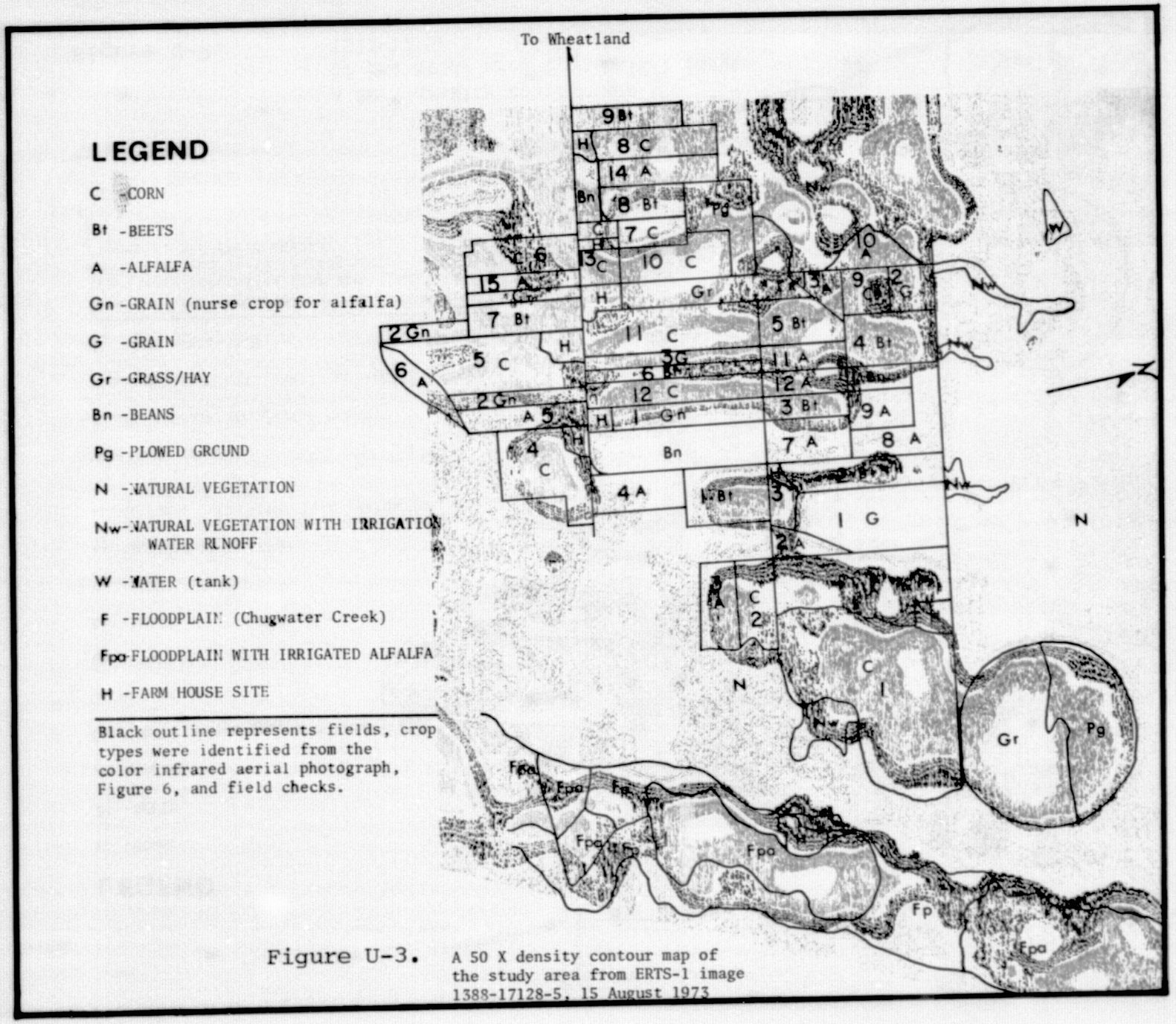


Figure U-3. A 50 X density contour map of the study area from ERTS-1 image 1388-17128-5, 15 August 1973

show as darker areas suggesting various amounts of vegetative cover.

The density contour map of Figure U-2 taken from ERTS-1 image 1352-17132-5, 10 July, shows the natural vegetation as lighter than in June, indicating dryer conditions or grazing pressure. The beets are darker and can be distinguished from the corn. The alfalfa and grain are generally darker than in June.

The isodensitracing shown in Figure U-3, from ERTS-1 image 1388-17125-5, 15 August, shows the corn and beets as darker than before. The alfalfa in fields 4, 7, and 8 is much lighter, after having been harvested. Similar observations drawn from other images and density contour maps serve as correlative data for interpretations regarding the vegetativetype and condition.

An additional application of the isodensity map lies in the enhancement of boundary and mix problems. Examination of the three density contour maps (Figures U-1, U-2, and U-3) shows that large, evenly vegetated fields are quite distinct, but, as the fields become progressively smaller or less even, or as contrast decreases, the crops become more and more difficult to map and identify. The density contour maps give the interpreter a good indication of the magnitude of this uncertainty.

Appendix V: ERTS-1 imagery as a tool for mapping major vegetation zones in Wyoming.

a previously unpublished report by:
M. A. Evans and R. W. Marrs on research performed under contract NAS 5-21799.

A false-color infrared ERTS-1 mosaic of Wyoming was used as an interpretation base for compiling general vegetation maps of Wyoming. Individual ERTS-1 images were then selected for more detailed interpretation of vegetative subzones in various kinds of terrain.

The earliest report concerning plant zones of Wyoming is by Nelson (1896). Later, Cary (1917) reported on the life zones of Wyoming while Kirkwood (1922) and Rydberg (1928) discussed forest distribution and life zones of the Rocky Mountain region. More recently, Costello (1954), Daubenmire (1943), and Porter (1962) have discussed vegetation zones of the Rocky Mountain region and Wyoming. Yet, there are still no comprehensive vegetation maps for Wyoming. The chief value of these previous works lies in the descriptions of the various vegetation zones observed. These descriptions provide much of the information necessary as background for mapping large areas with ERTS imagery. Individual locations where the vegetation and geology are known can be pinpointed on an ERTS-1 image and correlated with available field data to identify typical relationships between vegetative communities and spectral response. The texture, hue and tone of each zone has definite characteristics. Some zone boundaries contrast sharply and are easy to define. Other zones blend together and are difficult or impossible to distinguish. Experience and personal knowledge of the area and zone are a considerable asset in mapping these indistinct boundaries.

This report presents maps of the vegetation zones of Wyoming compiled from ERTS-1 images and illustrates the utility of ERTS-1 imagery in regional vegetation mapping. The project summarized in this report, including field work, required about two months total time. Although mapping vegetation from ERTS

imagery has advantages in speed and efficiency, some natural detail is missed. The resolution of the imagery is limited to features 70 meters or greater in diameter. Thus, to purists of the natural sciences, ERTS image interpretations may be practically useless. But, to many, ERTS offers a unique apportunity to obtain up-to-date general information previously difficult or impossible to obtain.

The Wyoming index map (Figure V-1) shows major drainage systems, water bodies, county boundaries and major cities for use as reference with the Wyoming vegetation maps (Figs. V-2, V-3, V-4 and V-5). The imagery used in compiling the regional vegetation maps was a false-color composite mosaic of Wyoming (see Fig. 1 this report) prepared by General Electric Photographic Engineering Laboratories. The vegetation zones were chosen to correspond to those defined by Porter (1962) and currently in use by Wyoming botanists (Dorn, 1972). The maps compiled from the ERTS image interpretations were partially field checked during summer and fall, 1973.

Vegetation zones of Wyoming are primarily controlled by altitude. The major vegetation zones descriminable from the ERTS-1 color composite mosaic are: 1) alpine, 2) timbered mountain slopes, 3) foothills scrub, 4) grassland including eastern plains and foothills (Great Plains) and interior grassland plains, 5) desert and basins, and 6) river bottoms. The major agricultural areas of Wyoming were also mapped. Major lakes are shown by double outlines. A list of the species found in each zone is given by Porter (1962).

The alpine zone of Wyoming includes the high mountain peaks and ridges above timberline, usually above 10,500 feet in elevation. Typical terrain includes rocky summits, scree slopes, lakes, alpine tundra, meadows, snowbanks, and in some places, glaciers. On the ERTS imagery, white to bluish areas are characteristic of the snow fields and bare rocky summits. Lakes appear as small black dots and alpine tundra and meadows appear light pink.

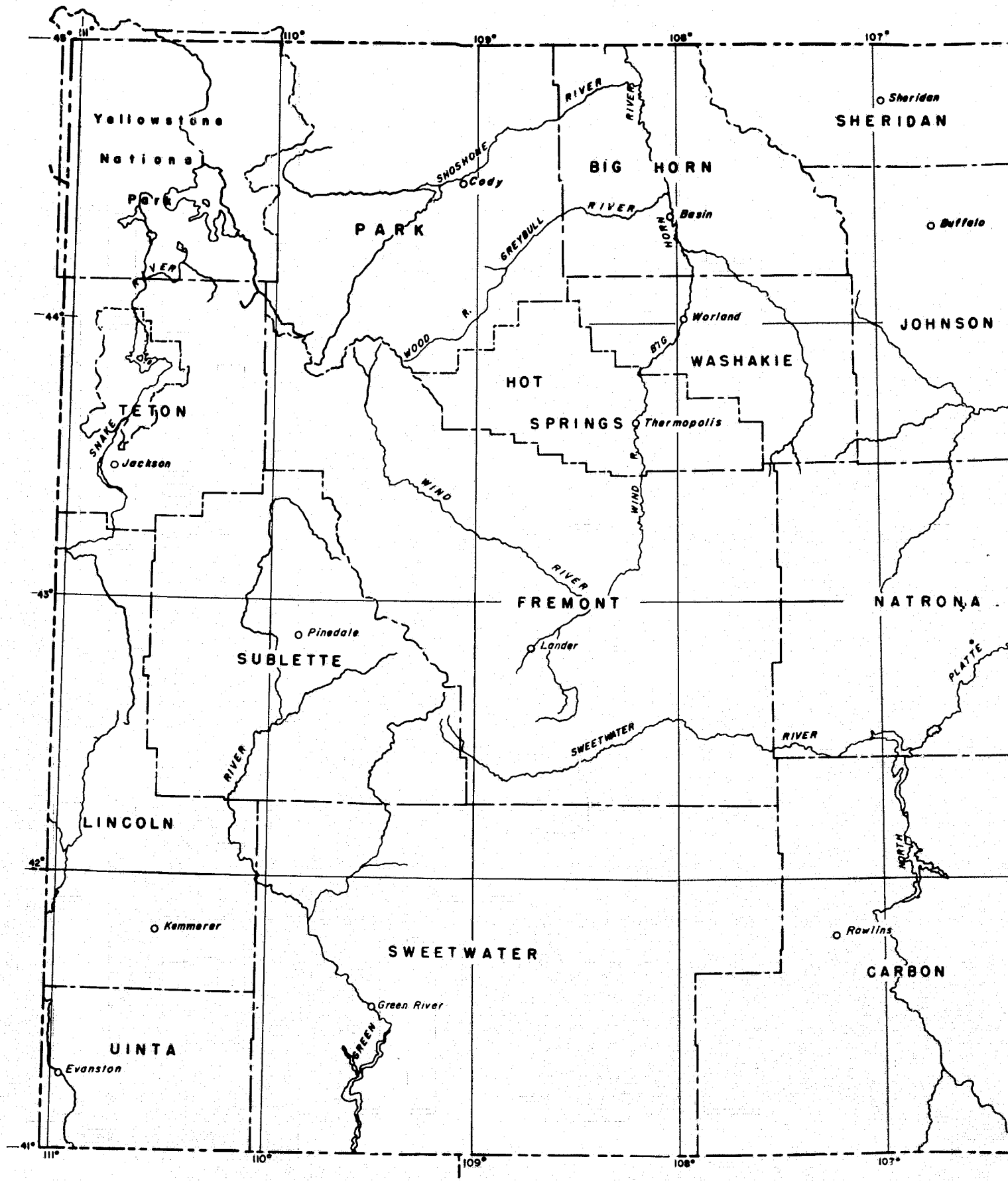
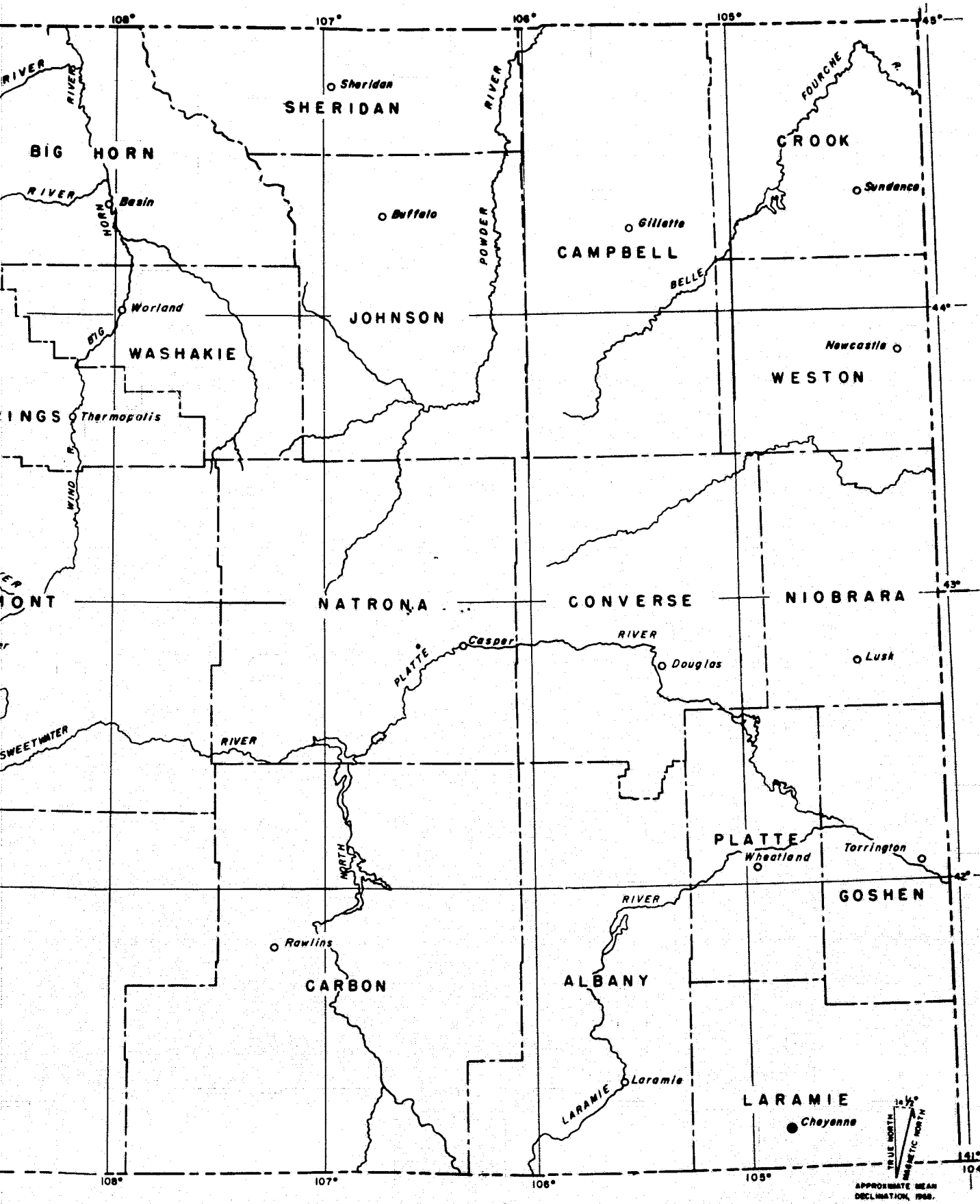


FIGURE V-1. INDEX MAP OF WYOMING.

OLDOUT FRA



MAP OF WYOMING.

ORIGINAL PAGE IS
OF POOR QUALITY

FOLDOUT FRAME

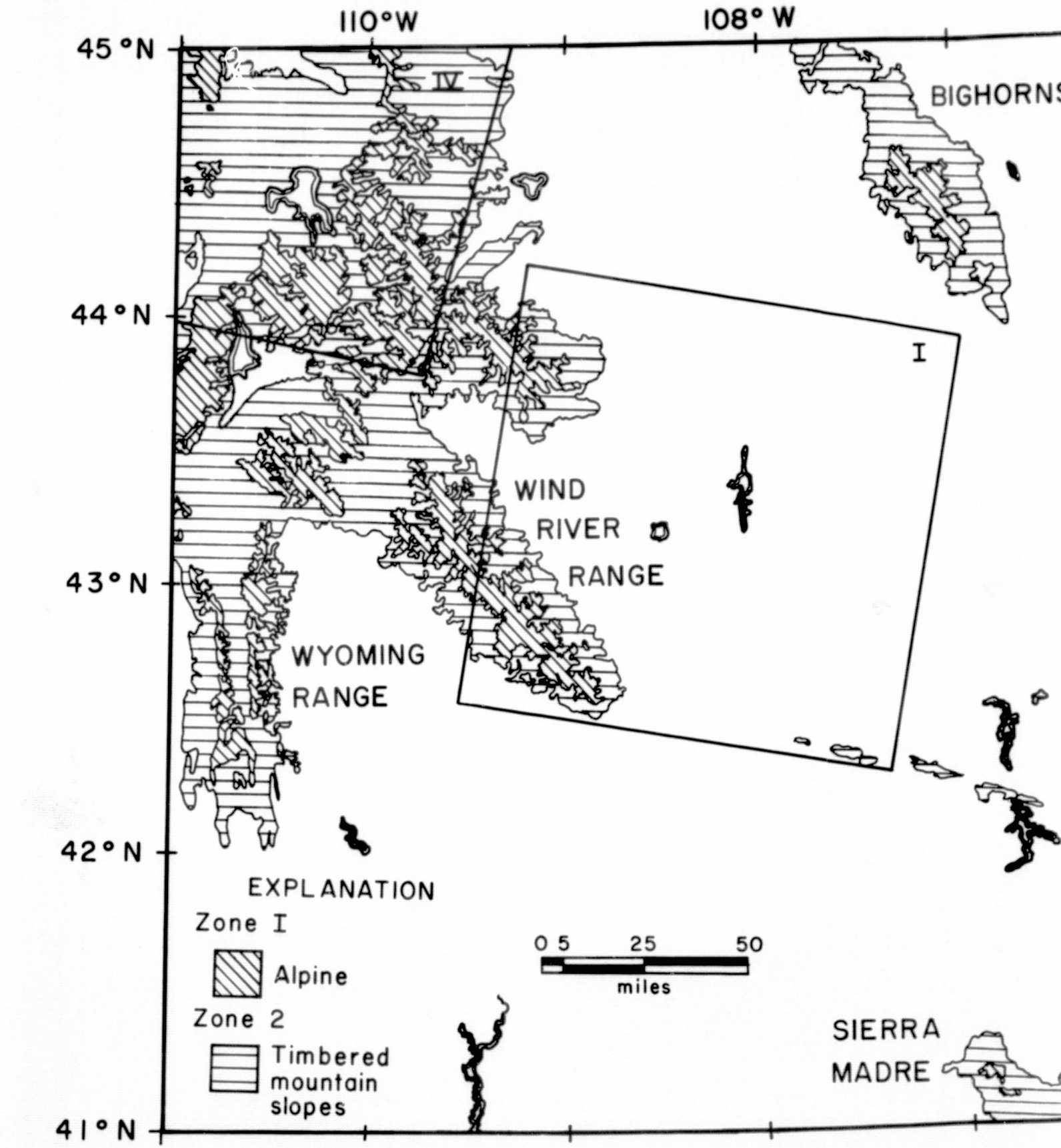
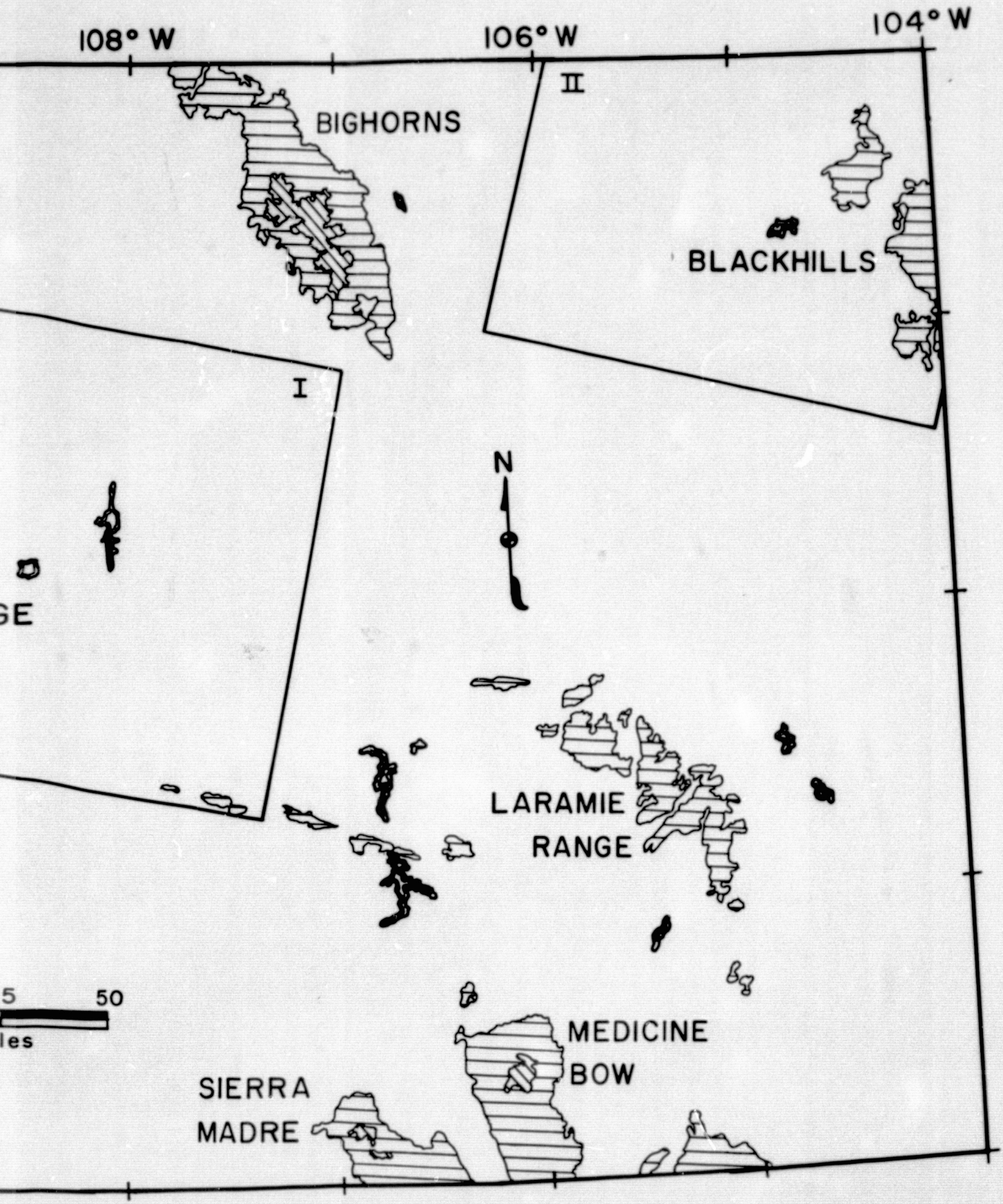


Figure V-2. Map I; A vegetation map of Wyoming showing Zone 2 (Timbered Mountain Slopes).

FOLDOUT FRAME
OUT FRAME
ORIGINAL PAGE IS
POOR QUALITY



on map of Wyoming showing Zone I (Alpine) and

imbered Mountain Slopes).

FOLDOUT FRAME

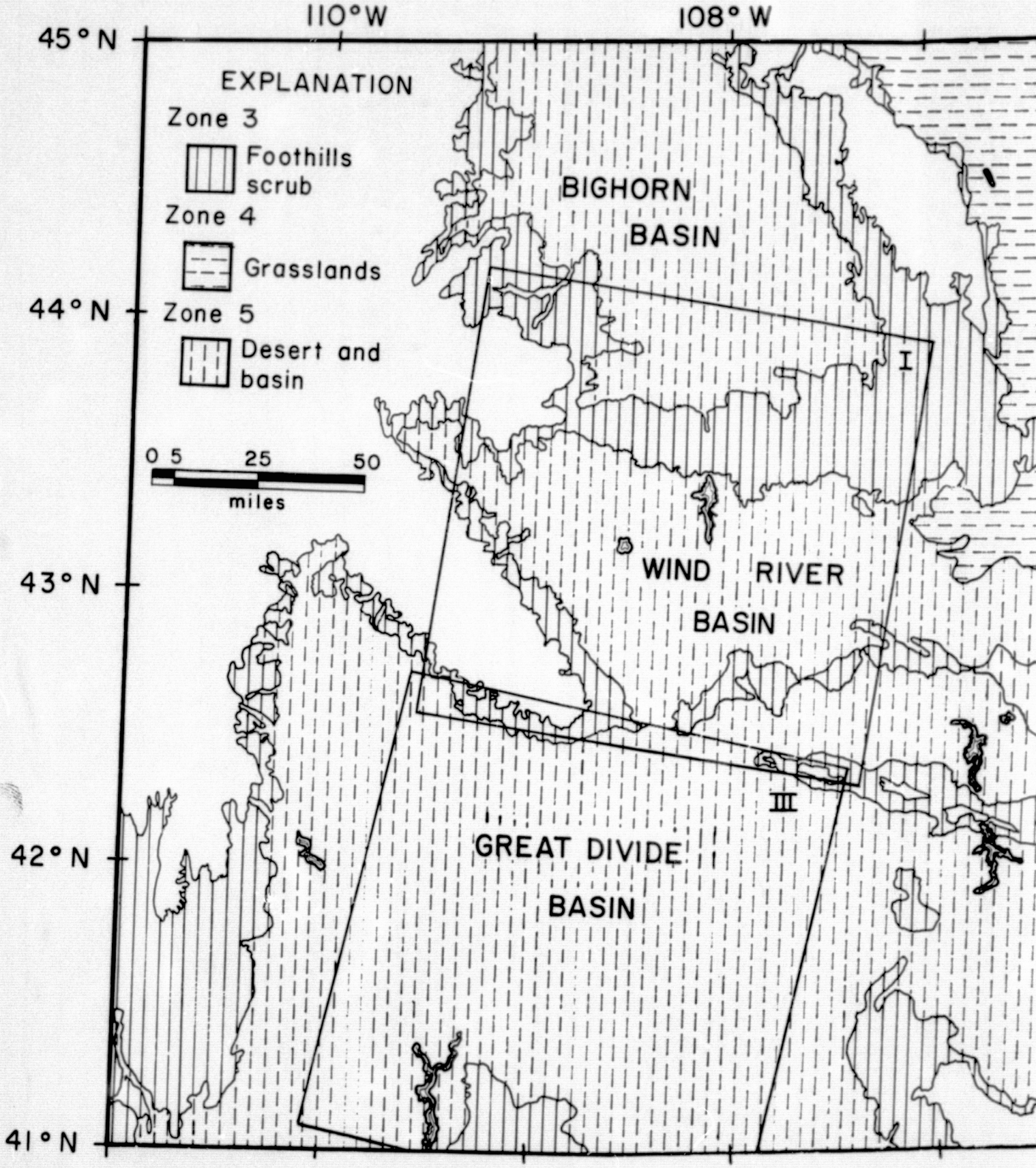
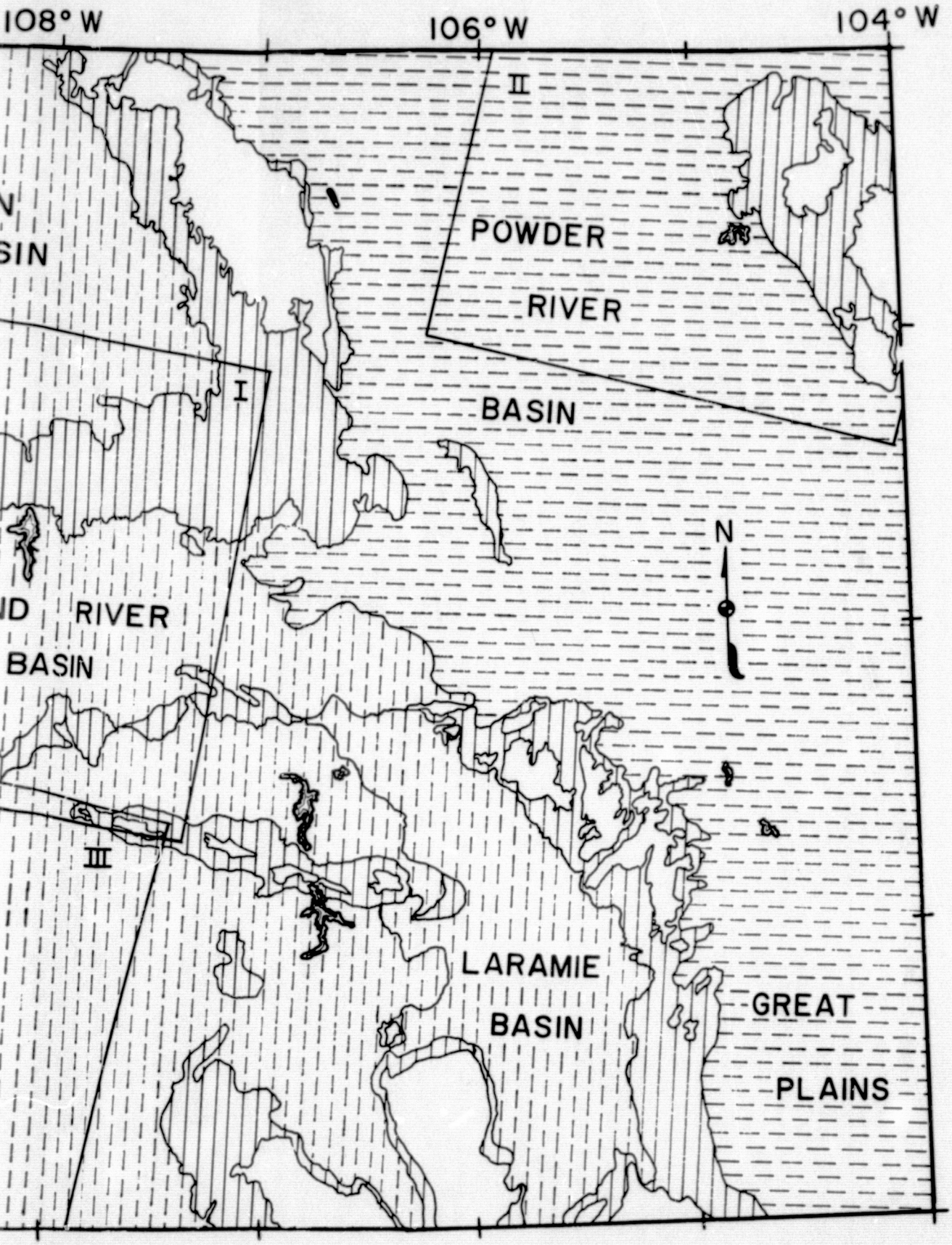


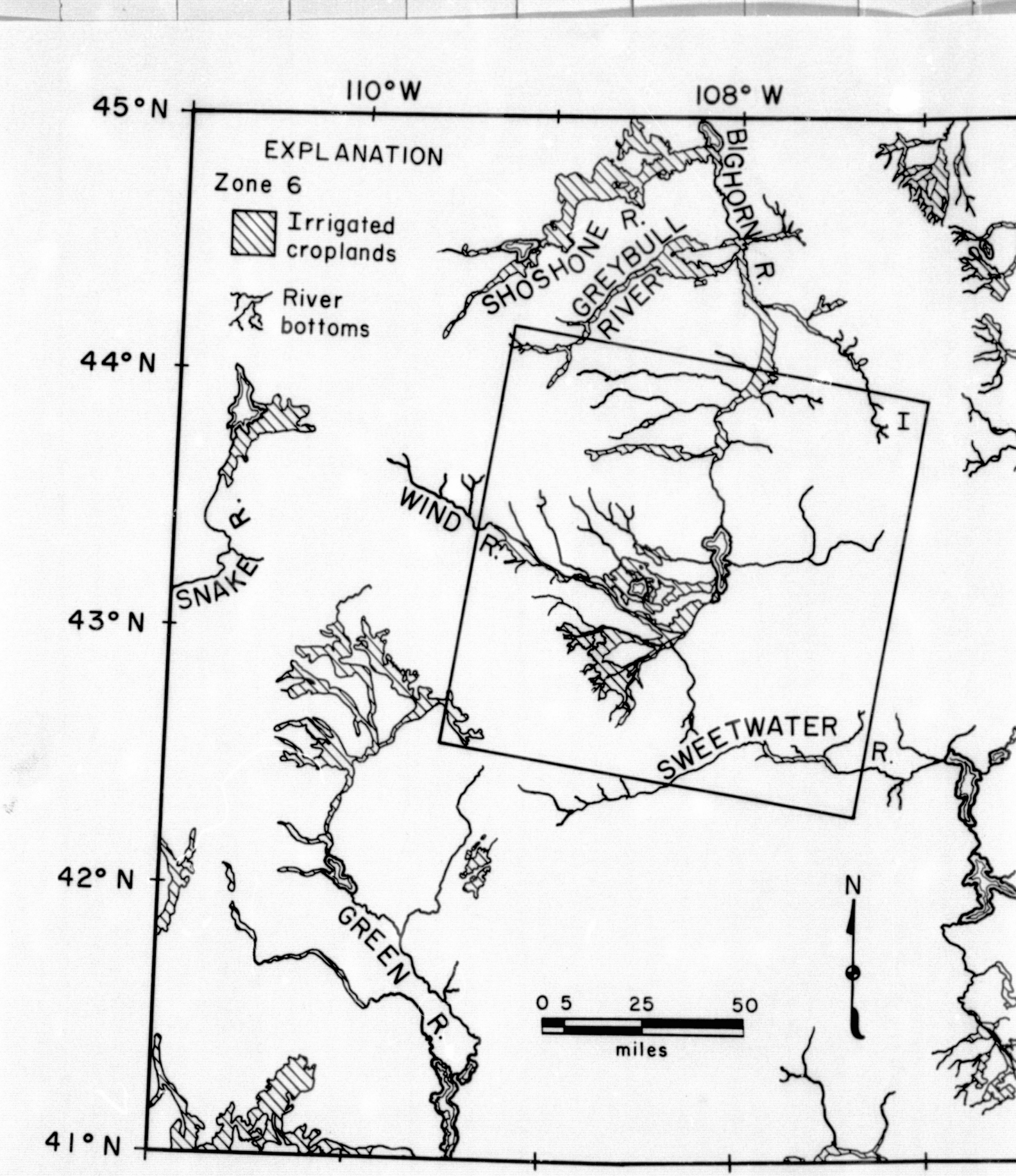
Figure V-3. Map II; A vegetation map of Wyoming showing Zone 4 (Grasslands) and Zone 5 (Desert



of Wyoming showing Zone 3 (Foothills Scrub),

ds) and Zone 5 (Desert and Basin).

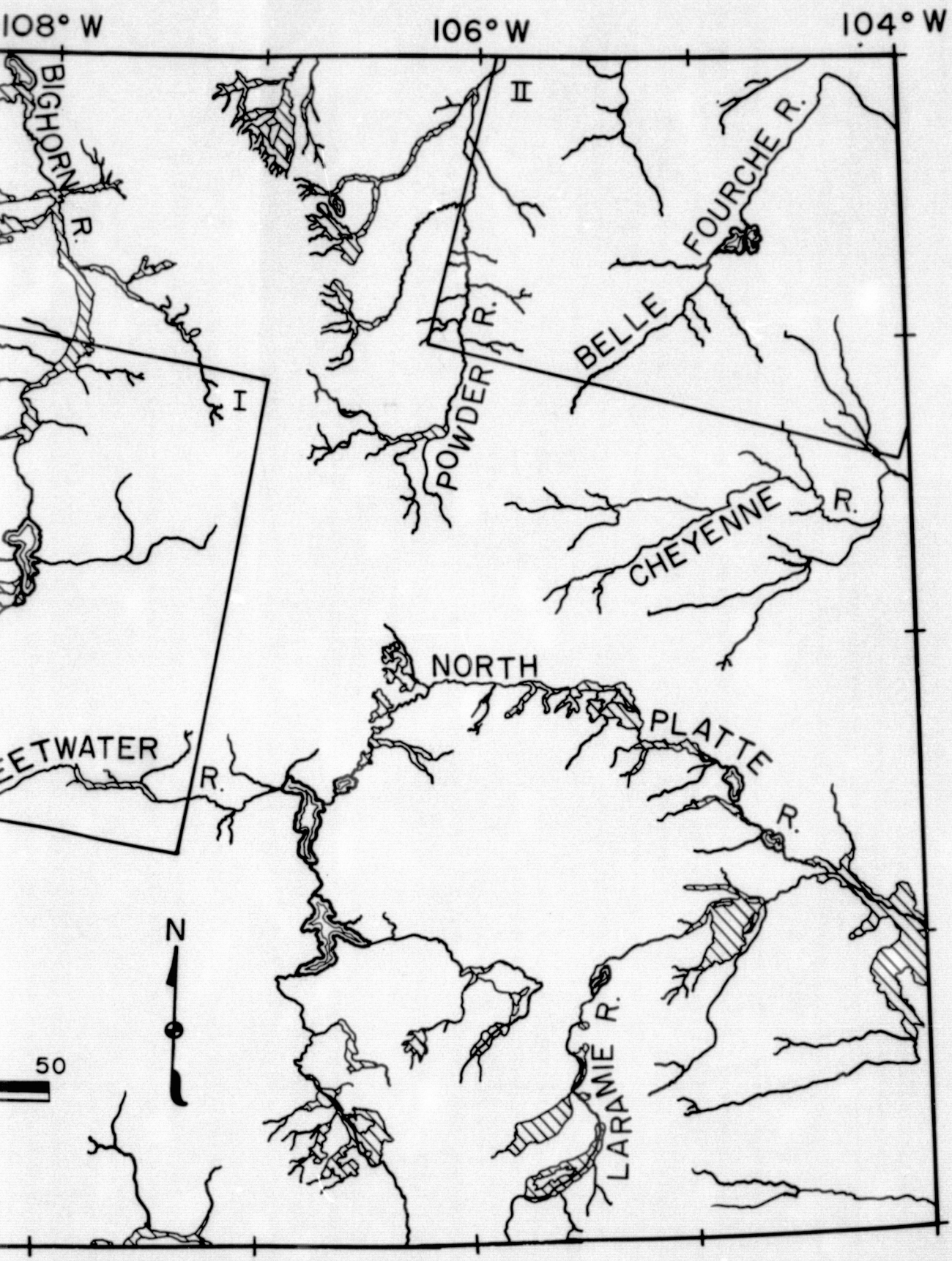
FOLDOUT FRAME



LDOUT FRAME

GINAL PAGE IS
POOR QUALITY

Figure V-4. Map III; A vegetation map of Wyoming showin
and Irrigated Croplands).



up of Wyoming showing Zone 6 (major River Bottoms
roplands).

FOLDOUT FRAME 2

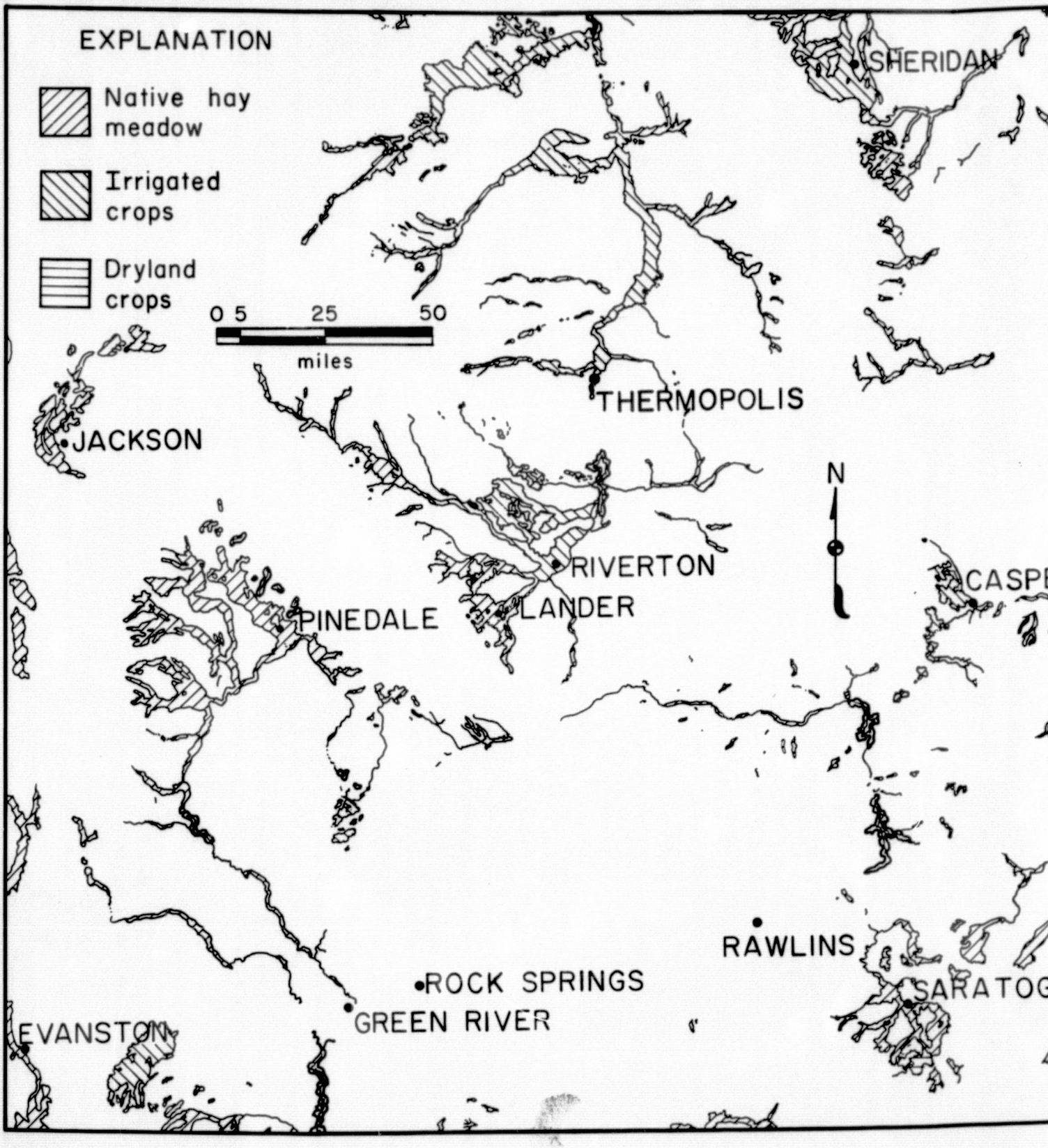
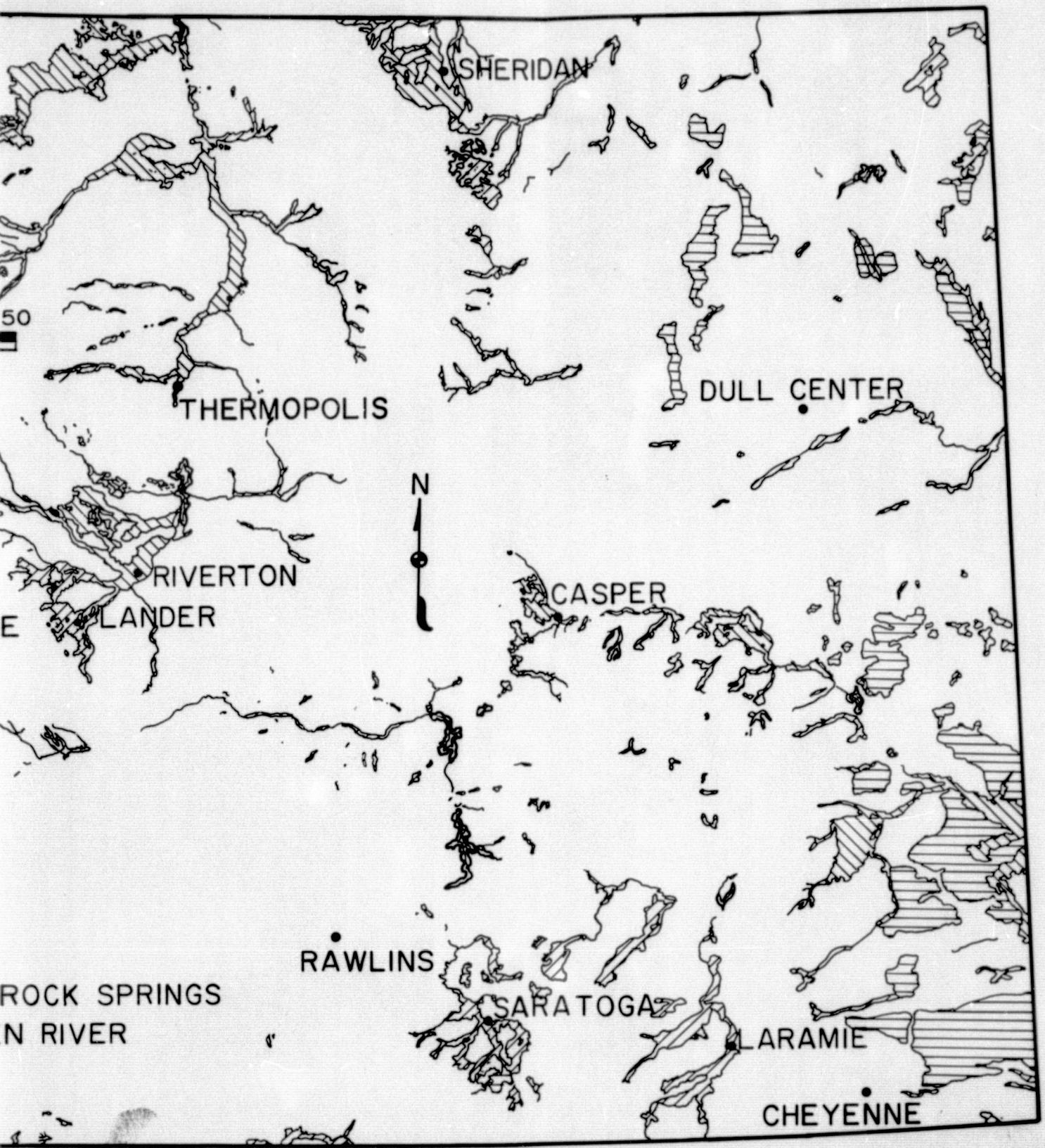


Figure V-5. Map IV; A general map defining the agricultural areas



neral map defining the agricultural areas of Wyoming.

Vegetation of the alpine zone is sparse, consisting chiefly of grasses and low-growing herbaceous flowering plants that flourish briefly in the short growing season. Some dwarf or scrubby woody shrubs are present.

Timbered mountain slopes (Fig. V-3) extend from the alpine zone to an elevation of about 6,000 feet. Conifers are the chief visible component of the vegetation community. Aspen and grassy meadows are interspersed throughout this zone. On the ERTS imagery, zone 2 appears dark red to black in color with small areas of bright red and pink representing meadows and aspen groves. Figures V-6 and V-8 are ERTS images illustrating vegetation zones 1 and 2. Figure V-6 corresponds to area IV, shown in Figure V-2, while Figure V-8 corresponds to area I of Figure V-2. Figures V-7, V-9, and V-10 are vegetation maps compiled from interpretations of the areas shown in Figures V-6 and V-8.

The Columbia Plateau element is found only in extreme northwestern Wyoming, primarily in the Yellowstone National Park and Jackson Hole area. Little data was available on this element. Consequently, it is mapped as open parks and meadows in Figure V-7.

The Black Hills element of northeastern Wyoming is mapped as timbered mountain slopes. On the ERTS false-color mosaic, this area has a mottled red to dark red appearance. The vegetation here is more related to the midwestern deciduous flora than to the Rocky Mountain flora. Figure V-11 is an ERTS image which shows the Black Hills element and the zone. Figure V-12 is a detailed zone map of this region.

Figure V-3 shows zone 3 (foothills scrub), zone 4 (grassland) and zone 5 (deserts and basins). Zone 3, foothills scrub, is found along the lower slopes of mountains. The vegetation of this zone is mostly shrubs and small trees with some grasses. The foothills scrub zone is often rocky and arid. Mountain mohogany, sagebrush,

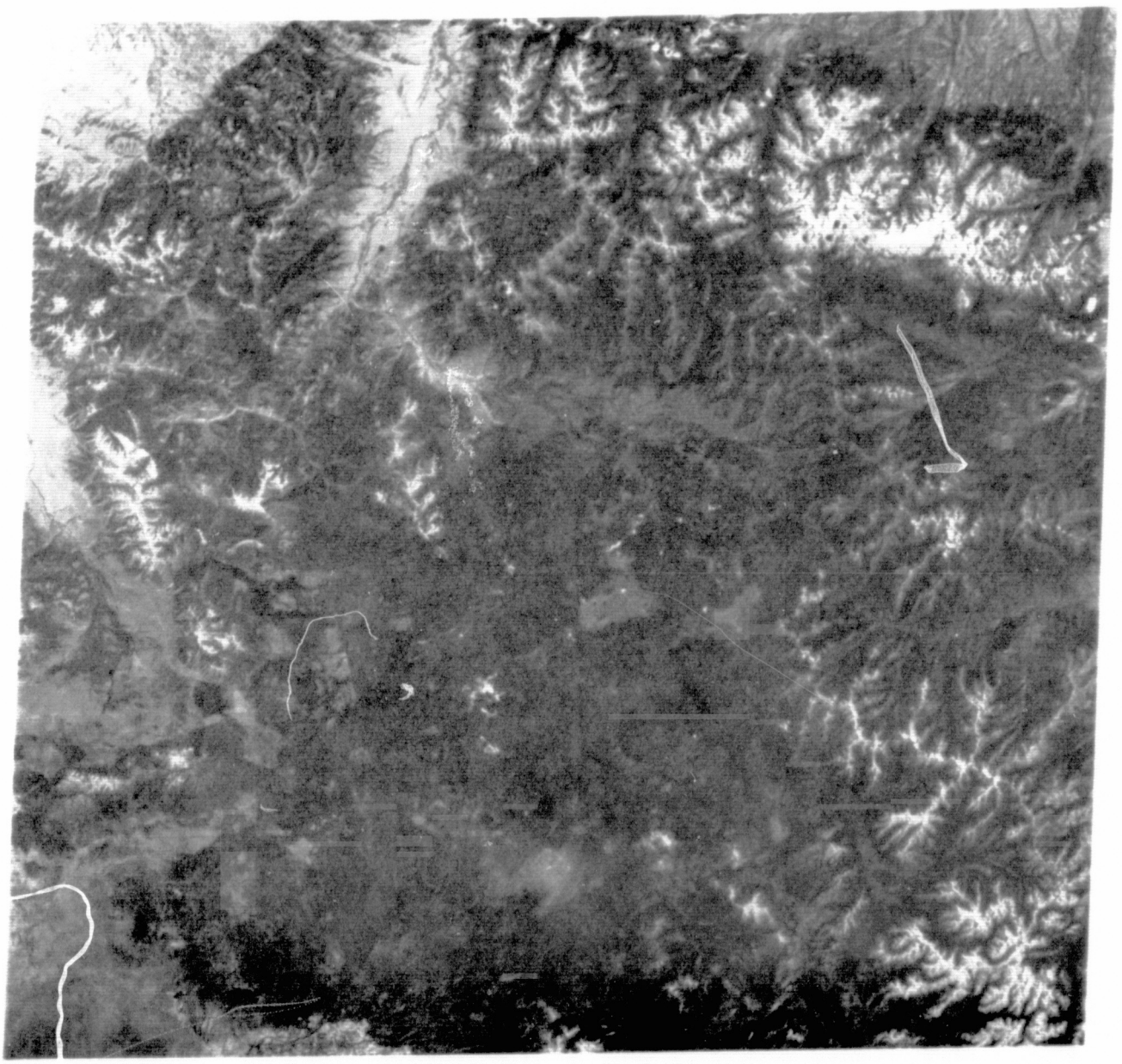


Figure V-6. ERTS-1 image 1015-17404-4,5,7, 7 August 1972, showing the Yellowstone Park and Columbia Plateau areas of Wyoming, Idaho, and Montana.

ORIGINAL PAGE IS
OF POOR QUALITY

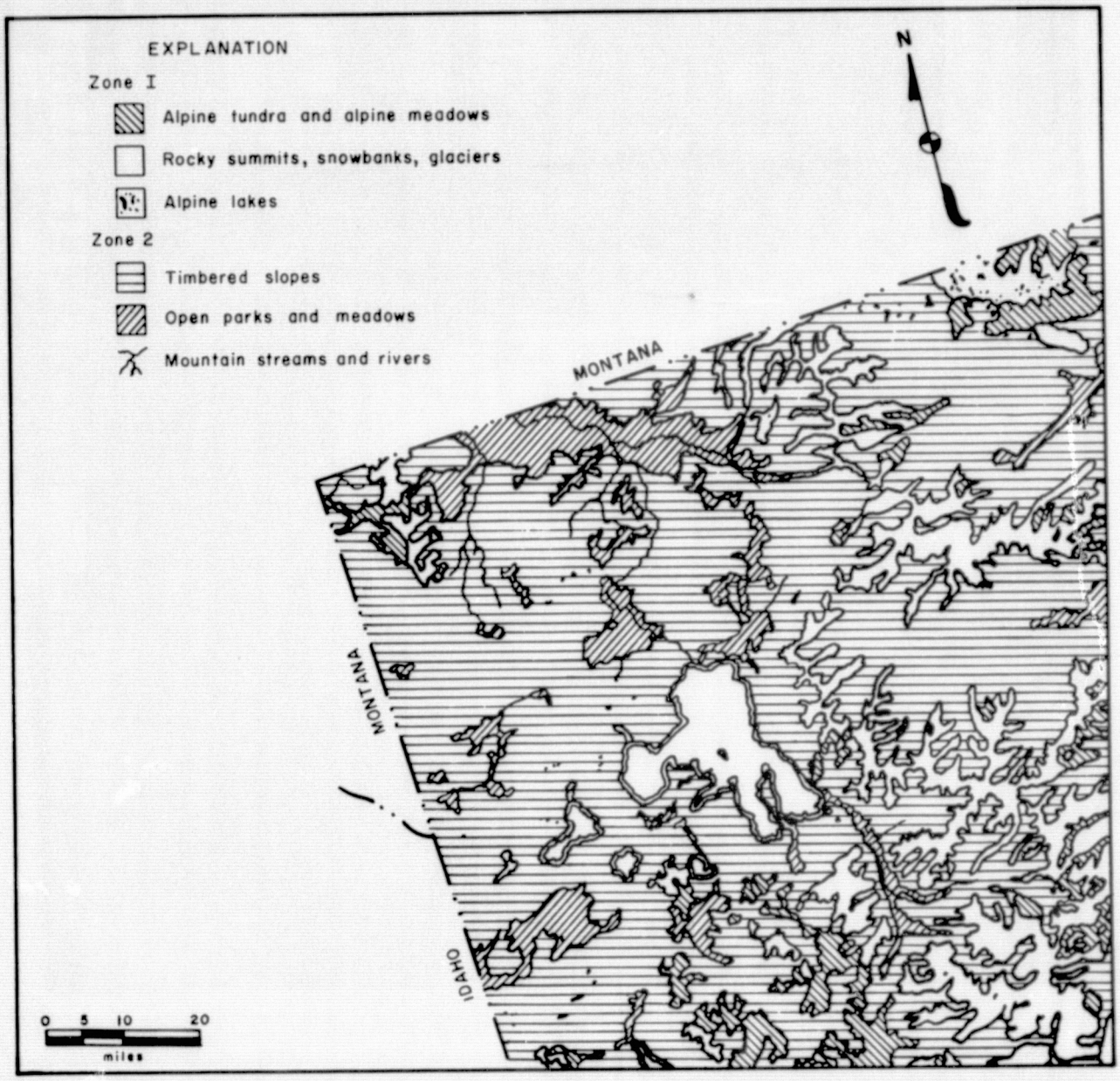


Figure V-7. A detailed map of Zones 1 and 2 taken from the original of Figure V-7.

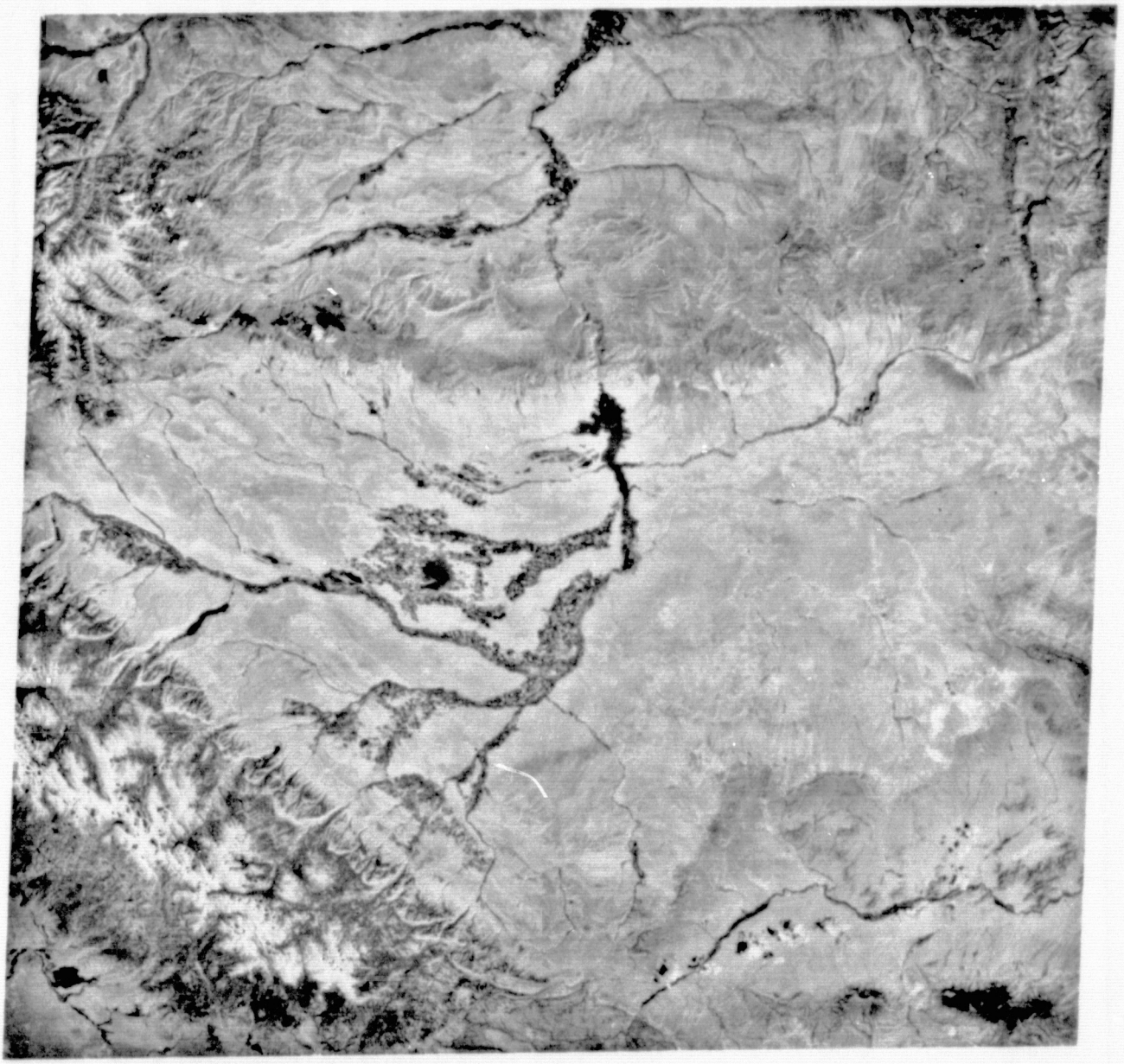


Figure V-8. ERTS-1 image 1013-17294-4,5,7, 5 August 1972, showing the Wind River Mountains and Wind River Basin of central Wyoming.

ORIGINAL PAGE IS
OF POOR QUALITY

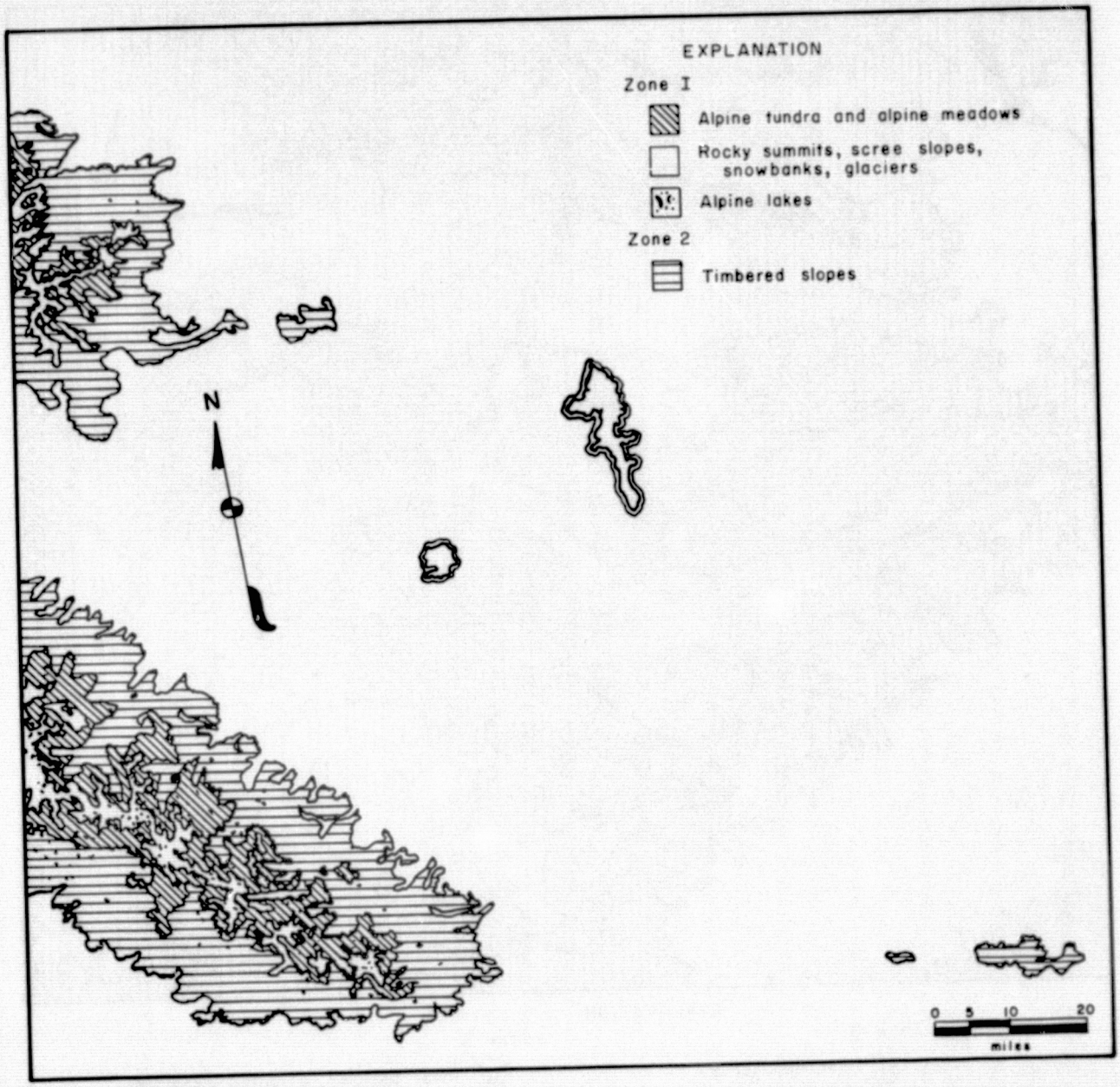


Figure V-9. A detailed map of Zones 1 and 2 taken from the original of Figure

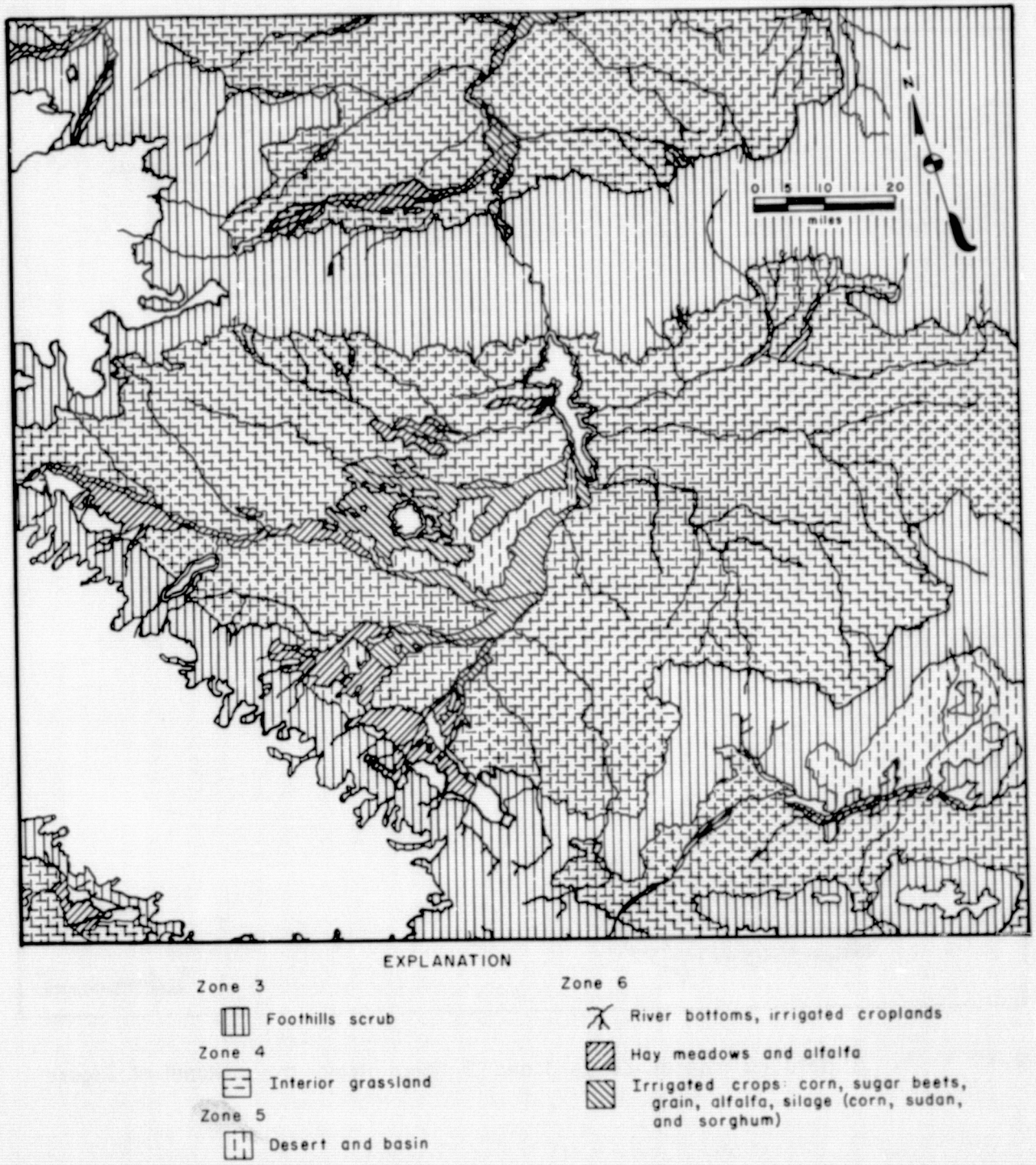


Figure V-10. A detailed map of Zones 3, 4, 5 and 6 taken from the original of Figure V-8.

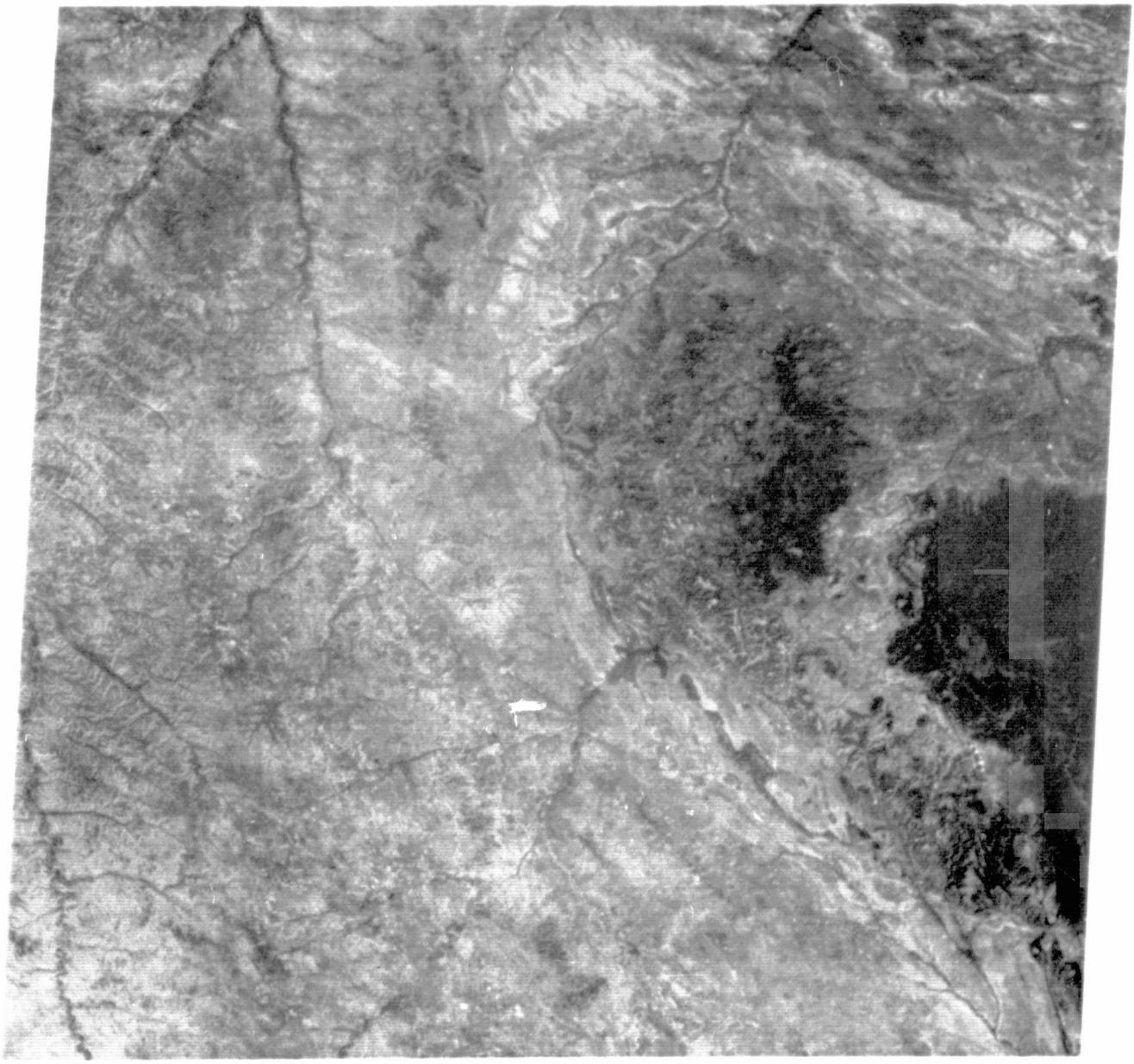


Figure V-11. ERTS-1 image 1047-17175-4,5,7, 8 September 1972, showing the Black Hills and Northern Powder River Basin of Wyoming, South Dakota, and Montana.

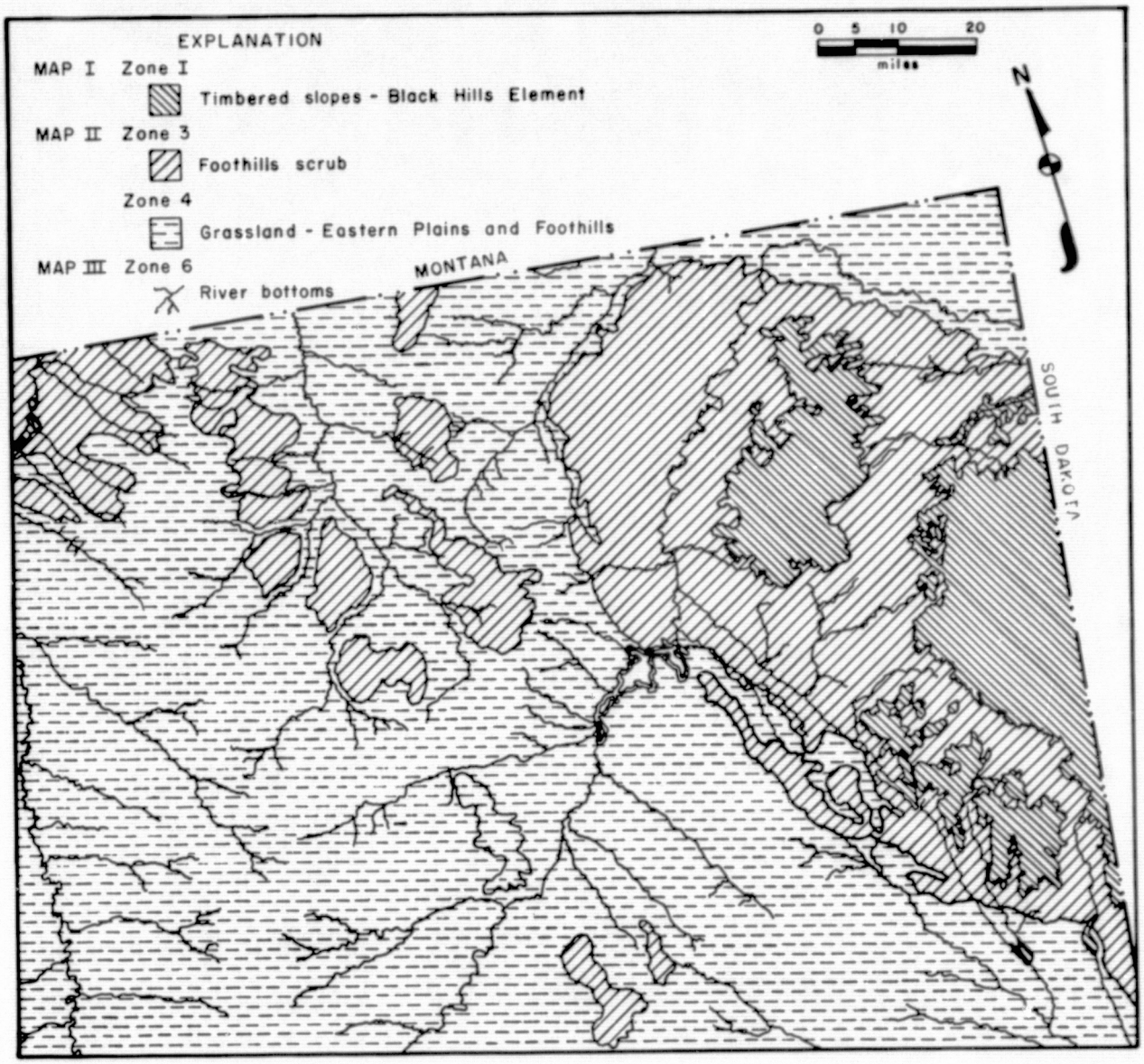


Figure V-12. A detailed map of Zone I (Black Hills Element of Timbered Mountain Slopes) and Zones 3, 4, and 6 taken from the original of Figure V-11.

scattered limber pine, and juniper are common shrubs and trees. On the ERTS mosaic this zone appears brown to reddish where more moisture is available.

Zone 4, grassland, is characteristic of the rolling plains and hills at lower elevations (3,000 to 6,000 feet). The grasslands of Wyoming can be divided into two major types, 1) eastern plains and foothills, and 2) interior grassland plains. In Figure V-3, only the eastern plains and foothills type are mapped as grassland. This general type is characterized by "relatively tall grasses and forbs" and a truly grassland type of flora. But this flora grades into a more arid basin northward (Powder River Basin). Much of the grassland in eastern Wyoming has been converted to agricultural uses (Fig. V-5). On the ERTS imagery, the eastern plains and foothills grasslands appear pale pink to green and are limited to a strip east of the Laramie Range and southwest of the Black Hills.

The interior grasslands are closely related to desert and basin flora. This type is a shortgrass prairie dominated by blue grama, bluegrass, and rabbit brush with some sagebrush present. The type is defined on ERTS as a mottled, off-white to light-brown color.

Zone 5, desert and basin, includes flat, undulating areas at elevations from 4,000 to 6,000 feet. These areas are very arid and often alkaline. Dry streambeds and playa lakes are also very common. The sparse vegetation is mostly xerophytic and saline tolerant. On the ERTS mosaic, these vast areas appear cream to white in color. In the Great Divide Basin area, Figure V-13, (Area III, Fig. V-3) the variety of tones and colors is due to change in soil and rock types and changes in density of vegetation. The blue to blue-green color represents areas covered by sagebrush.

Figure V-4 (Map III) shows zone 6, major river bottoms and irrigated croplands. This zone is limited by the effects of water. Natural river bottoms are covered by lush grasslands and dense growths of cottonwood and willows. In very arid



Figure V-13. ERTS-1 image 1013-17300-4,5,7, 5 August 1973, showing the Great Basin and Red Desert areas of Wyoming, Utah, and Colorado.

ORIGINAL PAGE IS
OF POOR QUALITY

areas there is no mappable river-bottom flora. Where topography permits, the water is often used to irrigate native hay meadows, alfalfa, and other crops. On the ERTS mosaic, zone 6 appears as ribbons or bands of light red to red.

Figure V-5 (Map IV) shows the major agriculture areas of Wyoming. A previous paper (Evans and Marrs, 1974) discusses the application of ERTS-1 imagery to mapping of irrigated croplands.

This mapping program demonstrates that ERTS-1 images are of considerable value in vegetation mapping. Tonal changes, color, brightness, hue, and texture of the ERTS mosaic can be related to vegetative zones and patterns. Often the ERTS imagery defines detail which can not be shown in the general mapping units used here. To map such detail, one must first conduct more intense field checking and make careful studies of smaller areas. He may then be able to expand the techniques to larger areas. Also, the ideal mapping base would be a mosaic compiled from images obtained on consecutive days or a series of such mosaics of the area representing different periods throughout the year or growing season.

The desert and basin and grasslands zones are the most difficult to map accurately due to the great variety of tones and changes in color. For the purpose of this program, the maps for these areas were generalized as described above. More detailed maps can be produced from the ERTS-1 imagery, but such mapping requires the careful analysis of the spectral reflectance values recorded by ERTS and correlation with a ground control such as that used by Gordon (Appendix W, this report).

Appendix W: The use of ERTS data for range mapping and estimation of above-ground, green biomass.

from a report on research performed under contracts NAS 5-21799 and NAS 9-13298.

Gordon, R. C. 1974, Multispectral imagery for range vegetation type mapping and estimation of above-ground green biomass, National Technical Information Service, Springfield, Virginia, 45 p.

Objectives

The objectives of this research were: (1) to determine whether or not the multispectral imagery available from the ERTS-1 satellite was useful for mapping the rangeland resource, and (2) to estimate above-ground green biomass by relating it to total scene reflectance, thereby diversifying the applications of remotely sensed data for use in the field by the resource manager.

Neither of these goals were set with the idea of eliminating field work but, to assist it by determining changes in the rangeland and its above-ground green biomass on a regular basis. The development and advancement of remote sensing techniques for range management will allow the conservationist to locate areas which require his attention.

Study Area

The study was conducted on 68,000 acres of rangeland in the southeastern portion of the Red Desert west of Baggs, Wyoming. Extending through the area are the southern structural rim of the Washakie Basin and a complex system of east-west oriented faults, synclines and anticlines (Gibbens, 1972). The irregular topography extends from 6,200 to 7,200 feet above sea level.

Shales, sandstone or alluvial mixtures of the two make up the major soil parent materials. The often calcareous, brown to pale-brown loams make up the majority of the soils described by the Soil Conservation Service. These loams have developed mainly from the Browns Park formation and the montmorillanitic clay soils from resid-

ual or transported shales. Both are neutral to very basic in reaction (Gibbens, 1972).

The climate consists of cold winters, broken by a short hot summer. Precipitation ranges from about 8 to 11 inches per annum with the majority of winter moisture in the form of snow. Gibbens (1972) states that the growing season is approximately 96 days.

The vegetation types are usually dominated by big sagebrush (Artemisia tridentata Nutt.) or Utah juniper (Juniperus osteosperma (Torr.) Little). These provide good cover for antelope, mule deer, and sage grouse populations.

Under the Bureau of Land Management supervision, the study area was divided into a four pasture rest-rotation unit, a two pasture deferred unit and one season-long grazing unit. Summer use of the pastures was confined to cattle, with sheep grazing the four-pasture rest-rotation unit during the winter.

Procedures

U. S. Geological Survey 1:24,000-scale topographic maps were used as a mapping base. Information was transferred, using a Bausch and Lomb ZT-4 zoom transfer scope, from colour and colour infrared aerial photography obtained from NASA flights 213 and 248 (Figs. W-1a and W-1b). The scales of these images were 1:43,400 and 1:104,500. Accuracy of the vegetation type lines was determined by field reconaissance.

The Skylab vegetation maps were prepared from colour photographs number 104-S190A and 35-S190B Track 48, taken on August 4, 1973, enlarged on the aforementioned zoom transfer to a scale of 1:250,000. This map was then enlarged with a Saltzman Projector system to 1:24,000 for direct comparison to the base map (Figs, W-2a and W-2b). Skylab images S190A and S190B, nine-inch format, were at scales of 1:712,917 and 1:477,979 respectively.

The third set of vegetation type maps was prepared from ERTS image number 1318-17253, band 5, taken on June 6, 1973 (Figs. W-3a and W-3b). This image was enlarged photographically to about 1:250,000, the information mapped directly on the print, and transferred to the Saltzman Projector for enlargement to 1:24,000. Band 5 was chosen over the other bands and the colour composites because of its high contrast and the difficulties encountered in making colour enlargements. Both the ERTS map and the Skylab range type maps covered the entire 68,000 acre study area.

Vegetation transects were established in the study area to adequately type the vegetation. Crown cover and basal cover were obtained for shrubs and for grasses and forbs respectively on these transects using the same procedure followed by Gibbens (1972). Duplication of this method allowed direct comparison of data.

Vegetation types were named for the dominant species in the area of the transect and other transects with similar composition and cover characteristics were grouped to form subtypes of a major type. The major range vegetation types and subtypes were designated on all three vegetation maps.

Prior to the first ERTS overpass of the 1973 study season, 10, two- by three-meter reference plots were established both in the Poison Buttes pasture and 10, in Pasture C, of the rotation pasture system. Meter readings of relative reflectance were obtained from each of these 20 plots during the five 1973 summer overpasses using a portable photometer manufactured by Science and Mechanics.

In addition to the 20 reference plots, 350 plots were established within which above-ground green biomass was determined. Above-ground green biomass included all green herbaceous material and leaves of shrubs but not perennial branches. The Pasture C and Poison Buttes biomass sites each had 175 of these plots.

Relative reflectance measurements were obtained for each plot under conditions similar to those occurring during the overpass and using the same techniques. Measurements were taken as soon after the overpass as possible.

Above-ground green biomass was sampled after each overpass using a double sampling technique described by Pechanec and Pickford (1937). After the July 30, 1973, overpass 50 plots were clipped in entirety to have an accurate above-ground green biomass weight for comparison with the estimates made on July 31, 1974.

Soil moisture was determined by collecting samples of the top inch of soil during each overpass in the 1973 field season and during the 1974 field season, when the comparative transects were being measured for relative reflectance.

Relative reflectance information was obtained with a calibrated photometer. The photometer was calibrated using the procedure followed by Raines and Lee (1974). Reference grey cards of known reflectance were then measured and the values were used as a standard for the field meter readings. Meter readings recorded in the field were converted to percent relative reflectance by plotting them on the graph of reflectance versus meter reading.

Results

Mapping with the ERTS imagery, although hampered by colour bias, cloud cover, loss of detail through enlargement and the resultant poor location association caused by the latter, was successful. Both ERTS and the Skylab images provided useful maps of the range vegetation types. The ERTS-1 map contained representatives of all the vegetation types except one and it was the smallest type. The type not included was a seeded patch of Agropyron cristatum, Type 0. The image used was band 5 (red, .6 to .7) and was taken in June, 1973. The map produced from this image would serve as a useful survey base for the resource manager.

Techniques for estimation of above-ground green biomass have not been confirmed due to the mechanical failure of the photometer. However, graphs of log transmittance versus above-ground green biomass (Fig. W-4) indicate two things. First, it appears possible, for the Poison Buttes site, to estimate above-ground green biomass by relating it to log transmittance. Secondly, for Pasture C, it may be possible to estimate the green biomass produced on this location by relating it directly to an area whose above-ground green biomass can be estimated from the ERTS imagery. These two conclusions may be tested by relating the 1974 summer imagery with the 1974 production data.

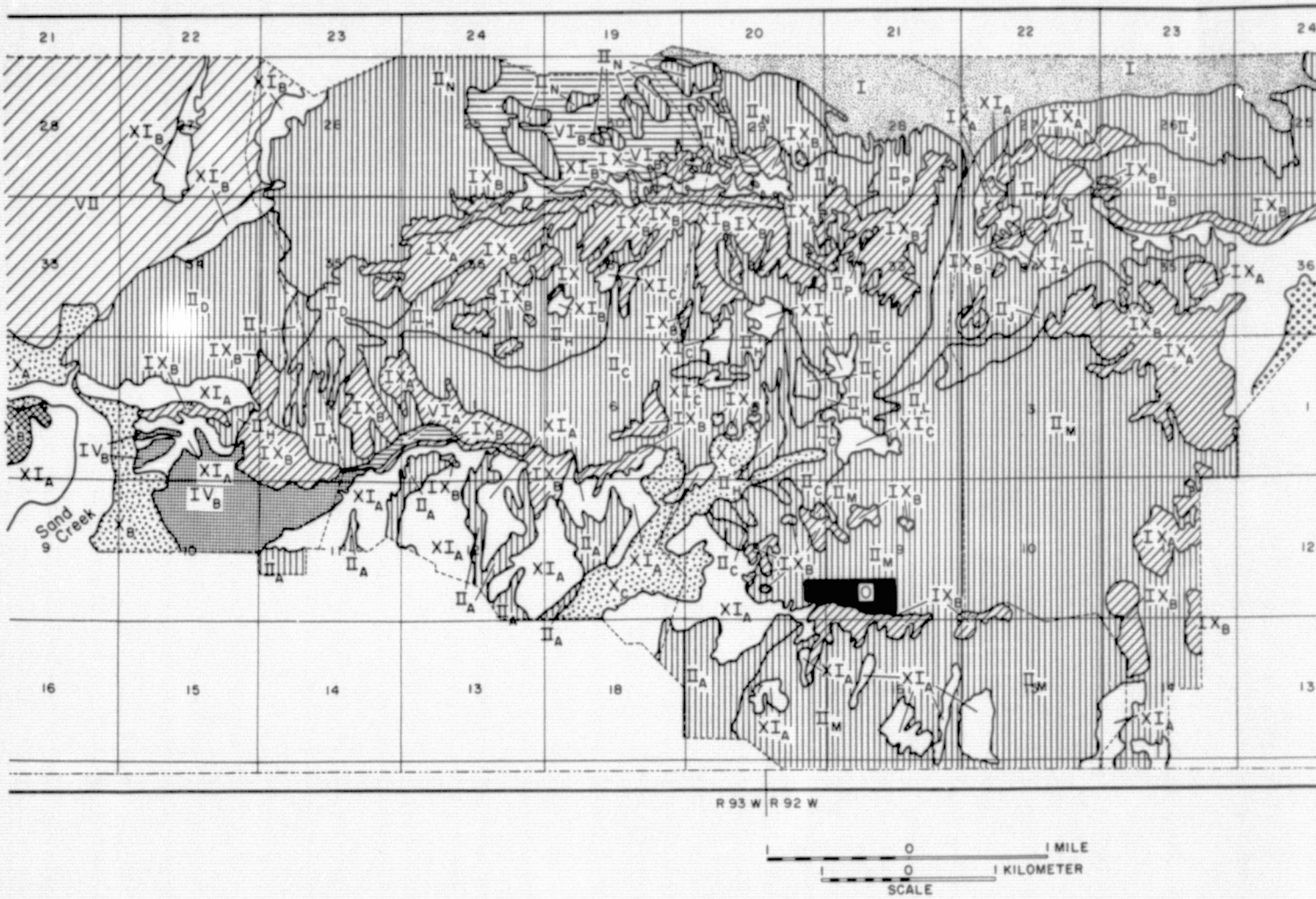
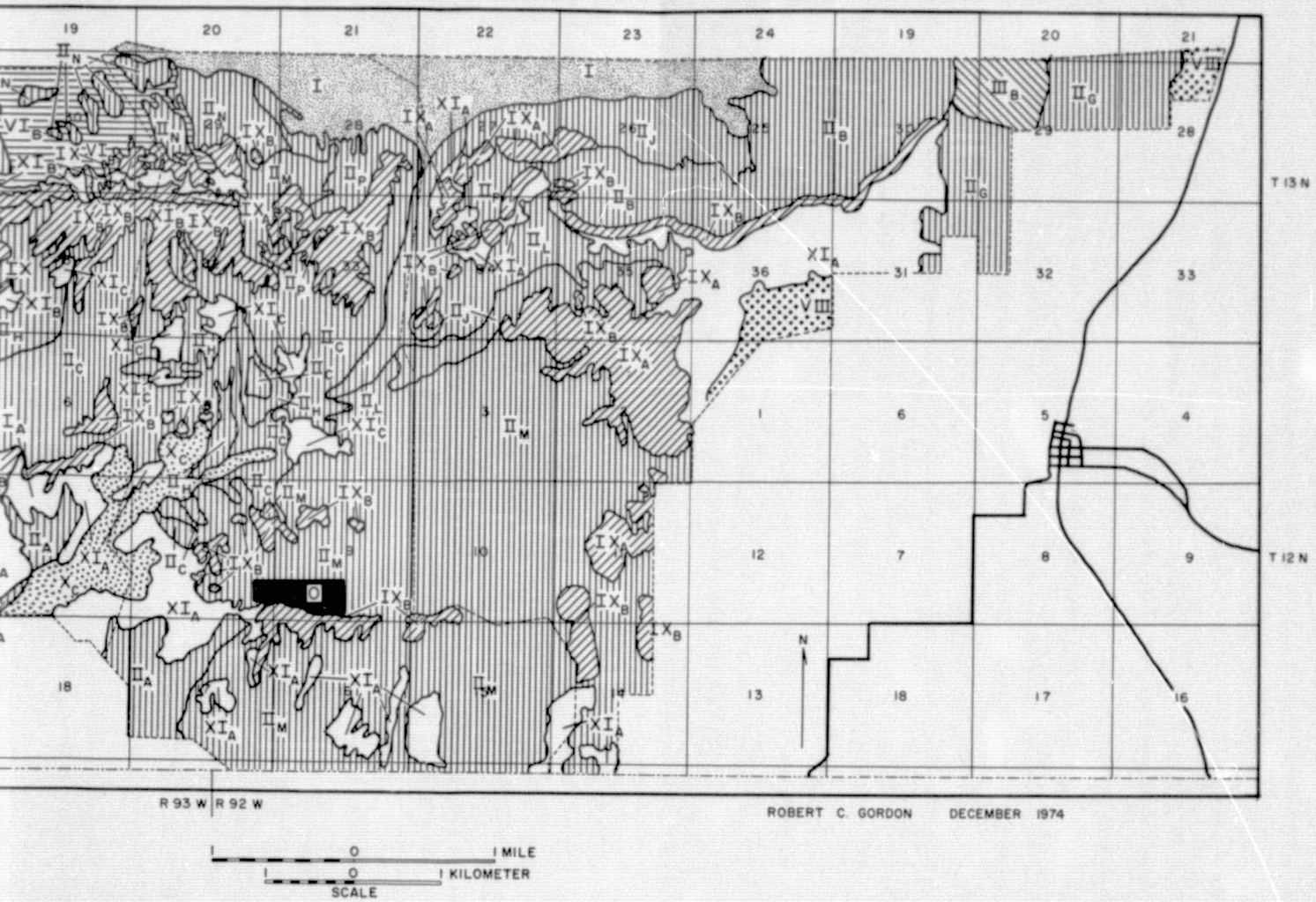


Figure W-1a Range vegetation map compiled from low level aerial photography supplemented with ground reconnaissance

RANGE VEGETATION TYPES

- Type O — Agropyron cristatum: Crested wheatgrass
- Type I — Agropyron smithii -- Artemisia tridentata: Western wheatgrass and basin big sagebrush
- Type II — Artemisia tridentata -- Agropyron smithii: Basin big sagebrush and western wheatgrass
- Type III — Artemisia tridentata -- Agropyron spicatum: Basin big sagebrush and bluebunch wheatgrass
- Type IV — Artemisia tridentata -- Atriplex species: Basin big sagebrush and saltbush
- Type V — Artemisia tridentata -- Carex eleocharis: Basin big sagebrush and needleleaf sedge
- Type VI
- Type VII
- Type VIII
- Type IX
- Type X
- Type XI

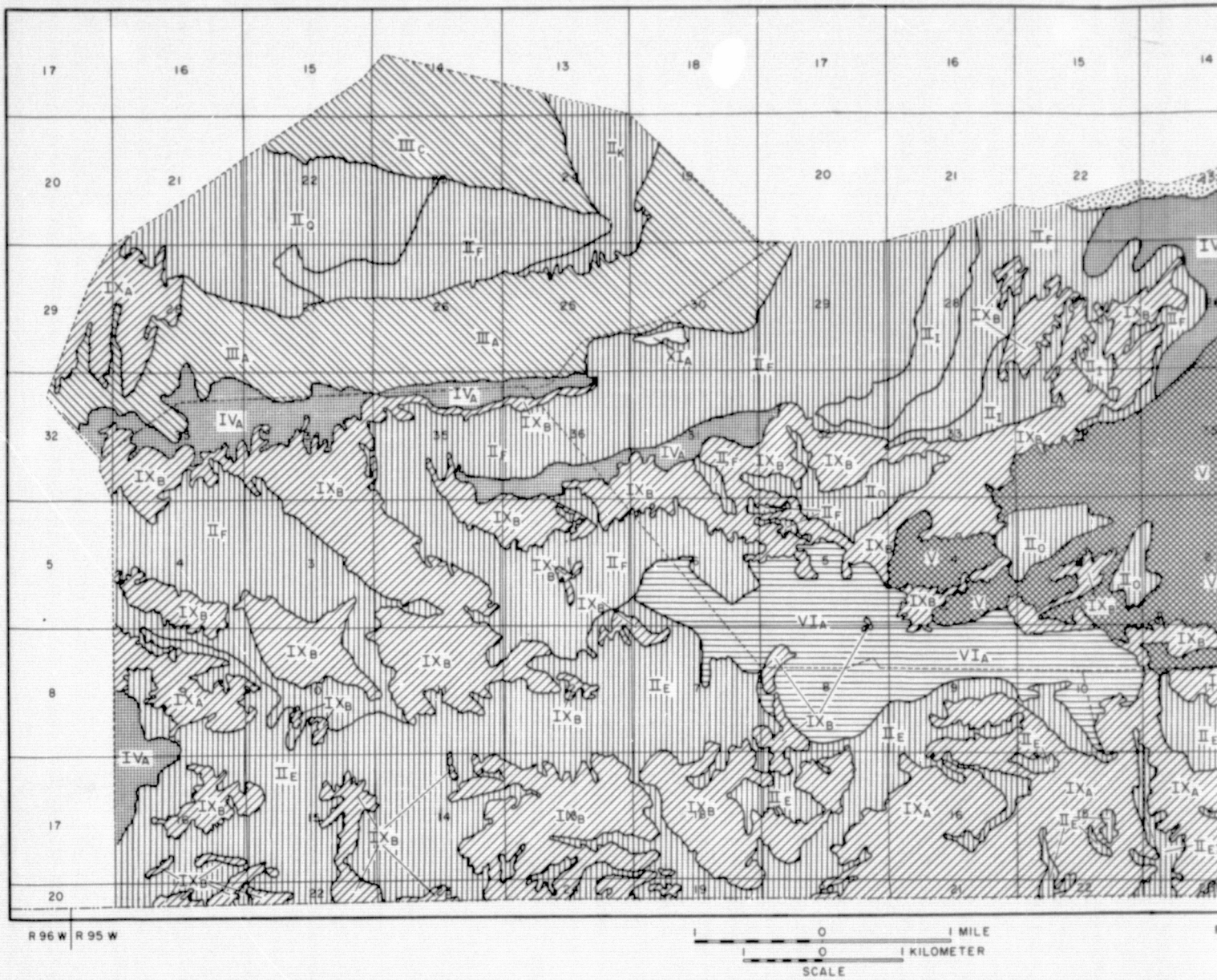
FOLDOUT FRAME



RANGE VEGETATION TYPES

- O — Agropyron cristatum: Crested wheatgrass
- I — Agropyron smithii -- Artemisia tridentata: Western wheatgrass and basin big sagebrush
- II — Artemisia tridentata -- Agropyron smithii: Basin big sagebrush and western wheatgrass
- III — Artemisia tridentata -- Agropyron spicatum: Basin big sagebrush and bluebunch wheatgrass
- IV — Artemisia tridentata -- Atriplex species: Basin big sagebrush and saltbush
- V — Artemisia tridentata -- Carex eleocharis: Basin big sagebrush and needleleaf sedge
- Type VI — Artemisia tridentata -- Gutierrezia sarothrae -- Agropyron smithii: Basin big sagebrush, broom snakeweed, and western wheatgrass
- Type VII — Artemisia tridentata -- Stipa comata: Basin big sagebrush and needleandthread
- Type VIII — Artemisia tridentata: Basin big sagebrush
- Type IX — Juniperus osteosperma: Utah juniper
- Type X — Sarcobatus vermiculatus -- Artemisia tridentata: Black greasewood and basin big sagebrush
- Type XI — Bare ground

COLORADO STATE

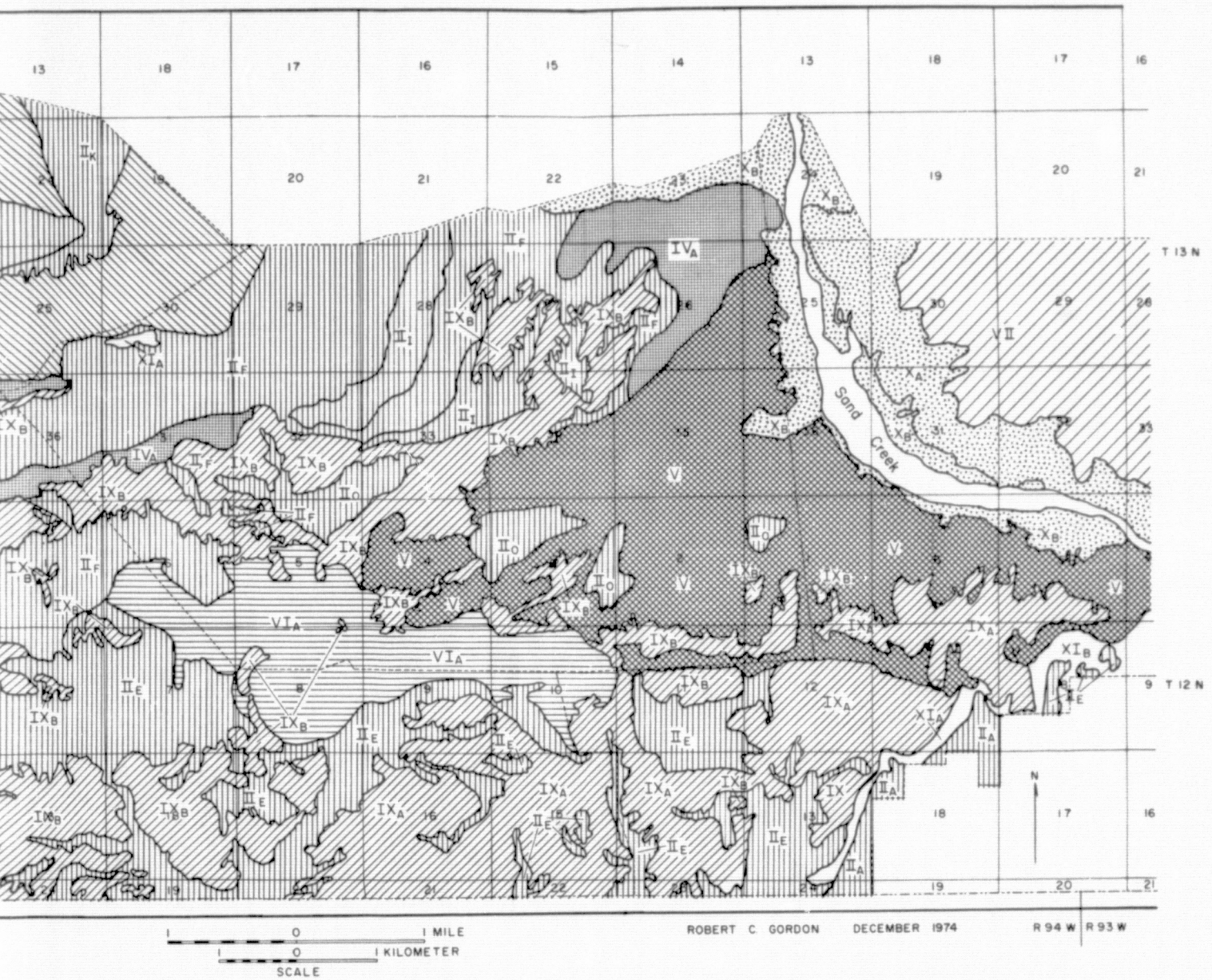


RANGE VEGETATION T

Type O	Agropyron cristatum: Crested wheatgrass	Typ
Type I	Agropyron smithii -- Artemisia tridentata: Western wheatgrass and basin big sagebrush	Typ
Type II	Artemisia tridentata -- Agropyron smithii: Basin big sagebrush and western wheatgrass	Typ
Type III	Artemisia tridentata -- Agropyron spicatum: Basin big sagebrush and bluebunch wheatgrass	Typ
Type IV	Artemisia tridentata -- Atriplex species: Basin big sagebrush and saltbush	Typ
Type V	Artemisia tridentata -- Carex eleocharis: Basin big sagebrush and needleleaf sedge	Typ

Figure W-1b Range vegetation map compiled from low level aerial photography supplemented with ground reconnaissance

DOUT FRAME



RANGE VEGETATION TYPES

- Type O — Agropyron cristatum: Crested wheatgrass
- Type I — Agropyron smithii -- Artemisia tridentata: Western wheatgrass and basin big sagebrush
- Type II — Artemisia tridentata -- Agropyron smithii: Basin big sagebrush and western wheatgrass
- Type III — Artemisia tridentata -- Agropyron spicatum: Basin big sagebrush and bluebunch wheatgrass
- Type IV — Artemisia tridentata -- Atriplex species: Basin big sagebrush and saltbush
- Type V — Artemisia tridentata -- Carex eleochoris: Basin big sagebrush and needleleaf sedge
- Type VI — Artemisia tridentata -- Gutierrezia sarothrae -- Agropyron smithii: Basin big sagebrush, broom snakeweed, and western wheatgrass
- Type VII — Artemisia tridentata -- Stipa comata: Basin big sagebrush and needleandthread
- Type VIII — Artemisia tridentata: Basin big sagebrush
- Type IX — Juniperus osteosperma: Utah juniper
- Type X — Sarcobatus vermiculatus -- Artemisia tridentata: Black greasewood and basin big sagebrush
- Type XI — Bare ground

FOLDOUT FRAM

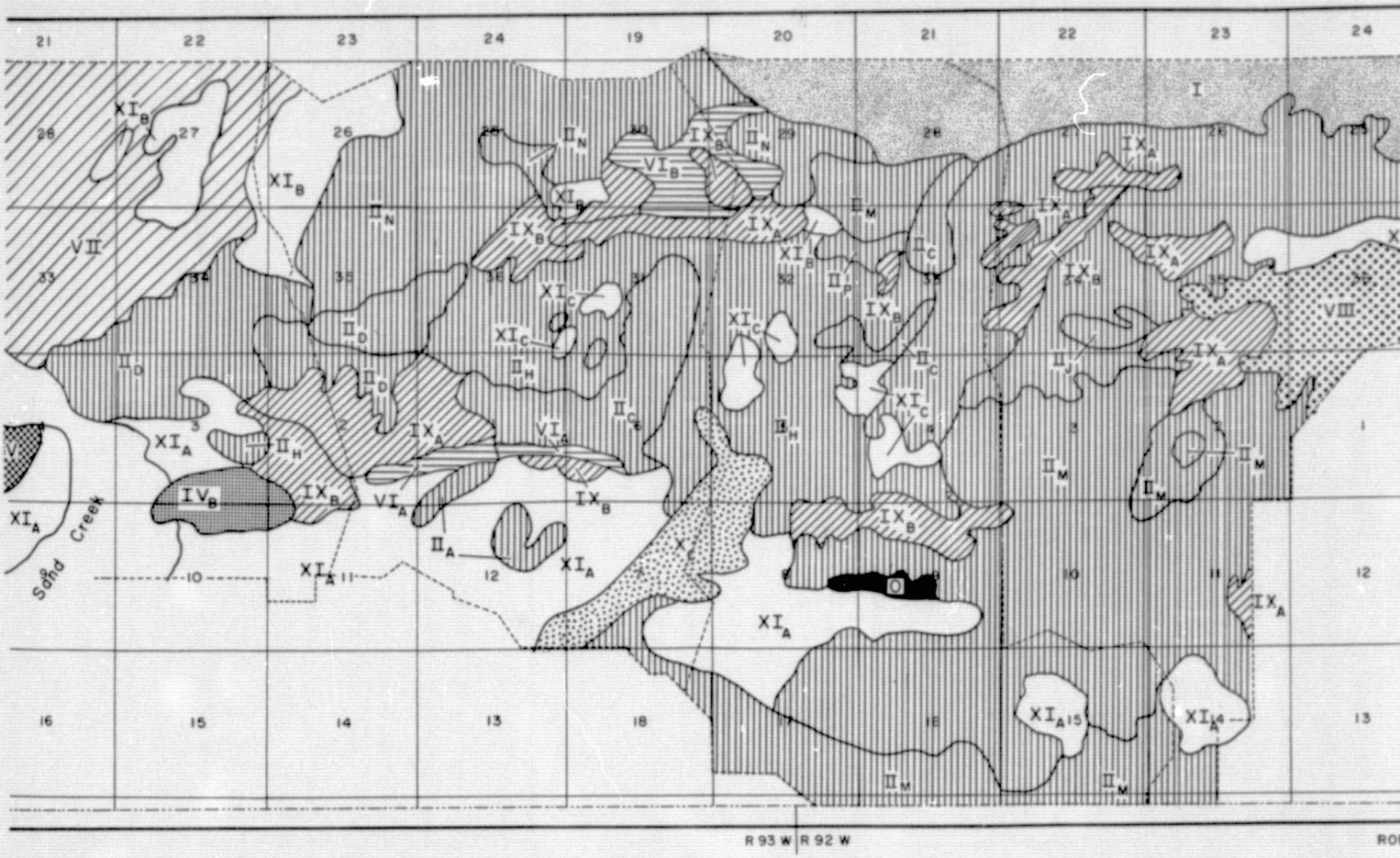
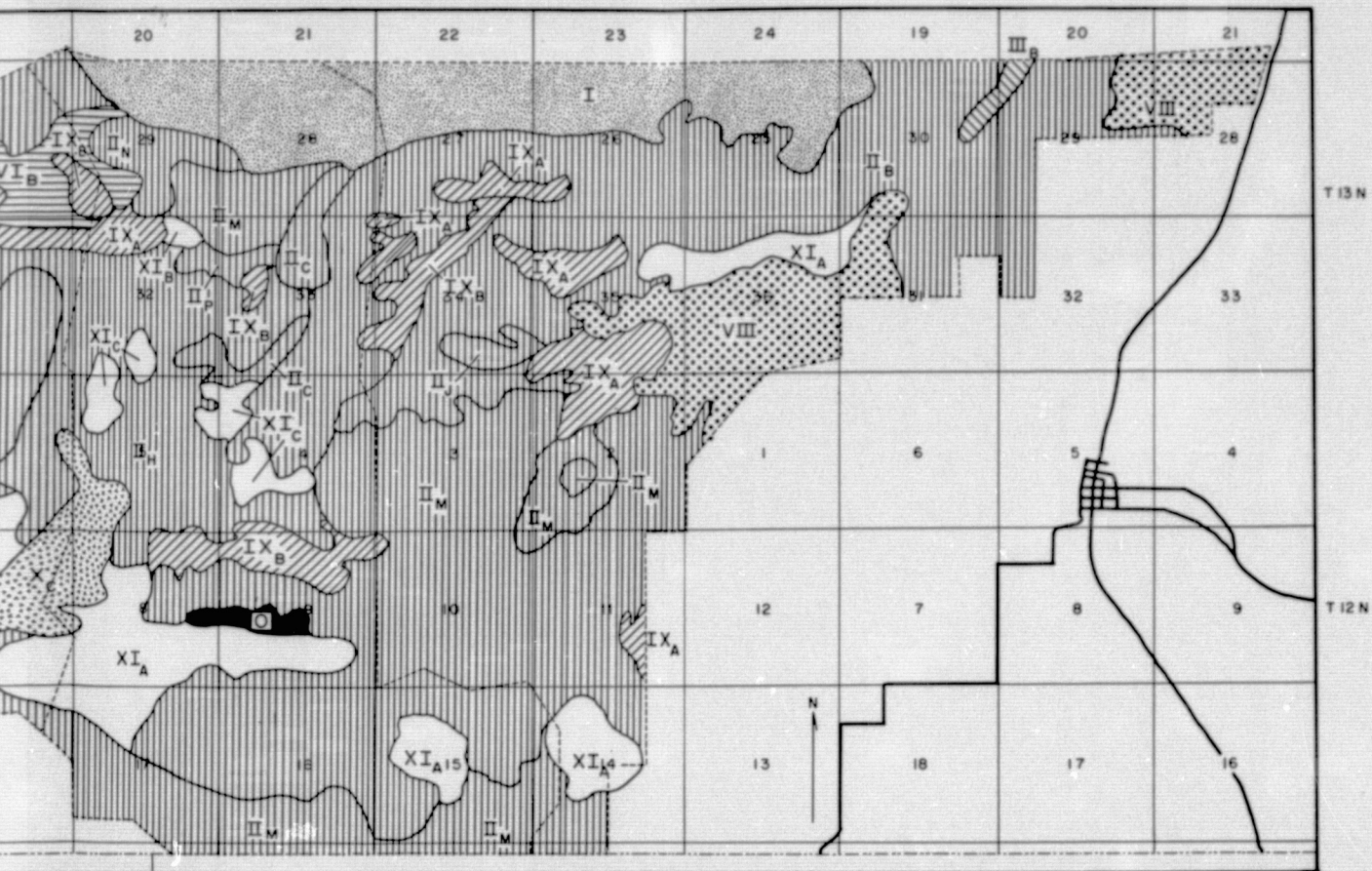


Figure W-2a. Range vegetation map interpreted from SKYLAB photographs

RANGE VEGETATION TYPES

- Type O — Agropyron cristatum: Crested wheatgrass
- Type I — Agropyron smithii -- Artemisia tridentata: Western wheatgrass and basin big sagebrush
- Type II — Artemisia tridentata -- Agropyron smithii: Basin big sagebrush and western wheatgrass
- Type III — Artemisia tridentata -- Agropyron spicatum: Basin big sagebrush and bluebunch wheatgrass
- Type IV — Artemisia tridentata -- Atriplex species: Basin big sagebrush and saltbush
- Type V — Artemisia tridentata -- Carex eleocharis: Basin big sagebrush and needleleaf sedge
- Type VI — Ar Ag sm
- Type VII — Ar Bo
- Type VIII — Ar Bo
- Type IX — Ju Ur
- Type X — Sc Bl
- Type XI — Bo

FOLDOUT FRAME



RANGE VEGETATION TYPES

Agropyron cristatum:
Crested wheatgrass

Agropyron smithii -- Artemisia tridentata:
Western wheatgrass and basin big sagebrush

Artemisia tridentata -- Agropyron smithii:
Basin big sagebrush and western wheatgrass

Artemisia tridentata -- Agropyron spicatum:
Basin big sagebrush and bluebunch wheatgrass

Artemisia tridentata -- Atriplex species:
Basin big sagebrush and saltbush

Artemisia tridentata -- Carex eleocharis:
Basin big sagebrush and needleleaf sedge

Type VI Artemisia tridentata -- Gutierrezia sarothrae -- Agropyron smithii: Basin big sagebrush, broom snakeweed, and western wheatgrass

Type VII Artemisia tridentata -- Stipa comata:
Basin big sagebrush and needleandthread

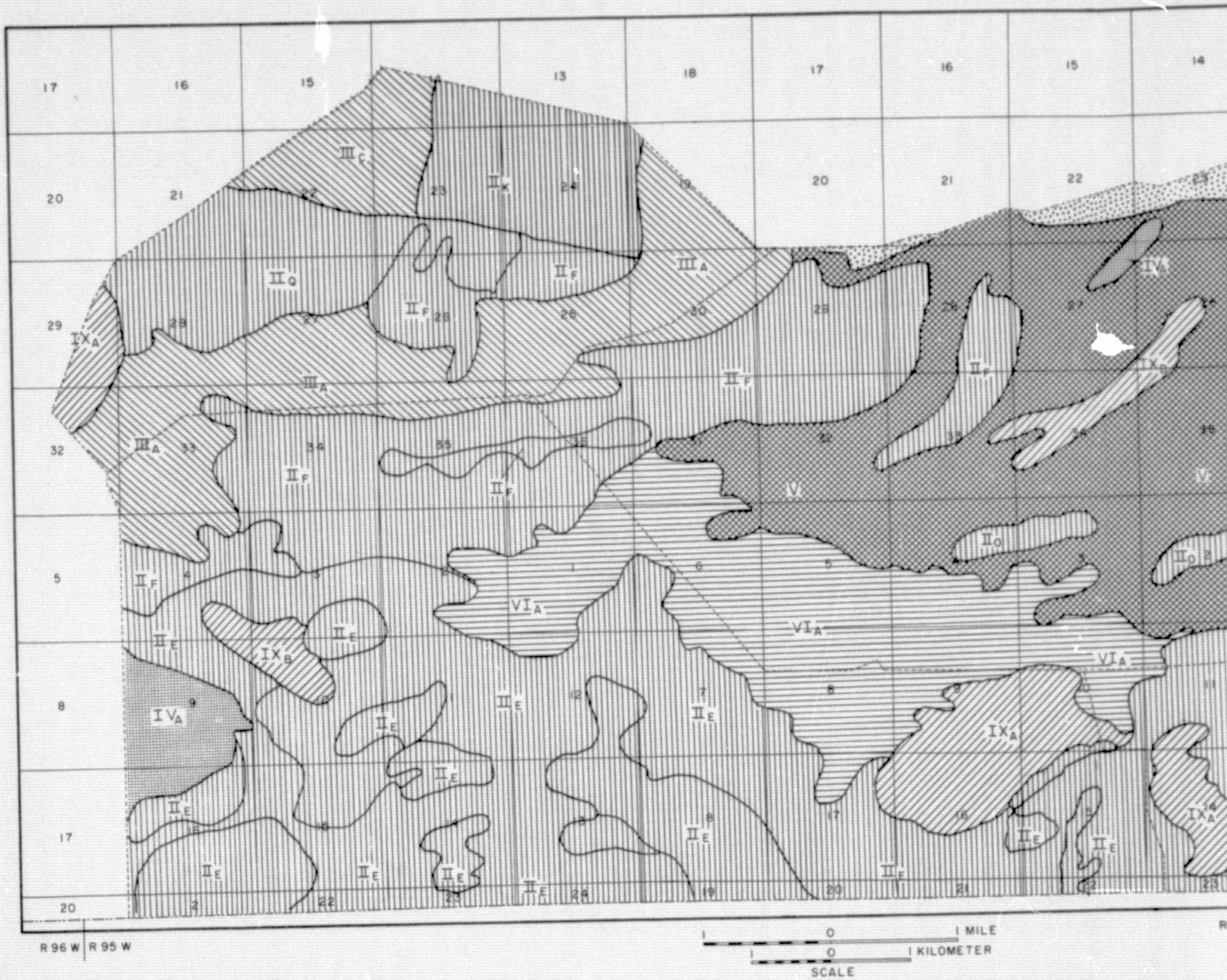
Type VIII Artemisia tridentata:
Basin big sagebrush

Type IX Juniperus osteosperma:
Utah juniper

Type X Sarcobatus vermiculatus -- Artemisia tridentata:
Black greasewood and basin big sagebrush

Type XI Bare ground

FOLDOUT FRAM

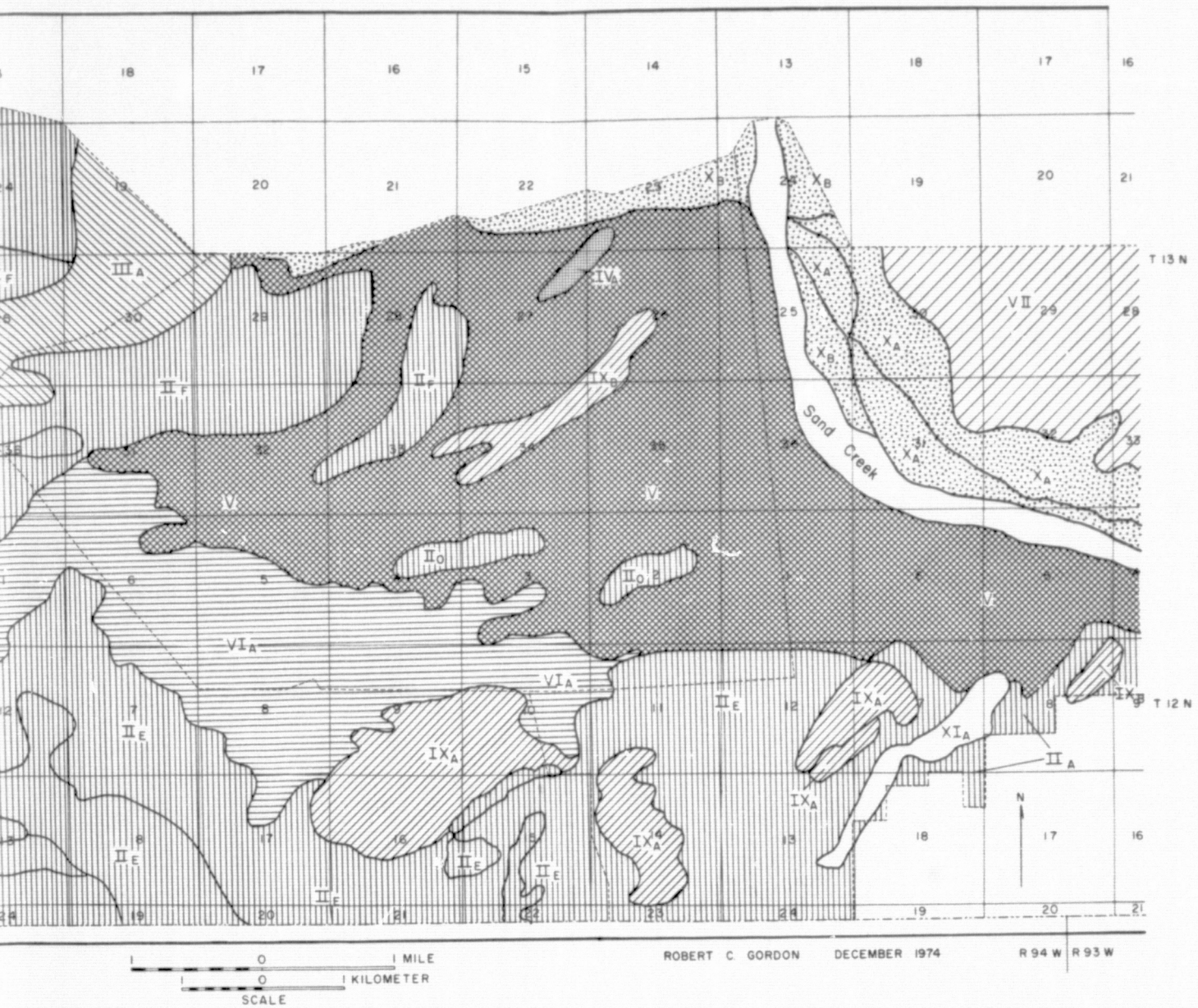


RANGE VEGETATION T

Type O	Agropyron cristatum: Crested wheatgrass	Typ
Type I	Agropyron smithii -- Artemisia tridentata: Western wheatgrass and basin big sagebrush	Typ
Type II	Artemisia tridentata -- Agropyron smithii: Basin big sagebrush and western wheatgrass	Typ
Type III	Artemisia tridentata -- Agropyron spicatum: Basin big sagebrush and bluebunch wheatgrass	Typ
Type IV	Artemisia tridentata -- Atriplex species: Basin big sagebrush and saltbush	Typ
Type V	Artemisia tridentata -- Carex eleocharis: Basin big sagebrush and needleleaf sedge	Typ

Figure W-2b Range vegetation map interpreted from SKYLAB photographs

OLDOUT FRAM



RANGE VEGETATION TYPES

Type O — Agropyron cristatum: Crested wheatgrass

Type I — Agropyron smithii -- Artemisia tridentata: Western wheatgrass and basin big sagebrush

Type II — Artemisia tridentata -- Agropyron smithii: Basin big sagebrush and western wheatgrass

Type III — Artemisia tridentata -- Agropyron spicatum: Basin big sagebrush and bluebunch wheatgrass

Type IV — Artemisia tridentata -- Atriplex species: Basin big sagebrush and saltbush

Type V — Artemisia tridentata -- Carex eleocharis: Basin big sagebrush and needleleaf sedge

Type VI — Artemisia tridentata -- Gutierrezia sarothrae -- Agropyron smithii: Basin big sagebrush, broom snakeweed, and western wheatgrass

Type VII — Artemisia tridentata -- Stipa comata: Basin big sagebrush and needleandthread

Type VIII — Artemisia tridentata: Basin big sagebrush

Type IX — Juniperus osteosperma: Utah juniper

Type X — Sarcobatus vermiculatus -- Artemisia tridentata: Black greasewood and basin big sagebrush

Type XI — Bare ground

FOLDOUT FRAME

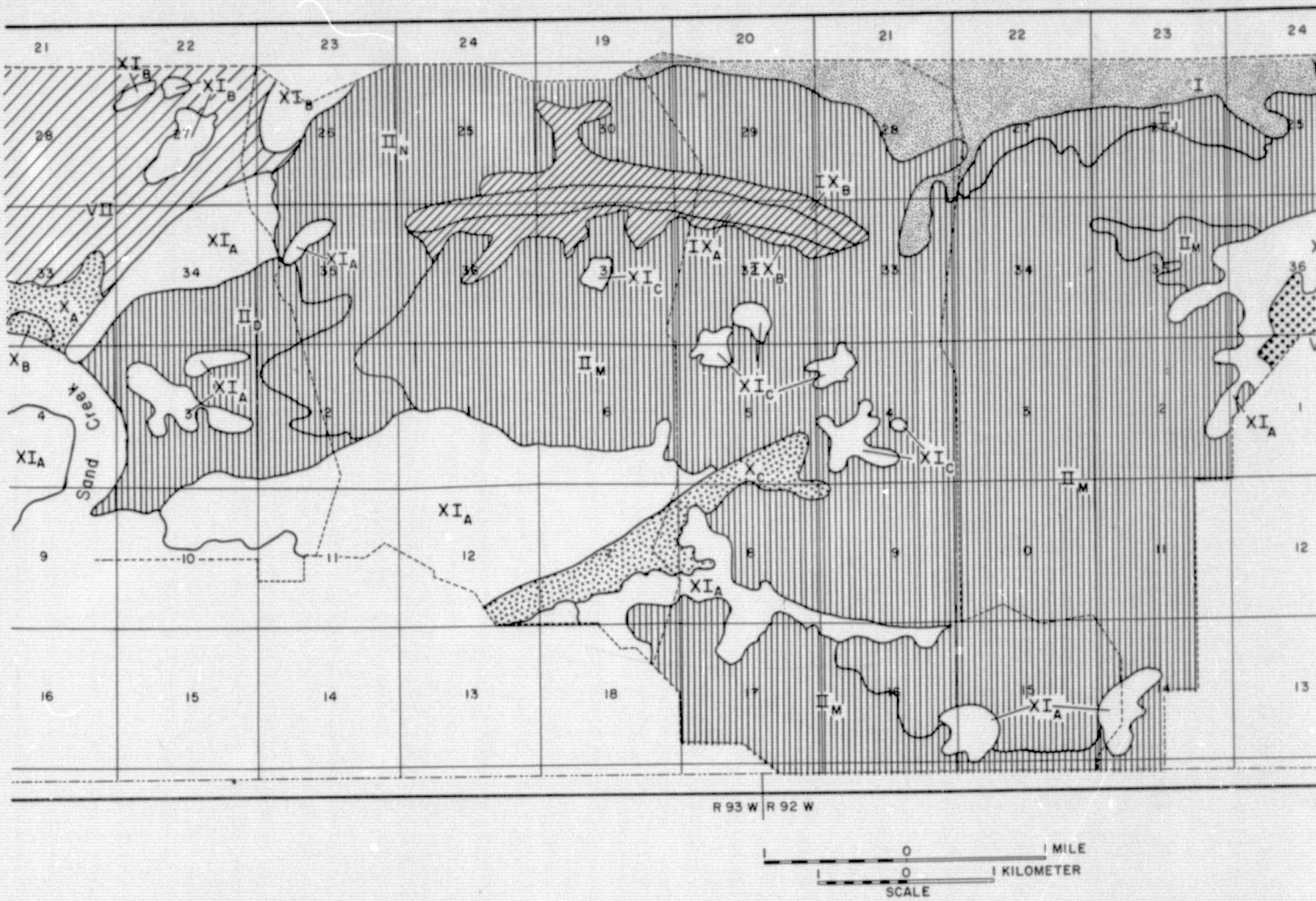
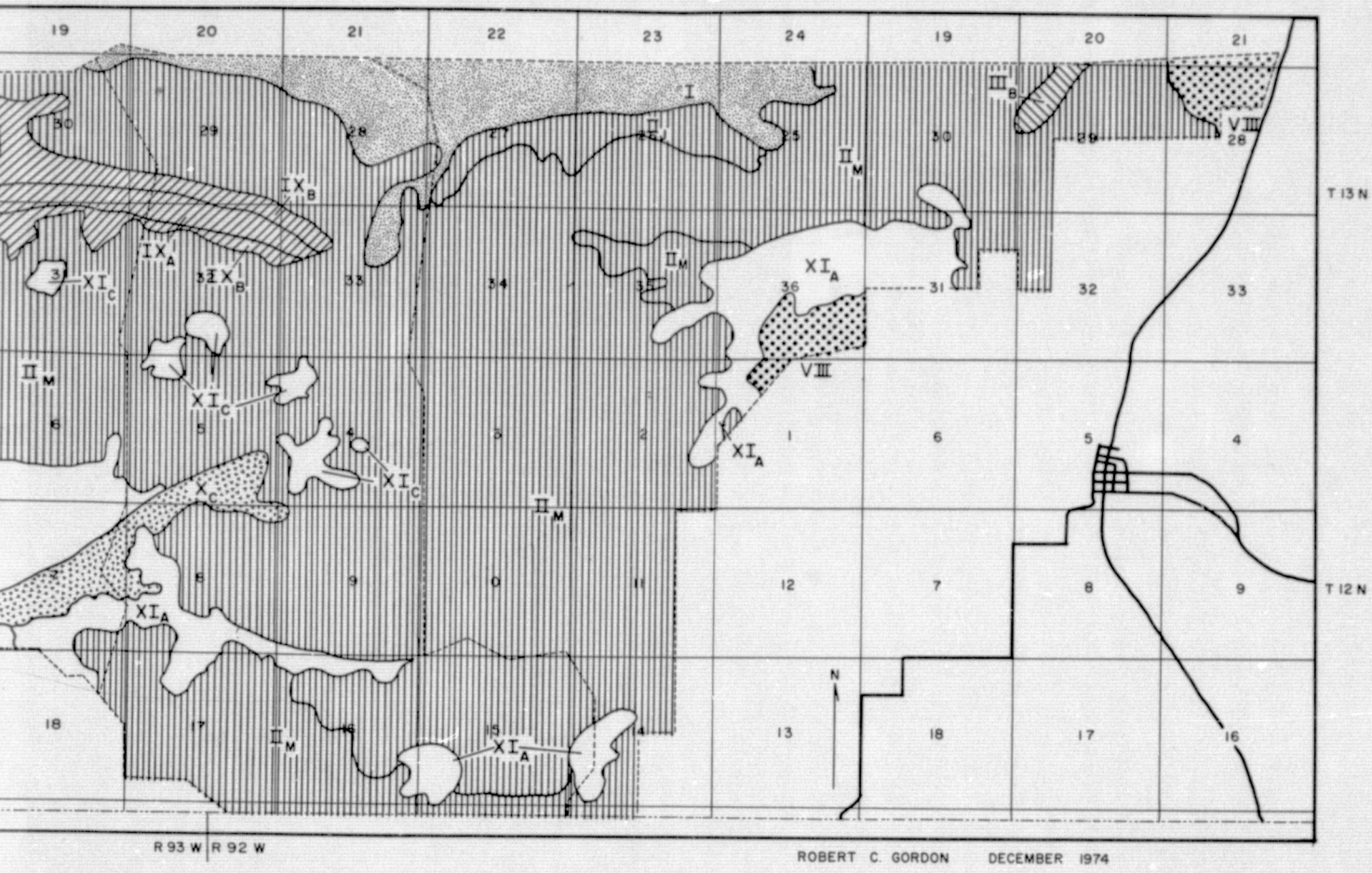


Figure W-3a. Range vegetation map developed from ERTS-1 imagery

RANGE VEGETATION TYPES

Type 0	Agropyron cristatum: Crested wheatgrass	Type VI
Type I	Agropyron smithii -- Artemisia tridentata: Western wheatgrass and basin big sagebrush	Type VII
Type II	Artemisia tridentata -- Agropyron smithii: Basin big sagebrush and western wheatgrass	Type VIII
Type III	Artemisia tridentata -- Agropyron spicatum: Basin big sagebrush and bluebunch wheatgrass	Type IX
Type IV	Artemisia tridentata -- Atriplex species: Basin big sagebrush and saltbush	Type X
Type V	Artemisia tridentata -- Carex eleocharis: Basin big sagebrush and needleleaf sedge	Type XI

FOLDOUT FRAME 1



RANGE VEGETATION TYPES

O Agropyron cristatum: Crested wheatgrass

I Agropyron smithii -- Artemisia tridentata: Western wheatgrass and basin big sagebrush

II Artemisia tridentata -- Agropyron smithii: Basin big sagebrush and western wheatgrass

III Artemisia tridentata -- Agropyron spicatum: Basin big sagebrush and bluebunch wheatgrass

IV Artemisia tridentata -- Atriplex species: Basin big sagebrush and saltbush

V Artemisia tridentata -- Carex eleocharis: Basin big sagebrush and needleleaf sedge

Type VI Artemisia tridentata -- Gutierrezia sarothrae -- Agropyron smithii: Basin big sagebrush, broom snakeweed, and western wheatgrass

Type VII Artemisia tridentata -- Stipa comata: Basin big sagebrush and needleandthread

Type VIII Artemisia tridentata: Basin big sagebrush

Type IX Juniperus osteosperma: Utah juniper

Type X Sarcobatus vermiculatus -- Artemisia tridentata: Black greasewood and basin big sagebrush

Type XI Bare ground

FOLDOUT FRAME

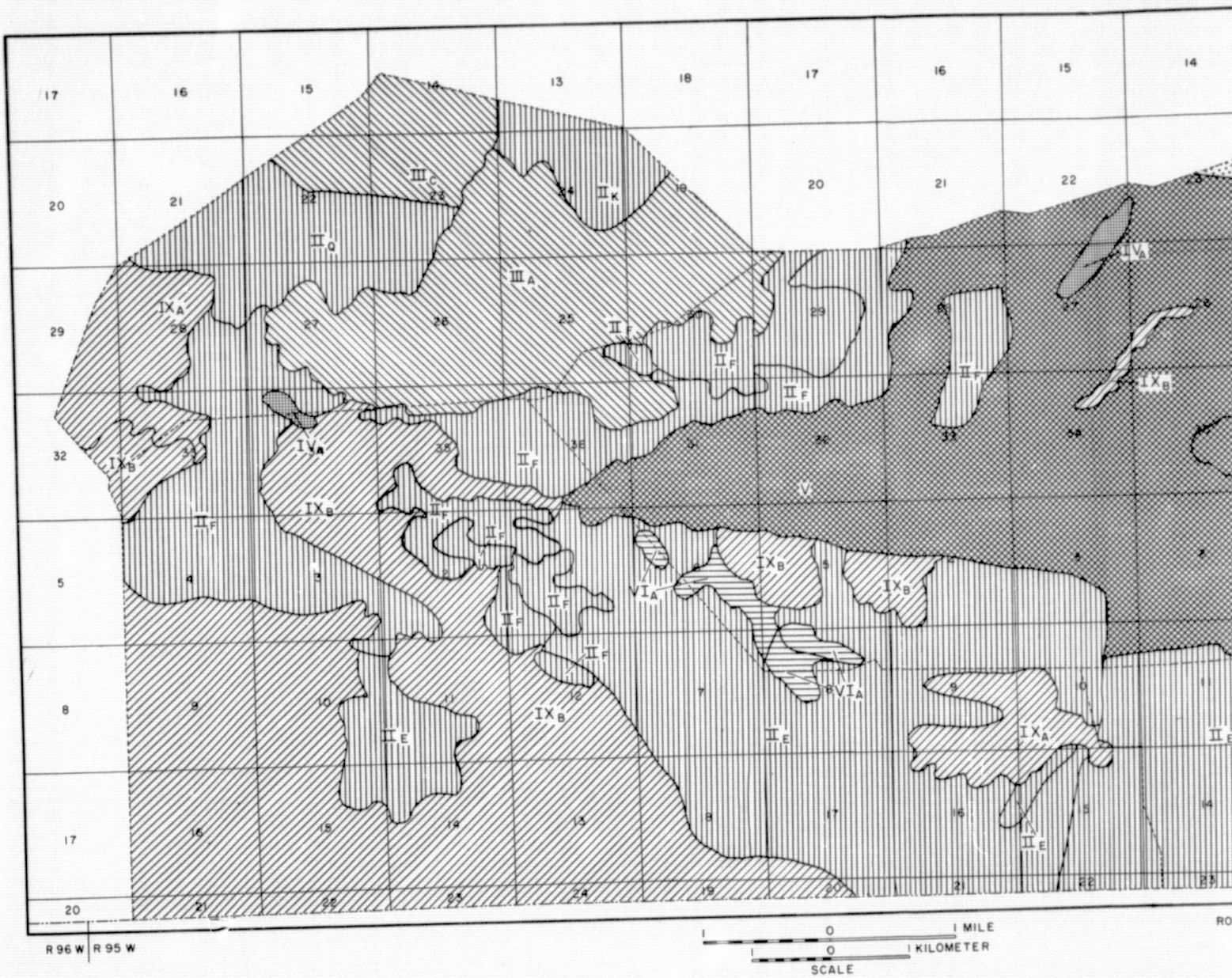
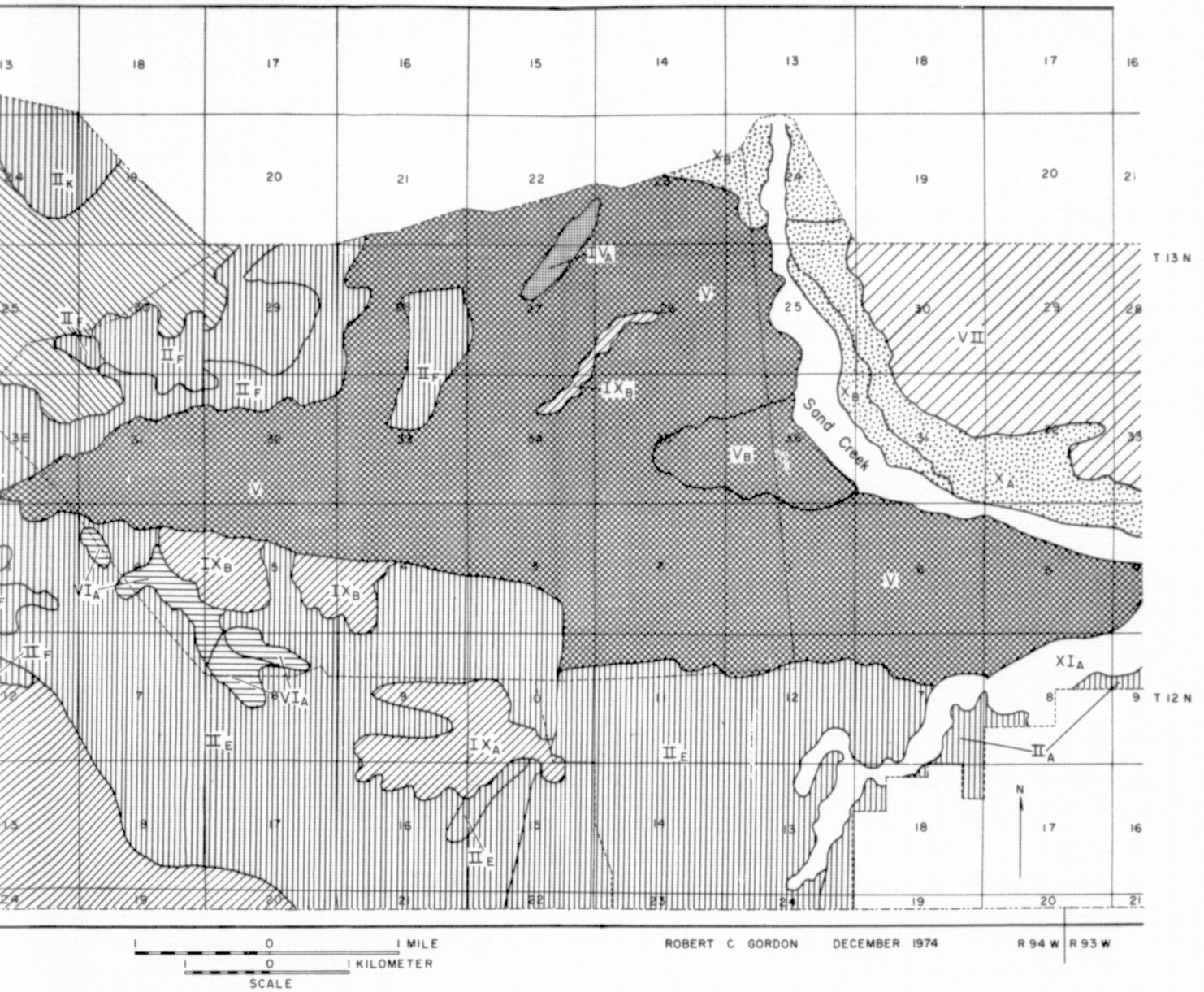


Figure W-4a. Range vegetation map developed from ERTS-1 imagery

LDOUT FRAME



RANGE VEGETATION TYPES

Type 0 Agropyron cristatum: Crested wheatgrass

Type I Agropyron smithii -- Artemisia tridentata: Western wheatgrass and basin big sagebrush

Type II Artemisia tridentata -- Agropyron smithii: Basin big sagebrush and western wheatgrass

Type III Artemisia tridentata -- Agropyron spicatum: Basin big sagebrush and bluebunch wheatgrass

Type IV Artemisia tridentata -- Atriplex species: Basin big sagebrush and saltbush

Type V Artemisia tridentata -- Carex eleocharis: Basin big sagebrush and needleleaf sedge

Type VI Artemisia tridentata -- Gutierrezia sarothrae -- Agropyron smithii: Basin big sagebrush, broom snakeweed, and western wheatgrass

Type VII Artemisia tridentata -- Stipa comata: Basin big sagebrush and needleandthread

Type VIII Artemisia tridentata: Basin big sagebrush

Type IX Juniperus osteosperma: Utah juniper

Type X Sarcobatus vermiculatus -- Artemisia tridentata: Black greasewood and basin big sagebrush

Type XI Bare ground

FOLDOUT F

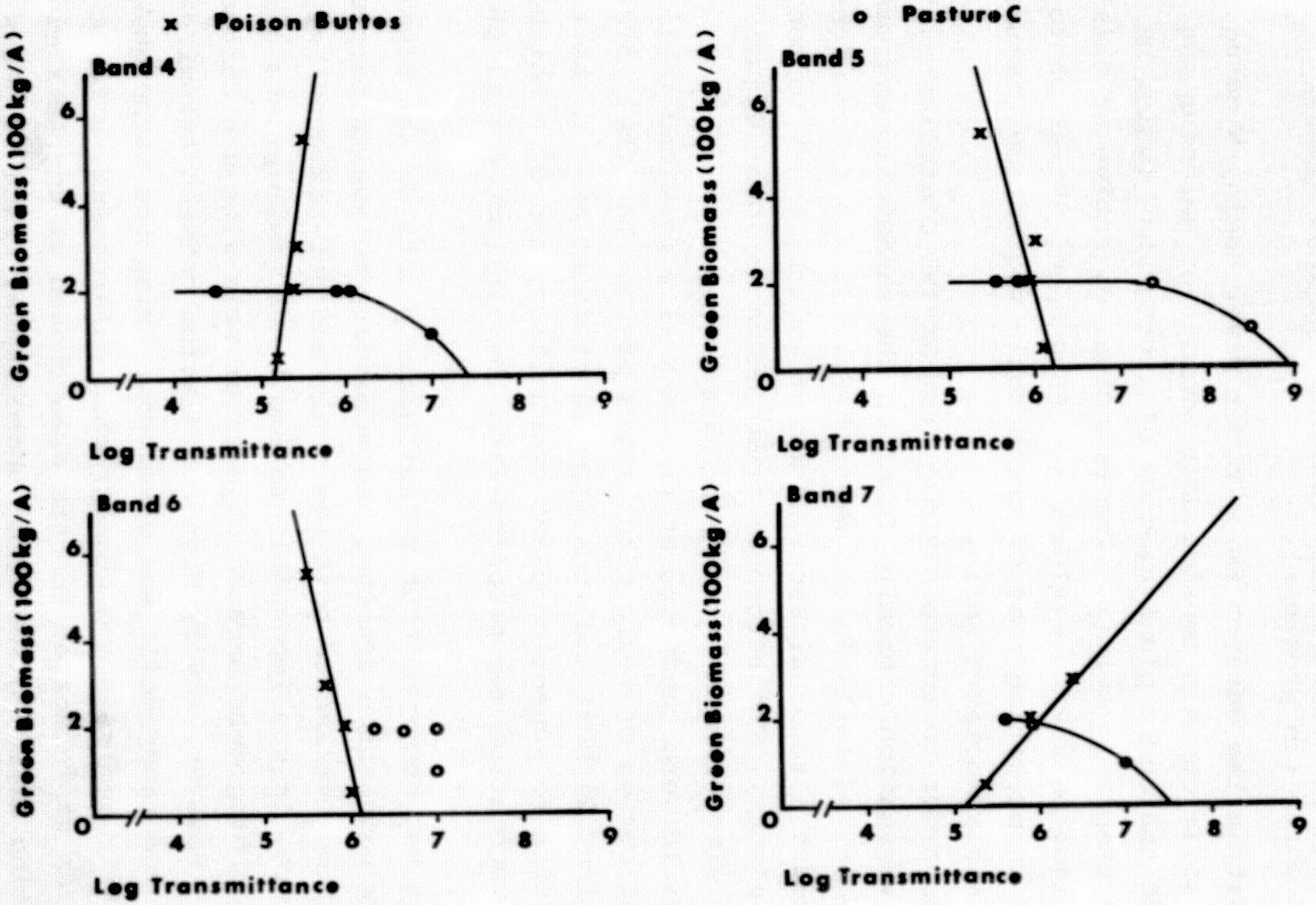


Figure W-4. Graphs of log transmittance versus above-ground green biomass.

Appendix X: Mapping of seleniferous soil units.

a summary of research for contract NAS 9-13298:
Kolm, K. E., 1975, The Location and Mapping of Seleniferous Soil Units in the Wasatch Fm., Powder River Basin, Wyoming, using Skylab Photographs; Dept. of Geology, University of Wyoming, Special Report, (in progress).

Within the Wasatch Fm., Powder River Basin, Wyoming, sandy soils contain considerable amounts of selenium and support the toxic plant species of Astragalus bisulcatus and Oxytropis lambertii. The principal objective of this investigation was to evaluate the success of Skylab photography in preparing maps of these toxic vegetation communities and their associated soils.

In order to accurately map from Skylab photographs, the toxic vegetation community found on the sandstones and sandstone-derived soils in the Wasatch Fm., it was first necessary to conduct a reconnaissance study of an area known to contain these plants. The reference area chosen is located just north of the site of AMAX's South Belle Ayr Mine.

Field work conducted at the AMAX site resulted in 1) identification of toxic plant types present and their distribution, 2) soil and rock type identification and their relationship to supported plant communities, and 3) a soils and toxic vegetation map prepared from low-altitude aerial photography.

It was observed that seleniferous plants do not display a heavy population density, and secondary non-seleniferous vegetation overlapped both the toxic and not-toxic soils. Therefore, it was impossible to map these toxic plants using Skylab photographs because objects of this size are unresolvable. However, a very high correlation between seleniferous plants and sandy soils was observed. Using the techniques of density analysis and photographic enlargement, a toxic soils map was prepared for the area chosen at the AMAX mine site using Skylab S190B color photographs, Track 59, Pass 28.

A regional map of these seleniferous soils in the Wasatch Fm., Powder River Basin, Wyoming, is now being prepared and will be field checked. A similar toxic soils map, using ERTS imagery, will not be attempted due to the seleniferous soil lenses being too small to be resolved at the ERTS scale.

Appendix Y: Programs employed in Q-mode factor analysis of ERTS-1 multispectral data.

ORIGINAL PAGE IS OF POOR QUALITY

```
0001            DIMENSION DATA(3,10),C(55),Z(3,10),SIG(10),AVG(10),R(100)
0002            DIMENSION V(10,10),E(10),TV(51),H(10),FF(10),B(10)
0003            DIMENSION F(3,10),FSTAR(3,10),VSTAR(10,10),CONTRL(4)
0004            DIMENSION INDEX(10),D(55)
0005       10   FORMAT (30F1.0)
0006            READ (105,10) ((DATA(I,J),J=1,10),I=1,3)
0007            CONTRL(1)=2.0
0008            CONTRL(4)=.995
0009            DO 2 I=1,2
0010            DO 3 J=1,2
0011            CONTRL(2)=I
0012            CONTRL(3)=J
0013            CALL SQFAC(CONTRL,3,10,10,3,DATA,AVG,SIG,Z,C,E,V,F,VSTAR,FSTAR,NC,
0014           1TV,H,FF,B,IER,D,INDEX,R)
0015        3   CONTINUE
0016        2   CONTINUE
0017            STOP
0018            END
```

```
0001              SUBROUTINE SQFAC(CONTRL,NVAR,NLOC,N,NSEC,DATA,AVG,SIG,Z,C,E,V,F,
0002             1  VSTAR,FSTAR,NC,TV,H,FF,B,IER,D,INDEX,R)
0003       C     MODE=1 FOR R-MODE, MODE=2 FOR Q-MODE FACTOR ANALYSIS
0004       C     MTYPE=1 FOR CORRELATION MATRIX, MTYPE=2 FOR COSINE MATRIX
0005       C     DATA=NVAR X NLOC DATA MATRIX
0006       C     NVAR=NUMBER OF VARIABLES
0007       C     NLOC=NUMBER OF LOCATIONS
0008       C     C= NXN COSINE OR CORRELATION MATRIX STORED AS A VECTOR ARRAY
0009       C     WITH C(1)=(1,1) ELEMENT, C(2)=(2,1) ELEMENT, C(3)=(2,2) ELEMENT
0010       C     C(4)=(3,1) ELEMENT, ETC.
0011       C     M=N*(N+1)/2
0012       C     N2=N**2
0013       C     NSEC=NLOC IF N=NVAR, NSEC=NVAR IF N=NLOC
0014       C     MAX=MAX(NVAR,NLOC)
0015       C     Z=NVAR X NLOC NORMALIZED DATA MATRIX. COMPONENTS OF Z=COMPONENTS
0016       C     OF DATA MINUS AVG (FOR R-MODE) DIVIDED BY SIG
0017       C     SIG=N COMPONENT VECTOR OF STD DEV (FOR R-MODE) OR RMS LENGTH (FOR
0018       C     Q-MODE)
0019       C     AVG=N COMPONENT VECTOR OF AVERAGES FOR R-MODE AND ZERO FOR Q-MODE
0020       C     V=NXN WORK MATRIX (EIGENVECTORS)
0021       C     E=N COMPONENT WORK VECTOR (EIGENVALUES)
0022       C     TV,H,F,B,IER ARE DEFINED BY COMMENTS IN SUBR VARMX
0023       C     ISIDE=1 IF LEFT MATRIX IS TO BE ROTATED AND RIGHT MATRIX USED
0024       C     FOR LOADINGS, ISIDE=2 IF RIGHT MATRIX IS TO BE ROTATED AND LEFT
0025       C     MATRIX USED FOR LOADINGS
0026       C     F=UNROTATED FACTOR MATRIX
0027       C     FSTAR=ROTATED FACTOR MATRIX
0028       C     VSTAR= ROTATED EIGENVECTOR MATRIX
0029       C     D=WORK MATRIX
0030       C     EF=FRACTION OF EIGENVALUE SUM TO BE USED IN FACTOR REPRESENTATION
0031                  DIMENSION CONTRL(4),DATA(NVAR,NLOC),AVG(1),SIG(1),Z(NVAR,NLOC)
0032                  DIMENSION C(1),E(1),V(N,N),F(NSEC,N),VSTAR(N,N),FSTAR(NSEC,N)
0033                  DIMENSION TV(51),H(1),FF(1),B(1),D(1),INDEX(1),R(1)
0034                  M=N*(N+1)/2
0035                  MODE=CONTRL(1)
0036                  MTYPE=CONTRL(2)
0037                  ISIDE=CONTRL(3)
0038                  EF=CONTRL(4)
0039                  CALL CO(CONTRL,NVAR,NLOC,N,DATA,AVG,SIG,Z,C)
0040                  CALL WRICO(CONTRL,NVAR,NLOC,N,DATA,AVG,SIG,Z,C,INDEX)
```

ORIGINAL PAGE IS
OF POOR QUALITY

```
0041              DO 1 I=1,M
0042              D(I)=C(I)
0043          1   CONTINUE
0044              CALL EIGEN(D,V,N,0)
0045              KK=0
0046              DO 2 J=1,N
0047              DO 3 I=1,N
0048              IF (I.GT.J) GO TO 3
0049              KK=KK+1
0050              IF (I.EQ.J) E(I)=D(KK)
0051          3   CONTINUE
0052          2   CONTINUE
0053              DO 60 L=1,N
0054              IF (E(L).LT.0.0) WRITE (108,61) E(L)
0055         61   FORMAT (1X,25HWARNING- NEG. EIGENVALUE(,F12.5,33H) MADE POSITIVE S
0056             1  O SQ. RT. EXISTS)
0057              E(L)=ABS(E(L))
0058         60   CONTINUE
0059              NEV=0
0060              S=0.0
0061              FN=N
0062              EP=EF*FN
0063              DO 5 K=1,N
0064              IF (S.GT.EP) GO TO 5
0065              S=S+E(K)
0066              NEV=NEV+1
0067          5   CONTINUE
0068              IF (MTYPE.EQ.1) P=NSEC
0069              IF (MTYPE.EQ.2) P=1.0
0070              IF (MODE.EQ.2) GO TO 6
0071              DO 7 I=1,NEV
0072              DO 8 J=1,NLOC
0073              S=0.0
0074              DO 9 K=1,NVAR
0075              S=S+V(K,I)*Z(K,J)
0076          9   CONTINUE
0077              F(J,I)=S/SQRT(E(I))
0078          8   CONTINUE
0079          7   CONTINUE
0080              GO TO 10
0081          6   DO 11 I=1,NVAR
0082              DO 12 J=1,NEV
```

```
0083                S=0.0
0084                DO 13 K=1,NLOC
0085                S=S+Z(I,K)*V(K,J)
0086          13    CONTINUE
0087                F(I,J)=S/SQRT(E(J))
0088          12    CONTINUE
0089          11    CONTINUE
0090          10    CONTINUE
0091                CALL WREIG(V,E,F,N,NSEC,NEV,INDEX)
0092                ERMS=0.0
0093                EMAX=0.0
0094                DO 14 I=1,NVAR
0095                DO 15 J=1,NLOC
0096                S=0.0
0097                DO 17 K=1,NEV
0098                IF (MODE.EQ.1) S=S+V(I,K)*SQRT(E(K))*F(J,K)
0099                IF (MODE.EQ.2) S=S+F(I,K)*SQRT(E(K))*V(J,K)
0100          17    CONTINUE
0101                Z(I,J)=Z(I,J)-S
0102                ERMS=ERMS+Z(I,J)**2
0103                IF (ABS(Z(I,J)).GT.EMAX) EMAX=ABS(Z(I,J))
0104          15    CONTINUE
0105          14    CONTINUE
0106                CALL WRERR(ERMS,EMAX,Z,NVAR,NLOC,INDEX)
0107                IF (MODE.EQ.2) GO TO 18
0108                IF (ISIDE.EQ.2) GO TO 19
0109                DO 20 J=1,NEV
0110                DO 21 I=1,NLOC
0111                FSTAR(I,J)=F(I,J)*SQRT(E(J))
0112          21    CONTINUE
0113          20    CONTINUE
0114                CALL VARMX(NLOC,NEV,FSTAR,NC,TV,H,FF,B,IER)
0115                DO 22 I=1,NEV
0116                DO 23 J=1,NEV
0117                MM=NEV*(J-1)+I
0118                S=0.0
0119                DO 24 K=1,NLOC
0120                S=S+FSTAR(K,J)*F(K,I)
0121          24    CONTINUE
0122                R(MM)=S/(SQRT(E(I))*P)
0123          23    CONTINUE
0124          22    CONTINUE
```

ORIGINAL PAGE IS
OF POOR QUALITY

```
0125              CALL WRTRA(NEV,R,INDEX)
0126              DO 25 I=1,NVAR
0127              DO 26 J=1,NEV
0128              S=0.0
0129              DO 27 K=1,NEV
0130              MM=NEV*(J-1)+K
0131              S=S+V(I,K)*R(MM)
0132        27    CONTINUE
0133              VSTAR(I,J)=S
0134        26    CONTINUE
0135        25    CONTINUE
0136              GO TO 28
0137        19    CONTINUE
0138              DO 29 J=1,NEV
0139              DO 30 I=1,NVAR
0140              VSTAR(I,J)=V(I,J)*SQRT(E(J))
0141        30    CONTINUE
0142        29    CONTINUE
0143              CALL VARMX(NVAR,NEV,VSTAR,NC,TV,H,FF,B,IER)
0144              DO 31 I=1,NEV
0145              DO 32 J=1,NEV
0146              MM=NEV*(J-1)+I
0147              S=0.0
0148              DO 33 K=1,NVAR
0149              S=S+V(K,I)*VSTAR(K,J)
0150        33    CONTINUE
0151              R(MM)=S/SQRT(E(I))
0152        32    CONTINUE
0153        31    CONTINUE
0154              CALL WRTRA(NEV,R,INDEX)
0155              DO 34 I=1,NLOC
0156              DO 35 J=1,NEV
0157              S=0.0
0158              DO 36 K=1,NEV
0159              MM=NEV*(J-1)+K
0160              S=S+F(I,K)*R(MM)
0161        36    CONTINUE
0162              FSTAR(I,J)=S
0163        35    CONTINUE
0164        34    CONTINUE
0165              GO TO 28
0166        18    CONTINUE
```

```
0167              IF (ISIDE.EQ.2) GO TO 37
0168              DO 38 J=1,NEV
0169              DO 39 I=1,NLOC
0170              VSTAR(I,J)=V(I,J)*SQRT(E(J))
0171        39    CONTINUE
0172        38    CONTINUE
0173              CALL VARMX(NLOC,NEV,VSTAR,NC,TV,H,FF,B,IER)
0174              DO 40 I=1,NEV
0175              DO 41 J=1,NEV
0176              MM=NEV*(J-1)+I
0177              S=0.0
0178              DO 42 K=1,NLOC
0179              S=S+V(K,I)*VSTAR(K,J)
0180        42    CONTINUE
0181              R(MM)=S/SQRT(E(I))
0182        41    CONTINUE
0183        40    CONTINUE
0184              CALL WRTRA(NEV,R,INDEX)
0185              DO 43 I=1,NVAR
0186              DO 44 J=1,NEV
0187              S=0.0
0188              DO 45 K=1,NEV
0189              MM=NEV*(J-1)+K
0190              S=S+F(I,K)*R(MM)
0191        45    CONTINUE
0192              FSTAR(I,J)=S
0193        44    CONTINUE
0194        43    CONTINUE
0195              GO TO 28
0196        37    CONTINUE
0197              DO 46 J=1,NEV
0198              DO 47 I=1,NVAR
0199              FSTAR(I,J)=F(I,J)*SQRT(E(J))
0200        47    CONTINUE
0201        46    CONTINUE
0202              CALL VARMX(NVAR,NEV,FSTAR,NC,TV,H,FF,B,IER)
0203              DO 48 I=1,NEV
0204              DO 49 J=1,NEV
0205              MM=NEV*(J-1)+I
0206              S=0.0
0207              DO 50 K=1,NVAR
0208              S=S+F(K,I)*FSTAR(K,J)
```

ORIGINAL PAGE IS
OF POOR QUALITY

```
0209        50      CONTINUE
0210                R(MM)=S/(SQRT(E(I))*P)
0211        49      CONTINUE
0212        48      CONTINUE
0213                CALL WRTRA(NEV,R,INDEX)
0214                DO 51 I=1,NLOC
0215                DO 52 J=1,NEV
0216                S=0.0
0217                DO 53 K=1,NEV
0218                MM=NEV*(J-1)+K
0219                S=S+V(I,K)*R(MM)
0220        53      CONTINUE
0221                VSTAR(I,J)=S
0222        52      CONTINUE
0223        51      CONTINUE
0224        28      CONTINUE
0225                CALL WRSTR(VSTAR,FSTAR,N,NSEC,NEV,INDEX)
0226                RETURN
0227                END
```

```
0001            SUBROUTINE WRICO(CONTRL,NVAR,NLOC,N,DATA,AVG,SIG,Z,C,INDEX)
0002       1    FORMAT (18H OUTPUT OF SUBR CO)
0003       2    FORMAT (8H MODE = ,I2,10X,9H MTYPE = ,I2,8H NVAR = ,I5,8H NLOC = ,
0004           1 I5,9H ISIDE = ,I5,6H EF = ,F10.5)
0005       3    FORMAT (1X,12H DATA MATRIX)
0006       4    FORMAT (1X)
0007       5    FORMAT (1X, 19H NORMED DATA MATRIX)
0008       6    FORMAT (6X,20H       VECTOR LENGTH)
0009       7    FORMAT (1X,I5,F20.5)
0010       8    FORMAT (6X,42H                    MEAN    STANDARD DEVIATION)
0011       9    FORMAT (1X,I5,2F20.5)
0012      10    FORMAT (1X,19H CORRELATION MATRIX)
0013      11    FORMAT (1X,14H COSINE MATRIX)
0014      12    FORMAT (1H1)
0015            DIMENSION DATA(NVAR,NLOC),Z(NVAR,NLOC),C(1),SIG(1),AVG(1),INDEX(1)
0016            DIMENSION CONTRL(1)
0017            MODE=CONTRL(1)
0018            MTYPE=CONTRL(2)
0019            ISIDE=CONTRL(3)
0020            EF=CONTRL(4)
0021            WRITE (108,12)
0022            WRITE (108,1)
0023            WRITE (108,2) MODE,MTYPE,NVAR,NLOC,ISIDE,EF
0024            WRITE (108,3)
0025            CALL WRMAT(DATA,NVAR,NLOC,INDEX)
0026            WRITE (108,4)
0027            IF (MODE.EQ.2) GO TO 100
0028            WRITE (108,8)
0029            DO 101 I=1,NVAR
0030            WRITE (108,9) I,AVG(I),SIG(I)
0031     101    CONTINUE
0032            GO TO 103
0033     100    WRITE (108,6)
0034            DO 102 I=1,NLOC
0035            WRITE (108,7) I,SIG(I)
0036     102    CONTINUE
0037     103    CONTINUE
0038            WRITE (108,4)
0039            WRITE (108,5)
```

ORIGINAL PAGE IS
OF POOR QUALITY

```
0040              CALL WRMAT(Z,NVAR,NLOC,INDEX)
0041              WRITE (108,4)
0042              IF (MTYPE.EQ.1) WRITE (108,10)
0043              IF (MTYPE.EQ.2) WRITE (108,11)
0044              CALL WRTRI(C,N,INDEX)
0045              RETURN
0046              END
```

ORIGINAL PAGE IS
OF POOR QUALITY

```
0001            SUBROUTINE WREIG(V,E,F,N,NSEC,NEV,INDEX)
0002          1 FORMAT (1H1)
0003          2 FORMAT (1X,30H INDEX EIGENVALUES CUM. SUM EV)
0004          3 FORMAT (1X,I6,2F12.5)
0005          4 FORMAT (1X)
0006          5 FORMAT (1X,23H EIGENVECTORS (COLUMNS))
0007          6 FORMAT (1X,18H FACTORS (COLUMNS))
0008          7 FORMAT (1X,7HE-VALUE,5(I3,F10.5))
0009          8 FORMAT (1X,3I10)
0010          9 FORMAT (1X,8HE-VECTOR,5(I3,F10.5))
0011         10 FORMAT (1X,6HFACTOR,5(I3,F10.5))
0012            DIMENSION V(N,N),E(1),F(NSEC,N),INDEX(1)
0013            WRITE (108,1)
0014            WRITE (108,2)
0015            S=0.0
0016            DO 50 I=1,N
0017            S=S+E(I)
0018            WRITE (108,3) I,E(I),S
0019         50 CONTINUE
0020            WRITE (108,4)
0021            WRITE (108,5)
0022            CALL WRMAT(V,N,NEV,INDEX)
0023            WRITE (108,1)
0024            WRITE (108,6)
0025            CALL WRMAT(F,NSEC,NEV,INDEX)
0026            WRITE (106,8) N,NSEC,NEV
0027            WRITE (106,7) ((I,E(I)),I=1,NEV)
0028            WRITE (106,9) (((J,V(I,J)),I=1,N),J=1,NEV)
0029            WRITE (106,10) (((J,F(I,J)),I=1,NSEC),J=1,NEV)
0030            RETURN
0031            END
```

```
0001              SUBROUTINE WRSTR(VSTAR,FSTAR,N,NSEC,NEV,INDEX)
0002     C      VSTAR=N X NEV MATRIX OF VARIMAX ROTATED EIGENVECTORS
0003     C      FSTAR=NSEC X NEV MATRIX OF VARIMAX ADJUSTED FACTORS
0004     C      N=NUMBER OF COMPONENTS IN EIGENVECTORS
0005     C      NSEC=OTHER DIMENSION FROM N (THAT IS, NSEC=NVAR IF N=NLOC AND
0006     C      NSEC=NLOC IF N=NVAR)
0007     C      NEV=NUMBER OF EIGENVALUES AND EIGENVECTORS USED
0008     C      INDEX=WORK VECTOR OF MAX COMPONENTS, MAX=MAX(NVAR,NLOC)
0009           1      FORMAT (1H1)
0010           3      FORMAT (1X,13H VSTAR MATRIX)
0011           4      FORMAT (1X,13H FSTAR MATRIX)
0012                  DIMENSION VSTAR(N,N),FSTAR(NSEC,N),INDEX(1)
0013                  WRITE (108,1)
0014                  WRITE (108,3)
0015                  CALL WRMAT(VSTAR,N,NEV,INDEX)
0016                  WRITE (108,1)
0017                  WRITE (108,4)
0018                  CALL WRMAT(FSTAR,NSEC,NEV,INDEX)
0019                  RETURN
0020                  END
```

```
0001                SUBROUTINE WRERR(ERMS,EMAX,Z,NVAR,NLOC,INDEX)
0002          1     FORMAT (1H1)
0003          2     FORMAT (1X,6H ERMS=,F20.5,6H EMAX=,F20.5)
0004          3     FORMAT (1X)
0005          4     FORMAT (1X,24H ERROR OF REPRESENTATION)
0006                DIMENSION Z(NVAR,NLOC),INDEX(1)
0007                WRITE (108,1)
0008                WRITE (108,2) ERMS,EMAX
0009                WRITE (108,3)
0010                WRITE (108,4)
0011                CALL WRMAT(Z,NVAR,NLOC,INDEX)
0012                RETURN
0013                END
```

```
0001                SUBROUTINE WRMAT(A,N,M,INDEX)
0002      C       PRINT A NXM MATRIX WITH COLUMN AND ROW NUMBERING. A=MATRIX
0003      C       INDEX= M-DIMENSIONAL WORK VECTOR
0004                DIMENSION A(N,M),INDEX(M)
0005            1   FORMAT (1X,I13,9I12)
0006            2   FORMAT (1X,I5,10F12.5)
0007            9   FORMAT (1X)
0008                MR=M+10
0009                ICB=-9
0010                DO 3 K=1,M
0011                INDEX(K)=K
0012            3   CONTINUE
0013            4   MR=MR-10
0014                ICB=ICB+10
0015                IF (MR-10) 5,5,6
0016            5   ICE=ICB+MR-1
0017                GO TO 7
0018            6   ICE=ICB+9
0019            7   WRITE (108,9)
0020                WRITE (108,1) (INDEX(K),K=ICB,ICE)
0021                DO 8 IR=1,N
0022                WRITE (108,2) IR,(A(IR,IC),IC=ICB,ICE)
0023            8   CONTINUE
0024                IF (MR.GT.10) GO TO 4
0025                RETURN
0026                END
```

```
0001                SUBROUTINE WRTRI(A,N,INDEX)
0002      C     A=TRIANGULAR MATRIX WRITTEN IN VECTOR SEQUENCE, A(1)=(1,1) ELEMENT
0003      C     A(2)=(2,1) ELEMENT, A(3)=(2,2) ELEMENT, A(4)=(3,1) ELEMENT, ETC.
0004      C     N=ORDER OF MATRIX
0005      C     M=N*(N+1)/2
0006          20      FORMAT (1X,I13,9I12)
0007          21      FORMAT (1X,I5,10F12.5)
0008          22      FORMAT (1X)
0009                  DIMENSION A(1),INDEX(1)
0010                  NC=0
0011                  MR=N+10
0012                  ICB=-9
0013                  DO 1 K=1,N
0014                  INDEX(K)=K
0015           1      CONTINUE
0016           6      CONTINUE
0017                  NC=NC+1
0018                  MR=MR-10
0019                  ICB=ICB+10
0020                  IF (MR-10) 2,2,3
0021           2      ICE=ICB+MR-1
0022                  GO TO 4
0023           3      ICE=ICB+9
0024           4      WRITE (108,22)
0025                  WRITE (108,20) (INDEX(K),K=ICB,ICE)
0026                  L=0
0027                  DO 5 IR=ICB,N
0028                  L=L+1
0029                  KRB=1+(IR-1)*IR/2+(NC-1)*10
0030                  IF (L.LE.10) KRE=KRB+L-1
0031                  IF (L.GT.10) KRE=KRB+9
0032                  WRITE (108,21) IR,(A(K),K=KRB,KRE)
0033           5      CONTINUE
0034                  IF (MR.GT.10) GO TO 6
0035                  RETURN
0036                  END
```

```
0001            SUBROUTINE WRTRA(NEV,R,INDEX)
0002            DIMENSION R(NEV,NEV),INDEX(1)
0003       1    FORMAT (1H1,23H VARIMAX TRANSFORMATION)
0004            WRITE (108,1)
0005            CALL WRMAT(R,NEV,NEV,INDEX)
0006            RETURN
0007            END
```

```
0001              SUBROUTINE CO(CONTRL,NVAR,NLOC,N,DATA,AVG,SIG,Z,C)
0002      C      N=NVAR IF MODE=1, N=NLOC IF MODE=2
0003      C      M=N*(N+1)/2= NUMBER OF ELEMENTS IN UPPER TRIANGULAR PART OF R
0004      C      MODE=1 FOR R-MODE ANALYSIS, MODE=2 FOR Q-MODE ANALYSIS
0005      C      DATA=NVAR X NLOC DATA MATRIX. COLUMNS ARE LOCATIONS, ROWS ARE
0006      C      VARIABLES.
0007      C      R=NXN CORRELATION MATRIX IF MTYPE=1
0008      C      R=NXN COSINE MATRIX IF MTYPE=2
0009      C      R IS STORED AS A VECTOR. THE UPPER TRIANGULAR PART IS STORED IN
0010      C      COLUMN ORDER.
0011                   DIMENSION CONTRL(4),DATA(NVAR,NLOC),AVG(1),SIG(1),Z(NVAR,NLOC)
0012                   DIMENSION C(1)
0013                   MODE=CONTRL(1)
0014                   MTYPE=CONTRL(2)
0015                   IF (MODE.EQ.2) GO TO 1
0016                   DO 2 I=1,NVAR
0017                   AVG(I)=0.0
0018              2    CONTINUE
0019                   IF (MTYPE.EQ.2) GO TO 14
0020                   DO 3 J=1,NLOC
0021                   DO 4 I=1,NVAR
0022                   AVG(I)=AVG(I)+DATA(I,J)
0023              4    CONTINUE
0024              3    CONTINUE
0025                   FNLOC=NLOC
0026                   DO 5 I=1,NVAR
0027                   AVG(I)=AVG(I)/FNLOC
0028              5    CONTINUE
0029                   DO 6 J=1,NLOC
0030                   DO 7 I=1,NVAR
0031                   Z(I,J)=DATA(I,J)-AVG(I)
0032              7    CONTINUE
0033              6    CONTINUE
0034                   GO TO 17
0035              1    CONTINUE
0036                   DO 8 J=1,NLOC
0037                   AVG(J)=0.0
0038              8    CONTINUE
0039                   IF (MTYPE.EQ.2) GO TO 14
0040                   DO 9 I=1,NVAR
0041                   DO 10 J=1,NLOC
```

```
0042                AVG(J)=AVG(J)+DATA(I,J)
0043          10    CONTINUE
0044           9    CONTINUE
0045                FNVAR=NVAR
0046                DO 11 J=1,NLOC
0047                AVG(J)=AVG(J)/FNVAR
0048          11    CONTINUE
0049                DO 12 I=1,NVAR
0050                DO 13 J=1,NLOC
0051                Z(I,J)=DATA(I,J)-AVG(J)
0052          13    CONTINUE
0053          12    CONTINUE
0054                GO TO 17
0055          14    DO 15 I=1,NVAR
0056                DO 16 J=1,NLOC
0057                Z(I,J)=DATA(I,J)
0058          16    CONTINUE
0059          15    CONTINUE
0060          17    IF (MODE.EQ.2) GO TO 18
0061                DO 19 I=1,NVAR
0062                SIG(I)=0.0
0063          19    CONTINUE
0064                DO 20 J=1,NLOC
0065                DO 21 I=1,NVAR
0066                SIG(I)=SIG(I)+Z(I,J)**2
0067          21    CONTINUE
0068          20    CONTINUE
0069                DO 22 I=1,NVAR
0070                IF (MTYPE.EQ.1) SIG(I)=SIG(I)/FNLOC
0071                SIG(I)=SQRT(SIG(I))
0072          22    CONTINUE
0073                DO 23 J=1,NLOC
0074                DO 24 I=1,NVAR
0075                Z(I,J)=Z(I,J)/SIG(I)
0076          24    CONTINUE
0077          23    CONTINUE
0078                GO TO 25
0079          18    DO 26 J=1,NLOC
0080                SIG(J)=0.0
```

```
0081        26      CONTINUE
0082                DO 27 I=1,NVAR
0083                DO 28 J=1,NLOC
0084                SIG(J)=SIG(J)+Z(I,J)**2
0085        28      CONTINUE
0086        27      CONTINUE
0087                FNVAR=NVAR
0088                DO 29 J=1,NLOC
0089                IF (MTYPE.EQ.1) SIG(J)=SIG(J)/FNVAR
0090                SIG(J)=SQRT(SIG(J))
0091        29      CONTINUE
0092                DO 30 I=1,NVAR
0093                DO 31 J=1,NLOC
0094                Z(I,J)=Z(I,J)/SIG(J)
0095        31      CONTINUE
0096        30      CONTINUE
0097        25      CONTINUE
0098                IF (MODE.EQ.2) GO TO 32
0099                KK=0
0100                DO 33 I=1,N
0101                DO 34 J=1,I
0102                KK=KK+1
0103                S=0.0
0104                DO 35 JJ=1,NLOC
0105                S=S+Z(I,JJ)*Z(J,JJ)
0106        35      CONTINUE
0107                IF (MTYPE.EQ.1) S=S/FNLOC
0108                C(KK)=S
0109        34      CONTINUE
0110        33      CONTINUE
0111                GO TO 39
0112        32      CONTINUE
0113                KK=0
0114                DO 36 I=1,N
0115                DO 37 J=1,I
0116                KK=KK+1
0117                S=0.0
0118                DO 38 II=1,NVAR
0119                S=S+Z(II,I)*Z(II,J)
0120        38      CONTINUE
0121                IF (MTYPE.EQ.1) S=S/FNVAR
0122                C(KK)=S
```

ORIGINAL PAGE IS
OF POOR QUALITY


```
0123          37      CONTINUE
0124          36      CONTINUE
0125          39      CONTINUE
0126                  RETURN
0127                  END
```

```
0001    C                                                                       EIGE  10
0002    C     ...................................................               EIGE  20
0003    C                                                                       EIGE  30
0004    C        SUBROUTINE EIGEN                                               EIGE  40
0005    C                                                                       EIGE  50
0006    C        PURPOSE                                                        EIGE  60
0007    C           COMPUTE EIGENVALUES AND EIGENVECTORS OF A REAL SYMMETRIC     EIGE  70
0008    C           MATRIX                                                      EIGE  80
0009    C                                                                       EIGE  90
0010    C        USAGE                                                          EIGE 100
0011    C           CALL EIGEN(A,R,N,MV)                                        EIGE 110
0012    C                                                                       EIGE 120
0013    C        DESCRIPTION OF PARAMETERS                                      EIGE 130
0014    C           A - ORIGINAL MATRIX (SYMMETRIC), DESTROYED IN COMPUTATION.  EIGE 140
0015    C               RESULTANT EIGENVALUES ARE DEVELOPED IN DIAGONAL OF      EIGE 150
0016    C               MATRIX A IN DESCENDING ORDER.                           EIGE 160
0017    C           R - RESULTANT MATRIX OF EIGENVECTORS (STORED COLUMNWISE,     EIGE 170
0018    C               IN SAME SEQUENCE AS EIGENVALUES)                        EIGE 180
0019    C           N - ORDER OF MATRICES A AND R                               EIGE 190
0020    C           MV- INPUT CODE                                              EIGE 200
0021    C                  0   COMPUTE EIGENVALUES AND EIGENVECTORS             EIGE 210
0022    C                  1   COMPUTE EIGENVALUES ONLY (R NEED NOT BE          EIGE 220
0023    C                      DIMENSIONED BUT MUST STILL APPEAR IN CALLING     EIGE 230
0024    C                      SEQUENCE)                                        EIGE 240
0025    C                                                                       EIGE 250
0026    C        REMARKS                                                        EIGE 260
0027    C           ORIGINAL MATRIX A MUST BE REAL SYMMETRIC (STORAGE MODE=1)   EIGE 270
0028    C           MATRIX A CANNOT BE IN THE SAME LOCATION AS MATRIX R         EIGE 280
0029    C                                                                       EIGE 290
0030    C        SUBROUTINES AND FUNCTION SUBPROGRAMS REQUIRED                  EIGE 300
0031    C           NONE                                                        EIGE 310
0032    C                                                                       EIGE 320
0033    C        METHOD                                                         EIGE 330
0034    C           DIAGONALIZATION METHOD ORIGINATED BY JACOBI AND ADAPTED     EIGE 340
0035    C           BY VON NEUMANN FOR LARGE COMPUTERS AS FOUND IN 'MATHEMATICAL EIGE 350
0036    C           METHODS FOR DIGITAL COMPUTERS', EDITED BY A. RALSTON AND    EIGE 360
0037    C           H.S. WILF, JOHN WILEY AND SONS, NEW YORK, 1962, CHAPTER 7   EIGE 370
0038    C                                                                       EIGE 380
0039    C     ...................................................               EIGE 390
0040    C                                                                       EIGE 400
0041            SUBROUTINE EIGEN(A,R,N,MV)                                      EIGE 410
```

```
0042            DIMENSION A(1),R(1)                                     EIGE 420
0043      C                                                             EIGE 430
0044      C     ...........................................................EIGE 440
0045      C                                                             EIGE 450
0046      C     IF A DOUBLE PRECISION VERSION OF THIS ROUTINE IS DESIRED, THE EIGE 460
0047      C     C IN COLUMN 1 SHOULD BE REMOVED FROM THE DOUBLE PRECISION EIGE 470
0048      C     STATEMENT WHICH FOLLOWS.                                EIGE 480
0049      C                                                             EIGE 490
0050      C      DOUBLE PRECISION A,R,ANORM,ANRMX,THR,X,Y,SINX,SINX2,COSX, EIGE 500
0051      C     1                 COSX2,SINCS,RANGE                     EIGE 510
0052      C                                                             EIGE 520
0053      C     THE C MUST ALSO BE REMOVED FROM DOUBLE PRECISION STATEMENTS EIGE 530
0054      C     APPEARING IN OTHER ROUTINES USED IN CONJUNCTION WITH THIS EIGE 540
0055      C     ROUTINE.                                                EIGE 550
0056      C                                                             EIGE 560
0057      C     THE DOUBLE PRECISION VERSION OF THIS SUBROUTINE MUST ALSO EIGE 570
0058      C     CONTAIN DOUBLE PRECISION FORTRAN FUNCTIONS.  SQRT IN STATEMENTS EIGE 580
0059      C     40, 68, 75, AND 78 MUST BE CHANGED TO DSQRT.  ABS IN STATEMENT EIGE 590
0060      C     62 MUST BE CHANGED TO DABS. THE CONSTANT IN STATEMENT 5 SHOULD EIGE 600
0061      C     BE CHANGED TO 1.0D-12.                                  EIGE 610
0062      C                                                             EIGE 620
0063      C     ...........................................................EIGE 630
0064      C                                                             EIGE 640
0065      C     GENERATE IDENTITY MATRIX                                EIGE 650
0066      C                                                             EIGE 660
0067            5 RANGE=1.0E-6                                          EIGE 670
0068              IF(MV-1) 10,25,10                                     EIGE 680
0069           10 IQ=-N                                                 EIGE 690
0070              DO 20 J=1,N                                           EIGE 700
0071              IQ=IQ+N                                               EIGE 710
0072              DO 20 I=1,N                                           EIGE 720
0073              IJ=IQ+I                                               EIGE 730
0074              R(IJ)=0.0                                             EIGE 740
0075              IF(I-J) 20,15,20                                      EIGE 750
0076           15 R(IJ)=1.0                                             EIGE 760
0077           20 CONTINUE                                              EIGE 770
0078      C                                                             EIGE 780
0079      C     COMPUTE INITIAL AND FINAL NORMS (ANORM AND ANORMX)      EIGE 790
0080      C                                                             EIGE 800
0081           25 ANORM=0.0                                             EIGE 810
0082              DO 35 I=1,N                                           EIGE 820
0083              DO 35 J=I,N                                           EIGE 830
```

```
0084                IF(I-J) 30,35,30                                          EIGE 840
0085          30    IA=I+(J*J-J)/2                                            EIGE 850
0086                ANORM=ANORM+A(IA)*A(IA)                                   EIGE 860
0087          35    CONTINUE                                                  EIGE 870
0088                IF(ANORM) 165,165,40                                      EIGE 880
0089          40    ANORM=1.414*SQRT(ANORM)                                   EIGE 890
0090                ANRMX=ANORM*RANGE/FLOAT(N)                                EIGE 900
0091    C                                                                     EIGE 910
0092    C           INITIALIZE INDICATORS AND COMPUTE THRESHOLD, THR          EIGE 920
0093    C                                                                     EIGE 930
0094                IND=0                                                     EIGE 940
0095                THR=ANORM                                                 EIGE 950
0096          45    THR=THR/FLOAT(N)                                          EIGE 960
0097          50    L=1                                                       EIGE 970
0098          55    M=L+1                                                     EIGE 980
0099    C                                                                     EIGE 990
0100    C           COMPUTE SIN AND COS                                       EIGE1000
0101    C                                                                     EIGE1010
0102          60    MQ=(M*M-M)/2                                              EIGE1020
0103                LQ=(L*L-L)/2                                              EIGE1030
0104                LM=L+MQ                                                   EIGE1040
0105          62    IF( ABS(A(LM))-THR) 130,65,65                             EIGE1050
0106          65    IND=1                                                     EIGE1060
0107                LL=L+LQ                                                   EIGE1070
0108                MM=M+MQ                                                   EIGE1080
0109                X=0.5*(A(LL)-A(MM))                                       EIGE1090
0110          68    Y=-A(LM)/ SQRT(A(LM)*A(LM)+X*X)                           EIGE1100
0111                IF(X) 70,75,75                                            EIGE1110
0112          70    Y=-Y                                                      EIGE1120
0113          75    SINX=Y/ SQRT(2.0*(1.0+( SQRT(1.0-Y*Y))))                  EIGE1130
0114                SINX2=SINX*SINX                                           EIGE1140
0115          78    COSX= SQRT(1.0-SINX2)                                     EIGE1150
0116                COSX2=COSX*COSX                                           EIGE1160
0117                SINCS =SINX*COSX                                          EIGE1170
0118    C                                                                     EIGE1180
0119    C           ROTATE L AND M COLUMNS                                    EIGE1190
0120    C                                                                     EIGE1200
0121                ILQ=N*(L-1)                                               EIGE1210
0122                IMQ=N*(M-1)                                               EIGE1220
0123                DO 125 I=1,N                                              EIGE1230
0124                IQ=(I*I-I)/2                                              EIGE1240
0125                IF(I-L) 80,115,80                                         EIGE1250
```

```
0126        80      IF(I-M) 85,115,90                                          EIGE1260
0127        85      IM=I+MQ                                                    EIGE1270
0128                GO TO 95                                                   EIGE1280
0129        90      IM=M+IQ                                                    EIGE1290
0130        95      IF(I-L) 100,105,105                                        EIGE1300
0131       100      IL=I+LQ                                                    EIGE1310
0132                GO TO 110                                                  EIGE1320
0133       105      IL=L+IQ                                                    EIGE1330
0134       110      X=A(IL)*COSX-A(IM)*SINX                                    EIGE1340
0135                A(IM)=A(IL)*SINX+A(IM)*COSX                                EIGE1350
0136                A(IL)=X                                                    EIGE1360
0137       115      IF(MV-1) 120,125,120                                       EIGE1370
0138       120      ILR=ILQ+I                                                  EIGE1380
0139                IMR=IMQ+I                                                  EIGE1390
0140                X=R(ILR)*COSX-R(IMR)*SINX                                  EIGE1400
0141                R(IMR)=R(ILR)*SINX+R(IMR)*COSX                             EIGE1410
0142                R(ILR)=X                                                   EIGE1420
0143       125      CONTINUE                                                   EIGE1430
0144                X=2.0*A(LM)*SINCS                                          EIGE1440
0145                Y=A(LL)*COSX2+A(MM)*SINX2-X                                EIGE1450
0146                X=A(LL)*SINX2+A(MM)*COSX2+X                                EIGE1460
0147                A(LM)=(A(LL)-A(MM))*SINCS+A(LM)*(COSX2-SINX2)              EIGE1470
0148                A(LL)=Y                                                    EIGE1480
0149                A(MM)=X                                                    EIGE1490
0150    C                                                                      EIGE1500
0151    C           TESTS FOR COMPLETION                                       EIGE1510
0152    C                                                                      EIGE1520
0153    C           TEST FOR M = LAST COLUMN                                   EIGE1530
0154    C                                                                      EIGE1540
0155       130       IF(M-N) 135,140,135                                       EIGE1550
0156       135       M=M+1                                                     EIGE1560
0157                 GO TO 60                                                  EIGE1570
0158    C                                                                      EIGE1580
0159    C           TEST FOR L = SECOND FROM LAST COLUMN                       EIGE1590
0160    C                                                                      EIGE1600
0161       140       IF(L-(N-1)) 145,150,145                                   EIGE1610
0162       145       L=L+1                                                     EIGE1620
0163                 GO TO 55                                                  EIGE1630
0164       150       IF(IND-1) 160,155,160                                     EIGE1640
0165       155       IND=0                                                     EIGE1650
0166                 GO TO 50                                                  EIGE1660
0167    C                                                                      EIGE1670
```

```
0168     C          COMPARE THRESHOLD WITH FINAL NORM                    EIGE1660
0169     C                                                               EIGE1690
0170        160      IF(THR-ANRMX) 165,165,45                            EIGE1700
0171     C                                                               EIGE1710
0172     C          SORT EIGENVALUES AND EIGENVECTORS                    EIGE1720
0173     C                                                               EIGE1730
0174        165      IQ=-N                                               EIGE1740
0175                 DO 185 I=1,N                                        EIGE1750
0176                 IQ=IQ+N                                             EIGE1760
0177                 LL=I+(I*I-I)/2                                      EIGE1770
0178                 JQ=N*(I-2)                                          EIGE1780
0179                 DO 185 J=I,N                                        EIGE1790
0180                 JQ=JQ+N                                             EIGE1800
0181                 MM=J+(J*J-J)/2                                      EIGE1810
0182                 IF(A(LL)-A(MM)) 170,185,185                         EIGE1820
0183        170      X=A(LL)                                             EIGE1830
0184                 A(LL)=A(MM)                                         EIGE1840
0185                 A(MM)=X                                             EIGE1850
0186                 IF(MV-1) 175,185,175                                EIGE1860
0187        175      DO 180 K=1,N                                        EIGE1870
0188                 ILR=IQ+K                                            EIGE1880
0189                 IMR=JQ+K                                            EIGE1890
0190                 X=R(ILR)                                            EIGE1900
0191                 R(ILR)=R(IMR)                                       EIGE1910
0192        180      R(IMR)=X                                            EIGE1920
0193        185      CONTINUE                                            EIGE1930
0194                 RETURN                                              EIGE1940
0195                 END                                                 EIGE1950
```

```
0001    C                                                                       VARM  10
0002    C     ...................................................               VARM  20
0003    C                                                                       VARM  30
0004    C        SUBROUTINE VARMX                                               VARM  40
0005    C                                                                       VARM  50
0006    C        PURPOSE                                                        VARM  60
0007    C           PERFORM ORTHOGONAL ROTATIONS OF A FACTOR MATRIX.  THIS      VARM  70
0008    C           SUBROUTINE NORMALLY OCCURS IN A SEQUENCE OF CALLS TO SUB-   VARM  80
0009    C           ROUTINES CORRE, EIGEN, TRACE, LOAD, VARMX IN THE PERFORMANCE VARM  90
0010    C            OF A FACTOR ANALYSIS.                                      VARM 100
0011    C                                                                       VARM 110
0012    C        USAGE                                                          VARM 120
0013    C           CALL VARMX (M,K,A,NC,TV,H,F,D,IER)                          VARM 130
0014    C                                                                       VARM 140
0015    C        DESCRIPTION OF PARAMETERS                                      VARM 150
0016    C           M      - NUMBER OF VARIABLES AND NUMBER OF ROWS OF MATRIX A. VARM 160
0017    C           K      - NUMBER OF FACTORS.                                VARM 170
0018    C           A      - INPUT IS THE ORIGINAL FACTOR MATRIX, AND OUTPUT IS VARM 180
0019    C                    THE ROTATED FACTOR MATRIX.  THE ORDER OF MATRIX A  VARM 190
0020    C                    IS M X K.                                          VARM 200
0021    C           NC     - OUTPUT VARIABLE CONTAINING THE NUMBER OF ITERATION VARM 210
0022    C                    CYCLES PERFORMED.                                  VARM 220
0023    C           TV     - OUTPUT VECTOR CONTAINING THE VARIANCE OF THE FACTOR VARM 230
0024    C                    MATRIX FOR EACH ITERATION CYCLE.  THE VARIANCE PRIOR VARM 240
0025    C                    TO THE FIRST ITERATION CYCLE IS ALSO CALCULATED.   VARM 250
0026    C                    THIS MEANS THAT NC+1 VARIANCES ARE STORED IN VECTOR VARM 260
0027    C                    TV.  MAXIMUM NUMBER OF ITERATION CYCLES ALLOWED IN VARM 270
0028    C                    THIS SUBROUTINE IS 50.  THEREFORE, THE LENGTH OF   VARM 280
0029    C                    VECTOR TV IS 51.                                   VARM 290
0030    C           H      - OUTPUT VECTOR OF LENGTH M CONTAINING THE ORIGINAL  VARM 300
0031    C                    COMMUNALITIES.                                     VARM 310
0032    C           F      - OUTPUT VECTOR OF LENGTH M CONTAINING THE FINAL     VARM 320
0033    C                    COMMUNALITIES.                                     VARM 330
0034    C           D      - OUTPUT VECTOR OF LENGTH M CONTAINING THE DIFFERENCES VARM 340
0035    C                    BETWEEN THE ORIGINAL AND FINAL COMMUNALITIES.      VARM 350
0036    C           IER    - ERROR INDICATOR                                    VARM 351
0037    C                    IER=0 - NO ERROR                                   VARM 352
0038    C                    IER=1 - CONVERGENCE WAS NOT ACHIEVED IN 50 CYCLES  VARM 353
0039    C                            OF ROTATION                                VARM 354
```

```
0040     C                                                                      VARM 360
0041     C       REMARKS                                                        VARM 370
0042     C          IF VARIANCE COMPUTED AFTER EACH ITERATION CYCLE DOES NOT     VARM 380
0043     C          INCREASE FOR FOUR SUCCESSIVE TIMES, THE SUBROUTINE STOPS     VARM 390
0044     C          ROTATION.                                                    VARM 400
0045     C                                                                       VARM 410
0046     C       SUBROUTINES AND FUNCTION SUBPROGRAMS REQUIRED                  VARM 420
0047     C          NONE                                                         VARM 430
0048     C                                                                       VARM 440
0049     C       METHOD                                                         VARM 450
0050     C          KAISER'S VARIMAX ROTATION AS DESCRIBED IN 'COMPUTER PROGRAM  VARM 460
0051     C          FOR VARIMAX ROTATION IN FACTOR ANALYSIS' BY THE SAME AUTHOR, VARM 470
0052     C          EDUCATIONAL AND PSYCHOLOGICAL MEASUREMENT, VOL XIX, NO. 3,   VARM 480
0053     C          1959.                                                        VARM 490
0054     C                                                                       VARM 500
0055     C     ..................................................................VARM 510
0056     C                                                                       VARM 520
0057           SUBROUTINE VARMX (M,K,A,NC,TV,H,F,D,IER)                         VARM 530
0058           DIMENSION A(1),TV(1),H(1),F(1),D(1)                              VARM 540
0059     C                                                                      VARM 550
0060     C     ..................................................................VARM 560
0061     C                                                                      VARM 570
0062     C     IF A DOUBLE PRECISION VERSION OF THIS ROUTINE IS DESIRED, THE    VARM 580
0063     C     C IN COLUMN 1 SHOULD BE REMOVED FROM THE DOUBLE PRECISION        VARM 590
0064     C                                                                      VARM 600
0065     C     DOUBLE PRECISION A,TV,H,F,D,TVLT,CONS,AA,BB,CC,DD,U,T,B,COS4T,   VARM 610
0066     C    1                 SIN4T,TAN4T,SINP,COSP,CTN4T,COS2T,SIN2T,COST,SINTVARM 620
0067     C                                                                      VARM 630
0068     C     THE C MUST ALSO BE REMOVED FROM DOUBLE PRECISION STATEMENTS      VARM 640
0069     C     APPEARING IN OTHER ROUTINES USED IN CONJUNCTION WITH THIS        VARM 650
0070     C     ROUTINE.                                                         VARM 660
0071     C                                                                      VARM 670
0072     C     THE DOUBLE PRECISION VERSION OF THIS SUBROUTINE MUST ALSO        VARM 680
0073     C     CONTAIN DOUBLE PRECISION FORTRAN FUNCTIONS.  SQRT IN STATEMENTS  VARM 690
0074     C     115, 290, 330, 350, AND 355 MUST BE CHANGED TO DSQRT.  ABS IN    VARM 700
0075     C     STATEMENTS 280, 320, AND 375 MUST BE CHANGED TO DABS.            VARM 710
0076     C                                                                      VARM 720
0077     C     ..................................................................VARM 730
0078     C                                                                      VARM 740
0079     C     INITIALIZATION                                                   VARM 750
0080     C                                                                      VARM 760
0081           IER=0                                                            VARM 761
```

```
0082                FPS=0.00116                                          VARM 770
0083                TVLT=0.0                                             VARM 780
0084                LL=K-1                                               VARM 790
0085                NV=1                                                 VARM 800
0086                NC=0                                                 VARM 810
0087                FN=M                                                 VARM 820
0088                FFN=FN*FN                                            VARM 830
0089                CONS=0.7071066                                       VARM 840
0090      C                                                              VARM 850
0091      C       CALCULATE ORIGINAL COMMUNALITIES                       VARM 860
0092      C                                                              VARM 870
0093                DO 110 I=1,M                                         VARM 880
0094                H(I)=0.0                                             VARM 890
0095                DO 110 J=1,K                                         VARM 900
0096                L=M*(J-1)+I                                          VARM 910
0097          110   H(I)=H(I)+A(L)*A(L)                                  VARM 920
0098      C                                                              VARM 930
0099      C       CALCULATE NORMALIZED FACTOR MATRIX                     VARM 940
0100      C                                                              VARM 950
0101                DO 120 I=1,M                                         VARM 960
0102          115   H(I)= SQRT(H(I))                                     VARM 970
0103                DO 120 J=1,K                                         VARM 980
0104                L=M*(J-1)+I                                          VARM 990
0105          120   A(L)=A(L)/H(I)                                       VARM1000
0106                GO TO 132                                            VARM1010
0107      C                                                              VARM1020
0108      C       CALCULATE VARIANCE FOR FACTOR MATRIX                   VARM1030
0109      C                                                              VARM1040
0110          130   NV=NV+1                                              VARM1050
0111                TVLT=TV(NV-1)                                        VARM1060
0112          132   TV(NV)=0.0                                           VARM1070
0113                DO 150 J=1,K                                         VARM1080
0114                AA=0.0                                               VARM1090
0115                BB=0.0                                               VARM1100
0116                LB=M*(J-1)                                           VARM1110
0117                DO 140 I=1,M                                         VARM1120
0118                L=LB+I                                               VARM1130
0119                CC=A(L)*A(L)                                         VARM1140
0120                AA=AA+CC                                             VARM1150
0121          140   BB=BB+CC*CC                                          VARM1160
0122          150   TV(NV)=TV(NV)+(FN*BB-AA*AA)/FFN                      VARM1170
0123                IF(NV-51)160,155,155                                 VARM1180
```

```
0124      155     IER=1                                                    VARM1181
0125              GO TO 430                                                VARM1182
0126      C                                                                VARM1190
0127      C       PERFORM CONVERGENCE TEST                                 VARM1200
0128      C                                                                VARM1210
0129        160     IF((TV(NV)-TVLT)-(1.E-7)) 170, 170, 190                VARM1220
0130        170     NC=NC+1                                                VARM1230
0131                IF(NC-3) 190, 190, 430                                 VARM1240
0132      C                                                                VARM1250
0133      C       ROTATION OF TWO FACTORS CONTINUES UP TO                  VARM1260
0134      C       THE STATEMENT 120.                                       VARM1270
0135      C                                                                VARM1280
0136        190     DO 420 J=1,LL                                          VARM1290
0137                L1=M*(J-1)                                             VARM1300
0138                II=J+1                                                 VARM1310
0139      C                                                                VARM1320
0140      C         CALCULATE NUM AND DEN                                  VARM1330
0141      C                                                                VARM1340
0142                DO 420 K1=II,K                                         VARM1350
0143                L2=M*(K1-1)                                            VARM1360
0144                AA=0.0                                                 VARM1370
0145                BB=0.0                                                 VARM1380
0146                CC=0.0                                                 VARM1390
0147                DD=0.0                                                 VARM1400
0148                DO 230 I=1,M                                           VARM1410
0149                L3=L1+I                                                VARM1420
0150                L4=L2+I                                                VARM1430
0151                U=(A(L3)+A(L4))*(A(L3)-A(L4))                          VARM1440
0152                T=A(L3)*A(L4)                                          VARM1450
0153                T=T+T                                                  VARM1460
0154                CC=CC+(U+T)*(U-T)                                      VARM1470
0155                DD=DD+2.0*U*T                                          VARM1480
0156                AA=AA+U                                                VARM1490
0157        230     BB=BB+T                                                VARM1500
0158                T=DD-2.0*AA*BB/FN                                      VARM1510
0159                B=CC-(AA*AA-BB*BB)/FN                                  VARM1520
0160      C                                                                VARM1530
0161      C         COMPARISON OF NUM AND DEN                              VARM1540
0162      C                                                                VARM1550
0163                IF(T-B) 280, 240, 320                                  VARM1560
0164        240     IF((T+B)-EPS) 420, 250, 250                            VARM1570
0165      C                                                                VARM1580
```

ORIGINAL PAGE IS
OF POOR QUALITY

```
0166     C          NUM + DEN IS GREATER THAN OR EQUAL TO THE                    VARM1590
0167     C          TOLERANCE FACTOR                                             VARM1600
0168     C                                                                       VARM1610
0169        250      COS4T=CONS                                                  VARM1620
0170                 SIN4T=CONS                                                  VARM1630
0171                 GO TO 350                                                   VARM1640
0172     C                                                                       VARM1650
0173     C          NUM IS LESS THAN DEN                                         VARM1660
0174     C                                                                       VARM1670
0175        280      TAN4T= ABS(T)/ ABS(B)                                       VARM1680
0176                 IF(TAN4T-EPS) 300, 290, 290                                 VARM1690
0177        290      COS4T=1.0/ SQRT(1.0+TAN4T*TAN4T)                            VARM1700
0178                 SIN4T=TAN4T*COS4T                                           VARM1710
0179                 GO TO 350                                                   VARM1720
0180        300      IF(B) 310, 420, 420                                         VARM1730
0181        310      SINP=CONS                                                   VARM1740
0182                 COSP=CONS                                                   VARM1750
0183                 GO TO 400                                                   VARM1760
0184     C                                                                       VARM1770
0185     C          NUM IS GREATER THAN DEN                                      VARM1780
0186     C                                                                       VARM1790
0187        320      CTN4T= ABS(T/B)                                             VARM1800
0188                 IF(CTN4T-EPS) 340, 330, 330                                 VARM1810
0189        330      SIN4T=1.0/ SQRT(1.0+CTN4T*CTN4T)                            VARM1820
0190                 COS4T=CTN4T*SIN4T                                           VARM1830
0191                 GO TO 350                                                   VARM1840
0192        340      COS4T=0.0                                                   VARM1850
0193                 SIN4T=1.0                                                   VARM1860
0194     C                                                                       VARM1870
0195     C          DETERMINE COS THETA AND SIN THETA                            VARM1880
0196     C                                                                       VARM1890
0197        350      COS2T= SQRT((1.0+COS4T)/2.0)                                VARM1900
0198                 SIN2T=SIN4T/(2.0*COS2T)                                     VARM1910
0199        355      COST= SQRT((1.0+COS2T)/2.0)                                 VARM1920
0200                 SINT=SIN2T/(2.0*COST)                                       VARM1930
0201     C                                                                       VARM1940
0202     C          DETERMINE COS PHI AND SIN PHI                                VARM1950
0203     C                                                                       VARM1960
0204                 IF(B) 370, 370, 360                                         VARM1970
0205        360      COSP=COST                                                   VARM1980
0206                 SINP=SINT                                                   VARM1990
0207                 GO TO 380                                                   VARM2000
```

```
0208      370      COSP=CONS*COST+CONS*SINT                                  VARM2010
0209      375      SINP= ABS(CONS*COST-CONS*SINT)                            VARM2020
0210      380      IF(T) 390, 390, 400                                       VARM2030
0211      390      SINP=-SINP                                                VARM2040
0212    C                                                                   VARM2050
0213    C          PERFORM ROTATION                                         VARM2060
0214    C                                                                   VARM2070
0215      400      DO 410 I=1,M                                              VARM2080
0216               L3=L1+I                                                   VARM2090
0217               L4=L2+I                                                   VARM2100
0218               AA=A(L3)*COSP+A(L4)*SINP                                  VARM2110
0219               A(L4)=-A(L3)*SINP+A(L4)*COSP                              VARM2120
0220      410      A(L3)=AA                                                  VARM2130
0221      420      CONTINUE                                                  VARM2140
0222               GO TO 130                                                 VARM2150
0223    C                                                                   VARM2160
0224    C      DENORMALIZE VARIMAX LOADINGS                                 VARM2170
0225    C                                                                   VARM2180
0226      430      DO 440 I=1,M                                              VARM2190
0227               DO 440 J=1,K                                              VARM2200
0228               L=M*(J-1)+I                                               VARM2210
0229      440      A(L)=A(L)*H(I)                                            VARM2220
0230    C                                                                   VARM2230
0231    C      CHECK ON COMMUNALITIES                                       VARM2240
0232    C                                                                   VARM2250
0233               NC=NV-1                                                   VARM2260
0234               DO 450 I=1,M                                              VARM2270
0235      450      H(I)=H(I)*H(I)                                            VARM2280
0236               DO 470 I=1,M                                              VARM2290
0237               F(I)=0.0                                                  VARM2300
0238               DO 460 J=1,K                                              VARM2310
0239               L=M*(J-1)+I                                               VARM2320
0240      460      F(I)=F(I)+A(L)*A(L)                                       VARM2330
0241      470      D(I)=H(I)-F(I)                                            VARM2340
0242               RETURN                                                    VARM2350
0243               END                                                       VARM2360
```

ORIGINAL PAGE IS
OF POOR QUALITY

OUTPUT OF SUBR CO
MODE = 2 MTYPE = 2 NVAR = 3 NLOC = 10 ISIDE = 1 EF = .99500

DATA MATRIX

	1	2	3	4	5	6	7	8	9	10
1	7.00000	4.00000	6.00000	8.00000	8.00000	7.00000	5.00000	9.00000	7.00000	8.00000
2	4.00000	1.00000	3.00000	6.00000	5.00000	2.00000	3.00000	5.00000	4.00000	2.00000
3	3.00000	8.00000	5.00000	1.00000	7.00000	9.00000	3.00000	8.00000	5.00000	2.00000

	VECTOR LENGTH
1	8.60232
2	9.00000
3	8.36660
4	10.04988
5	11.74734
6	11.57584
7	6.55744
8	13.03840
9	9.48683
10	8.48528

NORMED DATA MATRIX

	1	2	3	4	5	6	7	8	9	10
1	.81373	.44444	.71714	.79603	.68101	.60471	.76249	.69027	.73786	.94281
2	.46499	.11111	.35857	.59702	.42563	.17277	.45750	.38348	.42164	.23570
3	.34874	.88889	.59761	.09950	.59588	.77748	.45750	.61357	.52705	.23570

COSINE MATRIX

	1	2	3	4	5	6	7	8	9	10
1	1.00000									
2	.72332	1.00000								
3	.95870	.88978	1.00000							
4	.96007	.50857	.84440	1.00000						
5	.95988	.87963	.99710	.85550	1.00000					
6	.84355	.97905	.96024	.66188	.94863	1.00000				
7	.99275	.79638	.98426	.92562	.98660	.89582	1.00000			
8	.95399	.89479	.99920	.83947	.99891	.96071	.98247	1.00000		
9	.98029	.84327	.99531	.89153	.99601	.92881	.99664	.99440	1.00000	
10	.95899	.65473	.90150	.91468	.88283	.79410	.93455	.88580	.91927	1.00000

ORIGINAL PAGE IS

ORIGINAL PAGE IS
OF POOR QUALITY

INDEX	EIGENVALUES	CUM. SUM EV
1	9.15653	9.15653
2	.74683	9.90336
3	.09660	9.99996
4	.00000	9.99996
5	.00000	9.99996
6	.00000	9.99996
7	.00000	9.99996
8	.00000	9.99996
9	.00000	9.99996
10	.00000	9.99996

EIGENVECTORS (COLUMNS)

	1	2	3
1	.32285	-.24670	-.03507
2	.28223	.60175	.04605
3	.32957	.08500	-.02579
4	.29088	-.53799	-.30689
5	.32873	.06962	-.26704
6	.31009	.39336	.20233
7	.32846	-.11522	-.15149
8	.32886	.10142	-.14579
9	.33015	-.02084	-.12839
10	.30598	-.31112	.85373

FACTORS (COLUMNS)

	1	2	3
1	.75247	-.39561	.52657
2	.38153	-.38986	-.83810
3	.53685	.83157	-.14242

ERMS= .00000 EMAX= .00001

ERROR OF REPRESENTATION

	1	2	3	4	5	6	7	8	9	10
1	.00001	.00000	.00001	.00001	.00001	.00001	.00000	.00000	.00000	.00000
2	.00000	.00000	-.00000	.00000	.00000	.00000	.00001	.00000	.00001	.00000
3	.00000	.00001	.00001	.00000	.00001	.00000	.00000	.00000	.00000	.00000

ORIGINAL PAGE IS
OF POOR QUALITY

VARIMAX TRANSFORMATION

	1	2	3
1	.72733	.68439	.05078
2	-.68428	.72887	-.02227
3	-.05225	-.01854	.99846

ORIGINAL PAGE IS
OF POOR QUALITY

VSTAR MATRIX

	1	2	3
1	.85702	.51343	.04348
2	.26457	.96326	.04608
3	.67550	.73621	.04101
4	.96332	.26530	-.04018
5	.68667	.72618	-.03369
6	.44658	.88880	.10287
7	.79350	.60853	.00568
8	.66618	.74578	.00334
9	.74104	.67135	.01130
10	.84356	.43279	.31794

FSTAR MATRIX

	1	2	3
1	.79049	.21688	.57278
2	.58806	-.00749	-.80875
3	-.17112	.97616	-.13345

REFERENCES

Ahlbrandt, T. S., 1973, Sand dunes, geomorphology, and geology, Killpecker Creek area, north Sweetwater County, Wyoming; unpublished Ph.D. dissertation, Univ. of Wyoming, Dept. of Geology, Laramie, Wyoming, 174 p.

Anderson, J. R., Hardy, E. E., and Roach, J. T., 1972, A land-use classification system for use with remote-sensor data; U. S. Geological Survey Circ. 671, 16 p.

Andrews, D. A., Pierce, W. G., and Kirby, J. J., 1944, Structure contour map of the Bighorn Basin, Wyoming and Montana; U. S. Geol. Survey Oil and Gas Investigations Preliminary Map, no. 3.

Andrews, H. C. 1972, Introduction to mathematical techniques in pattern recognition; John Wiley and Sons, New York, 242 p.

Anuta, P. E., Kristof, S. J., Levandowski, D. W., Phillips, T. L., MacDonald, R. B., 1971, Crop, Soil, and geological mapping from digitized multispectral satellite photography; 7th International Symposium on Remote Sensing of Environment, vol. 111, Univ. of Mich., Ann Arbor, Mich., p. 1983-2016.

Barrus, R. B., 1968, The bedrock geology of the southeastern Alpine Lake quadrangle, Wind River Mountains, Wyoming; Washington State Univ. unpub. M.S. thesis, 46 p.

Barton, R., and Marrs, R. W., 1974, Location of geologic structures from interpretation of ERTS-1 imagery, Carbon County, Wyoming; National Technical Information Service, Springfield, Virginia, Report E74-10333, 7 p.

Bayley, R. W., 1965a, Geologic map of the South Pass City quadrangle, Fremont County, Wyoming; U. S. Geol. Survey Map GQ-458.

_____, 1965b, Geologic map of the Atlantic City quadrangle, Fremont Count, Wyoming; U. S. Geol. Survey Map GQ-459.

_____, 1965c, Geologic map of the Miners Delight quadrangle, Fremont County, Wyoming; U. S. Geol. Survey Map GQ-460.

_____, 1965d, Geologic map of the Louis Lake quadrangle, Fremont County, Wyoming; U. S. Geol. Survey Map GQ-461.

Bekkar, H., 1973, Laramide structural elements and relationship to Precambrian basement, southeastern Wyoming; unpub. M.S. thesis, University of Wyoming, Laramie, Wyoming.

REFERENCES (cont'd)

Bell, Wallace, 1955, Geology of the southeastern flank of the Wind River Mountains, Fremont County, Wyoming; Univ. of Wyoming unpub. Phd thesis, 204p.

Berg, Robert R., 1962, Mountain flank thrusting in Rocky Mountains foreland, Wyoming and Colorado; Bull. Amer. Assoc. Petroleum Geologists, v. 48, p. 2019-2032.

Blackstone, D. L., Jr., 1951, An essay on development of structural geology in Wyoming; Guidebook 6th Ann. Field Conference, Wyo. Geol. Assoc., p. 15-28.

_____, 1963, Development of geologic structure in Central Rocky Mountains; in backbone of the America's Am. Assoc. Petrol. Geologists, Mem. 2, p. 160-179.

_____, Nov. 22, 1972, Tectonic analysis of Southwestern Wyoming from ERTS-1 imagery; National Technical Information Service,Report E72-10377, Springfield, Virginia 10p.

_____, June 1, 1963, Analysis of photo linear elements, Laramie Mountains, Wyoming; National Technical Information Service, Report E73-10704, Springfield, Virginia, 16p.

_____, June 10, 1973, Analysis of linear photo elements, Boghorn-Pryor Mountains, Montana and Wyoming; National Technical Information Service, Report E73-10704, Springfield, Virginia, 15p.

_____, August 1, 1973, Geology of photo linear elements, Great Divide Basin, Wyoming; National Technical Information Service, Report E73-10958/WR, Springfield,Virginia, 14p.

Bradley, W. H., 1961, Geologic map of a part of southwestern Wyoming and adjacent states; U.S. Geol. Survey, Miscellaneous Geologic Investigations, Map I-332.

Breckenridge, R.M., 1973, Glaciation of northwestern Wyoming interpreted from ERTS-1; Symposium on Significant Results Obtained from ERTS-1, March 5-9, 1973, Report NASA-SP-327, NASA Scientific and Technical Information Office, Washington, D.C. p. 363-370.

Breckenridge, R.M., Marrs, R.W., and Murphy, D.J., 1973, Remote sensing applied to land-use studies in Wyoming; Symposium on Significant Results Obtained from ERTS-1; March 5-9, Report NASA SP-327, NASA Scientific and Technical Information Office, Washington, D.C. p.981-990.

REFERENCES (cont'd)

Brinker, W.F., and Blackstone, D.L., JR., (eds.), 1951, Guidebook for the 6th annual field conference - south central Wyoming; Wyo. Geol. Assoc. Guidebook; available from Petroleum Information Inc., Casper, Wyoming, 165p.

Carey, B.D., 1959, Geology of the Rattlesnake Hills Tertiary volcanic field, Natrona County, Wyoming; Univ. of Wyoming, unpublished Ph.d thesis, 247p. also in Wyoming Geol. Assoc. Guidebook 9th Ann. Field Conf., 1954, p.32-34.

Cary, Merritt, 1917, Life zone investigations in Wyoming; U.S. Dept. Agriculture, Biol. Survey Bull. 42.

Chamberlin, R.T., 1945, Basement control in Rocky Mountain deformation; American Jour. Science, v. 243-A, p. 98-116.

Christianson, R.L., and Blank, H.R., Jr., 1972, Volcanic stratigraphy of the Quaternary rhyolite plateau in Yellowstone National Park; U.S. Geological Survey, Prof. Paper 729-B, 18p.

Christianson, R.L., Pierce, K.L., Prostka, H.J., and Ruppel, E.T., 1966, Preliminary evaluation of radar imagery of Yellowstone Park, Wyoming; NASA Tech. Letter 30, 11p.

Condie, K.C., 1969, Petrology and geochemistry of the Laramie batholith and related metamorphic rocks of Precambrian age, eastern Wyoming; Geol. Soc. America Bull., v.80, p. 57-82.

Costello, D.F., 1954, Vegetation zones in Colorado; in Harrington, H.D., Manual of the plants of Colorado, Sage Books, Denver, Colorado, 666p.

Darton, N.H., Blackwelder, E., and Siebenthal, C.E., 1910, U.S. Geol. Survey, Geologic Atlas, Laramie - Sherman; Folio 173.

Daubenmire, R.F.,1943, Vegetation zonation in the Rocky Mountains; Botanical Review, v. 9, p. 325-393.

Davis, J.C., 1973, Statistics and data analysis in geology; John Wiley and Sons, New York, p.473-533.

Dobbin, C.E., Bowen, C.F., and Hoots, H.W., 1929, Geology and coal and oil resources of the Hanna and Carbon Basins, Carbon County, Wyoming; U.S. Geol. Survey Bull. 804, 88p.

Dorn, Robert D., 1972, Dept. of Botany, University of Wyoming, (personal communication).

REFERENCES (cont'd)

Dunbar, Robert O., 1944, Como Bluff anticline, Albany and Carbon Counties, Wyoming; Am. Assoc. Petrol. Geologists, vol. 28, p. 1196-1216.

Dunnewald, T.J., 1957, Wyoming soils and soil materials; Bull. 349, Agriculture experiment station, University of Wyoming, Laramie, Wyoming.

Embleton, C., and King, C.A.M., 1968, Glacial and Periglacial geomorphology; St. Martin's Press, New York, 608p.

Evans, M.A., and Marrs, R. W., 1974, Identification of irrigated crop types from ERTS-1 density contour maps and color infrared photography; National Technical Information Service, Springfield, Virginia, Report E 74-10312, 12p.

Evans, M.A., and Redfern, R.F., 1973, Vegetation analysis in the Laramie Basin, Wyoming from ERTS-1 imagery; National Technical Information Service, Springfield, Virginia, Report E 74-10145, 54p.

Fenneman, N.M., 1931 Physiography of the western United States; McGraw-Hill, New York, 534p.

Gates, D.M., Keegan, H.J., Schleter, J.C., and Weidner, V.R., 1965, Special Properties of Plants; Appl. Optics, v.4 p. 11-20.

Gibbens, R.P., and Fisser, H.G., 1972, Influence of grazing management systems on vegetation and wildlife habitat; Annual Report of Progress, July 1969 - July, 1970, Wyoming Agricultural Experiment Station, Scientific Report 414, 69p.

Gordon, R.C., 1974, Multispectral imagery for range vegetation type mapping and estimation of above ground green biomass; National Technical Information Service, Springfield, Virginia, 45p.

Granger, H.C., McKay, E.J., Mattick, R.E., Patten, E.L., and McIlroy, Paul, 1971, Mineral resources of the glacier primitive area, Wyoming; U.S. Geol. Survey Bull. 1319-F, 113p.

Griffiths, J.C., and Ondrick, C.W., 1969, Modeling the petrology of detrital sediments; in Computer Applications in Earth Science; Plenum Press, New York, p. 73-97.

Hoffer, R.M., and Goodrick, F.E., 1971 Variables in automatic classification over extended remote-sensing test sites; 7th Internation Symposium on Remote Sensing of Environment, Univ. of Mich., Ann Arbor, p. 1967-1981.

REFERENCES (cont'd)

_____, and Johannsen, C. J., 1969, Ecological potentials in spectral signature analysis; in Johnson, P. L., (ed.), Athens, Ga.

Houston, R. S., 1974, Geologic mapping using space images; in Houston and others, 1974, Some illustrations of the advantages of improved resolution in geologic studies; National Technical Information Service, Springfield, Virginia, report E 74-10628, p. 4-27.

Houston, R. S., and Marrs, R. W., 1974, Some preliminary results of the use of S-190A and S-190B Skylab sensors for photogeologic studies; 55th Annual Meeting of the American Geophys, Union, April, 1974, Washington, D. C., (abs.), EOS p. 344.

_____, 1974, Use of Skylab S-190A and S-190B photographs in Wyoming earth resource studies; Proceedings of the 20th Annual Meeting of the American Astronautical Soc., Los Angeles, Calif., Aug. 20-22, 1974. Paper AAS74-142.

Houston, R. S., Marrs, R. W., Breckenridge, R. M., and Blackstone, D. L. Jr., 1973; Application of the ERTS system to the study of Wyoming resources with emphasis on the use of basic data products, Third ERTS-1 Symposium, Dec. 10-14, NASA Scientific and Technical Information Office, Washington, D. C., Report NASA SP-551; p. 595-620.

Houston, R. S., and Short, Nicholas M., 1972, A first look at geological aspects of ERTS-1 imagery of Wyoming: NASA/ Goddard Space Flight Center, Greenbelt, Md., NASA-IM-X-68776, NTIS E 72-10041, 2p.

_____, 1972, Geologic interpretation of ERTS imagery of western Wyoming; First ERTS-1 Symposium; Sept. 29, 1972, Report X-650-73-10, NASA Scientific and Technical Information Office, Washington, D. C., p. 58-77.

Houston, R. S., and others, 1968, a regional study of rocks of Precambrain age in that part of the Medicine Bow Mountains lying in south-eastern Wyoming--with a chapter on the relationship between Precambrian & Laramide structure Wyoming Geological Survey Memoir no. 1, 167 p.

Hunt, Graham R., and Salisbury, John W., 1971, Visible and near-infrared spectra of minerals and rocks: v. I silicate minerals; Modern Geol., v. 1, p. 283-300.

REFERENCES (cont'd)

Hunt, G. R., Salisbury, J. W., and Lenhoff, C. V., 1971, Visible and near-infrared spectra of minerals and rocks: III oxides and hydroxides; Modern Geol., V. 2, p. 195-205; Visible and near-infrared spectra of minerals and rocks: IV: sulphides and sulphates; Modern Geology, V. 3, p. 1-14.

Imbrie, J., and Purdy, E. G., 1962, Classification of modern Bahamian carbonate sediments; American Assoc. Petroleum Geologists Memoir, n. 1, p. 253-272.

James. H. J., 1954, Sedimentary facies of iron formation; Econ. Geol., v. 49, n. 3, p. 235-293.

Kaabar, Salah M., 1971, Geology of the Pinto Creek Quadrangle, Albany County, Wyoming, unpublished Master's thesis, University of Wyoming.

Keefer, W. R., 1972, The geologic story of Yellowstone National Park; U.S. Geol. Survey Bull. 1347, 92p.

Kemp, J. F., 1897, The Leucite Hills of Wyoming: Geol. Soc. America Bull., v. 8, p. 169-182.

Kemp, J. F., and Knight, W. D., 1903, Leucite Hills of Wyoming, Geol. Soc. America Bull., v. 14, p. 305-336.

Kirkwood, J. E. 1922, Forest distribution in the northern Rocky Mountains; Montana State University Bull. 247.

Klovan, J. E., 1966, The use of factor analysis in determining depositional environments from grain-size distributions; Jour. Sedimentary Petrology, v. 36, p. 115-125.

Kolm, K. E., 1974, ERTS MSS imagery applied to mapping of sand dunes in Wyoming; Geol. Survey of Wyoming, Report of Investigations, n. 10, p. 34-39.

_____, 1974, ERTS MSS imagery applied to mapping and economic evaluation of sand dunes in Wyoming, National Technical Information Service, Springfield, Virginia, 31 p.

Kriegler, F. J., Malila, W. A., Nalepka, R. F., and Richardson, W., 1970, Preprocessing transformations and their effects on multispectral recognition; 6th International Symposium on Remote Sensing of Environment, University of Mich., Ann Arbor, p. 97-131.

Love, J. D., 1970, Cenozoic geology of the Granite Mountains area, central Wyoming; U.S. Geol. Survey Prof. Paper 495-C, 154 p.

Love, J. D., 1961, Reconnaissance study of Quaternary faults in and south of Yellowstone National Park, Wyoming; Geol. Soc. America Bull., v. 72, p. 1749-1764.

Love, J. D., Weitz, J. L., and Hose, R. K., 1955, Geologic map of Wyoming; U. S. Geol. Survey Map.

Lyon, R. J. P., and Patterson, J., 1969, Airborne geological mapping using infrared emission spectra; 6th International symposium on remote sensing of environment, v. 1, Univ. of Michigan, Ann Arbor, Michigan, p. 527-552.

Malahoff, Alexander, & Moberly, Ralph, Jr., 1968, Effects of structure on the gravity field of Wyoming; Geophysics, v. 33, p. 781-804.

Marrs, R. W., 1974, Remote sensing in mineral exploration; 17th Minerals Symposuim of the Society of Mining Engineers, Eastern Wyoming Subsection/AIME, May 11, 1973, 15 p.

Masarsky, Harold, 1962, Uranium-bearing coal in the eastern part of the Red Desert Area, Great Divide Basin, Sweetwater County, Wyoming; U. S. Geol. Survey Bull. 702.

McGrew, Paul O., & Berman, Jack E., 1955, Geology of the Tabernacle Butte area; Guidebook, 10th Ann. Field Conference, Wyo. Geol. Association, p. 108-111.

Miller, K. S., 1962, Multidimensional Gaussian distributions, John Wiley and Sons, New York, 129 p.

Moody, J. D., and Hill, M. J., 1956, Wrench fault tectonics; Geol. Soc. America Bull., v. 67, p. 1207-1246.

National Academy of Sciences, 1970, Remote sensing with special reference to agriculture and forestry; Natl. Acad. Sci., Wash. D. C., 424 p.

Nelson, Aven, 1896, First report on the flora of Wyoming; University of Wyoming, Agricultural Experiment Station Bull. 28, 218 p.

Newhouse, W. H., and Hagner, A. F., 1957, Geologic map of anorthesite areas, southern part of the Laramie Range, Wyoming; U. S. Geol. Survey, Mineral Investigations Field Studies Map, MF-119.

Odum, E. P., 1971, Fundamentals of Ecology, W. B. Saunders Co., Philadelphia.

Ohle, E. L., 1972, Evaluation of iron ore deposits; Econ. Geol., v. 67, no. 7, p. 953-964.

Parker, Ronald B., 1972, An Evaluation of ERTS-1 imagery for mapping of major earth fractures and related features; report E72-10349 available from National Technical Information Service, Springfield, Va., 7 p.

_____, 1973, Regional Fracture in the Wind River Mountains Precambrian from ERTS-1 Imagery; Geol. Soc. America, 26th Annual Meeting; Rocky Mountain Section; (abs.) p. 1520.

Parsons, W. H. (ed.), 1963, Structures and origin of volcanic rocks; Guidebook for National Science Foundation volcanic summer field conference, Wayne State University, Detroit, Mich., 61 p.

Pearson, R. L., and Miller, L. D., 1972, Remote spectral measurements as a method for determining plant cover; U. S. IBP Grassland Biome Tech. Report 167, Colo. State Univ., Fort Collins, Colo., 48 p.

Pearson, Robert C., Killsgaard, Thor H., and Patten, Lowell L., 1971, Mineral resources of the Popo Agie primitive area, Fremont and Sublette Counties, Wyoming; U. S. Geol. Survey Bull. 1353-B, 55 p.

Pechanec, J. F., and Pickford, G. D., 1936, A weight estimate method for determination of range or pasture production; Jour. American Soc. Agronomy, v. 29, p. 894-904.

Pierce, W. G., 1957, Heart Mountain and South Fork detachment thrusts of Wyoming; Amer. Assoc. Petroleum Geol. Bull., v. 41, no. 4, p. 591-626.

Pierce, W. G., and Nelson, W. H., 1969, Geologic map of the Wapiti Quadrangle, Park County, Wyoming, U. S. Geol. Survey map GQ-778.

Pipiringos, George N., 1961, Uranuim-bearing coal in the central part of the Great Divide Basin, Sweetwater County, Wyoming; U. S. Geol. Survey Bull. 1099-A.

Pohn, H. A., Offield, T. W., and Watson, Kenneth, 1972, Geologic material discrimination from Nimbus satellite data; 4th Ann. Earth Resources Program Review, v. 111, NASA/MSC-05937, Houston, Texas, p. 59-1 - 59-15.

Porter, C. L., 1962, A flora of Wyoming; Part I; University of Wyoming, Agricultural Experiment Station, Bull. 402, 39 p.

Ransome, F. L., 1915, The Tertiary orogeny of the North American Cordillera and its problems; in Problems of North American Geology, New Haven, p. 287-376.

Raines, G. L., and Lee, Keenan, 1974, Spectral reflectance measurements; Photogram. Eng., v. 40, no. 5, p. 547-550.

Renfro, H. B., and Feray, D. E., (no date), Geological highway map of the northern Rocky Mountain region; Amer. Assoc. Petroleum Geologists, Tulsa, Oklahoma.

Richmond, G. M., 1945, Geology and oil possibilities at the northwest end of the Wind River Mountains, Sublette County, Wyoming; U. S. Geol. Survey Oil and Gas Inv. Prelim. Map 31, (reprinted 1957).

Roehler, H. W., 1969, A review of Eocene stratigraphy in the Washakie Basin, Wyoming; U. S. Geol. Survey Guidebook, Field Conference on Tertiary Biostratigraphy of Southern and Western Wyoming, 1972, p. 3-19.

Rosenzweig, M. L., 1968, Net primary production of terrestrial communities; American Naturalist, v. 102, p. 67-74.

Rowan, Lawrence C., 1972, Near-infrared iron absorption bands; application to geologic mapping and mineral exploration; 4th Ann. Earth Resources Program Review, NASA, MSC, Houston, Texas, p. 60-1 - 60-18.

Rowan, L. C.,Werlaufter P. H., Billingsley, F. C., and Goetz, A. F. H., and others, 1973, Mapping of hydrothermal alteration zones and regional rock types using computer enhanced ERTS MSS images; Third ERTS Symposium, Dec. 10-14, 1973, Washingtion, D. C., NASA/Goddard Space Flight Center, Greenbelt, Maryland, v. 1, p. 807.

Rydberg, P. A., 1928, Life zones of the Rocky Mountains; Journal of the New York Botanical Gardens, v. 29, p. 282-284.

Sales, John K., 1968, Crustal mechanics of Cordilleran Foreland deformation; a regional and scale model approach; American Assoc. Petroleum Geologists Bull., v. 52, no. 10, p. 2016-2044.

Shelupsky, David, 1962, An introduction of spherical coordinates; American Mathematical Monthly, v. 69, no. 7, p. 644-646.

Sherer, Richard L., 1969, Nephrite deposits of the Granite, the Seminoe, and the Laramie Mountains, Wyoming; Univ. of Wyoming, unpub. Ph. D. thesis, 194 p.

Short, Nicholas M., and Lowman, Paul D., 1973, Earth observations from space; outlook for the geological sciences; NASA/Goddard Space Flt. Center, Greenbelt, Md., no. X-650-73-316, 115 p.

Smedes, H. W., 1971, Preprocessing of multispectral data and simulation of ERTS data channels to make computer terrain maps of a Yellowstone National Park test site; 7th International Symposium on Remote Sensing of Environment, Univ. of Mich., Ann Arbor, p. 2073-2094.

Smedes, H. W., Linnerud, A. J., Hawks, S. J., and Wodaver, L. B., 1971, Digital computer mapping of terrain by clustering techniques using color film as a three-band sensor; 7th International Symposium on Remote Sensing of Environment, Univ. of Mich., Ann Arbor, p. 2057-2071.

Smedes, H. W., Linnerud, H. J., Wodaver, L. B., Ming-Yang Su, and Jauror, R. R., 1972, Mapping of terrain by computer clustering techniques using multispectral scanner data and using color aerial film; 4th Ann. Earth Resources Program Rev., v. 111, NASA, MSC, No.-05937, Houston, Texas, p. 61-1 - 61-30.

Smedes, H. W., and Prostka, H. J., 1972, Absaroka volcanic supergroup in the Yellowstone National Park region; U. S. Geol. Survey Prof. Paper, 729-C.

Stone, D. S., 1969, Wrench faulting and Rocky Mountain tectonics; Mountain Geologist, v. 6, no. 2, p. 67-79.

Thorpe, J., 1939, Soil survey, Sheridan Co., Wyoming, U. S. Dept. Agriculture series 1932, no. 33, 48 p.

U. S. Dept. of Agriculture, 1973, Water supply outlook for Wyoming, U. S. Soil Conservation Service, January-August, 1973.

U. S. Geological Survey, 1972, Geologic map of Yellowstone National Park; U. S. Geol. Survey Miscellaneous Geologic Investigations Map I-711.

U. S. Geological Survey, 1973, Water resources data for Wyoming; Part I, Surface water records, U. S. Geol. Survey, 247 p.

Vincent, Robert, K., 1972, An ERTS multispectral scanner experiment for mapping iron compounds; 8th International Symposium on Remote Sensing of Environment, Ann Arbor, Michigan, p. 1239-1247.

_____, 1973, Ratio maps of iron ore deposits, Atlantic City District, Wyoming (abs.), Symposium of Significant Results Obtained from ERTS-1, NASA, Greenbelt, Md., p. 42.

Vincent, Robert K., and Thompson, F.J., 1971, Discrimination of basic silicate rocks by recognition maps processed from aerial infrared data; 7th International symposium on remote sensing of environment, v.1, University of Mich., Ann Arbor, Mich., p. 247-252.

Watson, Kenneth, Rowan, L.C., and Offield, T.W., 1971, Application of thermal modeling in the geologic interpretation of IR images; 7th International symposium on remote sensing of environment, v. III, Univ. of Mich., Ann Arbor, Mich., p. 2017-2041.

Watson, Robert D., 1972, Spectral reflectance and photometric properties of selected rocks; Remote sensing of Environment, v. 2, p. 95-100.

Watson, R.D., and Rowan, L.C., 1971, Automated geologic mapping using rock reflectances; 7th International symposium on remote sensing of environment; v. III, University of Mich., Ann Arbor, Mich., p. 2043-2053.

Welder, G.E., and McGreevy, L.J., 1966, Ground water reconcaissance of the Great Divide and Washakie basins and some adjacent areas of southwestern Wyoming; U.S. Geol. Survey Hydrologic Investigations Atlas HA-219.

Wilson, W.H., 1964, The Kirwin mineralized area, Park County, Wyoming; Wyoming Geol. Survey, Prelim. Report 2, 12p.

Wolff, A.J., 1974, Sequential Q-mode factor analysis; Unpub. Master Sci. Thesis, University of Wyoming, Dept. of Statistics, Laramie, Wyoming.

Zapp, A.D., 1956, Structure and contour map of the Tensleep sandstone in the Bighorn Basin, Wyoming and Montana; U.S. Geol. Survey Map OM 182.

INDEX

Absaroka Mountains 14, 19, 21
aeolian features 11, 15, 24, 25, 49
aerial photography 1, 3, 4, 15, 19, 21, 25, 29, 31, 33, 38, 41, 49, 50, 60
Agard, S. 12
agriculture 5, 6, 9, 27, 31, 38
aircraft 3
Air Force 1
alphanumeric maps 51, 56, 57
alteration 19, 20
American Association of Petroleum Geologists 7, 8
American Astronautical Society
American Geophysical Union 7
American Society of Mining and Melallurgical Engineers 7
Apperson, L. 13
aquifers 16, 33
archeology 49
Arminto area 17
Army 1

Badlands 49
Baggs 31
Baskett, S. 12
Bausch and Lomb ZT-4 38, 46
bias 24
Bighorn Basin 37
Bighorn Mountains 22, 23, 24. 33
biomass 31, 32
Black Hills 33
black sandstone 20
Blackstone, D. L. 10, 23, 24
Borgman, L. E. 10
botany 27, 29, 31
Breckenridge, R. M. 6, 10

caldera 14
Casper 42, 43
catalogue 1
change detection 38
cirques 15
climate 33, 49
coal 9, 11, 37, 38
color-additive viewing 13
color anomaly 19, 21
color composites 15, 17, 20, 33, 34, 36
computer processing 10, 12, 29, 31, 50, 51, 52, 61
converter plants 41
copper 19, 20
cost/benefit 59, 60
Cretaceous rocks 17, 20, 26

data:
  library 1, 12, 50;
  aquisition 1
  users 1. 62;
  interpretation 1, 19
Decker, E. R. 10
deer 46, 48, 49
demonstration project 5
density contouring 32, 40
development 5
Diem, K. L. 11
dikes 22
distortion 52

Earle, J. 12
Earth Resources Experiments Package (EREP)
  applications 4, 7
  data 1, 8, 9
  S192 8
  S190A 8
  S190B 8
Earth Resources Technology Satellite (ERTS)
  applications 5, 59
  data 1, 8, 24, 53, 54, 59, 61
  images 3, 5, 13, 14, 16, 17, 20,22, 23, 25, 27, 29, 30, 31, 33, 38, 44, 46, 49, 60
  magnetic tapes 50
  mosaic 2
  system 7
Earth Resources Technology Satellite B 3

INDEX

ecology 9, 41, 46
edge enhancement 13
eigenvalues 54, 55, 56
eigenvectors 54, 55, 56, 57
emission plumes 9, 41, 45
energy 6, 29, 37
engineering 5
environment 5, 6, 9, 10, 29, 32, 37, 38, 49, 50, 59
Evans, M. A. 12, 29
exploration 19, 20, 61

facies changes 15, 16
false color 2
fault 14, 21 24, 25, 37
federal agencies 3, 59
Federal Center, Denver
field data 8, 10, 14, 21, 22, 24, 25, 29, 46, 50, 60
film processing 50
fire 41, 44
Fisser, H. G. 10
flood plain 40
fluvial processes 49
fly-ash 9, 41
forestry 9, 27, 30, 31 38
fractures 7, 8, 21, 22, 23, 25
frequency space cluster 51, 56, 59, 61
Froman, N. 12
funding 1

game control 3, 49
General Electric Photographic Engineering Association 2
geochemistry 11, 61
Geological Society of America 7
geology:
mapping 4, 5, 6, 8, 9, 10, 11, 13, 14, 15, 27, 50, 59, 60, 61
geomorphic provinces 15
geomorphology 11, 15, 25
geophysics 19, 22, 25
geothermal 8, 10, 27, 28, 61
glaciation 6, 10, 15, 49
Glass, G. 11
Gordon, R. C. 6, 11
grassland 9, 30, 38
Great Divide Basin 24
Green River Basin 17, 26, 41
greenstone 21
grey-scale map 53
grooves 15
groundwater 20, 33, 37

Heartville Uplift 33
Houston, R. S. 6, 8, 9, 24
Huntoon, P. 11
hydrology 11, 12, 32

ice fields 15
illumination 24
image masks 13
impact 5, 29, 33, 38
interpretation techniques 7, 8, 13, 61
intrusive rock 14, 19
iron oxides 20
irrigation 32, 33
isodensity contouring 13, 42, 43

Joyce Loebl/Tech Ops isodensitracer 43

karst 37
Kern PG-2 38
Knight, D. H. 10
Kolm, K. E. 11

lakes 15, 32, 33, 35, 36
landforms 4, 15, 49
landslides 15
land-use 1, 3, 4, 5, 6, 10, 16, 38, 39, 40, 41, 60, 61,
Lane, D. 10
Laramide 24
Laramie Basin 29, 33, 35, 36
Laramie Mountains 17, 18, 22, 23, 24
LARS 29, 38, 51
Lauer, W. 12
limestone 37
linear features 10, 21, 22, 23, 24, 25
lithology 13, 23, 40
Love, J. D. 11

Marrs, R. W. 5, 8, 10, 29
McCarty, K. M. 12
Mears, B. 11
Medicine Bow Mountains 46
Meister, K. M. 13
Mesozoic rocks 14

INDEX

meteorology 8
minerals 4, 7, 8, 9, 19, 33, 40, 59, 61
mini computer 51, 52, 53
molybdenum 19
monitoring 8, 31, 38, 49
Montana 20
moraines 15
mosaic 2, 26, 31
multiband cameras 3
multi-level sensing 19, 20
multispectral data 14, 61
multivariate ratio 51, 57, 58
Murphy, D. J. 6

National Aeronautics and Space Administration (NASA) 1, 3, 49
Natural Resources 7, 59

objectives 1
oil shale 37
operational system 5
outwash fans 15

Parker, R. B. 7, 10, 22
pattern recognition 51, 53
pediments 15
permeability 37
petroleum 10, 21
Petroleum Ownership Map Company 26
photoprocessing 12
physiography 25
pilot study 3
planning 5, 29, 40, 59
plant science 5, 27
playa deposits 15, 16, 17
porosity 37
Powder River Basin 3, 4, 20, 32, 33, 37, 40, 41, 46
power plants 37
Precambrian rocks 5, 13, 14, 21, 22, 23
Pryor Mountains 23
public 1, 5
Pumpkin Buttes 59

Q-Mode analysis 51, 53, 55, 56, 57
Quaternary deposits 5, 15

range management 10, 11, 31, 40
ratio 55, 58
Rawlins 39, 60
Red Desert 24, 26
Redfern, R. F. 12, 29
remote-sensing applications 5, 6, 7
remote-sensing laboratory 1, 3, 4, 8, 38, 40, 51
residential areas 41
resolution 20, 25, 46, 51, 61
rivers 15
R-Mode analysis 54, 57
Rock Springs uplift 26
rural areas 41

sand dunes 5, 15, 16, 24, 49
sediment 33, 35, 36
sedimentary rocks 14, 18, 21
selenium 41
Short, N. M. 3, 6, 9, 24
Skylab:
  date 1
  photography 5, 8, 13, 25, 31, 33, 38, 41, 61
  system 7
slopes 40
snow 8, 15, 17, 18, 27, 28, 32, 33, 40, 41, 42, 45, 46, 47, 48, 49
soils 32, 40
  classification 4
  maps 1, 3, 4, 27
  moisture 32, 61
  surveys 7
special reports 1
spectral signatures 8, 9, 31, 32, 54, 59
spherical coordinates 58, 59
state agencies 3, 59
statistics 10, 19, 54, 55
stereo plotter 38
stereoscopic coverage 13, 61
stratigraphy 8
streams 15, 32, 33
Strickland, D. 11
strip mines 9, 38, 40
structure 10, 12, 22, 23, 24, 25, 26

INDEX

sun azimuth 23, 25
sun elevation 25
Surdam, R. C. 11
Sweetwater County 26

tectonics 8, 12, 25, 27, 57, 61
temperature 9, 27
terraces 15
tertiary rock 14, 17, 20
test site 1
thermal 8, 27
Thermopolis 27
Tomes, B. J. 12, 25
topical maps 15
topographic maps 40
trona 45

University of Wyoming 1, 3, 5, 6, 9, 10, 11, 12, 38, 50
uranium 20, 37, 59
urban areas 38, 40, 41
U. S. Geological Survey 3, 4, 11, 16, 40, 49
U. S. Soil Conservation Service 3, 4, 26

vegetation 8, 9, 10, 12, 13, 15, 16, 17, 25, 27, 29, 30, 31, 32, 33, 39, 40, 61
vegetation classification 29
volcanic rocks 14

Washakie Basin 26
water 34, 40
water table 33
Wheatland 29
wildlife 9, 11
Wind River Mountains 7, 22, 23, 25
winter range 46, 47, 48, 49
Wyoming 1
Wyoming Department of Economic Planning and Development 3
Wyoming Game and Fish Commission 3, 33
Wyoming Geological Society 7
Wyoming Geological Survey 4, 10, 11
Wyoming Highway Department 3

Yellowstone Park 27, 28
Yellowstone Plateau 15

zoom transfer scope 38